Universidade de Aveiro
2012

Departamento de Engenharia de Materiais e Cerâmica

Hugo Alexandre Gonçalves da Rocha Fernandes

Desenvolvimento de vitrocerâmicos à base de dissilicato de lítio

Development of lithium disilicate based glass-ceramics

Universidade de Aveiro
2012

Departamento de Engenharia de Materiais e Cerâmica

Hugo Alexandre Gonçalves da Rocha Fernandes

Desenvolvimento de vitrocerâmicos à base de dissilicato de lítio

Development of lithium disilicate based glass-ceramics

Tese apresentada à Universidade de Aveiro para cumprimento dos requisitos necessários à obtenção do grau de Doutor em Ciência e Engenharia de Materiais, realizada sob a orientação científica do Doutor José Maria da Fonte Ferreira, Professor Associado com Agregação do Departamento de Engenharia de Materiais e Cerâmica da Universidade de Aveiro e do Doutor Dilshat U. Tulyaganov, Professor do Turin Polytechnic University in Tashkent (Tashkent, Uzbequistão)

Apoio financeiro da FCT e do FSE no âmbito do III Quadro Comunitário de Apoio.

…Para a Rute e o Tomás

…Para os meus pais

o júri

presidente

Prof. Doutor Aníbal Guimarães da Costa
professor catedrático do Departamento de Engenharia Civil da Universidade de Aveiro

Prof. Doutor Jorge Ribeiro Frade
professor catedrático do Departamento de Engenharia de Materiais e Cerâmica da
Universidade de Aveiro

Prof. Doutor Amílcar Lopes Ramalho
professor associado com agregação da Faculdade de Ciências e Tecnologia da Universidade de Coimbra

Prof. Doutor José Maria da Fonte Ferreira
professor associado com agregação do Departamento de Engenharia de Materiais e Cerâmica da
Universidade de Aveiro

Prof. Doutor Dilshat Ubaydullayevich Tulyaganov
professor associado da Turin Polytechnic University in Tashkent, Uzbekistan

Prof. Doutor João Carlos Tomás Ramos
professor auxiliar da Faculdade de Medicina da Universidade de Coimbra

Prof. Doutora Maria Clara Henriques Baptista Gonçalves
professora auxiliar do Instituto Superior Técnico da Universidade Técnica de Lisboa

acknowledgements

I would like to sincerely express thanks to all who provided me with useful and helpful assistance. Without their knowledge, care and consideration, this work would likely not have matured.

I am deeply indebted to Prof. Doutor José Maria Ferreira, my supervisor, for all his support, interest, advices and encouragement. His support from the very first day of my work as a researcher is deeply appreciated. He strongly encouraged me even in the most difficult times. His contributions, detailed comments and insight have been of great value to me. He is a hard worker and a high-level scientist and professor which work I sincerely and extremely appreciate.

To my co-supervisor Prof. Dilshat Tulyaganov, my deeply gratitude for his support. I am honest thankful for his valuable teaching on glass science, for the interesting discussion moments and for his assistance from the very beginning. His collaboration was fundamental for this thesis. Prof. Dilshat Tulyaganov is more than a tutor – in spite of his high level scientific position, he is a really laboratory colleague and a truthfully friend.

I would like to express my gratitude to Paula Torres (also laboratory colleague) and Dr. Simeon Agathopoulos (former laboratory colleague) for their collaboration and friendship since the first day of my scientific research activity back in 2002, after my valuable experience in industry. They were excellent colleagues and their help and knowledge were essential during my starting days in the laboratory.

Appreciation also goes to my laboratory colleagues, whose expertise and knowledge added considerably to my experience. Their friendship was a great tonic to the most difficult times and doubts: Susana Olhero, Saurabh Kapoor, Allu Ammarnath Reddy, Sandra Pina, Avito Rebelo, Catarina Marques, Ajay Kaushal, Alexandra Lemos, Pedro Vale...

My gratitude to all co-authors of the papers presented in this thesis: Dr. Maria J. Pascual, Dr. Manuel Ribeiro, Dr. Ashutosh Goel and Ishu Goel, Dr. Vladislav Kharton and Dr. Aleksey Yaremchenko.

To all colleagues and technicians of DEMaC for the support to this work.

Financial support of the Portuguese Foundation for Science and Technology for the fellowship grant SFRH/BD/41307/2007 is gratefully acknowledged.

palavras-chave vidro, vitrocerâmicos, dissilicato de lítio, cristalização.

resumo

O principal objectivo deste estudo foi o desenvolvimento de vitrocerâmicos à base de dissilicato de lítio no sistema $Li_2O–K_2O–Al_2O_3–SiO_2$ contendo uma razão molar SiO_2/Li_2O muito afastada da do dissilicato de lítio ($Li_2Si_2O_5$) usando composições simples e a técnica tradicional de fusão-vazamento de vidro de forma a obter materiais com propriedades mecânicas, térmicas, químicas e eléctricas superiores que permitam a utilização destes materiais em diversas aplicações funcionais.

Investigou-se o fenómeno de separação de fases, a cristalização e as relações estrutura–propriedades de vidros nos sistemas $Li_2O–SiO_2$, $Li_2O–Al_2O_3–SiO_2$ e $Li_2O–K_2O–Al_2O_3–SiO_2$. Os vidros nos sistemas $Li_2O–SiO_2$ e $Li_2O–Al_2O_3–SiO_2$ apresentaram fraca densificação e resultaram em materiais frágeis, contrastando com a boa sinterização dos vidros no sistema $Li_2O–K_2O–Al_2O_3–SiO_2$. Pequenas adições de Al_2O_3 e K_2O ao sistema $Li_2O–SiO_2$ permitiram controlar a separação de fases devido à formação de espécies de Al(IV) que confirmaram o papel de Al_2O_3 como formador de rede. Os compactos de pó de vidro das composições contendo Al_2O_3 e K_2O tratados termicamente resultaram em vitrocerâmicos bem densificados, apresentando dissilicato de lítio como a principal fase cristalina, e valores de resistência mecânica à flexão, resistência química e condutividade eléctrica (173–224 MPa, 25–50 $\mu g/cm^2$ e $\sim 2\times10^{-18}$ S/cm, respectivamente) que possibilitam a utilização destes materiais em diversas aplicações funcionais.

A adição de P_2O_5, TiO_2 e ZrO_2 ao sistema $Li_2O–K_2O–Al_2O_3–SiO_2$ como agentes nucleantes revelou que os vidros contendo apresentaram cristalização em volume, com a formação de metassilicato de lítio a temperaturas mais baixas e dissilicato de lítio para as temperaturas mais elevadas, enquanto a adição de zircónia reduz o grau de segregação, aumenta a polimerização da matriz vítrea e desloca o valor de T_g para temperaturas superiores, inibindo a cristalização.

keywords glass, glass-ceramics, lithium disilicate, crystallization.

abstract

The purpose of the present study was developing lithium disilicate based glass–ceramics in the system $Li_2O–K_2O–Al_2O_3–SiO_2$ featuring SiO_2/Li_2O molar ratios far beyond that of lithium disilicate ($Li_2Si_2O_5$) stoichiometry using simple compositions and traditional glass melt-quenching technique in order to get enhanced mechanical, thermal, chemical and electrical properties which allow the use these materials in functional applications.

Phase separation phenomena as well as the crystallization behaviour and structure–properties relations of glasses in $Li_2O–SiO_2$, $Li_2O–Al_2O_3–SiO_2$ and $Li_2O–K_2O–Al_2O_3–SiO_2$ glass systems were investigated. The experimental glasses in $Li_2O–SiO_2$ and $Li_2O–Al_2O_3–SiO_2$ systems exhibited poor densification ability resulted in porous samples of brittle nature, contrasting with well sintered glass-powder compacts obtained from glasses in the $Li_2O–K_2O–Al_2O_3–SiO_2$ system. Small additions of Al_2O_3 and K_2O to glasses in the in the system $Li_2O–SiO_2$ allowed to control an extent of the phase separation due to the formation of tetrahedral four–coordinated Al(IV) species confirming the role of Al_2O_3 as network former. Moreover, Al_2O_3- and K_2O-containing sintered glass powder compacts resulted in well-densified and mechanically strong fine–grained glass–ceramics with lithium disilicate as the major crystalline phase, mechanical strength of 173–224 MPa, chemical resistance of 25–50 μg/cm^2 and low total conductivity (~2×10^{-18} S/cm) making the materials suitable for a number of practical applications.

The effects of single additions of P_2O_5, TiO_2 and ZrO_2 as nucleating agents in the $Li_2O–K_2O–Al_2O_3–SiO_2$ system revealed that addition of P_2O_5 led to bulk crystallization, with the formation of lithium metasilicate at lower temperatures and lithium disilicate at higher temperatures while the addition of zirconia reduces the degree of segregation, increases the polymerization of the glassy matrix, and shifts T_p to higher temperatures hindering crystallization.

Contents

1. Introduction 3
    1.1. Forward 5
    1.2. Research objectives 6
    1.3. Structure of thesis 7
    References 8
2. Bibliographic review 9
    2.1. Glass 11
        2.1.1. The nature of glass 11
        2.1.2. The glass transformation behaviour 12
        2.1.3. Principles of Glass formation: structure theories and kinetic considerations 15
            2.1.3.1. Structural theories 15
            2.1.3.2. Kinetic theories 17
        2.1.4. Silicate glasses 17
            2.1.4.1. Silica glass 20
            2.1.4.2. Alkali and alkaline-earth silicate glasses 20
    2.2. Glass-ceramics 21
        2.2.1. Development of glass-ceramics and its commercialization 22
        2.2.2. Glass-ceramic processing 27
            2.2.2.1. Nucleation 27
                2.2.2.1.1. Homogeneous nucleation 28
                2.2.2.1.1. Heterogeneous nucleation 30
            2.2.2.2. Crystal growth 32
    2.3. Liquid-liquid phase separation 35
        2.3.1. Stable and metastable miscibility gap 36
        2.3.2. The relation of the miscibility gap with the shape of the liquidus line 36
        2.3.3. Mechanisms of phase separation 38
        2.3.4. The effect of phase separation on crystallization 40
    2.4. The $Li_2O–SiO_2$ system 41
        2.4.1. Formation and properties of crystalline phases 41
        2.4.2. Research regarding lithium disilicate based glass-ceramics: a brief history 43
        2.4.3. Technological importance of lithium disilicate based glass-ceramics 52
            2.4.3.1. Dental materials 53
            2.4.3.2. Electronic applications 53
            2.4.3.3. Military applications 53
    References 56
3. Results and discussion 63
    3.1. Crystallization process and some properties of $Li_2O–SiO_2$ glass-ceramics doped with Al_2O_3 and K_2O 67
    3.2. Effect of Al_2O_3 and K_2O content on structure, properties and devitrification of glasses in the $Li_2O–SiO_2$ system 85
    3.3. Structural characterisation and thermo-physical properties of glasses in the $Li_2O–SiO_2–Al_2O_3–K_2O$ system 111

3.4. Effect of K_2O on structure–property relationships and phase transformations in $Li_2O–SiO_2$ glasses 127
3.5. The role of K_2O on sintering and crystallization of glass powder compacts in the $Li_2O–K_2O–Al_2O_3–SiO_2$ system 143
3.6. Structure, properties and phase formation in Al_2O_3/K_2O-containig non-stoichiometric lithium disilicate based glasses 165
3.7. The role of P_2O_5, TiO_2 and ZrO_2 as nucleating agents on microstructure and crystallization behaviour of lithium disilicate based glass 189
3.8. Al_2O_3/K_2O-containing non-stoichiometric lithium disilicate based glasses: a study of crystallization kinetics 207
3.9. Apatite crystallization from glasses in the $Ca_5(PO_4)_3F–CaAl_2Si_2O_8–CaMgSi_2O_6–NaAlSi_3O_8$ system 223
4. Conclusions and future directions 239
4.1. Conclusions 241
4.1.1. Bulk glasses 241
4.1.2. Glass powder compacts 242
4.2. Proposed application fields for the experimental glass-ceramics 243
4.3. Future directions 243

List of Publications

PhD Thesis

1. Crystallization process and some properties of $Li_2O–SiO_2$ glass-ceramics doped with Al_2O_3 and K_2O.
   H.R. Fernandes, D.U. Tulyaganov, J.M.F. Ferreira.
   J. American Ceramic Society 91 [11] (2008) 3698–3703.
   doi:10.1111/j.1551-2916.2008.02724.x

2. Effect of Al_2O_3 and K_2O content on structure, properties and devitrification of glasses in the $Li_2O–SiO_2$ system.
   H.R. Fernandes, D.U. Tulyaganov, A. Goel, M.J. Ribeiro, M.J. Pascual, J.M.F. Ferreira.
   J. European Ceramic Society 30 (2010) 2017–2030.
   doi: 10.1016/j.jeurceramsoc.2010.04.017

3. Structural characterisation and thermo–physical properties of glasses in the $Li_2O–SiO_2–Al_2O_3–K_2O$ system.
   H.R. Fernandes, D.U. Tulyaganov, A. Goel, M.J. Ribeiro, M.J. Pascual, J.M.F. Ferreira.
   J. of Thermal Analysis and Calorimetry 103 [3] (2011) 827–834.
   doi: 10.1007/s10973-010-1049-5

4. Effect of K_2O on structure–property relationships and phase transformations in $LiO_2–SiO_2$ glasses.
   H.R. Fernandes, D.U. Tulyaganov, A. Goel, J.M.F. Ferreira.
   J. European Ceramic Society 32 (2012) 291–298.
   doi: 10.1016/j.jeurceramsoc.2011.09.017

5. The role of K_2O on sintering and crystallization of glass powder compacts in the $Li_2O–K_2O–Al_2O_3–SiO_2$ system.
   H.R. Fernandes, D.U. Tulyaganov, M.J. Pascual, V.V. Kharton, A.A. Yaremchenko, J.M.F. Ferreira.
   J. European Ceramic Society 32 (2012) 2283–2292.
   doi: 10.1016/j.jeurceramsoc.2012.02.003

6. Structure, properties and phase formation in Al_2O_3/K_2O-containig non-stoichiometric lithium disilicate based glasses.
   H.R. Fernandes, D.U. Tulyaganov, M.J. Pascual, J.M.F. Ferreira.
   Materials Research Bulletin (2012, submitted).

7. The role of P_2O_5, TiO_2 and ZrO_2 as nucleating agents on microstructure and crystallization behaviour of lithium disilicate based glass.
   H.R. Fernandes, D.U. Tulyaganov, J.M.F. Ferreira.
   J. Materials Science (published online, 23 August 2012).
   doi: 10.1007/s10853-012-6793-4

8. Al_2O_3/K_2O-containig non-stoichiometric lithium disilicate based glasses: a study of crystallization kinetics.
   H.R. Fernandes, D.U. Tulyaganov, J.M.F. Ferreira.
   J. Thermal Analysis and Calorimetry (published online, 10 October 2012).
   doi: 10.1007/s10973-012-2692-9

9. Apatite crystallization from glasses in the $Ca_5(PO_4)_3F$–$CaAl_2Si_2O_8$–$CaMgSi_2O_6$–$NaAlSi_3O_8$ system.
H.R. Fernandes, D.U. Tulyaganov, M.J. Ribeiro, J.M.F. Ferreira.
J. Non-Crystalline Solids (2012, accepted).

Other publications

10. Preparation of mullite whiskers from kaolinite using $CuSO_4$ as fluxing agent.
S. Agathopoulos, H.R. Fernandes, D. Tulyaganov, J.M.F. Ferreira.
Materials Science Forum 455–456 (2004) 818–821.

11. Synthesis of lithium aluminosilacate glass and glass-ceramics from spodumene material.
D.U. Tulyaganov, S. Agathopoulos, H.R. Fernandes, J.M.F. Ferreira.
Ceramics International 30 (2004) 1023–1030.
doi:10.1016/j.ceramint.2003.10.022

12. Incorporation of granite cutting sludge in industrial porcelain tile formulations.
P. Torres, H.R. Fernandes, S. Agathopoulos, D.U. Tulyaganov, J.M.F. Ferreira.
J. European Ceramic Society 24 [10,11] (2004) 3177–3185.
doi:10.1016/j.jeurceramsoc.2003.10.039

13. Preparation and crystallization of glasses in the system tetrasilicic mica–fluorapatite–diopside.
D.U. Tulyaganov, S. Agathopoulos, H.R. Fernandes, J.M. Ventura, J.M.F. Ferreira.
J. European Ceramic Society 24 (2004) 3521–3528.
doi:10.1016/j.jeurceramsoc.2003.11.026

14. Synthesis and characterization of synthetic F–mica containing glass-ceramics in the system $SiO_2{\cdot}Al_2O_3{\cdot}B_2O_3{\cdot}CaO{\cdot}MgO{\cdot}Li_2O{\cdot}(K,Na)_2O{\cdot}F$.
D.U. Tulyaganov, S. Agathopoulos, H.R. Fernandes, J.M.F. Ferreira.
J. Materials Research 19 [4] (2004) 1234–1242.
doi:10.1557/JMR.2004.0160

15. Preparation and characterization of high compressive strength foams from sheet glass.
D.U. Tulyaganov, H.R. Fernandes, S. Agathopoulos, J.M.F. Ferreira.
J. Porous Materials 13 (2005) 133–139.
doi:10.1007/s10934-006-7014-9

16. Influence of Li_2O-doping on non-isothermal evolution of phases in K–Na containing aluminosilicate matrix.
D.U. Tulyaganov, S. Agathopoulos, H.R. Fernandes, O. Fabrichnaya, J.M.F. Ferreira.
J. American Ceramic Society 89 [1] (2006) 292–297.
doi:10.1111/j.1551-2916.2005.00696.x

17. Processing of glass-ceramics in the SiO_2–Al_2O_3–B_2O_3–MgO–CaO–Na_2O–(P_2O_5)–F system via sintering and crystallization of glass powder compacts.
D.U. Tulyaganov, S. Agathopoulos, H.R. Fernandes, J.M.F. Ferreira.
Ceramics International 32 (2006) 195–200.
doi:10.1016/j.ceramint.2005.02.006

18. Influence of lithium oxide as auxiliary flux on the properties of triaxial porcelain bodies.
D.U. Tulyaganov, S. Agathopoulos, H.R. Fernandes, J.M.F. Ferreira.
J. European Ceramic Society 26 (2006) 1131–1139.
doi:10.1016/j.jeurceramsoc.2005.01.036

19. The influence of incorporation of ZnO-containing glazes on the properties of hard porcelains.
D.U. Tulyaganov, S. Agathopoulos, H.R. Fernandes, J.M.F. Ferreira.
J. European Ceramic Society 27 (2007) 1665–1670.
doi:10.1016/j.jeurceramsoc.2006.05.011

20. Recycling of chromium-rich leather ashes in porcelain tiles production.
H.R. Fernandes, J.M.F. Ferreira.
J. European Ceramic Society 27 (2007) 4657–4663.
doi:10.1016/j.jeurceramsoc.2007.03.037

21. Nano-TiO_2 coated unidirectional porous structure prepared by freeze-drying and solution infiltration.
Zhen-Yan Deng, H.R. Fernandes, J.M. Ventura, S. Kannan, J.M.F. Ferreira.
J. American Ceramic Society 90 [4] (2007) 1265–1268.
doi:10.1111/j.1551-2916.2007.01602.x

22. Development of ceramic floor tile compositions based on quartzite and granite sludges.
P. Torres, R.S. Manjate, S. Quaresma, H.R. Fernandes, J.M.F. Ferreira.
J. European Ceramic Society 27 (2007) 4649–4655.
doi:10.1016/j.jeurceramsoc.2007.02.217

23. Preparation and characterization of foams from sheet glass and fly ash using carbonates as foaming agents.
H.R. Fernandes, D.U. Tulyaganov, J.M.F. Ferreira.
Ceramics International 35 [1] (2009) 229–235.
doi:10.1016/j.ceramint.2007.10.019

24. Damping associated with porosity in ceramics.
S.D. Panteliou, K. Zonios, I.T. Chondrou, H.R. Fernandes, S. Agathopoulos, J.M.F. Ferreira.
International Journal of Mechanics and Materials in Design 5 [2] (2009) 167–174.
doi:10.1007/s10999-008-9092-0

25. Incorporation of river silt in ceramic tiles and bricks.
P. Torres, R.S. Manjate, H.R. Fernandes, S.M. Olhero, J.M.F. Ferreira.
Industrial Ceramics 29 (2009) 1–8.

26. Incorporation of wastes from granite rocks cutting and polishing industries to produce roof tiles.
P. Torres, H.R. Fernandes, S. Olhero, J.M.F. Ferreira.
J. European Ceramic Society 29 (2009) 23–30.
doi:10.1016/j.jeurceramsoc.2008.05.045

27. Production and characterization of glass-ceramic foams from recycled materials.
H.R. Fernandes, D.U. Tulyaganov, J.M.F. Ferreira.
Advances in Applied Ceramics 108 [1] (2009) 9–13.
doi:10.1179/174367509X344971

"Pars Syriae, quae Phoenice vocatur, finitima Iudaeae intra montis Carmeli radices paludem habet, quae vocatur Candebia. ex ea creditur nasci Belus amnis quinque milium passuum spatio in mare perfluens iuxta Ptolemaidem coloniam. lentus hic cursu, insaluber potu, sed caerimoniis sacer, limosus, vado profundus, non nisi refuso mari harenas fatetur; fluctibus enim volutatae nitescunt detritis sordibus.

Tunc et marino creduntur adstringi morsu, non prius utiles. quingentorum est passuum non amplius litoris spatium, idque tantum multa per saecula gignendo fuit vitro. fama est adpulsa nave mercatorum nitri, cum sparsi per litus epulas pararent nec esset cortinis attollendis lapidum occasio, glaebas nitri e nave subdidisse, quibus accensis, permixta harena litoris, tralucentes novi liquores fluxisse rivos, et hanc fuisse originem vitri." [(a)]

Gaius Plinius Secundus

(Pliny the Elder , 23-79 AD)

In Naturalis Historia, Book XXXVI:190-191

[(a)] In the part of Syria adjoining Judea and Phoenicia the Candebia swamp is bounded by Mount Carmel. This is believed to be the source of the river Belus, which after five miles runs into the sea near Ptolemais. On the shores of the River Belus the sand is revealed only when the tides retreat. This sand does not glisten until it has been tossed about by the waves and had its impurities removed by the sea.
A ship belonging to traders in soda once called here, so the story goes, and they spread out along the shore to make a meal. There were no stones to support their cooking-pots, so they placed lumps of soda from their ship under them. When these became hot and fused with the sand on the beach, streams of an unknown liquid flowed, and this was the origin of glass.

Chapter

1

Introduction

"Science may set limits to knowledge, but should not set limits to imagination."
Bertrand Russell

1.1 Foreword

The multiple forms and uses of glasses are becoming increasingly important in science, industry and in general daily life. During the last century, new glass and glass-ceramic materials have been developed envisaging their use in several diverse functions ranging from common materials (*e.g.* cookware) to technological applications such as dental restorations, medical prosthesis, electronic devices and telescope mirrors, or even architectural materials.[1-2] In particular, lithium disilicate based glass-ceramics derived from non-stoichiometric compositions have proven to be potential candidates for different functional applications (*e.g.* dental restorations,[3-6] metal-glass seals,[7-8] magnetic media disks for hard disk drives,[9-11] etc.).

Modern science and technology constantly require new materials with special properties to achieve specific applications. Glass-ceramic materials combine the properties of conventional sintered ceramics with the distinctive characteristics of glasses. Moreover, developing glass-ceramics demonstrates the benefit of combining various remarkable properties in one material.[1]

The binary alkali silicate systems show liquid–liquid phase separation or immiscibility at temperatures below the *liquidus* temperature of crystallisation. This type of phase separation is often called metastable because crystalline phases are more stable than liquid at the temperature of phase separation.[1-2, 12] The presence of metastable immiscibility region is the main cause of S-like course of the *liquidus* curve and binary $Li_2O–SiO_2$ system is a typical example in this regard which demonstrates S-like course of the *liquidus* curve in silica-rich region. According to Vogel,[12] $Li_2O–SiO_2$ liquids containing less than 30 mol.% Li_2O lead to opalescent or opaque glasses on cooling owing to phase separation. However, mechanical properties and chemical durability of these glasses after devitrification are low.

A literature survey reveals that despite many comprehensive studies leading to the development of lithium disilicate glass-ceramics from different systems,[1, 13-19] the role of immiscibility phenomena and addition of Al_2O_3/K_2O on the crystallization behaviour of glasses far beyond the $Li_2Si_2O_5$ stoichiometry has not been thoroughly investigated. Therefore, this work aims to investigate the $Li_2O–SiO_2$ glass system, particularly the influence of Al_2O_3 and K_2O on glass structure–properties relationships, nucleation process and phase formation in both bulk glasses and sintered glass powder compacts. The effect of

some nucleating agents, such as TiO_2, P_2O_5 and ZrO_2, on glass crystallization and properties was also investigated.

Several experimental techniques were used throughout this investigation aiming at a better understanding of the glass structure (*e.g.* FTIR, MAS-NMR) and microstructure (SEM) as well as the crystallization mechanism of glass (*e.g.* FTIR, DTA, SEM, XRD) and the sintering and crystallization behaviour of the corresponding glass powder compacts (*e.g.* DTA, FTIR, HSM, SEM, XRD). Some glass and glass-ceramic properties such as density, mechanical strength, chemical resistance, electrical properties, CTE, etc., were also evaluated to achieve a better understanding concerning the structure–properties relations and the potential practical (functional) applications of the produced materials.

1.2 Research Objectives

The purpose of the present work was developing lithium disilicate based glass-ceramics in the system $Li_2O–K_2O–Al_2O_3–SiO_2$ featuring SiO_2/Li_2O molar ratios far beyond that of lithium disilicate ($Li_2Si_2O_5$) stoichiometry using simple compositions and traditional glass melt-quenching technique in order to get enhanced mechanical, thermal, chemical and electrical properties which allow the use these materials in functional applications.

The tasks of this research were:

1. Getting a deeper insight on phenomena related to metastable immiscibility and devitrification in $Li_2O–SiO_2$ glasses in relevance with Al_2O_3 and K_2O additions;
2. Investigating and comparing the phase separation phenomena as well as the crystallization behaviour and structure–properties relations of glasses in three different systems: (1) $Li_2O–SiO_2$, (2) $Li_2O–Al_2O_3–SiO$
3. $_2$ and $Li_2O–K_2O–Al_2O_3–SiO_2$;
4. Presenting an in-depth analysis pertaining to study the structure of $Li_2O–K_2O–Al_2O_3–SiO_2$ glasses and their devitrification mechanism;
5. Evaluating of the sintering behaviour and properties of the corresponding glass powder compacts;

6. Investigating the effect of diverse nucleating agents (TiO_2, P_2O_5 and ZrO_2) on the structure, properties and crystallization of glasses in the $Li_2O–K_2O–Al_2O_3–SiO_2$ system.

1.3 Structure of the thesis

This dissertation is structured in four chapters. The chapter 1 provides a succinct introduction to the thesis, the research objectives and an outlook of the content of each chapter. Chapter 2 presents a broad literature review that ranges from a brief introduction to glass science and technology, to lithium disilicate based glass and glass-ceramics comprising some important achievements and covering the subjects included on this thesis such as glass forming ability, liquid-liquid phase separation, thermal behaviour and crystallization of glasses. The outcome of the experimental work done on the frame of the proposed goals and its discussion is presented in Chapter 3. This chapter is divided in sub-chapters which correspond to the manuscripts that resulted from the research activity and had been published or submitted to ISI journals. Finally, Chapter 4 presents the overall conclusions and some suggestions for future work including some proposals for the application of the tested materials throughout the work done in the frame of this thesis.

References

1. Höland W, Beall G. Glass-ceramic Technology. Westerville, Ohio: The American Ceramic Society; 2002.
2. Shelby JE. Introduction to glass science and technology. Cambridge: The Royal Society of Chemistry; 1997.
3. Borom MP, Turkalo AM, Doremus RH. Strength and microstructure in lithium disilicate glass-ceramics. Journal of the American Ceramic Society 1975;58(9-10):385-91.
4. Guazzato M, Albakry M, Ringer SP, Swain MV. Strength, fracture toughness and microstructure of a selection of all-ceramic materials. Part I. Pressable and alumina glass-infiltrated ceramics. Dental Materials 2004;20(5):441-48.
5. Höland W, Apel E, van Hoen C, Rheinberger V. Studies of crystal phase formations in high-strength lithium disilicate glass-ceramics. Journal of Non-Crystalline Solids 2006;352(38-39):4041-50.
6. Iqbal Y, Lee WE, Holland D, James PF. Metastable phase formation in the early stage crystallisation of lithium disilicate glass. Journal of Non-Crystalline Solids 1998;224(1):1-16.
7. Bengisu M, Brow RK, White JE. Interfacial reactions between lithium silicate glass-ceramics and Ni-based superalloys and the effect of heat treatment at elevated temperatures. Journal of Materials Science 2004;39(2):605-18.
8. Goswami M, Kothiyal GP, Montagne L, Delevoye L. MAS-NMR study of lithium zinc silicate glasses and glass-ceramics with various ZnO content. Journal of Solid State Chemistry 2008;181(2):269-75.
9. Goto N, Yamaguchi K, inventors; Ohara, K.K., assignee. Magnetic disk substrate and method for manufacturing the same. 1997.
10. Beall GH, Kohli JT, inventors; Corning Inc., assignee. Glass-ceramics containing lithium disilicate and tridymite. 1998.
11. Goto N, Ishioka J, Kawashima Y, inventors; Ohara, K.K., assignee. Glass-ceramic substrate for an information storage medium. 2001.
12. Vogel W. Structure and Crystallization of Glasses. Leipzig: Pergamon Press; 1971.
13. Anspach O, Keding R, Rüssel C. Oriented lithium disilicate glass–ceramics prepared by electrochemically induced nucleation. Journal of Non-Crystalline Solids 2005;351:656-62.
14. Headley TG, Loehman RE. Crystallization of Glass–Ceramics by Epitaxial Growth. Journal of the American Ceramic Society 1984;67:620-25.
15. James PF. Kinetics of crystal nucleation in silicate glasses. Journal of Non-Crystalline Solids 1985;73:517-40.
16. McMillan PW. Glass–Ceramics. London: Academic Press; 1979.
17. Ota R, Mishima N, Wakasugi T, Fukunaga J. Nucleation of Li_2O–SiO_2 glass and its interpretation based on a new liquid model. Journal of Non-Crystalline Solids 1997;219:70-74.
18. Ray CS, Day DE, Huang W, Narayan KL, Cull TS, Kelton KF. Non-isothermal calorimetric studies of the crystallization of lithium disilicate glass. Journal of Non-Crystalline Solids 1996;204(1):1-12.
19. Zanotto ED. Metastable phases in lithium disilicate glasses. Journal of Non-Crystalline Solids 1997;219:42-48.

Chapter

2

Bibliographic review

“It's not that I'm so smart, it's just that I stay with problems longer.”
Albert Einstein

2.1 Glass

Glass is present in everyone's daily life. Although one doesn't realise its importance in everyday life, glass has a vast appliance field ranging from simple and common materials (*e.g.* bottles, cups, windows, containers, light bulbs, etc.) to technical applications (*e.g.* television tubes, computer screens, spectacles and telescope lenses, spectrometer prisms, laboratory ware, optical fibres, etc.) or artistic purposes.[1-8]

Glass has its history at the beginning of time, with naturally occurring volcanic glasses such as obsidian which was then appreciated and used to fabricate tools and jewellery during the stone-age.[9] However, in spite of the enormous technological achievements obtained during the industrial revolution only the last decades have witnessed great advances in glass science in particular concerning the study of glass structure and the development of new compositions aiming at specific applications.[5, 10-13]

2.1.1 The nature of glass

The origin of the word glass is the Latin term *glaesum* which was used to refer to a lustrous and transparent or translucent body. Glassy substances are also called vitreous, originating from the word *vitrum*, again denoting a clear, transparent body.[6, 14] Although glass became a popular commodity in the growth of civilization, perhaps because of its transparency, lustre (or shine), and durability, the current understanding of glass no longer requires any of these characteristics to distinguish it from other substances. Glass can be inorganic (non-carbon based) as well as organic (carbon-based), and fusion is not the only method to make a glass.

According to ASTM description of glass as issued by Committee C-14 in 1941 as a tentative standard glass is an inorganic product of fusion which has cooled to a rigid condition without crystallizing:[15-16] (1) glass is typically hard and brittle, and has a conchoidal fracture. It may be colourless or coloured, and transparent to opaque. Masses or bodies of glass may be made coloured, transparent, or opaque by the presence of dissolved, amorphous, or crystalline material; (2) when a specific kind of glass is indicated, such descriptive terms as flint glass, barium glass, and window glass should be used following the basic definition, but the qualifying term is to be used as understood by trade custom; (3) objects made of glass are

loosely and popularly referred to as glass, such as glass for a tumbler, a barometer, a window, a magnifier, or a mirror.

In common language the term *glass* is assigned to a fragile and transparent material well known since ancient times. However, in scientific language its range of meaning is much larger but difficult to define with precision. Many definitions for glass were proposed along the last decades including the attempt to distinguish between glass and amorphous solids.[1, 6, 8, 13, 17]

The definition and the understanding of the glassy state are fundamental to glass science and technology which traditionally need to face three main difficult problems: (1) glass is *non-crystalline* and thus is absent of long-range atomic order which is characteristic of most solid materials and unlike crystalline materials, the structure of glass cannot be defined in terms of a simple unit cell that is repeated periodically in space; (2) glass is *non-equilibrium* meaning that the glassy state cannot be described using equilibrium thermodynamics or statistical mechanics and the macroscopic properties of a glass depend on composition and thermal history; and (3) glass is *non-ergodic,* since we observe glass on a time scale that is much shorter than its structural relaxation time. As time elapses, ergodicity is gradually restored and the properties of a glass slowly approach their equilibrium values. The glass transition, *i.e.*, the process by which equilibrium, ergodic liquid is gradually frozen into a non-equilibrium, non-ergodic glassy state, is the key point to these questions.[18]

Glasses share two common characteristics: no glass has a long range, periodic atomic arrangement, and every glass exhibits time-dependent *glass transformation* behaviour. This behaviour occurs over a temperature range known as the glass transformation region. A glass can thus be defined as an amorphous solid completely lacking in long range, periodic atomic structure, and exhibiting a region of glass transformation behaviour. Thus, any material, inorganic, organic, or metallic, formed by any technique, which exhibits glass transformation behaviour is a glass.[5]

2.1.2 The glass transformation behaviour

The glass transformation behaviour is commonly analysed and discussed using enthalpy (or volume, since enthalpy and volume behave in a similar way) versus temperature diagrams (Fig. 1).[5, 14, 19] Considering a small volume of a liquid at a temperature well above its melting temperature (T_m) it is possible to follow the variation of its enthalpy (or volume) during the

cooling process. At a point in the equilibrium liquid region, as temperature decreases, the atomic structure of the melt will gradually changes and will be characteristic of the exact temperature at which the melt is held. Upon cooling, the volume of the liquid generally decreases. If cooling to any temperature below T_m of the crystal results in the conversion of the material to the crystalline state, the enthalpy will decline abruptly to the value suitable for the crystal. This is due to the formation of a long range, periodic atomic arrangement. Continued cooling of the crystal will result in a further decrease in enthalpy due to the heat capacity of the crystal.

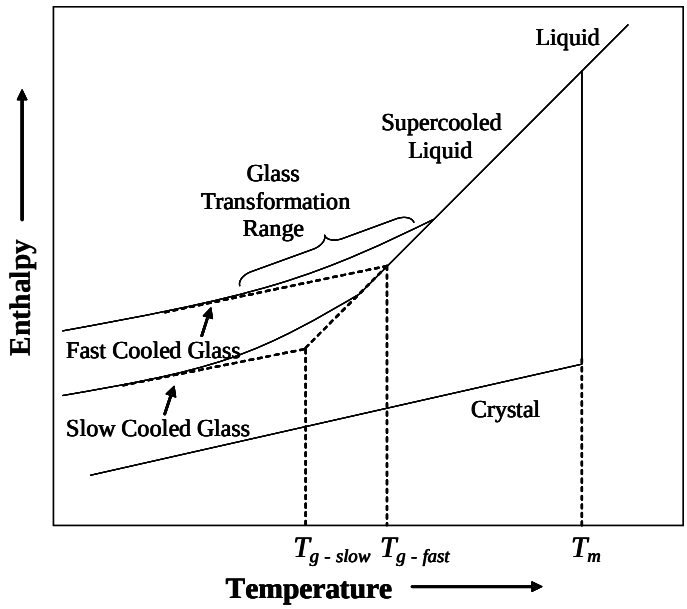

Fig. 1 – Effect of temperature on the enthalpy of a glass forming melt.

If no crystallization occurs when the liquid is cooled below the T_m of the crystal a supercooled liquid is obtained and its structure continues to rearrange as the temperature decreases, but there is no abrupt decrease in enthalpy due to discontinuous structural rearrangement. As the liquid is cooled further, the viscosity increases and eventually becomes so great that the atoms can no longer completely rearrange to the equilibrium liquid structure, during the time allowed by the experiment. The structure begins to lag behind that which would be present if sufficient time was allowed to reach equilibrium, resulting in a deviation of the enthalpy from the equilibrium line. In this case, enthalpy follows a curve of gradually decreasing slope, until it eventually becomes determined by the heat capacity of the frozen liquid, *i.e.*, the viscosity becomes so great that the structure of the liquid becomes fixed and is no longer temperature-dependent. The temperature region laying between the limits where the enthalpy is that of the

equilibrium liquid and that of the frozen solid is known as the glass transformation region. The frozen liquid is now a glass.[5, 14]

Since the temperature where the enthalpy departs from the equilibrium curve is controlled by kinetic factors (*i.e.* viscosity of the liquid), the use of a slower cooling rate will allow the enthalpy to follow the equilibrium curve to a lower temperature. In this case, the glass transformation region will shift to lower temperatures and the formation of a completely frozen liquid, or glass, will not occur until a lower temperature. The glass obtained will have a lower enthalpy than that obtained using a faster cooling rate. The atomic arrangement will be that characteristic of the equilibrium liquid at a lower temperature than that of the more rapidly cooled glass.[5]

Although the glass transformation actually occurs over a temperature range, it is convenient to define a term which allows us to express the difference in thermal history between these two glasses. If we extrapolate the glass and supercooled liquid lines, they intersect at a temperature defined as the *fictive temperature*. The structure of the glass is considered to be that of the equilibrium liquid at the fictive temperature. Although the fictive temperature concept is not a completely satisfactory method for characterizing the thermal history of glasses, it does provide a useful parameter for discussion of the effect of changes in cooling rate on glass structure and properties.

The glass transformation occurs over a range of temperatures and not at one specific temperature, thus it cannot be characterized by any single temperature.[5] However, it is useful and convenient to use just a single temperature as an indication of the onset of the glass transformation region during heating of a glass. This temperature is usually named the glass transformation (or transition) temperature (T_g). Thermal analysis curves or thermal expansion curves are generally used to evaluate T_g, which is rather vaguely defined by changes in either. Although the values obtained from these two methods are similar, they are not identical. Besides the experimental method to evaluate T_g, the heating rate used to produce these curves also influences the obtained value. Since T_g, is a function of both the experimental method used for the measurement and the heating rate used in that measurement, it cannot be considered to be a true property of the glass. We can, however, think of T_g, as a useful indicator of the approximate temperature where the supercooled liquid converts to a solid on cooling, or, conversely, of which the solid begins to behave as a viscoelastic solid on heating.[5-6, 11]

2.1.3 Principles of Glass formation: structure theories and kinetic considerations

Different cooling rates are required in order to form glasses in different chemical systems. Such experimental observation is on the basis of several attempts to produce an atomic theory of glass formation based on the nature of the chemical bonds and the shape of the structural units involved. Although proposing a structural theory seems contradictory for a material that is characterized by no long-range, periodic atomic ordering, some form of short-range ordering makes possible and reproducible to form the same glass from a nominal starting composition and control the overall properties.

Two main approaches[5] to explain glass formation are as follows: (a) the *structural theories of glass formation* based on structural considerations such as geometry, nature of bond forces, etc., (b) *kinetic approach* focuses emphasis to control of glass formation by changes in processing.

2.1.3.1 Structural theories

Inorganic glasses are readily formed from a wide variety of materials, principally oxides, chalcogenides, halides, salts, and combinations of each. There have been many attempts to relate the glass-forming tendency of a material to its molecular level structure. The first structural methods were proposed in the 1920s when Goldschmidt[20] suggested that the ability of an oxide to form a glass might be related to the way in which the oxygen ions were arranged around the cation to form the unit cell of the crystal structure. It can be shown from geometrical considerations that for an oxide M_xO_y, the coordination number of the M cations will be 4 if the radius R_M/R_O lies between approximately 0.2 and 0.4. Goldschmidt noted that for some glass-forming oxides (*e.g.* SiO_2, GeO_2 and P_2O_5) a tetrahedral arrangement occurred in the crystalline state and suggested that this might be a criterion of glass-forming ability. However, this theory has been subsequently shown to be incomplete, with a variety of systems inadequately explained by it. For instance, although all ionic glass-formers satisfy this rule, there are many systems that satisfy it but are not glass-formers (*e.g.*, BeO and most of the halides).

Later, Zachariasen[21] formulated the random network theory, according to which glass-formers are cations that have high valences (≥ 3) and can create three-dimensional networks of polyhedra. For instance, in silicate glasses, oxygen networks are formed by polymerization of polyhedra. By postulating that the oxygen polyhedra found in the oxide crystals would also be

present in the glasses, Zachariasen formed the concept of a continuous random network structure for a glass, with periodic structural arrangement is prevented by random orientations. He proposed that the structure of glass was similar to that of a crystal, but with a larger lattice energy resulting from the disordered arrangements of polyhedral units, to possess a random network lacking long-range periodicity (as shown schematically in Fig. 2) which can be demonstrated by the absence of sharp X-ray diffraction spectra of glasses. According to his experiments, Zachariasen listed four conditions for a structure to favour glass formation:

1. no oxygen atom must be linked to more than two cations;
2. the number of oxygen atoms surrounding any given cation must be small (typically 3 or 4);
3. oxygen polyhedra share only corners, not edges or faces;
4. at least three corners of each oxygen polyhedron must be shared – this rule was added to ensure that the network would be three-dimensional (although certain glasses can exist in structures describable in fewer dimensions).

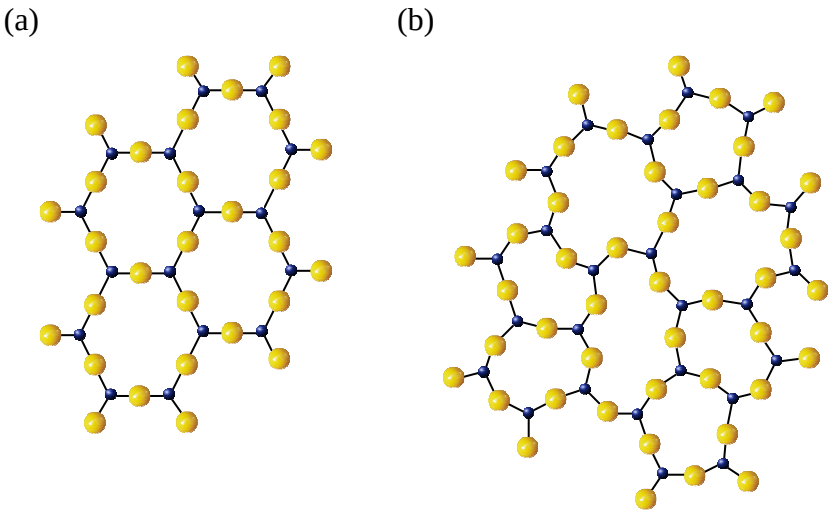

Fig. 2 – Schematic 2D representation of (a) a generic A_2O_3 crystalline compound (with A– ● and O – ●) and (b) a continuous random network of the same substance.[3]

These conditions lead to the open structures that can accommodate a distribution of inter-polyhedral bond angles that are associated with the loss of long-range structural order when a crystal forms a glass. Diffraction studies made by Warren[22] and later by Wright[23] confirmed

Zachariasen's prediction that glasses and crystals have similar short-range polyhedral structures but different long-range polyhedral arrangements. Structural approaches, however, do not take the thermal history of the melt into account.[24]

2.1.3.2 Kinetic theories

According to Tamman,[25] who introduced the kinetic concepts in the early 1920s, glasses are formed when the nucleation rate (U) *versus* temperature does not significantly overlap the growth rate (G) *versus* temperature curve. About 40 years later, Turnbull and Cohen[26] proposed the determination of kinetic stability on cooling experiments through the steady-state nucleation rate. Gutzow *et al*.[2] related glass stability to the non-steady-state time lag (τ). These kinetic approaches assume that one of the three parameters (U, G or τ) is dominant while the other two were neglect. In the early 1970s, Uhlmann *et al*.[27] considered U and G simultaneously, formulating a kinetic criterion for vitrification. Later, the kinetic theory of glass formation was extended to include non-steady state effects and heterogeneous nucleation. In 1989, Weinberg *et al*.[28-29] demonstrated that the volume fractions transformed and the resulting critical cooling rates (R_c) are quite sensitive to the method of calculation. The *nose method* which uses isothermal TTT curves, overestimates R_c by up to one order of magnitude. They also demonstrated that R_c is highly sensitive to the main physical properties that rule the nucleation and growth kinetics, *i.e.* crystal liquid surface energy, thermodynamic driving force and viscosity.[30] Later on, Weinberg[31] integrated the equation of overall crystallization kinetics to estimate and compare criteria for vitrification on cooling and glass stability against crystallization on heating.

However, Cabral *et al*.[32] used experimental values of crystal nucleation and growth rates for glasses that nucleate in the bulk to calculate critical cooling rates for glass formation (R_c) by the TTT method. The resulting values of R_c were consistent with their laboratory practice of melting and quenching the studied glasses and also with experimental data of R_c for one of the glasses, lithium disilicate.

2.1.4 Silicate glasses

Inorganic glasses can be produced starting from many compositions such as silicates, phosphates, borates, halides or chalcogenides. Silicate glasses are the most important regarding commercially impact because they have excellent transparency and good chemical

durability, and they can be made from inexpensive natural ingredients. However, glass is a brittle material susceptible to mechanical failure which is a disadvantage to consider it as a versatile ceramic material.[33]

Concerning their role in the glass production, oxides are usually classified into three groups: (1) network formers, such as Si, B, P, Ge, and As, having oxygen coordination numbers of 3 or 4 and tend to produce the basic cross-linked polymeric glass structure; (2) network modifiers, such as Na, K, Ca, and Ba, having coordination number of 6 or more and generally tend to reduce the degree of polymerization and viscosity; and (3) intermediate oxides with cations, such as Al, Zn, Mg, Pb, and Be having intermediate coordination of 4 to 6 and act either as network formers or modifiers, depending upon the glass composition.[5, 12, 19, 34]

Oxides with large coordination numbers and relatively weak bonds (network modifiers) alter the glass-forming network by replacing stronger BO bonds between glass-forming polyhedra with weaker, NBO bonds to modifying polyhedra. Figure 3 shows a schematic 2D representation of the random network of an alkali silicate glass. The network modifiers are important constituents to most technological glasses because they lower the melting temperature and control many useful properties. Modifiers are commonly used to facilitate the glass fabrication at lower temperatures because they promote the decreasing of the viscosity by disrupting the network of the glass melt.[12] Silica glass is difficult to process because its melting temperature is about 1713 ºC corresponding to cristobalite–liquid equilibrium. For instance, adding 25 wt.% of Na_2O to silica lowers the *liquidus* temperature to only about 793 ºC, which is a great advantage from the technological point of view.[35] Alkali metal ions are mobile and allow ion migration while alkaline-earth ions like ions (one alkaline earth ion is compensated electrically by two NBOs) are relatively immobile and can hinder the diffusion of other ions, in particular the alkali ones, and hence improve the chemical resistance of the glass.[12] For this reason, most of important commercial glasses are based on compositions comprising SiO_2 (network former), Na_2O and CaO (alkaline and alkaline-earth modifiers respectively).

The relative concentration of BO and NBO has an important influence on the structure and properties of glasses.[36] According to the number of bridging oxygen atoms in a tetrahedral unit, the following scenarios can be considered:

1. BO = 4 (*i.e.* [O]/[Si] = 2): each BO is shared by two silicon atoms and the network is three-dimensional with all four corners bridging.

2. BO = 3 (*i.e.* [O]/[Si] = 2.5), the network is two-dimensional with three corners bridging (note that some tetrahedra may be linked to four others and some therefore to less than three, the said number being the average value over the network).
3. BO = 2 (*i.e.* [O]/[Si] = 3), the network is formed by one-dimensional chains with one corner bridging.
4. BO < 2 (*i.e.* [O]/[Si] > 3), the network is composed of individual SiO_4 tetrahedral elements, some of these being bound together.

The rigidity of the glass network decreases gradually by replacing the bridging oxygen atoms by non-bridging ones until only individual isolated tetrahedra remain. Using the Q^n terminology (with n the number of BO on a tetrahedron), it is possible to refer to (1) Q^4, (2) Q^3, (3) Q^2 and (4) Q^1, Q^0 structures, respectively.

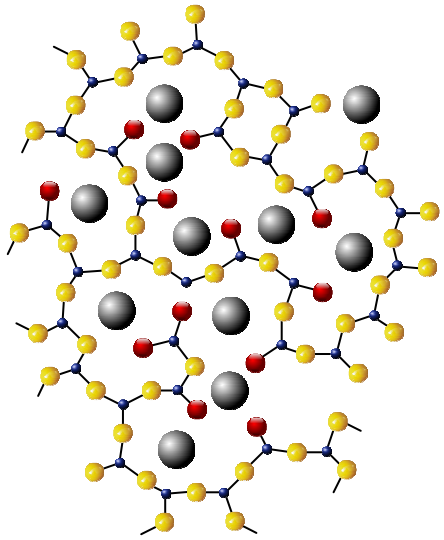

Fig. 3 – Schematic 2D representation of the random network of an alkali silicate glass (Si–●, BO– ●, NBO– ●, alkali ion–●).[3]

Considering an oxide glass of general composition $(A_2O)_x(SiO_2)_{1-x}$, with A the alkali metal, for x = 0 (*i.e.* pure silica) only BO exist (Q^4) while increasing alkali concentration yields a dramatic decrease of BO and an increase of NBO accordingly.[12] The intermediate oxides have coordination numbers and bond strengths between the network formers and network modifiers and tend to have an intermediate effect on glass properties.[19]

2.1.4.1 Silica glass

In the case of oxide glasses, the short-range structure can be extremely well-defined in terms of the coordination polyhedra of the network-forming cation such as silicon. These glasses are characterized by predominantly heteropolar bonding between network-forming cations and oxygen. Bond lengths and angles in the first coordination shell of oxygen around these cations vary only over a narrow range. Glass-forming cation–oxygen polyhedra like SiO_4 are usually corner-linked through 'bridging' oxygens (BO) and form a three-dimensional extended connected network. The properties of glass are mainly dependent on its structure which in the case of silica glass consists of well-defined SiO_4 tetrahedra connected to another neighbouring tetrahedron through each corner (Fig 2b). The Si–O distance in the tetrahedron as obtained by neutron diffraction studies is about 0.16 nm and that the shortest O–O distance is about 0.26 nm, the same dimensions as found in crystalline silica. The inter-tetrahedral (Si–O–Si) bond angle distribution is centred near ~143º, but is much broader than that found for crystalline silica, producing the loss in long-range order shown schematically in Fig. 2b.[23, 37]

2.1.4.2 Alkali and alkaline–earth silicate glasses

As in silicate glasses, the structure of alkali silicate glasses also consists of a network of SiO_4 tetrahedra, but some of the corners are now occupied by non-bridging oxygens that are linked to the modifying polyhedra (Fig. 3). Increasing the concentration of modifying oxide leads to the increasing of the relative fraction of non-bridging oxygens associated with the glass network which results in the reduction of T_g and melt viscosity and increasing values of thermal expansion coefficient and ionic conductivity.[38]

The changes in the silicate network, and so the compositional dependence of many of the glass properties, can be described by the relative fractions of bridging and non-bridging oxygens or by the types and concentrations of the different Si-tetrahedra (Q^n).[12] The rigidity of the network decreases gradually by replacing the bridging oxygen atoms by non-bridging ones until only individual isolated tetrahedra remain (Q^0). Glasses containing < 10 mol.% alkali oxides are considerably more difficult to melt due to higher viscosities.[5] Moreover, alkali-deficient glasses are prone to phase separation and devitrification on a scale of 0.1–1 μm.[39] Modifiers disrupt the network and are used in fact to lower the viscosity of the glass melt and hence to facilitate its fabrication at lower temperatures. Thus, as expected then, the

relative concentration of bridging and non-bridging oxygens has an important influence on the properties of glasses.[36]

2.2 Glass-ceramics

Glass-ceramics are fine-grained polycrystalline materials formed when glasses of suitable compositions are heat-treated and undergo controlled crystallisation to the lower energy crystalline state.[10-11] In many cases, the crystallization process can be almost complete but a small content of residual glassy phase is often present. In these materials, the crystalline phases are entirely produced by crystal growth from a homogeneous glass phase while in traditional ceramics most of crystalline phases are introduced when the ceramic composition is prepared although some recrystallization can occur or new crystal types can arise due to solid state reactions.[11]

Glass-ceramics are normally produced in two steps: (1) a glass is formed by a standard glass-manufacturing process; and (2) the glass article is shaped, cooled and reheated above its glass transition temperature. The second step is sometimes repeated as a third step. In these heat treatments, the article partly crystallizes in the interior. In most cases, nucleating agents (*e.g.*, noble metals, fluorides, ZrO_2, TiO_2, P_2O_5, Cr_2O_3 or Fe_2O_3) are added to the base glass composition to boost the nucleation process. A less frequently used method is to induce and control internal crystallization during the cooling path of a molten viscous liquid. This process is used sometimes to form relatively coarse-grained glass-ceramics from waste materials to be used in the construction industry.[10-11, 40]

Glass-ceramics also can be produced by concurrent sinter-crystallization of glass-particle compacts. In this case, crystallization starts at glass–particle interfaces. A main advantage of the sinter-crystallization process is that nucleating agents are not necessary, because the particle surfaces provide nucleation sites. A disadvantage of this method is the presence of some residual porosity (0.5–3.0 %). However, this can be sometimes minimized or even eliminated by hot-pressing techniques. The sintering route also is attractive to produce glass-ceramics from reluctant glass-forming compositions, which could be made as a “frit,” moulded and sinter-crystallized.[10, 40-43]

2.2.1 Development of glass-ceramics and its commercialization

Glass-ceramics derive particular interest for several end applications, such as thermal, chemical, biological and dielectric ones, because these systems provide great possibilities to manipulate their properties, such as transparency, strength, resistance to abrasion, coefficient of thermal expansion. These properties can be achieved by proper selection of the composition which can control the extent of crystallization, crystal morphology, crystal size and aspect ratio. The ease of fabrication techniques in conjunction with lower production cost offer additional advantages.[1, 5, 10-12, 44-45]

It has been known for a long time that glasses can be crystallized to form polycrystalline ceramics. In the eighteenth century, Réaumur[46] had the idea of fabricating polycrystalline materials by first forming glass and then nucleating and crystallizing it to form a highly crystalline material. Réaumur experiments resulted in the creation of opaque, porcelain-like objects that had low mechanical strength and a distorted shape compared to the original shape of the bottles because he was unable to control the crystallization process that is necessary for the production of true glass-ceramics.[11] However, a real breakthrough was made in the 1950's by S. D. Stookey when the theory of glass phase separation was advanced.[10, 47-48]

Over the last decades, glass-ceramics have gradually become established in a wide variety of technical and domestic applications. The interest in glass-ceramics has become greater because they comprise an important group of materials which have an enormous technological significance and commercial value.[49] This can be explained by the fact that glass-ceramics possess an extremely favourable combination of mechanical, thermal, chemical, electrical and physical properties. The properties of these materials are superior to those of the majority of conventional glass or traditional ceramics materials.[10] The following key points are in the basis of this importance[5, 10-11]:

1. Glass-ceramics can attain high mechanical strength and good electrical insulation due to a very fine-grain microstructure with almost no porosity. These particular properties can be acquired owing to uniform chemical composition of glass-ceramics which can be achieved from the homogeneity of the parent glasses.
2. Changes in the chemical composition of the parent glass and the thermal treatment permit producing glass-ceramics comprising diverse physical properties which in turn permit their application in a wide range of practical fields. It is possible for them to combine a variety of desired properties, for example: combining very low thermal

expansion coefficient with transparency in the visible wavelength range for cooking ware or combining very high strength and toughness with translucency, biocompatibility, chemical durability and relatively low hardness for dental applications.

3. The control of the shape and dimensions of the glass-ceramic materials is easier in comparison to conventional ceramic materials since the later usually feature a relatively large shrinkage during drying and firing processes, which can result in variation of dimensions and/or distortion.
4. Parent glasses can be easily shaped using several techniques such as pressing, blowing or drawing which offer certain advantages over the available techniques for shaping conventional ceramic materials.

The first use of glass-ceramics as commercially viable products was developed in the aerospace industry in the late 1950s. These glass-ceramics were used as radomes to protect radar equipment in the nosecones of aircraft and rockets.[10] For such applications, these materials must exhibit a challenging combination of properties to withstand critical conditions resulting from rain erosion and atmospheric re-entry such as: homogeneity; low dielectric constant; low coefficient of thermal expansion; low dielectric loss; high mechanical strength; and high abrasion resistance. No glass, metal or single crystal can simultaneously meet all of these relevant specifications. Glass-ceramics now are used in nose cones of high performance aircraft and missiles.[10]

Another class of traditional, but still modern and very interesting glass-ceramics, is represented by Corning's Fotoceram and Schott's Foturan. These glass-ceramics can be patterned by ultraviolet light and selectively crystallized by thermal treatments. The crystallized regions then are completely dissolved by acid etching. The patterned glass can be used as-is or can be heated once more to form polycrystalline glass-ceramic plates that have high-precision holes, channels or any desired intricate pattern. The products are used in electronics, chemistry, acoustics, optics, mechanics and biology in applications that include micro-channels in optical fibres, ink-jet printer heads, substrates for pressure sensors and acoustic systems in head-phones.[10-11, 44]

Commercial applications of sintered glass-ceramics include devitrifying frit solder glasses for sealing TV tubes, cofired multilayer substrates for electronic packaging, marble-like floor and wall tile and some bioactive glass-ceramics.[10, 41, 50] Commercially successful glass-ceramics

can be divided in several categories according to their applications, both technical and consumer, as proposed examples below:

Glass-ceramics for thermal uses – Glass-ceramics featuring low-CTE can be used for thermal applications such as panels for cooktops fireplaces and stoves.[51] A relevant thermal property of glass-ceramics is their limiting use temperature. Because of their residual glass phase, most glass-ceramics flow and deform at relatively low temperatures, typically below about 700 °C. However, some notable exceptions exist. An example is a celsian glass-ceramic in the SrO–BaO–Al_2O_3–SiO_2 system, which has use temperatures as high as 1450 °C and CTEs that match silicon, SiC and Si_3N_4.[52] Materials with low CTE values are also of high interest in applications for which thermal dimensional stability is of prime importance. Particularly demanding are the requirements in optical applications with service temperatures between −50 and +100 ºC. For these special applications, optical glass ceramics have been developed for which the thermal expansion characteristic has been optimized to be as close to zero as possible in the working temperature interval. The best example of low expansion optical glass ceramic is the glass-ceramic Zerodur®.[10]

Machinable glass-ceramics – These materials rely on mica crystals in their microstructure and usually present high CTE and very low porosity. They can be quickly and inexpensively machined to complex shapes and precision parts with ordinary metalworking tools. Some machinable glass-ceramics can be used as dental and some bioactive applications via modern CAD–CAM techniques.[10-11, 44] Machinable glass-ceramics found wide application in such diverse and speciality areas as precision electrical insulators, vacuum feedthroughs, windows for microwave-type parts, samples holders for field-ion microscopes, seismograph bobbins, gamma-ray telescope frames, and boundary retainers on the space shuttle.[10]

Glass-ceramics used as construction materials – Many glass-ceramics have been developed from a wide variety of waste materials (*e.g.* incinerator ashes, blast furnaces slags, steel slags and sugar-cane ashes), showing big variation of compositions and predominant crystal phases.[53-55] These low-cost, dark-coloured (because of the high level of transition elements in wastes) materials are generally strong, hard and chemically resistant. Their intended use is for abrasion and chemically resistant parts or floor and wall tiles used in chemical, mechanical and other heavy-duty industries or construction.[10]

High-strength glass-ceramics – The average fracture strength (100–250 MPa) and toughness (1–2.5 $MPa.m^{1/2}$) of most glass-ceramics are generally higher than those of commercial

glasses (50–70 MPa and 0.7 $MPa.m^{1/2}$, respectively). For instance, glass-ceramics with impressive mechanical properties have been reported for canasite glass-ceramics and for lithium disilicate glass-ceramics.[10] These glass-ceramics feature lath-shaped crystals that lead to crack deflection and toughening. Fibre reinforcement, chemical strengthening by ion-exchange methods and development of a thin surface layer with a lower thermal expansion than the interior to induce a compressive surface layer are other successful strategies to increase strength and toughness.

Glass-ceramics for medical applications – Bioactive glass-ceramics form *in-situ* a biologically active layer of hydroxycarbonate apatite that bonds to bone and teeth and sometimes even to soft tissue. Many products have reached commercial success and have been used as granular fillers, artificial vertebrae, scaffolds, iliac spacers, spinous spacers, intervertebral spacers, middle-ear implants and as other types of small-bone replacements. Another interesting class of bioactive glass-ceramics is heat-generating bioactive or biocompatible glass-ceramics intended for use for hyperthermic treatment of tumours.[56-58]

Glass-ceramics for dental restorations – Restorative dental materials are used to fabricate, *e.g.*, dental crowns, bridges, inlays, and veneers.[10, 59] These materials, therefore, are not implanted in bone. Instead, they are bonded to the living tooth by bonding or cementation systems. The main objective is to produce a new biomaterial featuring properties (mechanical properties, biochemical compatibility with the oral environment, abrasion resistance, and a degree of translucency, shade, opalescence, and fluorescence) similar to those of natural teeth. The new biomaterial must demonstrate higher chemical durability than natural teeth, to prevent it from being susceptible to decay. These biomaterials are an integral part of a system used to fabricate dental restorations.

Glass-ceramics for electrical and electronic applications – Some glass-ceramics (*e.g.* spinel-enstatite, spinel, lithium disilicate, and canasite types) are used as magnetic memory disk substrates.[10, 60-61] For instance, the development of spinel glass-ceramics from the SiO_2–Al_2O_3–ZnO–MgO–TiO_2 system represented a significant contribution to the fabrication of magnetic memory disk substrates due to a very special nanostructure. The crystallites of the gahnite type ($ZnA1_2O_4$), spinel ($MgAl_2O_4$) or the solid solution of both types of crystals are smaller than 0.1 μm. Enstatite ($MgSiO_3$) is an important accessory phase, increasing fracture toughness above 1 $MPa.m^{0.5}$ and the crystals grow in an isolated manner in a glass matrix. As a result, the spinel-enstatite material is suitable as a substrate for magnetic memory disks. It demonstrates a favourable low surface roughness compared with other materials. The local

roughness of the glass-ceramic after the polishing process is 5 Å, which is important because the electromagnetic recording head can fly well within 20 nm of the spinning disk surface. Solid oxide fuel cells (SOFC) are another example of the application of glass-ceramics in this field.[62] SOFC are ceramic solid-state energy conversion devices that produce electricity by electrochemically combining fuel (*e.g.*, hydrogen gas or natural gas) and oxidant (*e.g.*, air) gases across an ionic conducting oxide at operating temperatures of about 800 °C. The planar SOFC configuration provides a simple manufacturing process and high current densities, but it requires hermetic sealing to prevent fuel–oxidant mixing and to electrically insulate the stack. A suitable sealing material must meet several criteria: chemical stability at 800 °C under oxidizing and reducing wet atmospheres (air, hydrogen gas); electrically insulating; chemical compatibility (*i.e.*, must not poison other cell components); ability to form a seal at about 900 °C that results in a hermetic bond with high strength; CTE of $10–12\times10^{-6}$ /K; and long-term reliability during high-temperature operation and during thermal cycles to room temperature.

Optical glass-ceramics – Cookware that allows continuous visualization and monitoring of the cooking process; fireplace protection; transparent armours for visors or vehicle windows; substrates for LCD devices; ring laser gyroscopes; missile noses; fibre grating athermalization; precision photolithography; printed optical circuits; and small or very large telescope mirrors are just some examples of successful optical applications of glass-ceramics.[10, 40, 51] The keen interest in glass-ceramics for optical applications is caused by their advantages over glasses, single crystals and sintered transparent ceramics. Unlike glasses, glass-ceramics demonstrate properties similar to those of single crystals. In contrast with single crystals or sintered ceramics, glass-ceramics can be made in intricate shapes and sizes by fast and cost-efficient glass-manufacturing processes. Transparent glass-ceramics based on fluoride, chalcogenide and oxyfluoride doped with rare-earth ions have been successfully used for wavelength up-conversion devices for europium-doped waveguide amplifiers. Transparent mullite, spinel, willemite, ghanite or gelenite-based glass-ceramics doped with transition-metal ions have been developed for use in tunable and infrared lasers, solar collectors and high-temperature lamp applications. Other optically active applications include luminescent glass-ceramics for solar concentrators, up-conversion and amplification devices; illumination devices using IR; heat-resistant materials that absorb UV, reflect IR and are transparent to visible light; materials that absorb UV and fluoresce in red/IR; substrates for arrayed waveguide grating; solid-state lighting – white light; and laser pumps.[10]

2.2.2 Glass-ceramic processing

Glass-ceramics are fine-grained polycrystalline materials formed when glasses of suitable compositions are heat-treated and thus undergo controlled crystallization. The important feature of the processing of glass-ceramics is that the crystallization must be controlled. For instance, common window glass is too stable and difficult to crystallize, whereas other compositions crystallize in an uncontrolled manner resulting in undesirable microstructures. Usually, a glass-ceramic is not fully crystalline: typically the microstructure is 50–95 vol.% crystalline, with the balance volume being the residual glass. One or more crystalline phases may form during the heat treatment and their composition is normally different from the parent glass, and the composition of the residual glass is also different from that of the parent glass.[11-12]

Initially the glass batch is heated to form a homogeneous melt. The shape of the desired object is formed from the glass at the working point (when viscosity is ~10^3 Pa.s) by the usual processes such as pressing, blowing, rolling, or casting. After annealing to eliminate internal stresses, the glass object then undergoes a thermal treatment that converts it into a glass-ceramic.[63] Crystallization is the process by which the well ordered or regular periodic crystalline structures are produced from the non-periodic structure of glass. In its simplest form, crystallization is observed when a melt of a single pure element or compound is cooled. The crystallization process is generally considered as consisting of two independent processes: (1) *nucleation*, which corresponds to the formation of crystallization centres, and (2) *crystal growth* from the formed centres. The rate at which these two processes occur is a function of temperature. [5, 11, 63-64]

2.2.2.1 Nucleation

Nucleation is the key factor for controlling crystallization in glass-ceramics. Crystal nuclei must be present in the glass matrix to commence the crystallization process. Nucleation involves the initiation of regions of longer-range atomic order (*embryos*) which are normally present in molten materials or in the super-cooled liquid.[11] The temperature dependence of nucleation and crystallization in glasses can be described by the classic theory and the nucleation rate and crystal growth rate as a function of temperature are accurately measured experimentally.[10-11, 48] Two distinct types of nucleation can occur: (1) homogeneous nucleation and (2) heterogeneous nucleation.[5, 44, 65] In homogeneous nucleation the first small

seeds are of the same composition as the crystals which grow upon them, but in heterogeneous nucleation the nuclei are different chemically from the formed crystals. In heterogeneous nucleation, foreign boundaries such as substrates and grain boundaries are usually involved.[10] This is also called catalyzed nucleation. Heterogeneous nucleation is the typical mechanism used in the development of glass-ceramics, as boundaries cannot be excluded and are indeed generally effective in the development of most glass-ceramics. The embryos turn into nuclei when they attain a critical minimum size capable of developing spontaneously into gross particles of the stable phase.

2.2.2.1.1 Homogeneous nucleation

The theory of nucleation involves a thermodynamic parameter known as free Gibbs energy (*G*), which is a function of other thermodynamic parameters: the enthalpy (*H*), *i.e.*, the internal energy of the system, and the entropy (*S*), *i.e.*, a measurement of the disorder of the atoms or molecules. The change in free energy ΔG is an important thermodynamic parameter regarding the phase transformations, since a transformation will occur spontaneously only when ΔG has a negative value.

Considering that each nucleus is spherical and has a radius *r* the classical theory gives the work of formation ΔG as:[66-67]

$$\Delta G = -\frac{4}{3}\pi r^3 \Delta G_V + 4\pi r^2 \gamma + \Delta G_E \qquad \text{Eq. 1}$$

where ΔG_V is the free-energy change per unit volume associated with the formation of the new phase, γ is the interfacial energy (per unit area) of the new surface of the nucleus, and ΔG_E is the elastic distortion energy (often not considered because from a mathematical point of view, this contribution can be ignored for melt-crystal and vapour-crystal transformations[10]). These volume, surface, and total free energy contributions are plotted schematically as a function of nucleus radius in Fig. 4.[5, 65, 68]

The curve corresponding to the first term on the right-hand side of Eq. 1, the free energy (which is negative) decreases with the third power of *r* and the curve resulting from the second term for in Eq. 1, energy values are positive and increase with the square of the radius. Consequently, the curve associated with the sum of both terms first increases, passes through a maximum, and finally decreases. In a physical sense, this means that as a solid particle begins to form as atoms in the liquid cluster together, its free energy first increases. If this

cluster reaches a size corresponding to the critical radius r^*, then growth will continue with the accompaniment of a decrease in free energy. On the other hand, a cluster of radius less than the critical will shrink and redissolve. This subcritical particle is an embryo, whereas the particle of radius greater than r^* is termed a nucleus. A critical free energy (ΔG^*) occurs at the critical radius and, consequently, at the maximum of the curve in Fig 4 corresponds to an activation free energy, which is the free energy required for the formation of a stable nucleus. Equivalently, it may be considered an energy barrier to the nucleation process.

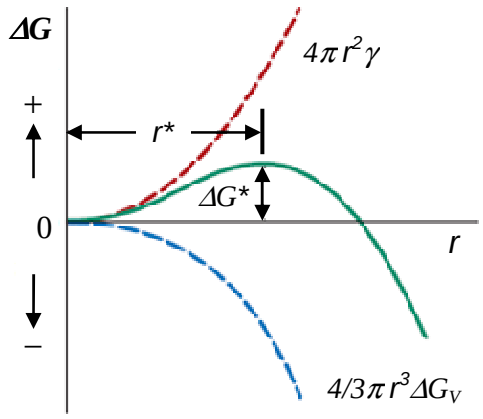

Fig. 4 – Schematic plot of free energy versus embryo/nucleus radius, on which is shown the critical free energy change (ΔG^*) and the critical nucleus radius (r^*).

Because r^* and ΔG^* appear at the maximum on the free energy *vs* radius curve of Fig 4, derivation of expressions for these two parameters is a simple matter. For r^*, we differentiate the ΔG equation without considering ΔG_E (Eq. 1) with respect to r, set the resulting expression equal to zero, and then solve for r (= r^*):[66, 69]

$$\left.\frac{\partial(\Delta G)}{\partial r}\right|_{r=r^*} = 4\pi\Delta G_V\, r^{*2} + 8\pi\gamma\, r^* = 0 \qquad \text{Eq. 2}$$

which leads to the result

$$r^* = -\frac{2\gamma}{\Delta G_V} \qquad \text{Eq. 3}$$

The critical nucleus size r^* corresponds to the critical free enthalpy ΔG^*. The critical free energy is determined by the substitution of this expression for r^* into Eq. 1:

$$\Delta G^* = \frac{16\pi\gamma^3}{3(\Delta G_V)^2} \qquad \text{Eq. 4}$$

This volume free energy change ΔG_V is the driving force for the transformation, and its magnitude is a function of temperature. At the equilibrium temperature, the value of ΔG_V is zero, and with diminishing temperature its value becomes increasingly more negative.

2.2.2.1.2 Heterogeneous nucleation

Heterogeneous nucleation involves phase boundaries, special catalysts, and foreign substrates that are distinct from the parent phase. This type of situation occurs when the driving forces involved in the formation of a new phase are stronger than those required by the parent phase for its transformation into a crystal. Fig. 5 shows the model on which heterogeneous nucleation is based. It is assumed that both the liquid and solid phases "wet" this flat surface, *i.e.*, both of these phases spread out and cover the surface. Three interfacial energies (represented as vectors) exist at two-phase boundaries (γ_{SI}, γ_{SL} and γ_{IL}) as well as the wetting angle θ (the angle between the γ_{SI} and γ_{SL} vectors).[10, 68]

The theory for the formation of critical free enthalpy in heterogeneous nucleation (ΔG_H^*) is derived from the contact angle (θ) relationship of Young's equation and is given by

$$\Delta G_H^* = \Delta G^* \, f(\theta), \quad \textit{where } f(\theta) = \frac{1}{4}(2+\cos\theta)(1-\cos\theta)^2 \qquad \text{Eq. 5}$$

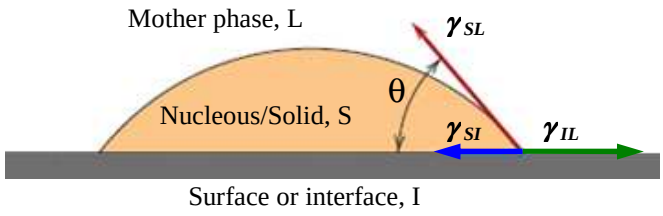

Fig. 5 – Model for heterogeneous nucleation. The solid–surface (γ_{SI}), solid–liquid (γ_{SL}) and liquid–surface (γ_{IL}) interfacial energies are represented by vectors. The wetting angle (θ) is also shown.[10, 68]

Considering Eq. 5 and Fig. 4, special situations should be taken into account: (1) if the heterogeneous substrate (I) is not wetted, θ = 180° and $f(\theta) = 1$, *i.e.*, this phenomenon returns to a homogeneous nucleation process; (2) if the surface of I is completely wetted and θ is

close to 0º, then $f(\theta) \geq 1$ and ΔG_H^* are very small; thus for $\theta < 180°$, heterogeneous rather than homogeneous nucleation will occur. Furthermore, nuclei with the critical size of r^* are preferentially formed. Heterogeneous nucleation is particularly effective if there is epitaxy between the nucleus and substrate. There can be an epitaxial relationship if the lattice geometry of the nucleus and substrate crystals is similar (less than 15% mismatch in lattice parameter). Further influences on epitaxy in glass ceramics include: the bonding state in the substrate and nucleus crystals, structure defects, and the degree of coverage of the nucleant surface with foreign nuclei. During the production of glass-ceramics, special nucleation agents can be incorporated into the base glass composition which acts as catalysts for the nucleation process in the glassy matrix. The relationships between the different interface energies of the three phases (γ_{SI}, γ_{SL} and γ_{IL}) will also provide several criteria for determining the effectiveness of the nucleating agent.

Taking a surface tension force balance in the plane of the flat surface leads to the following expression:

$$\gamma_{IL} = \gamma_{SI} + \gamma_{SL} \cos\theta \qquad \text{Eq. 6}$$

Using a similar procedure similar to the one presented above for homogeneous nucleation, it is possible to derive equations for r^* and ΔG_H^*; these are as follows:

$$r^* = -\frac{2\gamma_{SL}}{\Delta G_V} \qquad \text{Eq. 7}$$

$$\Delta G^* = \frac{16\pi\gamma_{SL}^{\ 3}}{3(\Delta G_V)^2} S(\theta) \qquad \text{Eq. 8}$$

The $S(\theta)$ term of Eq. 8 is a function only of θ (*i.e.*, the shape of the nucleus), which will have a numerical value between zero and 1 (For example, for θ angles of 30º and 90º, values of $S(\theta)$ are approximately 0.01 and 0.5, respectively. From Eq. 7, it is important to note that the critical radius r^* for heterogeneous nucleation is the same as for homogeneous, inasmuch as γ_{SL} is the same surface energy as γ in Eq. 3. It is also evident that the activation energy barrier for heterogeneous nucleation (Eq. 8) is smaller than the homogeneous barrier (Eq. 4) by an amount corresponding to the value of this $S(\theta)$ function, or

$$\Delta G_H^* = \Delta G^* S(\theta) \qquad \text{Eq. 9}$$

Figure 6 plots curves for both types of nucleation, and indicates the difference in the magnitudes of ΔG^*_{hom} ΔG^*_{het}, in addition to the constancy of r^*. This lower ΔG^* for heterogeneous means that a smaller energy must be overcome during the nucleation process (than for homogeneous), and, therefore, heterogeneous nucleation occurs more readily.[68]

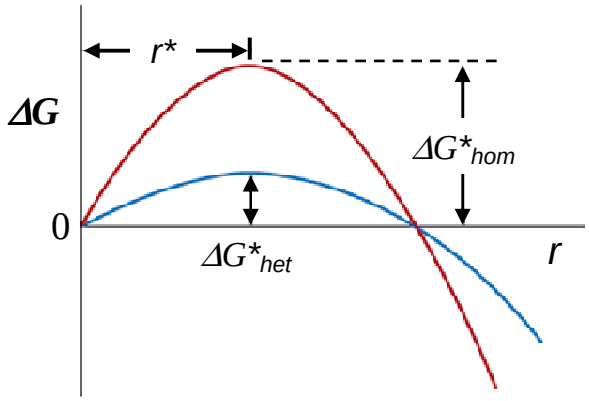

Fig. 6 – Schematic free energy *vs* embryo/nucleus radius plot on which are presented curves for both homogeneous (ΔG^*_{hom}) and heterogeneous nucleation (ΔG^*_{het}). Critical free energies and the critical radius are also shown.[68]

2.2.2.2 Crystal growth

The crystallization process will be concluded with the growth of crystals on the nucleated glasses, which should be heat-treated at higher temperatures. The growth step in a phase transformation begins once an embryo has exceeded the critical size, r^*, and becomes a stable nucleus.[10, 65, 68] Nucleation will continue to occur simultaneously with growth of the new phase particles, but cannot occur in regions that have already transformed to the new phase. Moreover, the growth process will finish in any region where particles of the new phase meet, because here the transformation will have reached completion.

The crystal growth is a complex stage of the crystallization process due to several motives: (1) more than one phase may crystallize simultaneously; (2) the composition of the crystals is usually different from the composition of the parent glass, implying that the crystal-glass interface is continuously changing in composition; (3) fractions of the primary crystal phase may start transformation into a new structural type.[72] The crystallization rates in glass can be enhanced or inhibited by the presence of some additives. For example, low concentrations of various transition metal ions such as Fe, Zn and V increase the rate of crystal growth,[73] while

Cr ions were found to decrease it.[74] Moreover, this effect may be specific to particular crystal surfaces.

The crystallization rate of glasses is determined by the extent to which material transport to the interface between the nucleus and the surrounding glass matrix is achieved.[10] Accordingly, particle growth occurs by long-range atomic diffusion, which normally involves several steps such as diffusion through the parent phase, diffusion across a phase boundary, and then into the nucleus. Consequently, the growth rate U is determined by the rate of diffusion, and its temperature dependence is the same as for the diffusion coefficient D,

$$D = D_0 \exp\left(-\frac{Q_d}{kT}\right) \qquad \text{Eq. 10}$$

where D_0 is a temperature-independent pre-exponential, Q_d is the activation energy for diffusion, R is the gas constant and T the absolute temperature. Thus, U can be express as

$$U = c \exp\left(-\frac{Q}{kT}\right) \qquad \text{Eq. 11}$$

where Q is the activation energy and c is a pre-exponential, both independent of temperature. Processes whose rates depend on temperature, as U in Eq. 11, are sometimes termed thermally activated and a rate equation having the exponential temperature dependence is termed an Arrhenius rate equation.[68]

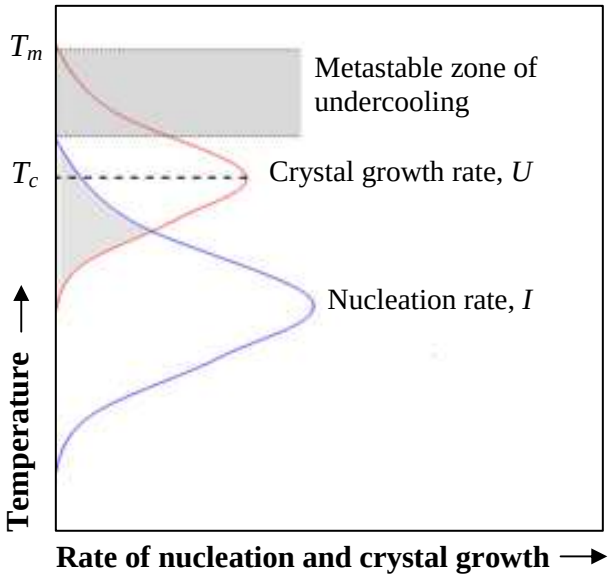

Fig. 7 – Schematic plot showing the variation of the nucleation rate (I) and growth rate (U) with the temperature.

Fig. 7 shows the temperature dependence of U and I (again, almost always the rate for heterogeneous nucleation). At a specific temperature, the overall transformation rate is the combined effect and is represented by a third curve. The general shape of this curve is the same as for the nucleation rate, presenting a peak or maximum that has been shifted upward relative to the curve for I.

In general, crystal growth, *i.e.* the rate of advance of a solid-liquid interface, can be described as a function of temperature [76-77] by:

$$U = \left(\frac{f\ D}{a_0}\right)\left[1 - \exp\left(-\frac{\Delta G}{R\,T}\right)\right] \qquad \text{Eq. 12}$$

where U is the growth rate, f is a site factor (fraction of sites at the interface where atoms can be preferentially added or removed), D is the diffusion coefficient for molecular transport across a solid liquid interface, a_0 is a jump distance, and ΔG is the difference in Gibbs free energy between the solid and liquid phase. Using the Stokes-Einstein relation it is possible to express D as a function of viscosity (η):[76]

$$D = \frac{k\,T}{3\,a_0\,\pi\,\eta} \qquad \text{Eq. 13}$$

where η is the viscosity and k is the Boltzmann constant. Replacing D by Eq. 13 in Eq. 12:

$$U = \left(\frac{f\ k\,T}{3\,a_0\ 2\,\pi\,\eta}\right)\left[1 - \exp\left(-\frac{\Delta G}{R\,T}\right)\right] \qquad \text{Eq. 14}$$

From Eq. 14, it can be seen that the crystal growth rate (U) in any glass system is controlled primarily by two factors: (1) the thermodynamic factor or barrier represented as [1 − exp ($-\Delta G/RT$)], and (2) a purely kinetic factor, *i.e.*, related to the motion or mobility of the ions or group of ions present in this glass, represented as ($f\,kT$ / ($3a_0\,2\pi\,\eta$)). From the analysis of Eq. 14, several scenarios can be considered:

1. At temperatures higher than the melting point ($T > T_m$), the change in the free energy (ΔG) is positive, hence the term [1 − exp($-\Delta G/RT$)] will be a negative number leading to a negative value of U. This is in agreement with the fact that the crystals start to dissolve at temperatures higher than the melting point.

2. For $T = T_m$, $\Delta G = 0$, which will yield $U = 0$. This is essentially in agreement with the definition of the melting point. As the temperature T is lowered below T_m, the

thermodynamic factor [1 − exp(−$\Delta G/RT$)] has a significant influence on crystal growth rate. At that region, because the viscosity is low, the thermodynamic factor will mainly control the crystal growth rate because of the higher driving force of ΔG is negative.

3. When the system is at a temperature far from equilibrium ($T \leq T_m$), the term [1 − exp(−$\Delta G/RT$)] approaches unity and the crystal growth rate is mostly governed by kinetic factors (viscosity and diffusivity). The conflicting changes in the crystal growth rate are due to changes in the thermodynamic and kinetic factors, resulting in a maximum in the temperature dependence of the crystal growth rate. As a result, the crystal growth rate curve is a skewed bell-shaped, reaching a maximum at T_c (somewhere below T_m) and reaching zero at both the high and low temperature ends.

2.3 Liquid–liquid phase separation

Liquid–liquid immiscibility is very common in glass melts, in fact so common that Shelby states that far more binary glass-forming melts exhibit liquid–liquid immiscibility than exhibit homogeneous behaviour.[5] Phase separation in glasses influences a variety of properties and has been an important subject of debate of modern glass research.[78] Shvetsov (1932) is referred as publishing the first account of metastable immiscibility as a cause for chemical inhomogeneity in glasses.[79] A number of review articles dealing with phase separation in glasses have been published, including frequently referenced publications by Mazurin[79-80], Tomozawa[81-82], Uhlmann[83] and James[84].

Phase separation occurs in many organic and inorganic materials including polymers, metallic alloys and ceramics.[2, 17, 45, 85] Some binary or multicomponent systems have the peculiar characteristic that over a certain region of temperature and composition, called *miscibility gap*, the system exists in equilibrium, or metastable equilibrium, as two liquid phases of different composition. This phenomenon is known as *liquid-liquid immiscibility*. The process whereby the homogeneous liquid separates into two liquids as it is brought into the two-liquid region is known as *phase separation*.[6, 13, 85-90]

2.3.1 Stable and metastable miscibility gap

In simple oxide mixtures such as $MgO–SiO_2$, $CaO–SiO_2$ and $SrO–SiO_2$, stable (above the *liquidus*) liquid immiscibility is often observed, which is readily evidenced by the tendency of the melt to segregate eventually as two bulk liquids. One or more glass phases are usually formed during the cooling of these two-phase melts: the silica-rich phase almost invariably forms a glass, while the other phase sometimes crystallizes.[91-92]

In systems such as $Li_2O–SiO_2$, $Na_2O–SiO_2$ and $BaO–SiO_2$, there are liquid miscibility gaps that occur somewhat below the *liquidus* but above the glass transition. These are known as *metastable miscibility gaps*.[78, 91-92] Cooling the melt of glasses of these systems results in the formation of two phases, usually on a microscopic scale. The supercooled liquid begins to unmix during the cooling through the miscibility gap and the unmixing process continues until it is stopped by (a) the interference of crystallization, or (b) by the high viscosity reached by the system as it passes through the glass transition region. The time that the system remains within the miscibility gap at high enough temperatures for the kinetic processes of separation to occur is determinant for the extent to which the phase separation proceeds. If crystallization does not occur, the resulting glass is a *phase separated glass*, *i.e.* a solid composed by two phases, both glass. If such a system is rapidly quenched to form a homogeneous or nearly homogeneous (slight separated) glass this is said to be *phase separable*, which means that the phase separation will occur upon heating to a suitable temperature for molecular transport to take place (although at these temperatures it will be competing with the crystallization process).

Many silicate glasses phase separate at temperatures well above T_g. There may be a much greater tendency for silicate glasses to separate than is presently thought, but in many systems the thermodynamic condition favouring immiscibility may occur only at sub-glass transition temperatures. For these glasses, the problems of observing the miscibility gaps are quite similar to the problems of getting any glass to relax to its metastable equilibrium configuration, once it is below its glass transition temperature. Such a glass cannot be termed phase separable since such behaviour is impossible by kinetic reasons.

2.3.2 The relation of the miscibility gap with the shape of the *liquidus* line

Observing phase diagrams such as the ones represented in Fig. 8, there are three possible positions of the miscibility gap with respect to the *liquidus*: (a) intercepting the *liquidus* (with

consequent stable two-liquid region); (b) tangent to the *liquidus*; and (c) entirely metastable. The slope of the *liquidus* can suggest the presence and possible position of a metastable miscibility gap.[91] Therefore, phase diagrams can give important information about what we may expect to be the nature of the resulting glass. Fig. 9 presents the series of binary alkaline-earth and alkali-metal oxide silicates whose *liquidus* curves for the composition range between 55 and 100 mol.% of SiO_2.[93] Stable liquid immiscibility is shown by the $MgO–SiO_2$, $CaO–SiO_2$ and $SrO–SiO_2$ systems. The $Li_2O–SiO_2$, $Na_2O–SiO_2$ and $BaO–SiO_2$ and $K_2O–SiO_2$ systems show successively decreasing S-shape tendencies in their *liquidus* curves. This would suggest that metastable miscibility gaps occur in the $Li_2O–SiO_2$, $Na_2O–SiO_2$ and $BaO–SiO_2$ and $K_2O–SiO_2$ systems at successively lower temperatures.

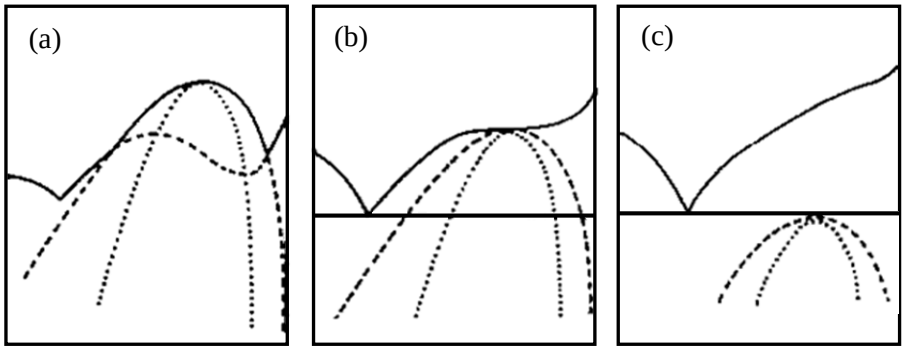

Fig. 8 – Three possible locations of a liquid immiscibility gap: (a) interrupting the *liquidus*, (b) tangent to the *liquidus*, and (c) entirely metastable.[91]

The greatest amount of phase separation would be expected to occur during glass formation in the $BaO–SiO_2$ system and the least in the $K_2O–SiO_2$ system because viscosity of each of these systems increases rapidly with decreasing temperatures. Indeed, it is extremely difficult to quench $BaO–SiO_2$ melts of composition between 5 and 10 mol.% of BaO to clear glasses. Phase separation occurs to such an extent during cooling that the glasses look opal-white, owing to light scattering by the resulting inhomogeneities in the index of refraction. In both the $Li_2O–SiO_2$ and $Na_2O–SiO_2$ systems, suitable heat treatments will develop such opalescence while no such opalescence has been found in the $K_2O–SiO_2$ system.

The investigations of the metastable miscibility gaps in the $BaO–SiO_2$, $Li_2O–SiO_2$ and $Na_2O–SiO_2$ systems made in recent years showed that they occur at successively lower temperatures (approximately 1450 ºC for $BaO–SiO_2$, 1200 ºC for $Li_2O–SiO_2$ and 850 ºC for $Na_2O–SiO_2$) as predicted by the *liquidus* shape.[94-95] Fig. 10 presents the $Li_2O–SiO_2$ system as

an example. No gap has been found in the $K_2O–SiO_2$ system, and it has been suggested that any tendency for such a gap most likely occurs below the glass transition temperature where it will never be observed.[96]

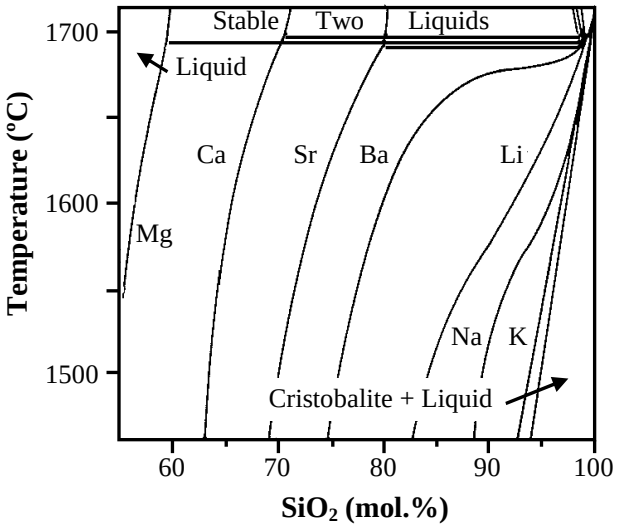

Fig. 9 – *Liquidus* curves for several binary silicate systems.[93]

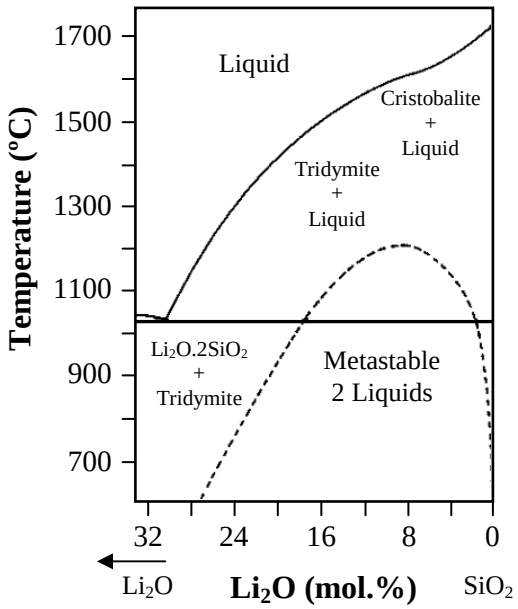

Fig. 10 – Metastable liquid immiscibility in the $Li_2O–SiO_2$ system.[94-95]

2.3.3 Mechanisms of phase separation

Models for phase separation, based on thermodynamics and the free energy of mixing arguments, are described in detail by several authors.[5, 79, 84, 96] Immiscibility in glasses is controlled by the Gibbs free energy of mixing and the competition between the enthalpy of mixing (ΔH_{mix}) and the entropy of mixing (ΔS_{mix}):

$$\Delta G_{mix} = \Delta H_{mix} - T\ \Delta S_{mix} \qquad \text{Eq. 15}$$

Above a critical temperature, T_c, the entropy term will always dominate and free energy of mixing will always be lower for the homogeneous melt. Below T_c, the free energy is lower if the melt separates into two phases of different compositions than if it remains a homogeneous melt. There are two distinct mechanisms by which phase separation can develop: (1) *nucleation and growth*; and (2) *spinodal decomposition*. These mechanisms have been characterised by many authors, for example: nucleation and growth mechanism – references [45, 90, 96-99]; spinodal decomposition – references [90, 96, 98, 100-103]. These mechanisms lead to very different microstructures and properties. The curvature of the free energy of mixing at the bulk composition of the melt will indicate the mechanism by which phase separation occurs. An idealized immiscibility diagram for the binary $Na_2O–SiO_2$ system is presented in Fig. 11.[5, 104] The inserted drawings represent the typical microstructures that will develop if allowed by kinetics, when heat treated within the various regions of the phase diagram.

Within the nucleation and growth region of the phase diagram, the formation of nuclei occurs if the free energy of the system decreases, thus a large change in composition must take place. This region is referred to as the metastable region because the system is unstable to small fluctuations in composition, but can be stable to larger changes in composition. After nucleation, the new phase will grow in size through diffusion and some regions may coalesce depending on their proximity. During the growth stage the chemical composition of the nucleated phase is invariant with respect to time at isothermal temperature. Phase separation resulting from nucleation and growth is characterized by distinctly separated spherical droplets of the nucleated phase in a continuous matrix of a second phase, as shown in Fig. 11. The spheres will have a composition of the phase which differs the greatest from the bulk composition. The spherical phase will nucleate randomly and have poor connectivity.

The phase separation in the spinodal region begins with small fluctuations in composition, which at a given time grow in compositional differences, resulting in two continuous interpenetrating phases. Because these changes occur spontaneously, and no energy barrier to separation is present, the region is considered unstable with respect to immiscibility. The system will lower its free energy by continually changing the composition of the two phases until the equilibrium compositions are reached. Once the equilibrium compositions are attained the free energy is at its lowest state. The spatial variations of the structure remain fairly constant until the equilibrium compositions are achieved, after which the phase separated regions will grow in size through diffusion, thereby reducing the interfacial energy

of the system. Both phases formed in the spinodal region will show a high degree of connectivity.

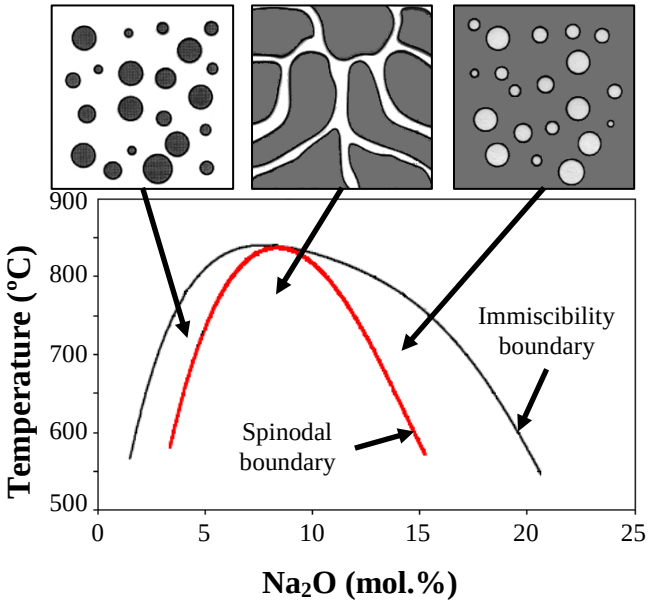

Fig. 11 – Metastable immiscibility diagram for the Na_2O–SiO_2 system with typical microstructures expected from the various regions of the system. Dark phase in drawings is sodium rich and light phase is silica rich. Immiscibility and spinodal boundaries were reproduced from data of Shelby[5].

2.3.4 The effect of phase separation on crystallization

Many glasses exhibit amorphous phase separation preceding the crystal nucleation and growth during the heat treatment schedule required to convert them to glass-ceramics. It is well known that such separation may aid subsequent crystallisation by producing a phase with a greater tendency to nucleate than the initial glass.[45]

Fine-grained glass-ceramics are obtained through a fine-scale, uniform dispersion of nuclei for the growth of the desired major crystalline phase. In general, this may be accomplished by one or more different mechanisms: (1) in the simplest one, although rarely encountered, the desired major crystalline phase nucleates homogeneously (without a catalyst) on a fine scale throughout the bulk of the glass; (2) the introduction of minor crystalline phase may homogeneously nucleate throughout the glass. The resulting finely dispersed crystalline precipitate may then act as a nucleation catalyst for the desired major crystalline phase, usually because of a favourable low interfacial energy between the nucleus and the growing crystal; (3) alternatively, the crystallization of a major phase may be initiated by a liquid-

liquid phase separation without the necessity of a crystalline nucleation catalyst. Such separation may result in a fine-scale dispersion of second-phase liquid droplets that are very poor glass formers and therefore crystallize very readily.[91] Moreover, Ohlberg *et al*. (1962) have presented evidence that crystal nucleation occurs at the two-liquid interface of certain two-phase glasses.[105]

2.4 The $Li_2O–SiO_2$ system

2.4.1 Formation and properties of crystalline phases

The phase diagram in Fig. 12 shows the crystallization tendency for the $Li_2O–SiO_2$ system.[94, 106] $Li_2O–SiO_2$ systems with composition close to lithium disilicate ($Li_2Si_2O_5$) are among the most studied systems regarding the control crystallization in glass–ceramic synthesis.[10, 78] The structure of orthorhombic lithium disilicate crystals involves corrugated sheets of $(Si_2O_5)^{-2}$ on the (010) plane that gives excellent mechanical properties for the glass-ceramic material.[10] The melting points of Li_2O and SiO_2 are 1727 and 1713 °C, respectively. The stoichiometric composition of lithium disilicate crystal phase ($Li_2Si_2O_5$) melts congruently at 1033 °C.[107] Different phases include lithium orthosilicate (Li_4SiO_4), lithium metasilicate (Li_2SiO_3) and lithium disilicate ($Li_2Si_2O_5$).[10, 108] A polymorphous transformation of the crystal phase was observed at approximately 936 ºC.[10, 94] As the Li_2O content increases, lithium metasilicate, Li_2SiO_3, crystallizes. Other crystalline phases can form depending on the starting glass composition.[109]

Lithium occupies a particular position in the periodic table, which confers to its compounds differentiated properties from those of the other alkalis, but not entirely similar to those of the alkaline-earths, with which they are often compared. Due to this particular behaviour, the lithium compounds with silica exhibited a kind of transition character in a remarkable manner, and hence the study of the $Li_2O–SiO_2$ system is of particular interest. The intermediate position of the lithium silicates between those of the alkalis and the alkaline earths is evidenced in the nature of the compounds formed and in their properties, such as the melting points, optical constants, crystallization ability, solubility in water.[94] Alkalis tend to form stable compounds of relatively high silica content due to their high basicity, such as the disilicates and the tetrasilicates (K, Rb, Cs), while the alkaline earths (with the exception of Ba) do not form disilicates. On the other hand, the orthosilicates of the alkalis are relatively

unstable, while those of the alkaline earths are very stable. Lithium forms a highly stable metasilicate ($Li_2O{\cdot}SiO_2$), with a higher melting point than that of any other alkali metasilicate. Lithium orthosilicate ($2Li_2O{\cdot}SiO_2$) is also stable at a higher temperature than the other alkali orthosilicates, but the disilicate ($Li_2O{\cdot}2SiO_2$) is only stable over a narrow region of composition in contact with the *liquidus*.

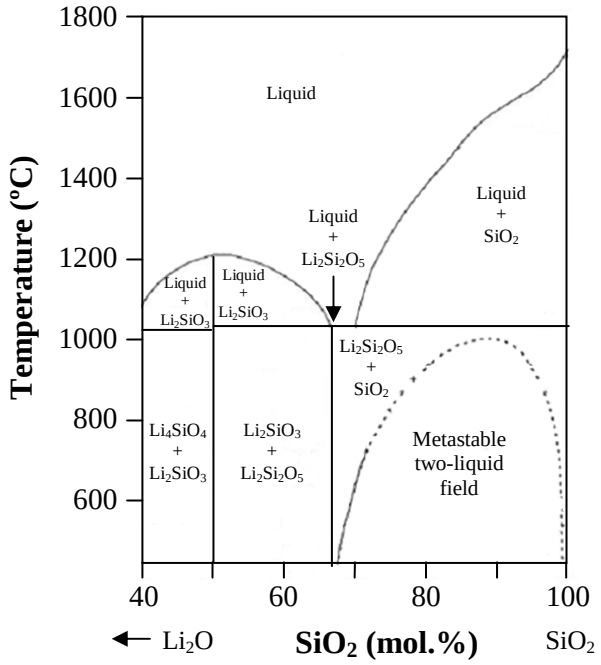

Fig. 12 – Phase diagram of the $Li_2O–SiO_2$ system.

Among the two-component alkali silicate glasses, the $Li_2O–SiO_2$ binary system is one the most important for the preparation of glass-ceramic materials.[110-111] In the $Li_2O–SiO_2$ phase diagram, an addition of approximately 30 mol.% of Li_2O to SiO_2 causes the *liquidus* temperature to drop rapidly from 1713 to 1030 °C, such that the resulting liquid forms a clear glass on cooling which is very easy to obtain. However, liquids containing less than 25 mol.% Li_2O give opalescent or opaque glass on cooling owing to phase separation within a metastable immiscibility dome.[78, 110, 112] Upon crystallization between the glass transition temperature (~500 °C), and the solidus temperature, *i.e.* the melting temperature (~1030 °C), $Li_2Si_2O_5$ is the main phase together with small amounts of either SiO_2 and/or Li_2SiO_3.[110-111] Usually, in order to produce a fine-grained lithium silicate glass-ceramic, the crystallization would typically involve nucleation followed by growth of the $Li_2Si_2O_5$ crystals, and nucleating catalysts, such as TiO_2 or P_2O_5, can generally be added.[10] However, the simple

$Li_2O–SiO_2$ system alone shows poor chemical durability and low mechanical characteristics. Addition of oxides acting as network former and modifier can greatly improve these properties and confer glass-ceramics very high thermal shock resistance and surface hardness, and low coefficients of conductivity and thermal expansion.[10-11, 110-111]

Lithium metasilicate crystallization was found to precede lithium disilicate crystallization as a metastable phase in some lithium silicate glasses and crystallizes at a lower temperature. Hench *et al.*[113] determined that lithium metasilicate crystals form before lithium disilicate in two glass compositions of 30 and 33 mol.% Li_2O, but the amount of lithium metasilicate was extremely limited and disappeared on further heat treatment at higher temperature. As the Li_2O content increases over the stoichiometric content of lithium disilicate, lithium metasilicate crystallizes and other crystalline phases can form depending on the starting glass composition. When the Li_2O is less than the stoichiometric content of the disilicate composition, metastable glass-in-glass phase separation occurs that influences crystal nucleation and crystal growth. Lithium disilicate and lithium metasilicate can crystallize by homogeneous bulk crystallization depending on the initial glass composition and temperature.

2.4.2 Research regarding lithium disilicate based glass-ceramics: a brief history

Simple silicate glass-ceramics are composed of alkali and alkali earth silicate crystals whose properties dominate that of the glass-ceramics. The most important ones were lithium silicates based glass-ceramics which consist of two main composition groups: (1) the first group based on lithium disilicate crystals ($Li_2O{\cdot}2SiO_2$), nucleated with P_2O_5, develops high expansion glass-ceramics which match the thermal expansion of several nickel based superalloys, and are used in variety of high strength hermetic seals, connectors, feedthroughs, and related materials based on a microstructure of fine-grained lithium disilicate crystals with dispersed nodules of quartz crystals have been extensively evaluated for use as magnetic disk substrates for computer hard drives;[114] (2) the second group based on lithium metasilicate crystals ($Li_2O{\cdot}SiO_2$), photosensitively nucleated by colloidal silver, produces a variety of chemically machined materials which are useful as fluidic devices, display screens, lens arrays, magnetic recording head pads, charged plates for inkjet printing, and other patterned devices.[40]

Numerous works have been published on the crystallization of lithium disilicate glass since it crystallizes by homogeneous bulk crystallization without changing composition.[45] Lithium disilicate glass crystallizes more easily than other alkali disilicate glasses and serves as the

model system for the study of glass-ceramics.[11, 115] Since the findings of Stookey [47-48, 116] in the 1950s, many researchers have dedicated their investigation works to lithium disilicate glasses and glass-ceramics. Experiments were carried out to shed some light in diverse fields such as crystallization mechanisms, crystallization kinetics, phase evolution and microstructure, use of nucleation agents and other additives, etc.. Some examples of research works regarding lithium disilicate system are presented below.

The initial works for the development of materials in the lithium disilicate system were compositions that were derived from the stoichiometric composition of lithium disilicate (or phyllosilicate) crystals.[10] The base glasses with stoichiometric composition of 33.33 Li_2O – 66.66 SiO_2 (mol.%) revealed certain opacity when the Li_2O content ranged between 5 mol.% and almost stoichiometric amount of Li_2O in lithium disilicate. Vogel explained this phenomenon as glass in glass phase separation (immiscibility of glasses).[78] These results demonstrated that phase separation processes are likely to play a part in the nucleation of lithium disilicate glass-ceramics. However, if glass-ceramics are produced from base glasses with the exact stoichiometric composition phase separation does not occur. For many years after Stookey's fundamental findings,[47-48] the mechanisms of nucleation were never completely determined although many comprehensive studies have been conducted regarding the nucleation of base glasses with stoichiometric composition of lithium disilicate for glass-ceramic manufacture.[11, 117]

Stookey[48] incorporated metal ions, such as silver (Ag^+) in glasses near the lithium disilicate composition as nucleating agents for controlling the crystallization of base glasses comprising the typical composition (wt.%): 80 SiO_2, 4 Al_2O_3, 10.5 Li_2O, 5.5 K_2O, 0.02 CeO_2, 0.04 AgCl. The formation of neutral silver was achieved by exposition to UV light. With subsequent heat treatment of the glasses (at about 600 ºC) colloids of metallic silver were obtained, which forms heterogeneous small nuclei (~8 nm) needed for the subsequent crystallization of lithium metasilicate primary crystal phase.[118] Lithium metasilicate possesses a chain silicate structure, features dendritic crystallization and its crystals are easily dissolved from the glass-ceramic in dilute hydrofluoric acid (HF). This knowledge permitted Stookey to develop a high-precision patterned glass-ceramic, the structure of which results from the etching.[47] High-precision structural parts in different shapes were produced by placing a mask on the material and exposing the open areas to UV light. This was the beginning of the production of a new product predominantly composed of a glass matrix and named Fotoform. If these products are

exposed to additional UV and thermal treatment, a lithium disilicate main crystal phase is produced.

Apart from the possibilities of shaping the glass-ceramic as desired, Stookey[116] and McMillan[11] discovered additional properties of these glass-ceramics, which were very promising for industrial applications of the material. These works were clear evidence of the importance of non-stoichiometric compositions in the $Li_2O–SiO_2$ system.

In the early 1960s, Kalinina and Filipovich[119] investigated the phases and the crystallization sequence in $Li_2O–SiO_2$ glasses using XRD analysis. They concluded that homogeneous bulk crystallization of both lithium disilicate and lithium metasilicate occurred, depending on the initial glass compositions. For example, the 34.2 mol.% Li_2O glass compositions crystallized into both lithium disilicate and lithium metasilicate, depending on the temperature. Heat treatment at lower temperature (*e.g.*, 480 °C) led to crystallization of lithium disilicate while heat treatment at higher temperatures (*e.g.*, 630 °C) led to crystallization of both lithium disilicate and lithium metasilicate. In general, the metasilicate phase has lower intensities on an X-ray diffraction pattern than the disilicate phase, so it is harder to detect. The glass composition comprising 43.7 mol.% Li_2O crystallized into lithium metasilicate after 24 h at 480 °C.

West and Glasser (1971)[120] performed an extensive study on the crystallization of $Li_2O–SiO_2$ glasses using X-ray diffraction. They did not detect lithium metasilicate crystallization at composition equal to or less than 36 mol.% Li_2O for any heat treatment time or temperature. Difficulties arose in determining phases from the XRD patterns of materials treated at lower temperatures due to the low intensities in X-ray diffraction patterns. Lithium metasilicate crystallization was found to precede lithium disilicate crystallization as a metastable phase in some silicate glasses. Hench *et al.* (1971)[113] determined that lithium metasilicate crystal forms before lithium disilicate in two glass compositions of 30 and 33 mol.% Li_2O, but the amount of lithium metasilicate was extremely small and it disappeared on further heat treatment.

In 1972, Tomozawa[121] and Doremus *et al.*[122] focused on the nucleation and growth behaviour of lithium disilicate crystal from glasses near lithium disilicate compositions. When the Li_2O content is less than the disilicate composition, metastable glass-in-glass phase separation occurs and influences crystal nucleation and crystal growth.[121]

In the late 1970s and early 1980s, several researchers focused on the nucleation kinetics for lithium disilicate glass.[117, 123-124] The experimentally determined nucleation rates obtained in

their research works were much higher than that predicted by the classical theory. The formation of a metastable crystalline precipitate prior to crystallization of the final equilibrium composition was suggested as a possible explanation for that difference. Joseph and Pye [123] stated that a metastable phase, whether glass or crystal, precedes lithium disilicate crystallization, but they failed to identify it. Further, prior heat treatment of the disilicate composition showed no metasilicate crystal or amorphous phase separation, only crystallization of lithium disilicate.[124]

In 1980 Ahmed *et al.* investigated the leaching of binary and ternary silicate glasses and glass-ceramics by HCl.[125] The leaching rate of binary lithium silicate glasses exhibiting liquid-liquid phase separation increases with the increase of the volume fraction of the easily leachable phase.[125] When a third component was introduced, the leachability of glass was remarkably affected by the effect of the third component on phase separation. Oxides which eliminate phase separation are the most effective in improving the leachability of glass. If the oxide promotes phase separation the deteriorating effect of the easily leachable phase will rapidly become the dominant factor. For glass-ceramics, the solubilities of both the formed crystals and the residual glass phase in the leaching solution have an almost equally important influence on the stability of glass-ceramics as exemplified by lithium silicate glass-ceramics containing ZnO or B_2O_3.

The chemical durability of lithium disilicate glass-ceramics was improved by Barret *et al.* [126] to a significant extent by incorporating additions such as Al_2O_3 and K_2O to the stoichiometric base glass. Improving the chemical durability of these glass-ceramics was essential to make the material suitable for use as a biomaterial in human medicine and, in particular, as a restorative material in dentistry. It must be noted that a significant improvement of the chemical durability of lithium disilicate glass-ceramics was achieved later in the development of glass ceramics with non-stoichiometric compositions (non-stoichiometric implies that the SiO_2:Li_2O molar ratio deviates from 2:1 and that the system is rendered considerably more complex with numerous additional components).[10]

A nucleating agent may be broadly defined as a constituent added to a glass, typically in amount of a few percent, which promote volume nucleation and enable a glass-ceramics to be produced. Examples are metallic particles, oxides and non-oxides. P_2O_5 is common nucleating agent for lithium silicate glass-ceramics, which promotes heterogeneous nucleation and produces a fine grained interlocking morphology after heat treatment.[127] James (1982)[65] found that the crystal nucleation rate of lithium disilicate in $33.3Li_2O{\cdot}65.7SiO_2{\cdot}1P_2O_5$ (mol.%) glass

were 1000 times greater than in $Li_2O{\cdot}2SiO_2$ base glass at 500 °C. Amorphous phase separation was observed in the glass containing P_2O_5 but not in the $Li_2O{\cdot}2SiO_2$ base glass.

Headley and Loehman (1984)[114] found that Li_3PO_4 crystals were precipitated from a $Li_2O–Al_2O_3–SiO_2$ based glass after treatment at high temperature in the range 800–1000 °C. Lithium disilicate, lithium metasilicate and cristobalite were observed to crystallize by epitaxial growth on the Li_3PO_4 crystals.

In the beginning of 1990s, Beall[128] and Echeverría[129] achieved notable results in the development of a new lithium disilicate glass-ceramic. The new material is distinguished by the particular ratios of SiO_2 and Li_2O, which are responsible for the formation of the main crystal phase; the nucleating agents; and the components of the glass matrix. The chemical components were selected to confer good chemical durability.

Jacquin and Tomazawa (1995)[130] investigated the crystallization behaviour of lithium disilicate glass powder heated in molten $LiNO_3$ salt using X-ray diffraction techniques. Heat treatment with $LiNO_3$ molten salt caused a lithium metasilicate crystal phase to appear after 5–96 h. By contrast, glass powder heat-treated in air at 500 °C remained amorphous after 5 h and turn into lithium disilicate crystal after 40 h. Glass powder heat treated at 575 °C in both molten salt and in air turned into lithium disilicate crystal. Metasilicate crystallization occurs with $LiNO_3$ molten salt at 500 and 400 °C due to the incorporation of lithium into the sample glass powder from the melt during crystallization. An increase in lithium content in the sample after molten salt heat treatment was confirmed by chemical analysis using dc plasma emission spectroscopy.

In addition to the examination of the nucleation mechanism of lithium disilicate glass-ceramics, the analysis of the microstructure and the improvement of the chemical durability of glass-ceramics with a stoichiometric composition were also major concern for glass researchers. On the pursuit of this goal, Schmidt and Frischat[131] (1997) got images of various structures by using scanning electron microscopy in conjunction with atomic force microscopy. Furthermore, they were also able to control the development of these structures.

Goto *et al.* [132] developed a lithium disilicate glass-ceramic with composition (wt.%) 65–83 SiO_2, 8–13 Li_2O, 0–7 K_2O, 0.5–5.5 (sum of MgO, ZnO, PbO), with 0–5 ZnO, 0–5 PbO, 1–4 P_2O_5, 0–7 Al_2O_3 and 0–2 (As_2O_3, Sb_2O_3) for magnetic memory disk substrates.

In 1998, Iqbal *et al.*[133] investigated $Li_2O–SiO_2$ glass containing P_2O_5 by XRD, TEM and NMR. They found metastable phases of lithium disilicate phase increased. No evidence was

found for the presence of Li_3PO_4 crystalline phase from XRD, possible because of the small percentage present. However, preliminary result using ^{31}P MAS NMR of 1 mol.% P_2O_5 glass did indicate possible formation of the Li_3PO_4 phase in the heat treated glasses and even in the as-quenched glasses. For the composition containing 5 mol.% P_2O_5 XRD revealed crystalline Li_3PO_4 in the as-quenched glass and after an extend heat treatment. TEM revealed the presence of high density of fine volume nucleated crystals in the P_2O_5 containing glasses, much higher than in the base lithium disilicate glass after similar heat treatment.

Using a special hot-press procedure, Schweiger *et al.* developed a powder-processed lithium disilicate glass-ceramic.[134-135] To optimize the viscous properties for the hot-press procedure at approximately 920 ºC, components such as La_2O_3, MgO, and pigments were added to the main components SiO_2, Li_2O, P_2O_5, K_2O and ZnO. An ingot is transformed into a viscous state at approximately 10^5–10^6 Pa.s in a special hot-press apparatus (EP 500, Ivoclar Vivadent AG, Lichtenstein). Thereafter, it is pressed at approximately 920 ºC for about 15 min to form a glass-ceramic body. This glass-ceramic of the lithium disilicate type does not require additional heat treatment and the end-product contains main crystal phases of $Li_2Si_2O_5$ and Li_3PO_4.

Soares *et al.* (2003)[136] studied the early crystallization of lithium disilicate glasses using TEM and XRD techniques. Three lithium silicate glasses nearby the $Li_2O{\cdot}2SiO_2$ composition were heat treated at ~T_g = 454 °C, two distinct crystalline phases, stable lithium disilicate and metastable lithium metasilicate coexist up to 120 h at 454 °C (crystalline fraction < 1 vol.%). For longer treatments (240–600 h) only the stable phase ($Li_2O{\cdot}2SiO_2$) was observed.

Mishima *et al.* (2004)[137] studied the crystallization behaviour of $xLi_2O{\cdot}(1–x)Na_2O{\cdot}2SiO_2$ glass doped with platinum (Pt). It was found that the addition of Pt induced the crystallization of $Li_2O{\cdot}SiO_2$ in the interior of crystallized glasses with high Na_2O (x = 0.4 to 0.6) and $Li_2O{\cdot}2SiO_2$ were observed in crystallized glasses with high $Li_2O{\cdot}SiO_2$ were observed also in the range of x = 0.6 to 0.8.

Morimoto and Emem (2004)[138] studied the properties of the glass-ceramic with composition $77.7SiO_2{\cdot}2.2Al_2O_3{\cdot}18.8Li_2O{\cdot}1.2P_2O_5$ (mol.%). They found that the transparent glass-ceramics can be obtained by heat treatment below 800 °C. The main crystalline phase is $Li_2O{\cdot}2SiO_2$. The percent crystallinity and crystal size ranged from 60 to 70% and from 20 to 60 nm, respectively. The density of glass-ceramics increases with increasing heating

temperature and time of crystallization. The fracture strength of transparent glass-ceramics increases linearly with crystal size ranging from 20–60 nm.

Morimoto[139] investigated the effect of K_2O on the crystallization in $Li_2O–SiO_2$ glass. It was found that a small amount of K_2O affected the mechanism of phase separation and crystallization process. Moreover, it was also concluded that K_2O suppressed the crystallization of $Li_2O{\cdot}2SiO_2$, but promotes the precipitation of $Li_2O{\cdot}SiO_2$ crystal. $Li_2O{\cdot}SiO_2$ crystal can precipitate in Li_2O rich continuous phase containing K_2O.

In 2006, Fuss *et al.*[140] studied the effect of pressure on crystal growth rate *U* of lithium disilicate glasses. They conclude that the crystal growth rate in a $Li_2O{\cdot}2SiO_2$ glass is suppressed and the *U*-curve shifts to higher temperatures with increasing pressure up to 6 GPa. They attributed this behaviour to an increase in viscosity. The glass partially crystallized under a hydrostatic pressure of 4.5 GPa has a density higher than that of crystalline $Li_2O{\cdot}2SiO_2$, comparable to or smaller than the density of $Li_2O{\cdot}SiO_2$ crystals. The density of the glass becomes comparable or larger than that of crystalline $Li_2O{\cdot}SiO_2$ when pressed at 6 GPa.

Kuzielová and co-workers,[141] presented a preliminary investigation of the lithium disilicate and the fluoroapatite crystallization in bio-glass ceramics. Composite glass-ceramics with various content of P_2O_5 in oxide system $SiO_2–Li_2O–CaO–CaF_2–P_2O_5$ were prepared by heat treatment of glass at different temperatures and lithium disilicate and fluorapatite were developed in the samples depending on P_2O_5 content and temperature. It was evidenced that addition of P_2O_5 has caused the formation of fluoroapatite, whereas the amorphous fluorapatite inhibited the crystallization of $Li_2O{\cdot}2SiO_2$, the crystalline fluorapatite promoted it. The obtained glass-ceramics featured hardness values that satisfy the requirements set on implants used in loading parts of human organism.

Apel *et al.* [142] (2007) evaluated the effect of the incorporation of ZrO_2 on phase formation, microstructure, biaxial flexural strength and translucency for glasses in the $Li_2O–SiO_2–Al_2O_3–K_2O–P_2O_5$ system. According to this study, ZrO_2 influences the reaction kinetics of the crystallization processes of both lithium metasilicate and lithium disilicate. The ZrO_2-free glass-ceramic has a very fine and strong microstructure. The incorporation of ZrO_2 into the glass matrix does not increase the strength due to an increase in the viscosity content in the glass-ceramic and the linked reduction in crystal growth of Li_2SiO_3 and $Li_2Si_2O_5$. The addition of ZrO_2 increases the translucent properties of the glass-ceramic leading to contrast

ratio values between 0.35 and 0.80. Therefore, the translucency of this lithium disilicate glass-ceramic can be customized for applications in aesthetic restorative dentistry.

The effects of P_2O_5 content and heat treatment on the species of crystalline phase and microstructure of lithium disilicate glass ceramics were studied by Zheng *et al.*.[143] According to this work, the crystallization temperature decreased and nucleation density increased with increasing P_2O_5 content (from 0 to 4 mol.%). Therefore, the microstructure was refined from plate-like polycrystalline aggregates to interlocking rod-shaped crystals and even spherical crystalline phases. The results suggested that Li_3PO_4 crystals acted as the heterogeneous nucleation sites for Li_2SiO_3 crystals, which could be the precursors of $Li_2Si_2O_5$ crystals. Furthermore, $Li_2Si_2O_5$ probably crystallized by epitaxial growth on Li_2SiO_3 crystals. With increasing P_2O_5 content, the relative content of $Li_2Si_2O_5$ crystals decreased and Li_2SiO_3 and Li_3PO_4 crystals increased in one- and two-stage treatments. Moreover, the precipitation of $Li_2Si_2O_5$ crystals was hampered during the one-stage treatment and the two-stage treatment was favourable for the growth of stable $Li_2Si_2O_5$ crystals.

The mechanism and kinetics of crystallization as functions of grain size and rate of heating in lithium disilicate glasses with and without fluorapatite were investigated by Palou *et al.*.[144] Their results showed that smaller particles crystallize preferentially by surface crystallization, which is replaced by volume crystallization at larger particle sizes. Moreover, the inclusion of fluorapatite in the lithium disilicate glasses favours crystallization through the surface mechanism. The calculated activation energies of the glasses indicate that the tendency of glass to crystallize is enhanced by the presence of fluorapatite. Also, *in vitro* testing demonstrated an improvement in bioactivity for the glasses and glass-ceramics containing fluorapatite.

Abd El All and Ezz-Eldin[145] studied some physical properties of lithium disilicate glasses doped with different ratios of V_2O_5 were investigated before and after gamma-rays irradiation. Results indicate that crystallization is predominantly controlled by a surface nucleation mechanism, even though a partial bulk nucleation has been encountered in composition containing more than 2 wt.% of doping oxide. The microstructure of the glass-ceramic materials clearly shows a marked dependence upon the amount of V_2O_5 due to the presence of phase separation for content higher than 0.5 wt.%. Increasing V_2O_5 ratio causes remarkable changes in the properties studied. The observed variations in the properties may be correlated with the changes in internal glass network with changes in the chemical composition.

Vanadium ions are believed to be present in three possible valence states V^{3+}, V^{4+} and V^{5+}, and the ratios of these states depend on glass composition.

The possibility of using P_2O_5 and Nb_2O_5 as nucleation agent in the TiO_2–ZrO_2–Li_2O–CaO–Al_2O_3–SiO_2 system was investigated by Goharian *et al.*.[146] They showed that in glass-ceramics comprising nano and submicron P_2O_5, the main crystalline phase was lithium disilicate. The results also showed that change of P_2O_5 particle's size had significant effect on the crystalline phases and microstructure, *i.e.*, with decreasing the size of P_2O_5 particles, the relative content of $Li_2Si_2O_5$ crystals was increased and the microstructure of glass-ceramic was changed, leading to better mechanical properties. By replacement of submicron P_2O_5 with submicron Nb_2O_5, crystallization mechanism was changed from volume to surface crystallization.

Recently, Bischoff *et al.* [147] used quantitative ^{29}Si MAS-NMR and ^{29}Si{7Li} rotational echo double resonance (REDOR) NMR spectroscopy to evaluate the crystallization mechanism of a high-strength lithium disilicate glass-ceramic in the SiO_2–Li_2O–P_2O_5–Al_2O_3–K_2O–(ZrO_2) system, used as restorative dentistry material. According to them, although the SiO_2/Li_2O ratio is higher than 2, the formation of Li_2SiO_3 (SiO_2/Li_2O=1) plays a prominent role in the crystallization mechanism, contrary to the situation in stoichiometric glasses where $Li_2Si_2O_5$ is formed directly. In the studied system, the first crystallization product is lithium metasilicate (formed at 650 to 700 ºC). At higher temperature, this material reacts with amorphous SiO_2 to produce the final lithium disilicate crystallization product. The obtained results illustrated that the lithium ions tend to be clustered in the glassy starting material and remain clustered to some extent in the glassy phase that stays behind after Li_2SiO_3 crystallization via reaction $2Q^3_{(glass)} \leftrightarrow Q^2_{(cryst.)} + Q^4_{(glass)}$. This crystallization process also results in some segregated glassy SiO_2 material. At higher temperatures, lithium metasilicate reacts with the surrounding glassy material via reaction $Q^4_{(glass)} + Q^2_{(cryst.)} \leftrightarrow 2Q^3_{(cryst.)}$, resulting in the formation of crystalline lithium disilicate in addition to a residual glass matrix in which the lithium ions are quite well-dispersed. Moreover, the absence of a well-ordered crystalline Li_3PO_4 phase below crystallization temperatures (850 ºC) suggests that the formation of the crystalline silicate phases cannot be understood as heterogeneous nucleation processes through epitaxy, but as a heterogeneous nucleation at the interface of an amorphous lithium phosphate phase and the glass matrix.

The effects of densification and crystallization at high pressure of lithium disilicate glasses on the mechanical properties were evaluated by Buchner and co-workers.[148] They concluded that

the hardness and elastic modulus of the samples submitted to high pressure at room temperature decreased with increasing pressure. On the other hand, the hardness and elastic modulus of the samples submitted simultaneously to high pressure (up to 7.7 GPa) and high temperature increased noticeably, showing that the high temperature treatment under high pressure improved the mechanical properties of lithium disilicate glass-ceramics.

Khalkhali and collaborators[149] evaluated the Weibull modulus, flexural strength, fracture toughness, Vickers microhardness, and chemical durability of sintered lithium disilicate glass ceramic specimens doped with P_2O_5 or ZrO_2. They observed that phase formation induced by the addition of P_2O_5 led to precipitation of Li_3PO_4, which in turn caused more intensive crystallization of Li_2SiO_3. The high-temperature crystalline phase $Li_2Si_2O_5$ was precipitated more intensively in P_2O_5 containing specimens resulting in an interlocked microstructure of needle like disilicate crystals, conferring to the materials good mechanical and chemical properties (values of 3-point flexural strength and chemical resistance of 181±15 MPa and 53±9 μg cm^{-2}, respectively). Addition of ZrO_2 led to a high glass viscosity which deteriorate both sintering and crystallization.

Mahmoud *et al.* [150] investigated the crystallization of lithium disilicate glass using a variable frequency microwave (VFM) processing technique, showing that it was possible to crystallize lithium disilicate glass in a significantly shorter time and lower temperature, when compared with conventional heating process.

2.4.3 Technological importance of lithium disilicate based glass-ceramics

Lithium disilicate glass-ceramics feature highly interesting properties such as high flexural strength, outstandingly high fracture toughness and high electrical resistivity.[10, 151] These electrical properties combined with a low loss factor are impressive for a glass-ceramic with a high alkaline ion content. Lithium disilicate glass-ceramics also demonstrate a relatively high linear coefficient of thermal expansion (~105×10^{-7} K^{-1}). This property is favourable for the fabrication of special composite materials, *e.g.* for sealing to metal substrates in the electrical industry.[128] Therefore, these properties presented ideal prerequisites for applications in electrical engineering. Some specific and interesting application fields of lithium disilicate based glass-ceramics are listed below as examples for the technological importance of these materials.

2.4.3.1 Dental materials

All-ceramic dental restorations are attractive to dentists and patients, because they are biocompatible, have superior aesthetics and their low thermal conductivity makes them comfortable in the mouth.[10] Moreover, the material is extremely durable, and it is relatively easy to manufacture to customized units. All-ceramic restorations can be used to cover even dark tooth cores (*e.g.*, if the tooth is severely discoloured or a titanium abutment is used). Current commercial lithium disilicate glass-ceramics, *e.g.*, IPS e.max® (Ivoclar, Liechtenstein) are ideal for fabricating single-tooth restorations.[59] This innovative glass-ceramic produces highly aesthetic results. Its hardness is similar to that of natural teeth, and it is two to three times stronger than other dental glass-ceramics. The material can be either pressed or machined to the desired shape in the dental laboratory and restorations fabricated with this material can be cemented by various techniques. These glass-ceramics possess true-to-nature shade behaviour, natural looking aesthetics, natural-looking light transmission, versatile applications and a comprehensive spectrum of indications.[10, 59]

2.4.3.2 Electronic applications

Electrically insulating materials such as lithium disilicate based glass-ceramics, *e.g.* produced by Corning Inc. (U.S.A.)[152] or Ohara Inc. (Japan)[132, 153], are used in magnetic media disks for hard disk drives. These materials offer the key properties necessary for today's higher areal density, smaller, thinner drive designs. They have high toughness, provide low surface roughness and good flatness, ultralow glide heights and excellent shock resistance. On the other hand, lithium-ion conducting glass-ceramics are promising solid electrolytes for lithium batteries.

2.4.3.3 Military applications

Some patents have been filed and others have been granted for inventions related to armour materials for the protection of people or equipment against high-speed projectiles or fragments. Ceramic materials are used particularly in armours for which low weight is important: bullet-proof vests; and armour for automobiles, aircraft and helicopters, especially in cockpits or seats and for protection of functionally important parts. The first and still-used ceramic armour materials consist of high modulus and hard Al_2O_3, although its density is quite high (about 4 g cm^{-3}). Other very hard, but less dense materials, such as SiC and B_4C,

can be produced only at very high temperatures by costly manufacturing processes and are, hence, expensive.

Most glass-ceramics have lower hardness and Young's modulus than the above-described ceramics, but have the great advantage of low density and much lower cost. Moreover, glass-ceramics can be transparent to visible light. For instance, TransArm (Alstom Grid Ltd, UK) is a transparent glass-ceramic armour based on lithium disilicate.[154] It originally was developed for protective visors for bomb disposal work. The preferred composition for the glass-ceramic armour is 71.8 SiO_2, 11 Li_2O, 8 ZrO_2, 2 P_2O_5, 4.5 Al_2O_3, 0.5 ZnO, 2.2 K_2O (wt.%). The manufacturing of the armour is carried out by heat-treating a base lithium disilicate glass to a transparent glass-ceramic, which is then submitted to a molten-salt to promote ion exchange at the surface of the material, resulting in an even higher level of resistance. The glass-ceramic armour can be attached to a transparent back-up plate (*e.g.* polycarbonate), so as to avoid the shards of the ballistic impacted sheet to spread, but also to absorb part of the impacting energy through ductility. This innovative armour material can be used in visors, vehicle observation and helicopter windscreens.[154]

However, there is little available information on this particular use of glass-ceramics, compared with other applications, due to the sensitive nature of this military-related research.

Lithium disilicate based glasses and glass-ceramics have been subject of many research works, ranging from stoichiometric to non-stoichiometric compositions, from simple binary system to very complex compositions, regarding just theoretical concepts or aiming functional applications. Glass crystallization kinetics, structure-properties relationships, or sintering and crystallization of glass powder compacts are just some examples of scientific and technological interest about lithium disilicate based glasses and glass-ceramics. Commercial lithium disilicate glasses and glass-ceramics feature complex compositions with the presence of nucleating agents (usually P_2O_5). Nevertheless, a systematic research work aiming to develop and characterize lithium disilicate glasses and glass-ceramics based on a very simple system such as $Li_2O–K_2O–Al_2O_3–SiO_2$ aiming both scientific and technological (functional applications) has not been yet published. Thus, the present manuscript aims to present the results of the scientific research work carried on the $Li_2O–K_2O–Al_2O_3–SiO_2$ glass system, including the study of glass structure, crystallization kinetics, sintering behaviour, evaluation of properties and possible (purposed) functional applications for the obtained materials.

References

1. Doremus RH. Glass Science. New York: Wiley; 1994.
2. Gutzow I, Schmelzer J. The vitreous state. Berlin: Springer-Verlag; 1995.
3. Paul A. Chemistry of Glasses. 2nd ed: Chapman and Hall; 1990.
4. Rawson H. Inorganic Glass Forming Systems. New York: Pergamon Press; 1967.
5. Shelby JE. Introduction to glass science and technology. Cambridge: The Royal Society of Chemistry; 1997.
6. Varshneya AK. Fundamentals of Inorganic Glasses. London: Academic Press; 1994.
7. Vogel W. Glass Chemistry. Berlin: Springer; 1994.
8. Zarzycki J. Glasses and the Vitreous State. Cambridge: Cambridge University; 1991.
9. Phillips CJ. Glass, the miracle maker: its history, technology, manufacture and applications. 2nd ed. New York: Pitman; 1948.
10. Höland W, Beall G. Glass-ceramic Technology. Westerville, Ohio: The American Ceramic Society; 2002.
11. McMillan PW. Glass–Ceramics. London: Academic Press; 1979.
12. Le Bourhis E. Glass: Mechanics and Technology. Weinheim: Wiley-VCH Verlag; 2008
13. Scholze H. Glass: Nature, Structure and Properties. Berlin: Springer; 1991.
14. Harper CA. Handbook of Ceramics, Glasses and Diamonds. New York: McGraw-Hill; 2001.
15. C162 - Compilation of ASTM Standard Definitions. Philadelphia: The American Society for Testing Materials; 1945.
16. Varshneya AK, Mauro JC. Comment on misconceived ASTM definition of glass by A. C. Wright. Glass Technology: European Journal of Glass Science and Technology Part A 2010;51(1):28-30.
17. Elliott SR. Physics of Amorphous Materials. London: Longman; 1990.
18. Mauro JC, Loucks RJ, Varshneya AK, Gupta PK. Enthalpy landscapes and the glass transition. Scientific Modeling and Simulation 2008;15(1-3):241-81.
19. Yamane M, Asahara Y. Glasses for photonics. Cambridge: Cambridge University Press; 2004.
20. Goldschmidt VM. Geochemische Vertailungsgesetze der Elemente. Oslo: Skrifter Norske Videnskaps-Akademie; 1926.
21. Zachariasen WH. The atomic arrangement in glass. Journal of the American Chemical Society 1932;54(10):3841-51.
22. Warren BE. X-ray determination of the structure of glass. Journal of the American Ceramic Society 1934;17(1-12):249–54.
23. Wright AC. Neutron and X-ray amorphography. Journal of Non-Crystalline Solids 1988;106(1-3):1-16.
24. Avramov I, Zanotto ED, Prado MO. Glass-forming ability versus stability of silicate glasses. II. Theoretical demonstration. Journal of Non-Crystalline Solids 2003;320:9-20.
25. Tamman G. Die Aggregatzustaende. Leipzig: Leopold Voss; 1922.
26. Turnbull D, Cohen M. Crystallization Kinetics and Glass Formation. London: Butterworths; 1960.
27. Uhlmann DR. A kinetic treatment of glass formation. Journal of Non-Crystalline Solids 1972 7(4):337-48.

28. Weinberg MC, Uhlmann DR, Zanotto ED. Nose method of calculating critical cooling rates for glass formation. Journal of the American Ceramic Society 1989;72(11):2054-58.
29. Weinberg MC, Zanotto ED. Calculation of the volume fraction crystallised in nonisothermal transformations. Physics and Chemistry of Glasses 1989;30(3):110-15.
30. Uhlmann DR, Zelinski BJJ, Zanotto ED, Weinberg MC. Sensitivity of critical cooling rate to model and material parameters. Paper presented at: XV International Congress on Glass, 1989; Leningrad, USSR.
31. Weinberg MC. Glass-forming ability and glass stability in simple systems. Journal of Non-Crystalline Solids 1994;167(1-2):81-88.
32. Cabral Jr. AA, Fredericci C, Zanotto ED. A test of the Hrubÿ parameter to estimate glass-forming ability. Journal of Non-Crystalline Solids 1997;219:182-86.
33. Volf BM. Technical approach to glass. New York: Elsevier science; 1990.
34. Rao KJ. Structural chemistry of glasses. Amsterdam: Elsevier Science & Technology Books; 2002.
35. Jones GO. Glass. Methuen: Wiley; 1956.
36. Kurkjian CR, Prindle WR. Perspectives on the History of Glass Composition. Journal of the American Ceramic Society 1998;81(4):795-813.
37. Wright AC, Bachra B, Brunier TM, Sinclair RN, Gladden LF, Portsmouth RL. A neutron diffraction and MAS-NMR study of the structure of fast neutron irradiated vitreous silica. Journal of Non-Crystalline Solids 1992;150(1-3):69-75.
38. Kirk RE, Othmer DF, Grayson M, Eckroth D. Encyclopedia of chemical technology. 5th ed. New Jersey: John Wiley & Sons; 2007.
39. Uhlmann DR, Kolbeck AG. Phase sepa- ration and the revolution in concepts of glass structure. Physics and Chemistry of Glasses 1976;17:146-58.
40. Pinkney LR. Glass ceramics. In: Buschow KHJ, Cahn R, Flemings MC, Ilschner B, Kramer EJ, Mahajan S, et al., editors. Encyclopedia of Materials: Science and Technology. Oxford: Pergamon; 2001.
41. Prado MO, Nascimento MLF, Zanotto ED. On the sinterability of crystallizing glass powders. Journal of Non-Crystalline Solids 2008;354:4589-97.
42. Rabinovich EM. Preparation of glass by sintering. Journal of Materials Science 1985;20(12):4259-97.
43. Scherer GW. Sintering of low density glasses: I. Theory. Journal of the American Ceramic Society 1977;60(5-6):236-39.
44. Strnad Z. Glass-ceramic Materials. Amsterdam: Elsevier; 1986.
45. James PF. Glasses and Glass-Ceramics London: Chapman and Hall; 1989.
46. Réaumur M. Memoires de l'Academie des Sciences, 1739. 1739:370-88.
47. Stookey SD. Chemical machining of photosensitive glass. Industrial and Engineering Chemistry 1953;45(1):115-18.
48. Stookey SD. Catalyzed Crystallization of glass in theory and practice. Industrial and Engineering Chemistry 1959;51(7):805-08.
49. Barsoum MW. Fundamentals of Ceramics. New York: McGraw-Hill International Editions; 1997.
50. Prado MO, Ferreira EB, Zanotto ED. Sintering kinetics of crystallizing glass particles: A Review. Paper presented at: 106th Annual Meeting of The American Ceramic Society, 2004; Indianapolis, Indiana, USA.
51. Pannhorst W. Glass ceramics: state-of-the-art. Journal of Non-Crystalline Solids 1997;219:198-204.
52. Beall GH. Refractory glass-ceramics aased on alkaline-earth aluminosilicates. Journal of the European Ceramic Society 2009;29:1211-19.

53. Andreola F, Barbieri L, Corradi A, Lancellotti I, Falcone R, Hreglich S. Glass-ceramics obtained by the recycling of end of life cathode ray tubes glasses. Waste Management 2005;25(2):183-89.
54. Liu H, Lu H, Chen D, Wang H, Xu H, Zhang R. Preparation and properties of glass-ceramics derived from blast-furnace slag by a ceramic-sintering process. Ceramics International 2009;35:3181-84.
55. Suzdal'tsev EI, Zaichuk TV, Rozhkova TI. The waste used in the production of glass ceramics of lithium alumina-silicate composition. Refractories and Industrial Ceramics 2003;44(4):273-76.
56. Aza PN, Aza HH, Pena P, Aza S. Bioactive glasses and glass-ceramics. Boletin da la Sociedad Espanola de Cerámica e Vidrio 2007;46(2):45-55.
57. Dubok VA. Bioceramics – Yesterday, today, tomorrow. Powder Metallurgy and Metal Ceramics 2000;39(7-8):381-94.
58. Hench LL, Day DE, Höland W, Rheinberger VM. Glass and medicine. International Journal of Applied Glass Science 2010;1(1):104-17.
59. Höland W, Rheinberger V, Apel E, van Hoen C, Höland M, Dommann A, et al. Clinical applications of glass-ceramics in dentistry. Journal of Materials Science: Materials in Medicine 2006;17:1037-42.
60. Onyiriuka EC. AM 2001 lubricant film on canasite glass-ceramic magnetic memory disk. Chemistry of Materials 1993;5(6):798-801.
61. Sohn S-B, Choi S-Y. Crystallization behavior in the glass system $MgO–Al_2O_3–SiO_2$: influence of CeO_2 addition. Journal of Non-Crystalline Solids 2001;282:221-27.
62. Mahapatra MK, Lu K. Glass-based seals for solid oxide fuel and electrolyzer cells - A review. Materials Science and Engineering 2010;R 67:65-85.
63. Carter CB, Norton MG. Ceramic materials - Science and engineering. New York: Springer; 2007.
64. Tammann G. Glass as supercooled liquids. Journal of Society of Glass Technology 1925;9:166-85.
65. James PF. Nucleation and crystallization in glasses. In: Simmons JH, Uhlmann DR, Beall GH, editors. Advances in ceramics. Columbus: American Ceramic Society; 1982.
66. Burke J. The Kinetics of Phase Transformation in Metals. New York: Pergamon Press; 1965.
67. Fokin VM, Zanotto ED. Crystal nucleation in silicate glasses: the temperature and size dependence of crystal/liquid surface energy. Journal of Non-Crystalline Solids 2000;265(1-2):105-12.
68. Callister Jr WD. Fundamentals of materials science and engineering. New York: John Wiley & Sons; 2001.
69. Kingery WD, Bowen HK, Uhlmann DR. Introduction to Ceramics. New York: Wiley; 1975.
70. Beall GH, Duke DA. Glass-ceramic technology. In: Uhlmann DR, Kreidl NJ, editors. Glass science and technology. Orlando: Academic; 1983.
71. Pannhorst W. Surface nucleation: collection of papers. Charleroi: International Commission on Glass; 2000.
72. Pye LD, Stevens HJ, LaCourse WC. Introduction to glass science. New York: Plenum Press; 1972.
73. Rogers PS. The initiation of crystal growth in glasses. Mineralogical Magazine 1970;37(291):741-58.
74. Williamson J. The kinetics of crystal growth in an aluminosilicate glass containing small amounts of transition-metal ions. Mineralogical Magazine 1970;37(291):759-70.

75. Uhlmann DR. Crystal Growth in Glass-Forming Systems: A Ten-Year Perspective. In: Simmons JH, Uhlmann DR, Beall GH, editors. Advances in Ceramics. Columbus: American Ceramic Society; 1982. p. 80-124.
76. Uhlmann DR, Uhlmann EV. Crystal growth and melting in glass-forming systems, a view from 1992. Ceramic Transactions 1993 30:109-40.
77. Uhlmann DR, Hays JF, Turnbull D. The effect of high pressure on crystallization kinetics with special reference to fused silica. Physics and Chemistry of Glasses 1966;7:159-68.
78. Vogel W. Structure and Crystallization of Glasses. Leipzig: Pergamon Press; 1971.
79. Mazurin OV, Porai-Koshits EA. Phase Separation in Glasses. Amsterdam: North-Holland; 1984.
80. Mazurin OV. Physical properties op phase separated glasses. Journal of Non-Crystalline Solids 1987;95-96 71-82.
81. Tomozawa M. Immiscibility of glass forming systems. Journal of Non-Crystalline Solids 1986;84(1-3):142-50.
82. Tomozawa M, McGahay V, Hyde JM. Phase separation of glasses. Journal of Non-Crystalline Solids 1990;123 (1-3):197-207.
83. Uhlmann DR. Microstructure of glasses: Does it really matter?. Journal of Non-Crystalline Solids 1982;49(1-3):439-60.
84. James PF. Liquid-phase separation in glass-forming systems. Journal of Materials Science 1975;10(10):1802-25.
85. Filipovich VN, Mazurin OV, Porai-Koshits EA. Phase Separation in Glass. Amsterdam: North Holland; 1984.
86. Levin EM, Block S. Structural interpretation of immiscibility in oxide systems: I, Analysis and calculation of immiscibility. Journal of the American Ceramic Society 1957;40(3):95-106.
87. Block S, Levin EM. Structural interpretation of immiscibility in oxide systems: II, Coordination principles applied to immiscibility. Journal of the American Ceramic Society 1957;40(4):113-18.
88. Levin EM, Block S. Structural interpretation of immiscibility in oxide systems: III, Effect of alkalis and alumina in ternary systems. Journal of the American Ceramic Society 1958;41(2):49-54.
89. Levin EM. Structural interpretation of immiscibility in oxide systems: IV, Occurrence, extent, and temperature of the monotectic. Journal of the American Ceramic Society 1967;50(1):29-38.
90. Vogel W. Phase separation in glass. Journal of Non-Crystalline Solids 1977;25(1-3):170-214.
91. Seward TP. Metastable phase diagrams and their application to glass-forming ceramic systems. In: Alper AM, editor. Phase Diagrams - Materials Science and Technology. New York: Academic Press; 1970.
92. Levin EM. Liquid immiscibility in oxide systems. In: Alper AM, editor. Phase Diagrams - Materials Science and Technology. New York: Academic Press; 1970.
93. Kracek FC. The cristobalite liquidus in the alkali oxide-silica systems and the heat of fusion of cristobalite. Journal of the American Chemical Society 1930;52(4):1436-42.
94. Kracek FC. The binary system $Li_2O–SiO_2$. Journal of Physical Chemistry 1930;34(12):2641-50.
95. Charles RJ. Activities in $Li_2O–$, $Na_2O–$, and $K_2O–SiO_2$ Solutions. Journal of the American Ceramic Society 1967;50(12):631-41.
96. Cahn JW, Charles RJ. Initial stages of phase separation in glasses. Physics and Chemistry of Glasses 1965;6(5):181-91.

97. Kreidl N. Phase separation in glasses. Journal of Non-Crystalline Solids 1991;129(1-3):1-11.
98. Uhlmann DR, Kolbeck AG. Phase separation and revolution in concepts of glass structure. Physics and Chemistry of Glasses 1976;17(5):146-58.
99. Weinberg MC, Shneidman VA, Osborne ZA. On the composition of the critical nucleus in phase separating glasses. Physics and Chemistry of Glasses 1996;37 (2):49-50.
100. Zarzycki J, Naudin F. Spinodal decomposition in the B_2O_3–PbO–Al_2O_3 system. Journal of Non-Crystalline Solids 1969;1(3):215-34.
101. Haskell RW. Introduction to the thermodynamics of spinodal decomposition. Journal of the American Ceramic Society 1973;56(7):355-60.
102. Seward TP, Uhlmann DR, Turnbull D. Development of two-phase structure in glasses, with special reference to the system BaO–SiO_2. Journal of the American Ceramic Society 1968;51(11):634-42.
103. Jantzen CM, Schwahn D, Schelten J, Herman H. The SiO_2-Al_2O_3 system: I Later stage spinodal decomposition and metastable immiscibility. Physics and Chemistry of Glasses 1981;22:122-37.
104. Wheaton BR, Clare AG. Evaluation of phase separation in glasses with the use of atomic force microscopy. Journal of Non-Crystalline Solids 2007;353:4767-78.
105. Ohlberg SM, Golub HR, Strickler DW. In: Reser MK, Smtih G, Insley H, editors. Symposium on Nucleation and Crystallization in Glasses and Melts. Columbus: American Ceramic Society; 1962.
106. Kim SS, Sanders TH. Thermodynamic modeling of phase diagrams in binary alkali silicate systems. Journal of the American Ceramic Society 1991;74(8):1833-40.
107. Glasser FP. Crystallization of lithium disilicate from $Li_2O.SiO_2$ glasses. Physics and Chemistry of Glasses 1967;8(6):224-32.
108. El-Meliegy E, van Noort R. Glasses and Glass Ceramics for Medical Applications. New York: Springer; 2012.
109. West AR, Glasser FP. Crystallisation of lithium trisilicate, $Li_2Si_3O_7$, from Li_2O–SiO_2 melts. Materials Research Bulletin 1970;5:837-42.
110. Strnad Z. Glass Science and Technology. New York: Elsevier; 1986.
111. Lewis MH. Glasses and Glass-Ceramics. London: Chapman and Hall; 1989.
112. West AR. Solid State Chemistry and its Applications. New York: John Wiley and Sons; 1984.
113. Hench LL, Frieman SW, Kinser DL. Early stages of crystallization in a Li_2O–$2SiO_2$ Glass. Physics and Chemistry of Glasses 1971;12(2):58-63.
114. Headley TG, Loehman RE. Crystallization of Glass–Ceramics by Epitaxial Growth. Journal of the American Ceramic Society 1984;67:620-25.
115. Matusita K, Tashiro M. Rate of homogeneous nucleation in alkali disilicate glasses. Journal of Non-Crystalline Solids 1973;11(5):471-84.
116. Stookey SD, inventor; Corning Glass Works, assignee. Photosensitively opacifiable glass. 1954.
117. James PF. Kinetics of crystal nucleation in silicate glasses. Journal of Non-Crystalline Solids 1985;73:517-40.
118. Beall GH. Design and properties of glass-ceramics. Annual Review of Materials Science 1992;22:91-119.
119. Kalinina A, Filipovich VN. The structure of glass-catalyzed crystallization of glass. In: Porai-Koshits EA, editor. The structure of glass. New York: Consultan Bureau; 1964.

120. West AR, Glasser FP. Advances in nucleation and crystallization in glasses. Columbus: American Ceramic Society; 1971.
121. Tomozawa M. Liquid phase separation and crystal nucleation in $Li_2O–SiO_2$. Physics and Chemistry of Glasses 1972;13(6):161-66.
122. Doremus RH, Turkalo AM. Crystallization of lithium disilicate in lithium silicate-glasses. Physics and Chemistry of Glasses 1972;13(1):14-&.
123. Joseph I, Pye LD. Collected papers. Paper presented at: 14th International Congress on Glass, 1986; Calcutta.
124. Neilson GF, Weinberg MC. A test of classical nucleation theory: crystal nucleation of lithium disilicate glass. Journal of Non-Crystalline Solids 1979;34(1):137-47.
125. Ahmed AA, El-Batal HA, Ghoneim NA, Khalifa FA. Leaching of some lithium silicate glasses and glass-ceramcs by HCl. Journal of Non-Crystalline Solids 1980;41:57-70.
126. Barrett JMG, FL), Clark, David E. (Gainesville, FL), Hench, Larry L. (Gainesville, FL), inventor; The Board of Regents, State of Florida, University of Florida (Tallahassee, FL), assignee. Glass-ceramic dental restorations. 1980.
127. von Clausbruch CS, Schweiger M, Holand W, Rheinberger V. The effect of P_2O_5 on the crystallization and microstructure of glass-ceramics in the $SiO_2–Li_2O–K_2O–ZnO–P_2O_5$ system. Journal of Non-Crystalline Solids 2000;263(1-4):388-94.
128. Beall G. Glass-ceramics: Recent developments and application. Ceramic Transactions 1993;30:241-66.
129. Echevería LM. New lithium disilicate glass-ceramics. Boletin da la Sociedad Espanola de Cerámica e Vidrio 1992;5:183–88.
130. Jacquin JR, Tomozawa M. Crystallization of lithium metasilicate from lithium disilicate glass. Journal of Non-Crystalline Solids 1995;190(3):233-37.
131. Schmidt A, Frischat GH. Atomic force microscopy of early stage crystallization in $Li_2O.SiO_2$ glasses. Physics and chemistry of glasses 1997;38(3):161-66.
132. Goto N, Yamaguchi K, inventors; Ohara, K.K., assignee. Magnetic disk substrate and method for manufacturing the same. 1997.
133. Iqbal Y, Lee WE, Holland D, James PF. Metastable phase formation in the early stage crystallisation of lithium disilicate glass. Journal of Non-Crystalline Solids 1998;224(1):1-16.
134. Schweiger M, Frank M, Rheinberger V, Höland W, inventors; Ivoclar AG, assignee. Lithium disilicate glass ceramics dental product 1999.
135. Schweiger M, Höland W, Frank M, Drescher H, Rheinberger V. IPS Empress 2: A new pressable high-strength glass-ceramic for esthetic all-ceramic restorations. Quintessence Dental Technology 1999;22:143-51.
136. Soares PC, Zanotto ED, Fokin VM, Jain H. TEM and XRD study of early crystallization of lithium disilicate glasses. Journal of Non-Crystalline Solids 2003;331(1-3):217-27.
137. Mishima N, Wakasugi T, Ota R. Nucleation behavior of $Li_2O–Na_2O–SiO_2$ glass doped with platinum. Journal of the Ceramic Society of Japan 2004;112(1306):350-53.
138. Morimoto S, Emem W. Strength of $Li_2O–SiO_2$ system transparent glass-ceramics. Journal of the Ceramic Society of Japan 2004;112:259-62.
139. Morimoto S. Effect of K_2O on crystallization of $Li_2O–SiO_2$ glass. Journal of the Ceramic Society of Japan 2006;114(1326):195-98.

140. Fuss T, Ray CS, Lesher CE, Day DE. In situ crystallization of lithium disilicate glass: Effect of pressure on crystal growth rate. Journal of Non-Crystalline Solids 2006;352:2073-81.
141. Kuzielová E, Hrubá J, Palou M, Smrcková E. Influence of P_2O_5 upon the crystallization of lithium disilicate and fluorapatite in bio-glass ceramics. Ceramics-Silikáty 2006;50(3):159-62.
142. Apel E, van't Hoen C, Rheinberger V, Holand W. Influence of ZrO_2 on the crystallization and properties of lithium disilicate glass-ceramics derived from a multi-component system. Journal of the European Ceramic Society 2007;27:1571-77.
143. Zheng X, Wen G, Song L, Huang X. Effects of P_2O_5 and heat treatment on crystallization and microstructure in lithium disilicate glass ceramics. Acta Materialia 2008;56(3):549-58.
144. Palou M, Kuzielová E, Vitkovič M, Noaman MSM. Mechanism and kinetics of glass-ceramics formation in the LiO_2–SiO_2–CaO–P_2O_5–CaF_2 system. Central European Journal of Chemistry 2009;7(2):228-33.
145. Abd El All S, Ezz-Eldin FM. Electrical conductivity of gamma-irradiated V_2O_5 doped lithium disilicate glasses doped and their glass-ceramics derivatives. Nuclear Instruments and Methods in Physics Research B 2010;268:49-56.
146. Goharian P, Nemati A, Shabanian M, Afshar A. Properties, crystallization mechanism and microstructure of lithium disilicate glass–ceramic. Journal of Non-Crystalline Solids 2010;356(4-5):208-14.
147. Bischoff C, Eckert H, Apel E, Rheinberger VM, Holand W. Phase evolution in lithium disilicate glass–ceramics based on non-stoichiometric compositions of a multi-component system: structural studies by ^{29}Si single and double resonance solid state NMR. Physical Chemistry Chemical Physics 2011;13:4540-51.
148. Buchner S, Lepienski CM, Soares Jr PC, Balzaretti NM. Effect of high pressure on the mechanical properties of lithium disilicate glass ceramic. Materials Science and Engineering A 2011;528:3921-24.
149. Khalkhali Z, Yekta BE, Marghussian VK. Mechanical and Chemical Properties of Zr and P-Doped Lithium Disilicate Glass Ceramics in Dental Restorations. International Journal of Applied Ceramic Technology 2012;9(3):497-506.
150. Mahmoud MM, Folz DC, Suchicital CTA, Clark DE. Crystallization of lithium disilicate glass using microwave processing. Journal of the American Ceramic Society 2012;95(2):579-85.
151. Borom MP, Turkalo AM, Doremus RH. Strength and microstructure in lithium disilicate glass-ceramics. Journal of the American Ceramic Society 1975;58(9-10):385-91.
152. Beall GH, Kohli JT, inventors; Corning Inc., assignee. Glass-ceramics containing lithium disilicate and tridymite. 1998.
153. Goto N, Ishioka J, Kawashima Y, inventors; Ohara, K.K., assignee. Glass-ceramic substrate for an information storage medium. 2001.
154. Budd MI, Darrant JG, inventors; GEC Alsthom Ltd, assignee. Glass-ceramic armour. 1995.

Chapter

3

Results and discussion

“We've arranged a civilization in which most crucial elements profoundly depend on science and technology.”
Carl Sagan

This chapter gathers the outcome of the experimental work done on the frame of the proposed goals and its discussion. It is divided in sub-chapters which correspond to the manuscripts that resulted from the research activity and had been published or submitted to ISI journals. The first three papers regard the experiments in the simple $Li_2O–K_2O–Al_2O_3–SiO_2$ glass system. Sub-chapters 3.4 and 3.5 consider the effect of adding excess of K_2O to glass G3 (*i.e.* $K_2O/Al_2O_3 > 1$), while sub-chapters 3.6 and 3.7 compares the systems $Li_2O–SiO_2$, $Li_2O–Al_2O_3–SiO_2$ and $Li_2O–K_2O–Al_2O_3–SiO_2$, including a study of crystallization kinetics. The role of nucleating agents on the microstructure and crystallization behaviour of lithium disilicate based glass is presented in 3.8. Finally, sub-chapter 3.9 introduces the apatite crystallization from glasses in the $Ca_5(PO_4)_3F–CaAl_2Si_2O_8–CaMgSi_2O_6–NaAlSi_3O_8$ system, aiming to estimate the potential of these compositions for applications as fine grade glass-ceramic coatings on ceramic substrates with compositions similar to that of G3.

3.1 Crystallization process and some properties of $Li_2O–SiO_2$ glass–ceramics doped with Al_2O_3 and K_2O

Hugo R. Fernandes[a], Dilshat U. Tulyaganov[a,b], Ishu K. Goel[a], José M. F. Ferreira[a]

[a] Department of Ceramics and Glass Engineering, University of Aveiro, CICECO, 3810-193 Aveiro, Portugal

[b] State Committee of Geology and Mineral Resources, Centre of Remote Sensing and GIS Technologies, Tashkent, Uzbekistan

Journal of the American Ceramic Society, 91 [11] 3698–3703 (2008)

DOI: 10.1111/j.1551-2916.2008.02724.x

Abstract

We report on the role of Al_2O_3 and K_2O on crystallization in glasses featuring a SiO_2/Li_2O ratio (3.13 to 4.88) far beyond that of lithium disilicate (LD, $Li_2Si_2O_5$) stoichiometry. Glasses in both bulk and frit form were produced by the conventional melt-quenching technique. Scanning electron microscopy analysis revealed surface nucleation as the dominant crystallization mechanism in glass-ceramics (GCs) derived from bulk glasses richer in Al_2O_3 and K_2O in the temperature range 800–900 ºC and dendritic skeletal surface growth of lithium metasilicate crystalline phase (LS, Li_2SiO_3). The glasses with lower amounts of Al_2O_3 and K_2O showed an intermediate type of crystallization mechanism (simultaneous surface and volume nucleation) resulting in the preferential formation of $Li_2Si_2O_5$. The formation of LD GCs by sintering and the crystallization of glass-powder frits seems to occur via the precursor phase of LS, resulting in high-strength materials.

1. Introduction

Since the fundamental research of Stookey referred to by Höland and Beall[1] on the stoichiometric composition of layered phyllosilicate lithium disilicate (LD, $Li_2Si_2O_5$), many comprehensive studies have been undertaken that led to the development of LD glass–ceramics (GCs) from a variety of systems.[1-8] In particular, the main emphasis was addressed on the investigation of compositions in the binary[9] Li_2O–SiO_2 or in the multicomponent systems.[10] According to Vogel,[9] Li_2O–SiO_2 liquids containing <30 mol.% Li_2O appeared as opalescent or opaque glasses upon cooling, owing to phase separation. He explained this phenomenon on the basis of the segregation of glassy phase into droplet-like zones of Li-rich phase and SiO_2-rich glass matrix. Moreover, within the Li_2O content range of 14–16 mol.% in the entire glass, LD composition was already reached in the droplet phase.[9] Further increasing the Li_2O content in the entire glass reduced the surface tension of the two phases because Li_2O entered into the SiO_2-rich phase surrounding the droplets and the size of the droplets reduced continuously. Subsequently, with a Li_2O content of 33.3 mol.% (LD composition) in the entire glass, the droplet phase and the phase surrounding the droplets had the same composition, and glass of LD composition had the most homogeneous possible structure. However, this simple Li_2O–SiO_2 system alone showed poor chemical durability and mechanical properties. Therefore, there was a need to add different oxides into the parent glasses, improving these properties as discussed briefly in the following paragraph.

The introduction of SiO_2-excess to stoichiometric LD glass along with additives, such as ZrO_2, Al_2O_3, ZnO, CaO, K_2O, and P_2O_5, has been suggested by Echeverria[11] and Beall[12-13] for developing LD GCs featuring translucency, smoothness, shiny surface, high mechanical stability, and fracture toughness. The chemical durability was improved by developing GCs with nonstoichiometric compositions1 or via the addition of Al_2O_3 and K_2O into stoichiometric LD glass.[14-15] The addition of P_2O_5 into LD glass was observed to induce amorphous phase separation and increase the crystal nucleation rate, simultaneously.[16-18] Subsequently, the addition of P_2O_5 (as nucleating agent) in amounts of 1.5–2.5 mol.% resulted in GCs with fine-grained interlocking microstructures, conferring high mechanical strength to the final products.[19-20]

A Li_2O–Al_2O_3–SiO_2 system with low Al_2O_3 content has been proposed as a potential candidate material for the substrate of hard discs in computers because of its excellent mechanical characteristics (impact resistance and hardness).[21-22] Kim *et al.* [22-23] demonstrated

that the replacement of MgO by K_2O improved the glass-forming ability of Al_2O_3-poor Li_2O–Al_2O_3–SiO_2 melts and the surface quality of polished GC disks.

LD GCs in a multicomponent system with a wide compositional range of (in wt.%) 57–80 SiO_2, 11–19 Li_2O, 0–13 K_2O, 0–5 Al_2O_3, 0–8 ZnO, 0.1–6 La_2O_3, and 0.1–11 P_2O_5 were thoroughly investigated to produce the material, using the IPS Empresss 2 via hot pressing technique.[24] Höland *et al.*,[25] Frank *et al.*,[26] and Schweiger *et al.*[27] have reported its properties. The reaction mechanism in the GC powders, used for the synthesis of LD GCs, is complex.[1, 28] In Al_2O_3-containing GCs, the predominant crystallization of $Li_2Si_2O_5$ occurs via the precursor lithium metasilicate. In the Al_2O_3-free glass composition of (in mol.%) 63.2 SiO_2, 29.1 Li_2O, 2.9 K_2O, 3.3 ZnO, and 1.5 P_2O_5, both LS and LD form as primary crystalline phases at ca. 600 ºC.[29] The growth of LD increases at 680 ºC because of the solid-state reaction as in the following chemical equation

$$Li_2SiO_3 + SiO_2 \rightarrow Li_2Si_2O_5 \quad (1)$$

The machinability features of LS have motivated the production of GCs, in the composition range of (in wt.%) 64–73 SiO_2, 13–17 Li_2O, 0.5–5 Al_2O_3, 2–5 K_2O, and 2–5 P_2O_5, via CAD/CAM, where machining is applied at an early stage of production, when crystallization of LS is predominant. Further heat treatment causes crystallization of LD, according to Eq. (1), resulting in high-strength LD GCs.[30]

Novaes de Oliveira *et al.*[31] investigated sintering and crystallization of glass powder having a composition (in mol.%) of 23.12 Li_2O, 11.10 ZrO_2 and 65.78 SiO_2. Crystallization took place just after completion of sintering and was almost complete at about 900 ºC in 20 min. Secondary porosity prevailed over the primary porosity during the crystallization stage. The glass-powder compacts first crystallized into LS, which transformed into LD, zircon ($ZrSiO_4$), and tridymite (SiO_2) after the crystallization process was essentially complete. The microstructure was characterized by fine crystals uniformly distributed and arbitrarily oriented throughout the residual glass phase.

A literature survey reveals that despite many comprehensive studies leading to the development of LD GCs from different systems, the role of Al_2O_3 and K_2O on the crystallization behaviour of glasses with a SiO_2/Li_2O ratio far beyond that of LD stoichiometry has not been thoroughly investigated. Therefore, the present work aims at investigating how the crystallization processes and some properties of Li_2O–SiO_2 GCs are affected by doping the batch formulations with different amounts of Al_2O_3 and K_2O. These

oxides were added at the expense of Li_2O in order to underline the influence of the SiO_2/Li_2O ratio on the crystallization features of the experimental glasses.

2. Experimental procedure

Three experimental glass compositions designated as G1, G2, and G3 with Li_2O contents 15.22, 19.09, and 22.96 mol.% and the corresponding SiO_2/Li_2O ratios 4.88, 3.83, and 3.13, respectively, were investigated in this work (Table 1). Doping by Al_2O_3 and K_2O was performed on an equimolecular basis, and the amount of additives decreased from G1 to G3.

Table 1 – Compositions of the experimental glasses.

	Oxides (mol.%)				
	Li_2O	K_2O	Al_2O_3	SiO_2	SiO_2/Li_2O
G1	15.23	5.24	5.24	74.30	4.88
G2	19.08	3.94	3.94	73.04	3.83
G3	22.96	2.63	2.63	71.78	3.13

Powders of technical grade SiO_2 (purity > 99.5%) and of reactive grade Al_2O_3, Li_2CO_3, and K_2CO_3 were used. Homogeneous mixtures of batches (~100 g), obtained by ball milling, were preheated at 800 ºC for 1 h for calcination and then melted in alumina crucibles at 1550 ºC for 1 h in air. Glasses in bulk form were produced by pouring the melts on preheated bronze moulds followed by annealing at 550 ºC for 1 h. In order to study the crystallization behaviour of the bulk glasses, the annealed bulk glasses were heat treated at 800 and 900 ºC for 1 h, respectively, at a heating rate of 2 K/min.

The glass-powder compacts were produced from glass frits, which were obtained by quenching the glass melts in cold water. The frits were dried and then milled in a high-speed agate mill in order to obtain fine glass powders. The fine glass powders had a mean particle size of 5–10 μm as determined by the light scattering technique (Coulter LS 230, Fraunhofer optical model, Amherst, MA). Rectangular bars with dimensions of 4 mm × 5 mm × 50 mm were prepared by uniaxial pressing (80 MPa). The bars were sintered under non-isothermal conditions for 1 h at 800, 850, and 900 ºC at a low heating rate of 2 K/min aimed to prevent deformation of the samples.

The coefficient of thermal expansion (CTE) of the samples was determined by dilatometry, using prismatic samples of bulk glasses and sintered glass-powder compacts with a cross section of 3 mm × 4 mm (BÄHR Thermo Analyse GmbH 2000, model DIL 801 L, Hüllhorst, Germany, heating rate 5 K/min). Differential thermal analysis of fine glass powders was carried out in air (DTA-TG, Labsys Setaram, Caluire France; heating rate 10 K/min).

The crystalline phases were determined by X-ray diffraction (XRD) analysis (Rigaku Geigerflex D/Mac, C Series, CuKα radiation, Japan). CuKα radiation (λ = 1.5406 Å), produced at 30 kV and 25 mA, scanned the range of diffraction angles (2θ) between 10 and 60º with a 2θ step of 0.02 º/s. The phases were identified by comparing the obtained diffractograms with patterns of standards complied by the International Centre for Diffraction Data (ICDD). Microstructure observations were done at the polished (mirror finishing) and then etched (by immersion in 2 vol.% HF solution for 5 min) surfaces of samples using field emission scanning electron microscopy (FE-SEM, Hitachi S-4100, Hitachi, Tokyo, Japan; 25 kV acceleration voltage, beam current 10 μA) under secondary electron mode. Archimedes' method (*i.e.*, immersion in diethyl phthalate) was used to measure the apparent density of the samples. Three-point bending strength tests were performed on rectified parallelepiped bars (3 mm × 4 mm × 50 mm) of sintered GCs (Shimadzu Autograph AG 25 TA, Tokyo, Japan 0.5 mm/min displacement); the results were obtained from at least 10 different independent samples.

3. Results

3.1 Characterization and properties of glasses

Melting at 1550 ºC for 1 h was adequate to obtain transparent and colourless glasses. Nevertheless, the presence of bubbles was evident in all the experimental glasses, which disappeared after remelting of glass frits at 1550 ºC for 1 h. The amorphous nature of the as-quenched glasses was confirmed by XRD (not shown).

Dilatometry curves of the cast and annealed bulk glasses (glass blocks) are plotted in Fig. 1. The transition points (T_g) and softening points (T_s) for the investigated glasses ranged between 485–501 ºC and 512–550 ºC, respectively (Table 2). Glass G1 exhibits the highest T_g and T_s, while the lowest is shown by glass G3. From the slope of the linear part of these plots (*i.e.*, 200–400 ºC), the thermal expansion coefficients (CTE) of the glasses G1, G2, and G3 were

calculated as 8.00×10^{-6}, 9.39×10^{-6}, and 10.23×10^{-6} /K, respectively. Consequently, the increase in Al_2O_3 and K_2O in the as-investigated proportions (Table 1) favours the decrease in CTE and the increase in T_g and T_s of the glasses (Table 2).

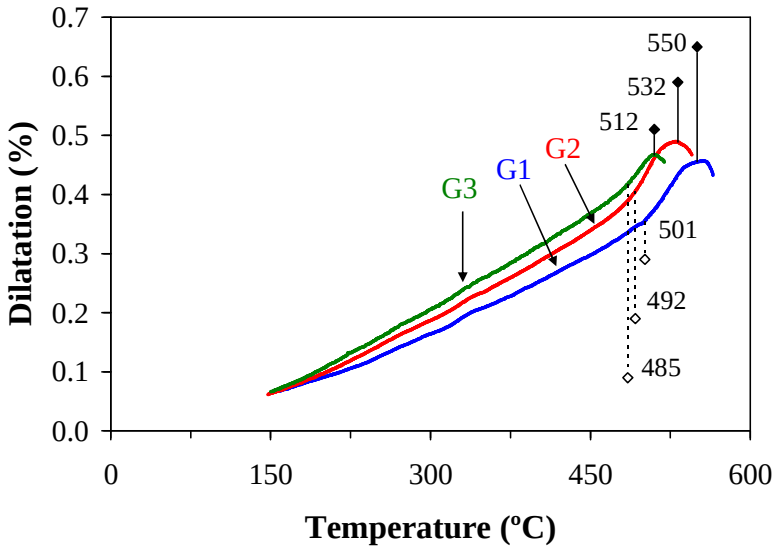

Fig. 1 – Dilatometry curves obtained from as-cast and annealed bulk glasses with reference to T_g (◇) and T_s (◆) temperatures.

The experimental results showed that the density of the glasses decreases in the order G3 > G2 > G1. The molar volume (V_m), oxygen molar volume (V_o), and excess molar volume (V_e) were calculated using the apparent density data for the bulk glasses using following relations:

$$V_m = \frac{M}{\rho} \quad (2)$$

where M is the molar mass of the glass and ρ is the apparent density of the bulk glasses. Similarly, excess molar volume of the glasses can be expressed as

$$V_e = V_m - \sum_i x_i V_{m(i)} \quad (3)$$

Here, x_i is the molar concentration of every oxide and $V_{m(i)}$ is the molar volume of every oxide. Oxygen molar volume of the glasses was calculated using the following relation:

$$V_o = \frac{\sum_i x_i M_i}{\rho \sum_i n_i x_i} \quad (4)$$

where M_i is the molar weight of the oxide, and i and n_i are the oxygen contents in the ith oxide, respectively. The lowest values of V_m, V_o, and V_e were obtained for glass G3, while the highest value of these parameters were calculated for glass G1 (Table 2).

Table 2 – Properties of the experimental glasses.

	G1	G2	G3
Density (g/cm^3)	2.34 ±0.01	2.35 ±0.01	2.36 ±0.01
T_g (ºC)	501	492	485
T_s (ºC)	550	532	512
$CTE_{200\text{-}400ºC}$ (10^{-6} /K)	8.00	9.39	10.23
Molar volume, V_m (cm^3/mol)	25.38 ±0.14	24.34 ±0.01	23.35 ±0.05
Oxygen molar volume, V_o (cm^3/mol)	15.23 ±0.09	14.89 ±0.01	14.57 ±0.03
Excess molar volume, V_e (cm^3/mol)	2.06 ±0.15	1.60 ±0.01	1.19 ±0.05

The DTA thermographs, as obtained from the fine glass powders at a heating rate of 10 K/min, revealed a single broad exothermic crystallization curve for both G1 and G2 (Fig. 2) with a peak temperature of crystallization (T_p) at 737 and 659 ºC, respectively. In the case of G3, an exothermic shoulder at T_p = 600 ºC followed by a stronger exothermic curve with T_p = 656 ºC were observed. The T_p of the investigated glasses was found to depend on the Al_2O_3 and K_2O molecular fraction because it increased from glass G3 to glass G1.

3.2 Crystallization behaviour of bulk glasses

Transparent parent glasses transformed into the white translucent opaque GC materials after heat treatment at 800 ºC. The degree of opacity significantly increased with further heat treatment at 900 ºC. SEM images of glass blocks heat treated at 800 and 900 ºC for 1 h are presented in Fig. 3 while their X-ray diffractograms are presented in Fig. 4. The crystallization process of the bulk glasses, as followed by XRD and SEM analyses, was found to depend on the contents of Al_2O_3 and K_2O. Dendritic microstructure for LS was observed in the SEM image of glass G1 heat treated at 800 ºC (Fig. 3(a)) while nucleated droplet phase separation was evident in the inner part (part B) of the sample (Fig. 3(b)). Li_2SiO_3 crystals grew from the surface of the glass specimen toward the interior, and the crystal growth rate

increased at 900 ºC (Fig. 3(c)). This type of dendritic skeletal crystal growth and surface crystallization has been previously documented for the other systems.[1, 32]

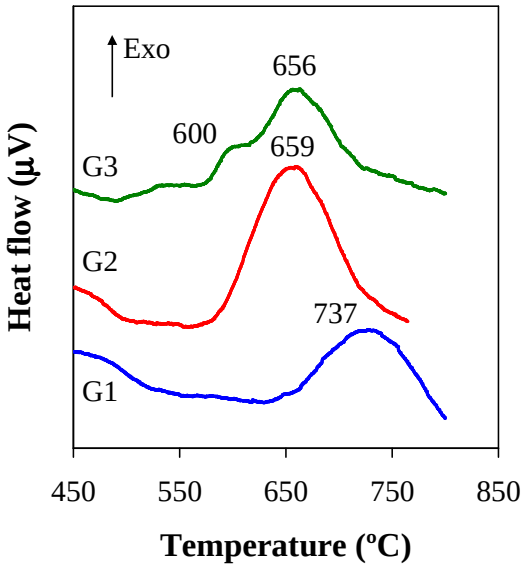

Fig. 2 – Differential thermal analysis (DTA) of the investigated compositions.

The XRD results are in good agreement with SEM observations depicting the presence of very low-intensity peaks of Li_2SiO_3 among the amorphous halo for the G1 specimen at both 800 and 900 ºC (Fig. 4(a)). Figure 3(d) presents the SEM image of specimen G3 at a comparatively low magnification (×40), after heat treatment at 800 ºC, evidencing the existence of simultaneous surface and bulk crystallization in the form of dendrites, and big droplets (designated as B), respectively. The detailed observation of the skeletal surface dendrites (part S, similar to G1) can be assigned to Li_2SiO_3 (Fig. 3(e)).

The SEM image of oriented structure, presented in Fig. 3(f), was extracted from the inner part of specimen G3 (Fig. 3(d), part B), which, under higher magnification (Fig. 3(g)), was found to be composed of fine cylindrically shaped nanocrystals. According to XRD (Fig. 4(c)), the relatively big droplets as observed in Fig. 3(d) are LD crystals, assuming that LS crystals (which also were registered by XRD analysis in Fig. 4(c)) have been mostly formed at the surface of the specimen (Fig. 3(e)).

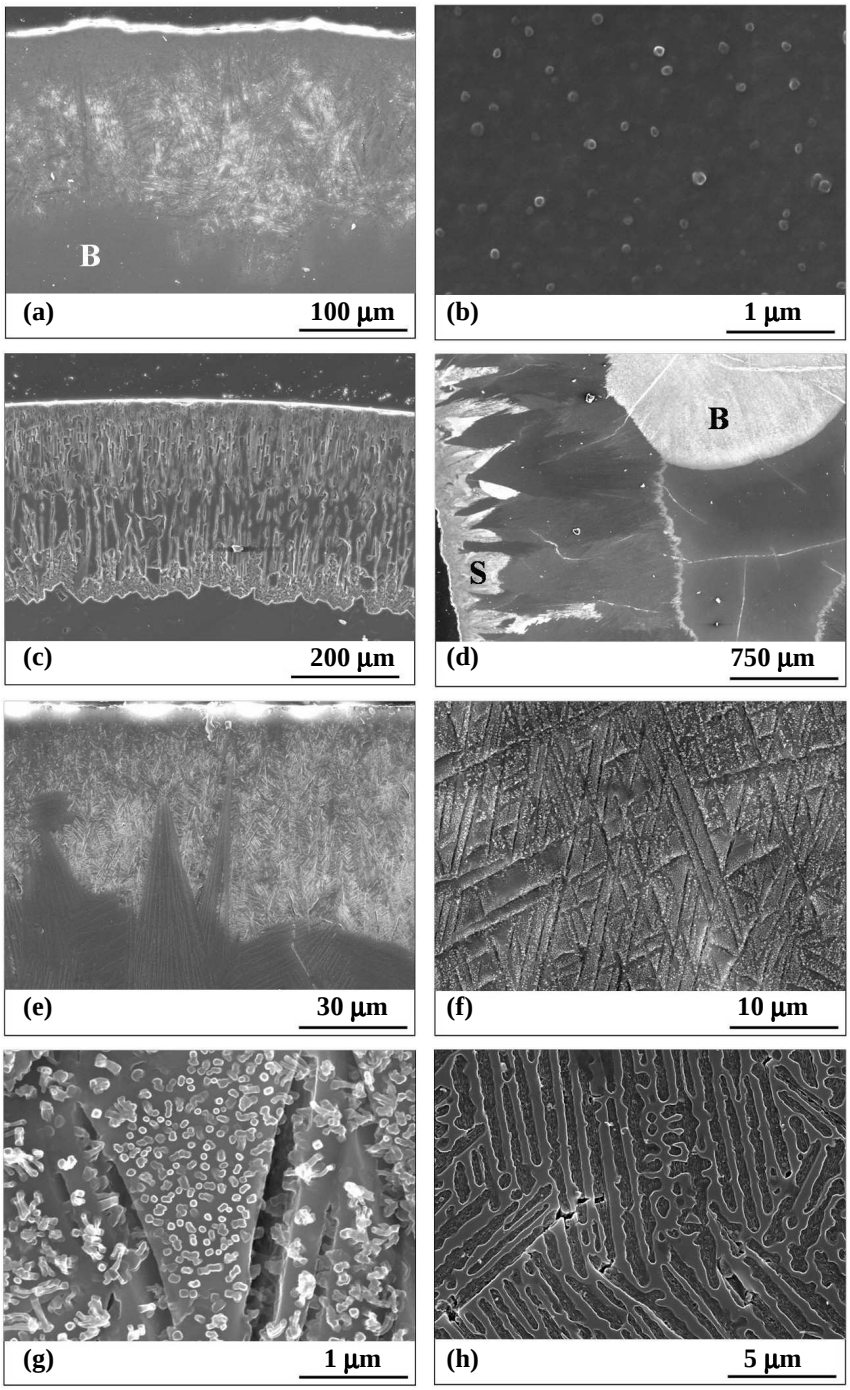

Fig. 3 – Scanning electron microscopy images of bulk glasses G1 and G3 heat treated at 800 ºC and 900 ºC for 1 h: (a)–(b) G1, heat treated at 800 ºC; (c) G1, heat treated at 900 ºC; (d)–(g) G3, heat treated at 800 ºC; (h) G3, heat treated at 900 ºC.

Heat treatment at 900 ºC caused further growth of LD peaks in the XRD pattern (Fig. 4(c)), while LS peaks were suppressed and very low-intensity peaks of quartz appeared. It is worth noting that the XRD patterns of composition G2 heat treated at 800 and 900 ºC (Fig. 4(c)) are very similar to those obtained for G3 under similar conditions. Homogeneous microstructure

composed of configured lathes and fine-grained crystals of LD in chemically etched zones (Fig. 3(h)) were observed for the G3 specimen after heat treatment at 900 ºC.

3.3 Crystallization behaviour of glass-powder compacts

Fully dense GC materials were obtained after sintering of the glass-powder compacts at 800–850 ºC. Crystallization seems to start after the completion of sintering because the intensity of the reflections related to crystalline phases at 800 ºC are relatively low, evidencing a more amorphous structure (Fig. 5). In particular, X-ray diffractograms revealed LS as the single crystalline phase in GC1 after sintering at 800 ºC (Fig. 5(a)), while highly amorphous GC2 and GC3 comprised low-intensity LS, quartz (Q), and LD peaks (Figs. 5(b) and (c)). Significant changes in phase assemblage occurred in the temperature interval of 800–850 ºC, resulting in the appearance of LD phase in GC1 and a tremendous growth of LD intensity peaks in GC2 and GC3. Therefore, LD precipitated out to become the major phase in all investigated compositions after sintering at 850 and 900 ºC, probably occurring via the precursor phase of LS.[33] LS and orthoclase (F) in GC1, and LAS in both GC2 and GC3 were found as minor crystalline phases.

SEM images of compositions GC1 and GC3 sintered at 900 ºC reveal the existence of a densely packed microstructure. The evidences of porosity derived from both the entrapment of air during the preparation route (so-called primary porosity) and the differences in density of the parent glass and crystalline phases (so-called secondary porosity) are also evident (Fig. 6). The insert presented in the Fig. 6(b) shows the existence of fine-grained LD crystals forming endless chains in the region free from superficial glassy phase.

The variation in density and the bending strength of GCs along with the firing temperature are plotted in Fig. 7. The density values were stable for GC1 (2.34 g/cm^3) at both 800 and 850 ºC followed by a smooth decrease after firing at 900 ºC. On the contrary, the density for GC2 and GC3 showed a significant increase within the temperature interval 800–850 ºC, reaching the maximum value 2.35 g/cm^3 for both compositions. A negligible decrease in density for GC2 and GC3 was observed after firing at 900 ºC.

The relatively low degree of crystallinity (Fig. 5(b)) resulted in poor mechanical properties for the GC3 fired at 800 ºC (58.1±2.3 MPa). However, under the same conditions GC2 featured better mechanical properties (92.2±3.0 MPa) in comparison with GC3, while the highest flexural strength value was recorded for GC1 (124.9±2.3 MPa). The mechanical strength

increased significantly for all experimental compositions at 850 ºC. The flexural strength for all the investigated GCs varied between 152 and 165 MPa with GC1 exhibiting the maximum. Similar results were recorded for GC1 at 900 ºC (162.5±30.7 MPa), while GC2 and GC3 demonstrated significant further increases to values of 181.3±30.4 and 201.4±14.0 MPa, respectively. A smooth surface effect of the samples as a result of self-glazing was also observed.

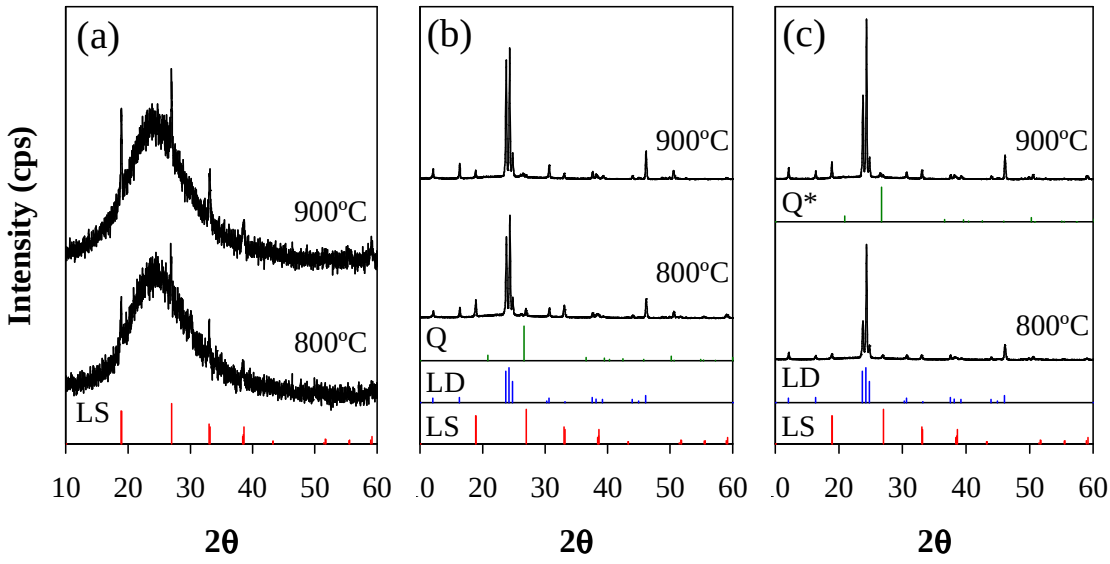

Fig. 4 – X-ray diffractograms of bulk glasses heat-treated at 800 and 900 ºC: (a) G1, (b) G2, and(c) G3. LS, lithium metasilicate (Li_2SiO_3, ICDD card 01-070-0330); LD, lithium disilicate ($Li_2Si_2O_5$, ICDD card 00-049-0803); Q, quartz (SiO_2, ICDD card 00-046-1045); Q*, quartz (SiO_2, ICDD card 01-085-0794) [scale bar: (a) = 2150 cps; (b) and (c) = 63000 cps].

The CTE (200–700 ºC) values of the GC1, GC2, and GC3 sintered at 900 ºC were calculated as 8.46×10^{-6}, 9.20×10^{-6}, and 9.21×10^{-6} /K, respectively. A similar trend, *i.e.* decreasing CTE values with increasing Al_2O_3 and K_2O molecular fraction, was also observed for the parent glasses (Fig. 1).

4. Discussion

The roles of Al_2O_3 and K_2O on the crystallization behaviour of glasses with SiO_2/Li_2O ratios (3.13 to 4.88) far beyond that of LD stoichiometry revealed some interesting features. Transparent bulk glasses were obtained after annealing at 550 ºC, contrasting to the cloudy glasses obtained by Vogel[9] when investigating compositions with similar Li_2O contents (15–

23 mol.%). The different crystallization behaviours observed can only be attributed to the presence of Al_2O_3 and K_2O (besides Li_2O and SiO_2) in the glasses used in the present investigation. It is well documented in the literature that the addition of Al_2O_3 simultaneously suppresses the immiscibility temperature while raising the T_g of the glasses so that immiscibility no longer occurs at any temperature unless not prevented by slow kinetics. It is worth noting that the existence of immiscibility in potassium silicate glasses has not been conclusively established.[34] Metastable immiscibility may be formed in the glasses investigated, but with such a fine scale of morphology that the glasses appear homogeneous to the naked eye. The slightly higher upper immiscibility temperatures of the lithium disilicate melt in simple Li_2O–SiO_2 system often leads to a slightly coarser morphology.[35]

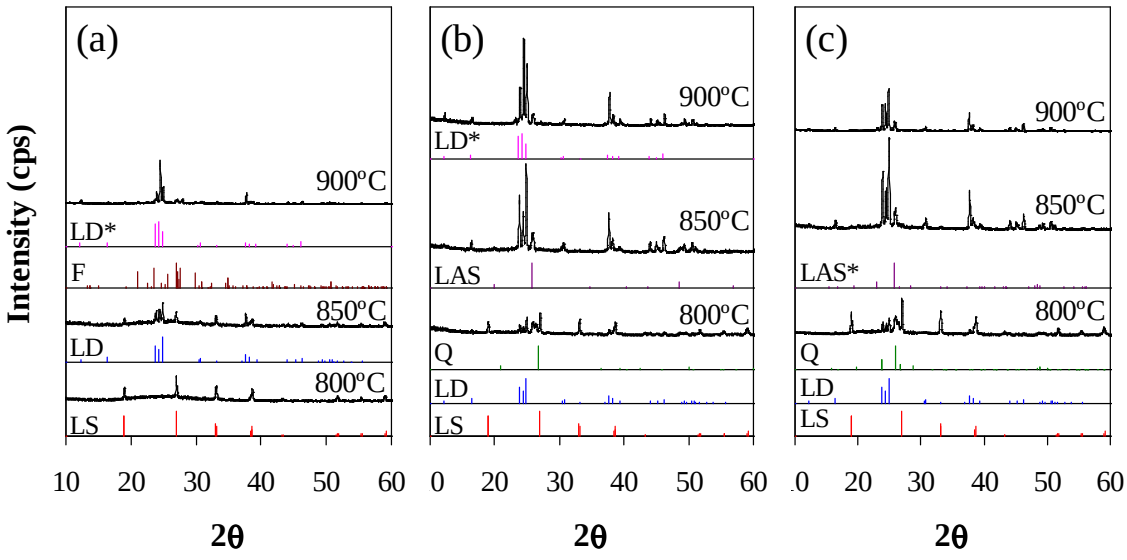

Fig. 5 – X-ray diffractograms of glass-powder compacts sintered for 1 h at different temperatures: (a) GC1, (b) GC2, and (c) GC3. LS, lithium metasilicate (Li_2SiO_3, ICDD card 01-070-0330); LD, lithium disilicate ($Li_2Si_2O_5$, ICDD card 00-040-0376); LD*, lithium disilicate ($Li_2Si_2O_5$, ICDD card 00-049-0803); LAS, lithium aluminum silicate ($LiAlSi_3O_8$, ICDD card 00-040-0073); LAS*, lithium aluminum silicate ($LiAlSi_3O_8$, ICDD card 00-035-0794); F, potassium feldspar ($KAlSi_3O_8$, ICDD card 01-071-0957); Q, quartz (SiO_2, ICDD card 01-076-0912) [scale bar = 13000 cps].

It can be assumed that due to the presence of alkali cations in the glasses, Al will exist in a four-coordinated position. To maintain local charge neutrality, $(AlO_4)^{5-}$ units will be charge compensated by alkali cations, which must be present in the vicinity of each such tetrahedron.

Therefore, the $(AlO_4)^{5-}$ tetrahedral will substitute directly into the network for silicon–oxygen tetrahedral, causing an increase in T_g and a decrease in CTE. This phenomenon was observed in the experimental glasses when the Al_2O_3 and K_2O molecular fraction increased from glass G3 to G1. Also, glass G3 exhibited the lower values of V_m, V_o, and V_e in comparison with G2 and G1. This can be explained by a higher volume fraction of network modifiers in this composition.

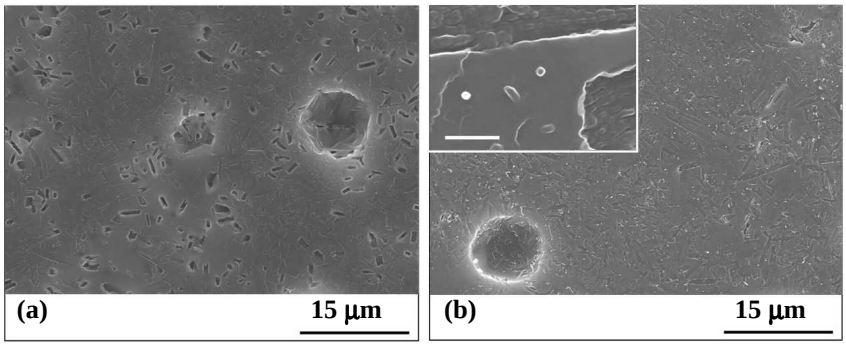

Fig. 6 – Typical microstructures of glass ceramics sintered for 1 h: (a) GC1 (900 ºC); (b) GC3 (900 ºC).

Both crystallization process and liquid–liquid phase separation seem to have contributed to the transformation of transparent parent bulk glasses into the opaque GC materials after heat treatment at 800 ºC. SEM images of bulk glass G1 (containing the highest amounts of Al_2O_3 and K_2O) after heat treatment at 800 ºC revealed dendritic surface crystallization of LS at 800 ºC (Fig. 3(a)) and nucleated droplet phase separation zones in the silica-rich matrix (Fig. 3(b)). Li_2SiO_3 crystals grew from the surface toward the interior (Fig. 3(c)) and no LD crystals were formed, while the sample continued to be highly amorphous after further heat treatment at 900 ºC (Fig. 4(a)). Because glass G1 has the highest T_g (Table 2), it can be suggested that the embedded disilicate zones (droplet phase in Fig. 3(b)) will be unable to grow as they are separated from one another by the inert highly viscous SiO_2-rich glass phase.[9] This can be also supported by the fact that crystallization of LS removes an equimolar quantity of Li_2O and SiO_2 from the molten glass, thus increasing the SiO_2 content of the remaining glass, leading to an increase in its viscosity.[34]

SEM images of bulk glass G3 at 800 ºC (Figs. 3(d) and (e)) also revealed the dendritic surface crystallization of LS, which most probably precipitated first because of its lower activation energy for crystallization in comparison with LD.[36-37] LD crystals were formed in the interior

of this specimen G3 (Fig. 3(g)) via a bulk crystallization mechanism; that was, however, not the case for G1. This type of LD formation most probably is attributed to the separation of glassy phase into droplet-like zones of Li-rich phase and SiO_2-rich glass matrix (Fig. 3(d)) that occurs during heat treatment of the parent glass as a result of a flow process. Note that G3 features the lower T_g (Table 2) and, hence, a less viscous glassy phase. On further heat treatment at 900 ºC, a highly homogeneous microstructure comprising of fine-grained crystals of LD were formed (Fig. 3(h)). It is worth noting that apart from the high intensity of reflections related to LD crystalline phase, traces of LS and quartz were also present in the XRD spectra of both GC2 and GC3 at 900 ºC (Fig. 4(c)).

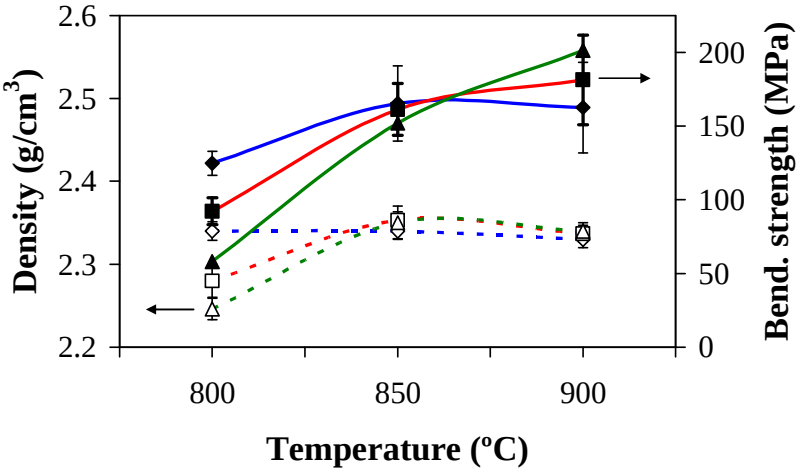

Fig. 7 – Evolution of density (dashed lines) and bending strength (full lines) of glass-powder compacts GC1 (◆), GC2 (■), and GC3 (▲) with sintering temperature.

During the preparation of GCs via sintering of glass-powder compacts, the crystallization of LD seems to occur via the precursor phase of LS due to the solid-state reaction as in chemical Eq. (1). In particular, LS was exclusively formed in G1 at 800 ºC. However, with temperature increase, the intensity of the reflections related to LS decreased, and LD appeared as a major crystalline phase in GC1 at both 850 and 900 ºC (Fig. 5(a)). Interestingly, LD was not formed in the heat-treated bulk glass blocks of glass G1. This behaviour may be associated with the difference in preparation routes of the parent glasses, as water quenching of the glass increases the OH content. The hydroxyl groups may act as a modifier and break the silicate network, thus reducing the viscosity and activation energy of viscous flow.[2, 38] Therefore, the appearance of orthoclase (F) in GC1 and LAS in both GC3 and GC4 as minor crystalline phases (Fig. 5) also can be explained. Moreover, precipitation of F and LAS phases evidences

that $(AlO_4)^{5-}$ units, charge compensated by alkali cations, are present in the structure of parent glasses.

The mechanical strength of GCs produced from glass-powder compacts increased significantly at 850–900 ºC, resulting in high-strength GCs (Fig. 6). This can be explained by the precipitation of fine LD crystals uniformly distributed in the glass matrix. It has been documented in the literature that the presence of $Li_2Si_2O_5$ crystals enhances the strength, whereas the presence of Li_2SiO_3 crystals does not change the strength of the parent glass.[39]

Nevertheless, further experimental investigations on the microstructural features of as-received bulk glasses and their crystallization kinetics are needed in order to have a better understanding about the phenomenon related to metastable immiscibility and crystallization processes in this system. In particular, a challenge to compare the microstructural features of the investigated experimental glasses with relevant glasses free from Al_2O_3 and K_2O in a Li_2O–SiO_2 system will be undertaken and presented in our forthcoming publication.

5. Conclusions

The parent bulk glasses featuring a high degree of LD non-stoichiometry appeared transparent after annealing, while the compositions with a similar amount of Li_2O in the Li_2O–SiO_2 system were previously found to be cloudy. Al_2O_3 may simultaneously suppress the immiscibility temperature while raising the T_g of experimental glasses. After heat treatment, seemingly both crystallization process and liquid–liquid phase separation contribute to the transformation of transparent glasses into opaque GC materials. The crystallization process, as followed by XRD and SEM analyses, was found to be dependent on the amount of Al_2O_3 and K_2O components as well as on the SiO_2/Li_2O ratio. In the composition of G1, featuring the highest Al_2O_3 and K_2O and the maximum SiO_2/Li_2O ratio (4.88), dendritic surface crystallization of LS was observed. For glasses with lower amounts of Al_2O_3 and K_2O and a lower SiO_2/Li_2O ratio, the mechanism seems to be a mix of surface and bulk crystallization resulting in the preferential formation of $Li_2Si_2O_5$.

During the preparation of GCs via sintering of glass-powder compacts, crystallization of LD seems to occur via the precursor phase of LS as a result of the solid-state reaction as in chemical Eq. (1). LS was exclusively formed in G1 at 800 ºC followed by LD, which appeared as the major crystalline phase in this composition at both 850 and 900 ºC. LD was not formed in the heat-treated bulk glass blocks of the same composition.

Finally, the mechanical strength specimens produced from glass-powder compacts increased significantly at 850–900 ºC resulting in high-strength GCs.

Acknowledgments

The first author is grateful for the financial support of CICECO and for the PhD grant from the University of Aveiro, Portugal.

References

1. Höland W, Beall G. Glass-ceramic Technology. Westerville, Ohio: The American Ceramic Society; 2002.
2. McMillan PW. Glass–Ceramics. London: Academic Press; 1979.
3. James PF. Kinetics of crystal nucleation in silicate glasses. Journal of Non-Crystalline Solids 1985;73:517-40.
4. Headley TG, Loehman RE. Crystallization of Glass–Ceramics by Epitaxial Growth. Journal of the American Ceramic Society 1984;67:620-25.
5. Zanotto ED. Metastable phases in lithium disilicate glasses. Journal of Non-Crystalline Solids 1997;219:42-48.
6. Ota R, Mishima N, Wakasugi T, Fukunaga J. Nucleation of $Li_2O–SiO_2$ glass and its interpretation based on a new liquid model. Journal of Non-Crystalline Solids 1997;219:70-74.
7. Ray CS, Day DE, Huang W, Narayan KL, Cull TS, Kelton KF. Non-isothermal calorimetric studies of the crystallization of lithium disilicate glass. Journal of Non-Crystalline Solids 1996;204(1):1-12.
8. Anspach O, Keding R, Rüssel C. Oriented lithium disilicate glass–ceramics prepared by electrochemically induced nucleation. Journal of Non-Crystalline Solids 2005;351:656-62.
9. Vogel W. Structure and Crystallization of Glasses. Leipzig: Pergamon Press; 1971.
10. Höland W, Apel E, van Hoen C, Rheinberger V. Studies of crystal phase formations in high-strength lithium disilicate glass-ceramics. Journal of Non-Crystalline Solids 2006;352(38-39):4041-50.
11. Echevería LM. New lithium disilicate glass-ceramics. Boletin da la Sociedad Espanola de Cerámica e Vidrio 1992;5:183–88.
12. Beall G. Design of glass-ceramics. Solid State Sciences 1989;3:333–54.
13. Beall G. Glass-ceramics: Recent developments and application. Ceramic Transactions 1993;30:241-66.
14. Barrett JMG, FL), Clark, David E. (Gainesville, FL), Hench, Larry L. (Gainesville, FL), inventor; The Board of Regents, State of Florida, University of Florida (Tallahassee, FL), assignee. Glass-ceramic dental restorations. 1980.
15. Wu J-mT, TW), Cannon, Warren R. (East Brunswick, NJ), Panzera, Carlino (Belle Mead, NJ), inventor; Johnson & Johnson Dental Products Company (East Windsor, NJ), assignee. Castable glass-ceramic composition useful as dental restorative. 1985.

16. Doremus RH, Turkalo AM. Crystallization of lithium disilicate in lithium silicate-glasses. Physics and Chemistry of Glasses 1972;13(1):14-&.
17. Iqbal Y, Lee WE, Holland D, James PF. Crystal nucleation in P_2O_5-doped lithium disilicate glasses. Journal of Materials Science 1999;34(18):4399-411.
18. James PF, McMillan PW. Quantitative measurements of phase separation in glasses using transmission electron microscopy. Part 1. Experimental technique and method of analysis. Physics and Chemistry of Glasses 1970;11(3):59-&.
19. Schweiger M. Microstructure and mechanical properties of a lithium disilicate glass–ceramic in the SiO_2–Li_2O–K_2O–ZnO–P_2O_5 system. Glastechnische Berichte-Glass Science and Technology 2000;73:43–50.
20. von Clausbruch CS, Schweiger M, Holand W, Rheinberger V. The effect of P_2O_5 on the crystallization and microstructure of glass-ceramics in the SiO_2–Li_2O–K_2O–ZnO–P_2O_5 system. Journal of Non-Crystalline Solids 2000;263(1-4):388-94.
21. Goto N, Yamaguchi K, inventors; Ohara, K.K., assignee. Magnetic disk substrate and method for manufacturing the same. 1997.
22. Kim KD. Crystallization behavior during cooling and glass-forming ability of Al_2O_3-poor Li_2O–Al_2O_3–SiO_2 melts. Journal of Non-Crystalline Solids 2008;354(15-16):1715-20.
23. Kim K-D, Kim YJ, Hwang JH. Surface topography of polished Li_2O–Al_2O_3–SiO_2 glass ceramics with low Al_2O_3 content. Glass Technology 2002;43C:202-06.
24. Höland W. Material science fundamentals of the IPS Empress 2 Glass-Ceramic. Ivoclar-Vivadent Report; 1998. p. 3-10.
25. Höland W, Schweiger M, Frank M, Rheinberger V. A comparison of the microstructure and properties of the IPS Empress®2 and the IPS Empress® glass-ceramics. Journal of Biomedical Materials Research 2000;53(4):297-303.
26. Frank M, Schweiger M, Rheinberger V, Höland W. High-strength translucent sintered glass-ceramics for dental application. Glastechnische Berichte-Glass Science and Technology 1998;71C:345-48.
27. Schweiger M, Frank M, Von Clausbruch CS, Höland W, Rheinberger V. Microstructure and properties of pressed glass–ceramic core to zirconia. Quintessence Dental Technology 1998;21:73-79.
28. Jacquin JR, Tomozawa M. Crystallization of lithium metasilicate from lithium disilicate glass. Journal of Non-Crystalline Solids 1995;190(3):233-37.
29. von Clausbruch CS, Schweiger M, Höland W, Rheinberger V. The effect of P_2O_5 on the crystallization and microstructure of glass–ceramics in the SiO_2–Li_2O–K_2O–ZnO–P_2O_5 system. Glastechnische Berichte-Glass Science and Technology 2001;74:223-29.
30. Höland W, Rheinberger V, Apel E, Van Hoen C. Principles and phenomena of bioengineering with glass–ceramics for dental restoration. Journal of the European Ceramic Society 2007;27:1521-26.
31. Oliveira APN, Manfredini T, Barbieri L, Leonelli C, Pelacani CC. Sintering and crystallization of a glass powder in the Li_2O–ZrO_2–SiO_2 system. Journal of the American Ceramic Society 1988;81(3):777-80.
32. Höland W, Frank M, Rheinberger V. Surface crystallization of leucite in glass. Journal of Non-Crystalline Solids 1995;180:292-307.
33. Oliveira APN, Manfredini T, Barbieri L, Leonelli C, Pelacani CC. Sintering and crystallization of a glass powder in the Li_2O–ZrO_2–SiO_2 system. Journal of the American Ceramic Society 1998;81(3):777-80.
34. Shelby JE. Introduction to glass science and technology. Cambridge: The Royal Society of Chemistry; 1997.

35. Oliveira APN, Corradi AB, Barbieri L, Leonelli C, Manfredini T. The effect of the addition of $ZrSiO_4$ on the crystallization of $30Li_2O/70SiO_2$ powdered glass. Thermochimica Acta 1996;286:375-86.
36. Oliveira APN, Leonelli C. Properties of glasses belonging to $Li_2O–ZrO_2–SiO_2$ system. Physics and Chemistry of Glasses 1998;39:213-21.
37. Pavlik V, Jona E, Sapietova M, Snircova S. Thermal stability vs. crystallization of the lithium silicate glasses with addition zirconium dioxide and titanium dioxide. Advances in Materials Research 2008;39-40:399-401.
38. Cattell MJ, Chadwick TC, Knowles JC, Clarke RL. The crystallization of an aluminosilicate glass in the $K_2O–Al_2O_3–SiO_2$ system. Dental Materials 2005;21:811-22.
39. Borom MP, Turkalo AM, Doremus RH. Strength and microstructure in lithium disilicate glass-ceramics. Journal of the American Ceramic Society 1975;58(9-10):385-91.

3.2 Effect of Al_2O_3 and K_2O content on structure, properties and devitrification of glasses in the $Li_2O–SiO_2$ system

Hugo R. Fernandes[a], Dilshat U. Tulyaganov[a,b], Ashutosh Goel[a], Manuel J. Ribeiro[c], Maria J. Pascual[d], José M.F. Ferreira[a]

[a] Department of Ceramics and Glass Engineering, University of Aveiro, CICECO, 3810-193 Aveiro, Portugal

[b] Turin Polytechnic University in Tashkent, 17 Niyazova str., 100174 Tashkent, Uzbekistan

[c] UIDM, ESTG, Polytechnic Institute of Viana do Castelo, 4900 Viana do Castelo, Portugal

[d] Instituto de Cerámica y Vidrio (CSIC), C/Kelsen 5, Campus de Cantoblanco, 28049 Madrid, Spain

Journal of the European Ceramic Society 30 (2010) 2017–2030

DOI:10.1016/j.jeurceramsoc.2010.04.017

Abstract

The effect of Al_2O_3 and K_2O content on structure, sintering and devitrification behaviour of glasses in the $Li_2O–SiO_2$ system along with the properties of the resultant glass–ceramics (GCs) was investigated. Glasses containing Al_2O_3 and K_2O and featuring SiO_2/Li_2O molar ratios (3.13–4.88) far beyond that of lithium disilicate ($Li_2Si_2O_5$) stoichiometry were produced by conventional melt-quenching technique along with a bicomponent glass with a composition $23Li_2O–77SiO_2$ (mol.%) ($L_{23}S_{77}$). The GCs were produced through two different methods: (a) nucleation and crystallization of monolithic bulk glass, (b) sintering and crystallization of glass powder compacts.

Scanning electron microscopy (SEM) examination of as cast non-annealed monolithic glasses revealed precipitation of nanosize droplet phase in glassy matrices suggesting the occurrence of phase separation in all investigated compositions. The extent of segregation, as judged from the mean droplet diameter and the packing density of droplet phase, decreased with increasing Al_2O_3 and K_2O content in the glasses. The crystallization of glasses richer in Al_2O_3 and K_2O was dominated by surface nucleation leading to crystallization of lithium

metasilicate (Li_2SiO_3) within the temperature range of 550–900 ºC. On the other hand, the glass with lowest amount of Al_2O_3 and K_2O and glass $L_{23}S_{77}$ were prone to volume nucleation and crystallization, resulting in formation of $Li_2Si_2O_5$ within the temperature interval of 650–800 ºC.

Sintering and crystallization behaviour of glass powders was followed by hot stage microscopy (HSM) and differential thermal analysis (DTA), respectively. GCs from composition $L_{23}S_{77}$ demonstrated high fragility along with low flexural strength and density. The addition of Al_2O_3 and K_2O to Li_2O–SiO_2 system resulted in improved densification and mechanical strength.

Keywords: Sintering; Microstructure-final; Glass; Glass–ceramics; Lithium disilicate

1. Introduction

Phase separation, nucleation and crystallization of glasses in the Li_2O–SiO_2 system have been the subject of many theoretical studies.[1-9] According to Vogel,[8] Li_2O–SiO_2 liquids containing less than 30 mol.% Li_2O lead to opalescent or opaque glasses on cooling owing to phase separation. TEM investigation revealed segregation into droplet like zones of Li-rich phase and SiO_2-rich glass matrix. Moreover, within the Li_2O content range of 14–16 mol.% in the entire glass, $Li_2Si_2O_5$ (here after referred as LD) composition was already reached in the droplet phase.[8] Further increasing the Li_2O content in the entire glass reduced the surface tension of the two phases because Li_2O entered into the SiO_2-rich phase surrounding the droplets and the size of the droplets reduced continuously. Subsequently, with Li_2O content of 33.3 mol.%, corresponding to $Li_2Si_2O_5$ in the entire glass, the droplet phase and the phase surrounding the droplets had the same composition, with this stoichiometric LD glass composition exhibiting the most homogeneous possible structure.

Generally, slight changes in lithium silicate glass composition may have significant effects on chronology and morphology of phases formed. The addition of P_2O_5 to LD glass was observed to induce amorphous phase separation and to increase the crystal nucleation rate, simultaneously.[3, 5, 10-12] The incorporation of TiO_2 in addition to P_2O_5 greatly affected phase evolution, morphology and thereby thermo-physical properties of crystallized glasses in low

alumina $Li_2O–SiO_2$ glasses.[13] The conventional nucleating agent ZrO_2 in $Li_2O–SiO_2$ glass enhanced the polymerization of the silicate network, and caused a significant red shift in Raman frequencies for Q^2 species and amorphous phase separation before crystallization.[14] Recently it was demonstrated that very small amount of MnO_2 and V_2O_5 (less than 1 wt.% in total) might decrease the critical cooling rate of the LD melt and so increase the glass forming tendency.[15] The occurrence of this phenomenon was attributed to the following possible reasons: (a) an increase of melt viscosity and, therefore, of the kinetic barrier against crystallization; (b) an increase of the surface energy difference between the Li-silicate crystals and residual melt, thus enhancing the surface energy barrier against nuclei formation.[15]

The role of Al_2O_3 and K_2O on crystallization in glasses featuring SiO_2/Li_2O ratios (3.13–4.88) far beyond of LD stoichiometry was recently studied.[16] Glasses in both bulk and frit form were produced by the conventional melt-quenching technique using alumina crucibles. Therefore, an unavoidable alumina uptake from the crucibles cannot be neglected. To eliminate this anomaly leading to uncontrolled compositional variations, Pt crucibles were used in the present work to prepare the same glass compositions along a new bicomponent (23 mol.% Li_2O and 77 mol.% SiO_2) glass denoted as $L_{23}S_{77}$. The aim of this work was, therefore, to get a deeper insight on phenomena related to a metastable immiscibility and devitrification in $Li_2O–SiO_2$ glasses in relevance with Al_2O_3 and K_2O content. Particular emphasis was also given to the investigation of sintering behaviour and the properties of the corresponding glass powder compacts. Significant differences between $L_{23}S_{77}$ composition and its Al_2O_3 and K_2O containing counterparts were encountered in terms of structure, crystallization kinetics, thermal behaviour and properties.

2. Experimental procedure

Table 1 presents the compositions of the glasses investigated in the present study along with the corresponding SiO_2/Li_2O ratios. The addition of Al_2O_3 and K_2O was performed on equimolecular basis and the amount of additives decreased from glass G1 to G3. The glass $L_{23}S_{77}$ containing the same amount of Li_2O (22.96 mol.%) as glass G3, but richer in SiO_2 (77.04 mol.%) due to complete exclusion of Al_2O_3 and K_2O from its composition was also prepared and investigated for comparison purposes.

Table 1 – Compositions of the experimental glasses.

	Oxides (mol.%)				
	Li_2O	K_2O	Al_2O_3	SiO_2	SiO_2 /Li_2O
G1	15.23	5.24	5.24	74.30	4.88
G2	19.08	3.94	3.94	73.04	3.83
G3	22.96	2.63	2.63	71.78	3.13
$L_{23}S_{77}$	22.96	–	–	77.04	3.35

Powders of technical grade SiO_2 (purity > 99.5%) and of reactive grade Al_2O_3, Li_2CO_3, and K_2CO_3 were used. Homogeneous mixtures of batches (~100 g), obtained by ball milling, were calcined at 800 ºC for 1 h and then melted in Pt crucibles at 1550 ºC for 1 h, in air. Glasses were produced in bulk (monolithic) and frit form as described below.

2.1 Crystallization behaviour of bulk glasses

Two sets of bulk glasses for each composition were obtained by pouring the glass melt on preheated bronze mould. The first set of glasses was allowed to cool down in the air while second set of glasses was subjected to annealing at 450 ºC for 1 h.

The coefficient of thermal expansion (CTE) of the annealed samples was determined by dilatometry using prismatic samples of bulk glasses with cross section of 3 mm × 4 mm (Bahr Thermo Analyse DIL 801 L, Germany; heating rate 5 K/min).

The onset of crystallization, T_c and peak temperature of crystallization, T_p for the investigated glasses were obtained from DTA thermographs of glass grains with sizes in the range of 415–1000 μm, collected by sieving of grounded non-annealed glass blocks. The DTA was carried out in air (Netzsch 402 EP, Germany) from room temperature to 1000 ºC at different heating rates (β = 2, 5, 10 and 15 K/min). The kinetics of crystallization was studied using the formal theory of transformation kinetics as developed by Johnson and Mehl[17] and Avrami,[18-20] for non-isothermal processes:

$$\ln\left(\frac{T_p^2}{\beta}\right) = \frac{E_c}{RT_p} - \ln q = 0 \quad (1)$$

which is the equation of a straight line, whose slope and intercept gives the activation energy, E_c, and the pre-exponential factor, $q = Q^{1/n}K_0$, respectively, and the maximum crystallization rate by the relationship[21]:

$$\left.\frac{d\chi}{dt}\right|_p = 0.37\,\beta\,E_c\,n\left(RT_p^2\right)^{-1} \quad (2)$$

which enables obtaining, for each heating rate, a value of the kinetic exponent, n. In Eq. (2), χ corresponds to the crystallization fraction and $\left.\frac{d\chi}{dt}\right|_p$ is the crystallization rate, which may be calculated by the ratio between the ordinates of the DTA curve and the total area of the crystallization curve.

In order to study the evolution of crystallization phases in monolithic glasses, the annealed glasses were cut into cubes (1 cm × 1 cm × 1 cm) and heat treated non-isothermally at 550, 650, 750, 800 and 900 ºC for 1 h, respectively, at heating rate of 2 K/min.

2.2 Sintering and crystallization of glass powder compacts

The glass frits were produced by quenching of melt in cold water. Further, the glass frits were dried and milled in high speed agate mill resulting in fine glass powders with mean particle size of 5–10 μm as determined by light scattering technique (Coulter LS 230, UK, Fraunhofer optical model). Infrared spectra of the glass powders were obtained using an infrared Fourier spectrometer (FTIR, model Mattson Galaxy S-7000, USA) in the range of 300–1500 /cm. For this purpose, each sample was mixed with KBr in the proportion of 1/150 (by weight) for 15 min and pressed into a pellet using a hand press.

A side-view hot-stage microscope Leitz Wetzlar (Germany) equipped with a Pixera video-camera and image analysis system was used to investigate the sintering behaviour of glass powder compacts. The measurements were conducted in air with a heating rate of 5 K/min. The cylindrical shaped samples from glass powder compacts with height and diameter of ~3 mm were prepared by cold-pressing the glass powders. The cylindrical samples were placed on a 10 mm × 15 mm × 1 mm alumina (> 99.5 wt.% Al_2O_3) support. The temperature was measured with a chromel–alumel thermocouple contacted under the alumina support. The temperatures corresponding to the characteristic viscosity points (first shrinkage (T_{FS}),

maximum shrinkage (T_{MS}), softening (T_D), half ball (T_{HB}) and flow (T_F)) were obtained from the graphs and photomicrographs taken during the hot-stage microscopy experiment.[22-23]

Rectangular bars with dimensions of 4 mm × 5 mm × 50 mm were prepared by uniaxial pressing (80 MPa). The bars were sintered under non-isothermal conditions for 1 h at 800, 850 and 900 ºC using a low heating rate of 2 K/min aimed to prevent deformation of samples.

Archimedes' method (*i.e.* immersion in diethyl phthalate) was employed to measure the apparent density of the samples. The three-point bending strength tests were performed on rectified parallelepiped bars (3 mm × 4 mm × 50 mm) of sintered GCs (Shimadzu Autograph AG 25 TA, 0.5 mm/min displacement): the results were obtained from at least 10 different independent samples.

2.3 Crystalline phase analysis and microstructural evolution in glass-ceramics

The amorphous nature of the parent glasses and the nature of crystalline phases present in the GCs were determined by X-ray diffraction (XRD) analysis (Rigaku Geigerflex D/Mac, C Series, Japan; Cu Kα radiation, 2θ = 10–60º with a 2θ-step of 0.02 º/s). The crystalline phases were identified by comparing the obtained diffractograms with patterns of standards complied by the International Centre for Diffraction Data (ICDD).

Microstructure observations were done at polished (mirror finishing) and then etched surfaces of samples (by immersion in 2 vol.% HF solution for 5–7 min) by field emission scanning electron microscopy (FE-SEM, Hitachi S-4100, Japan, 25 kV acceleration voltage, beam current 10 μA) under secondary electron mode.

3. Results

3.1 Microstructure and properties of glasses

Melting at 1550 ºC for 1 h was adequate to obtain bubble free, transparent and colourless glasses G1, G2 and G3, while in case of $L_{23}S_{77}$ transparent melt transformed into a cloudy hazy glass on cooling. SEM images of as cast non-annealed samples presented in Fig. 1 revealed the precipitation of a nanosize droplet phase in glassy matrices suggesting the occurrence of liquid–liquid phase separation in all investigated compositions. However, the mean droplet diameter and the population density of droplets decreased by adding Al_2O_3 and

K_2O into the Li_2O–SiO_2 system. Accordingly, homogeneous and transparent appearance was conferred to the glasses G1, G2 and G3 due to finer scale morphology and a relatively lower volume fraction of the droplets.

Infrared (FTIR) spectra of the experimental glasses G1, G3 and $L_{23}S_{77}$ are plotted in Fig. 2. All samples show lack of sharpness and a broad band in the region 850–1300 /cm. Two smaller absorption bands can be observed at ~470 (a) and ~800 /cm (b).

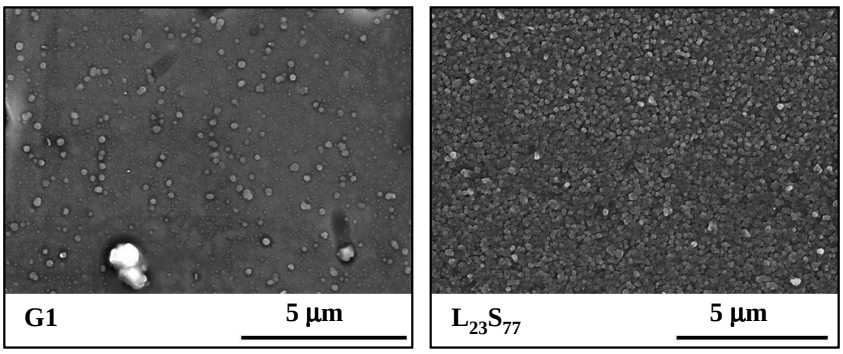

Fig. 1 – SEM images of non-annealed bulk glasses G1 and $L_{23}S_{77}$.

Some properties of experimental glasses are presented in Table 2. The transition points (T_g) and softening points (T_s) for the investigated glasses ranged between 477–498 and 501–537 ºC, respectively. Glass G1 exhibits the highest T_g and T_s, while the lowest is shown by glass $L_{23}S_{77}$. The measured CTE (200–400 ºC) values for the glasses $L_{23}S_{77}$, G1, G2, and G3 were 8.16, 8.47, 8.69 and 9.65 ($\times 10^{-6}$ /K), respectively. Consequently, an increase in Al_2O_3 and K_2O in the as-investigated proportions favours the decrease in CTE and increase in T_g and T_s of the glasses. These results are in accordance with our earlier study,[16] while some discrepancies in the CTE values might be attributed to differences in the preparation of glasses (using Pt crucibles in this study) and in the annealing procedures.

Density of glass $L_{23}S_{77}$ was 2.31 g/cm^3 while for other glasses the measured density was 2.36 g/cm^3. It was observed that molar volume (V_m), oxygen molar volume (V_o) and excess molar volume V_e (calculated using density values of annealed glasses[16]) diminished with decreasing Al_2O_3 and K_2O content as well as SiO_2/Li_2O content in the glasses (Table 2). It is worthy noting that no significant differences were observed in the values of V_m, V_o and V_e for annealed and non-annealed glasses.

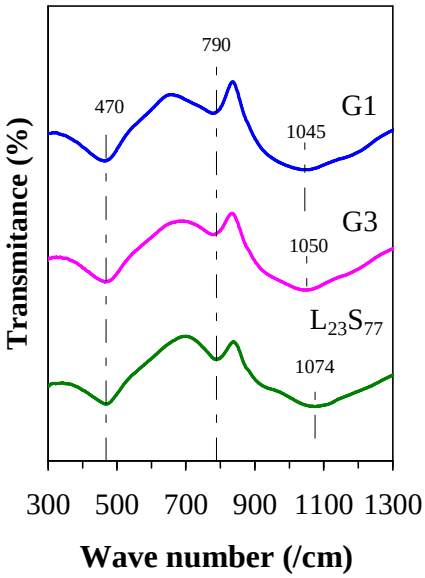

Fig. 2 – FTIR spectra of the non-annealed bulk glasses G1, G3 and $L_{23}S_{77}$.

Table 2 – Properties of the experimental glasses.

	$L_{23}S_{77}$	G1	G2	G3
Density (g/cm^3)	2.31 ± 0.01	2.36 ± 0.01	2.36 ± 0.01	2.36 ± 0.01
NBO/T	0.60	0.36	0.47	0.60
T_g (ºC)	477	498	495	477
T_s (ºC)	501	537	531	514
$CTE_{200\text{-}400ºC}$ (10^{-6} /K)	8.16	8.47	8.69	9.65
Molar volume, V_m (cm^3/mol)	23.02 ± 0.01	25.24 ± 0.01	24.27 ± 0.02	23.38 ± 0.01
Oxygen mol. vol., V_o (cm^3/mol)	13.90 ± 0.01	15.14 ± 0.02	14.85 ± 0.01	14.58 ±0.01
Excess mol. vol., V_e (cm^3/mol)	1.34 ± 0.01	1.92 ± 0.01	1.53 ± 0.01	1.22 ± 0.01

3.2 Crystallization of bulk glasses

The changes in the appearance of monolithic glasses after heat treatment at 550, 650, 750, 800 and 900 ºC for 1 h is presented in Table 3. Fig. 3 presents the DTA thermographs for all the investigated glasses at β =15 K/min.

As is evident from Fig. 3, the exothermic crystallization peaks for the G1 and G2 glasses were significantly less pronounced in comparison to those of G3 and $L_{23}S_{77}$ compositions. Using lower heating rates of 2, 5 and 10 K/min, the tendency is the same, *i.e.*, the crystallization

peaks for the glasses G1 and G2 could be hardly distinguished, while the glasses G3 and $L_{23}S_{77}$ exhibit sharp exothermic crystallization peaks under the same experimental conditions (not shown). The values of T_p for glasses $L_{23}S_{77}$, G3, G2 and G1 are 749, 823, 835 and 831 ºC, respectively, and T_p tends to shift towards higher temperatures with increasing heating rates.

Table 3 – Changes in the appearance of monolithic bulk glasses after heat treatment at different temperatures for 1 h.

	G1	G2	G3	$L_{22}S_{77}$
As-cast glass	Transparent	Transparent	Transparent	Cloudy
450 ºC	Transparent	Transparent	Transparent	Cloudy
550 ºC	Transparent	Transparent	Semi transparent	Cloudy
650 ºC	Transparent	Transparent	Semi transparent	White opaline
750 ºC	Semi transluc. opaline	White translucent opaline	Semi translucent opaline	White opaline
800 ºC	Semi transluc. opaline	White transluc.opaline	White transluc. opaline	White opaline
900 ºC	Semi transluc. opaline	White transluc. opaline	White transluc. opaline	White opaque

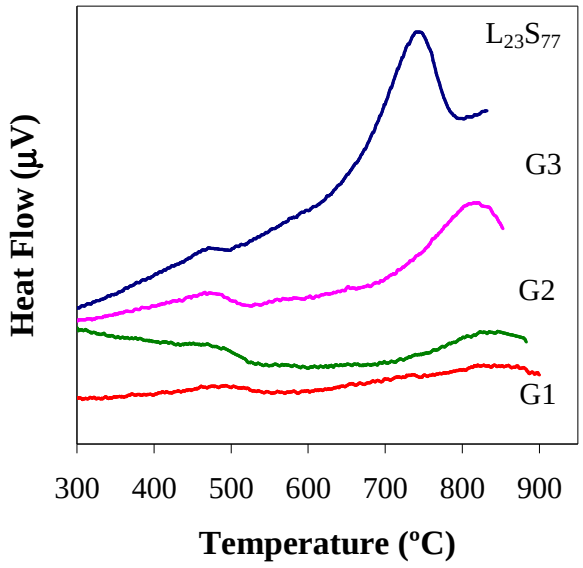

Fig. 3 – DTA thermographs for all the investigated glasses at β =15 K/min.

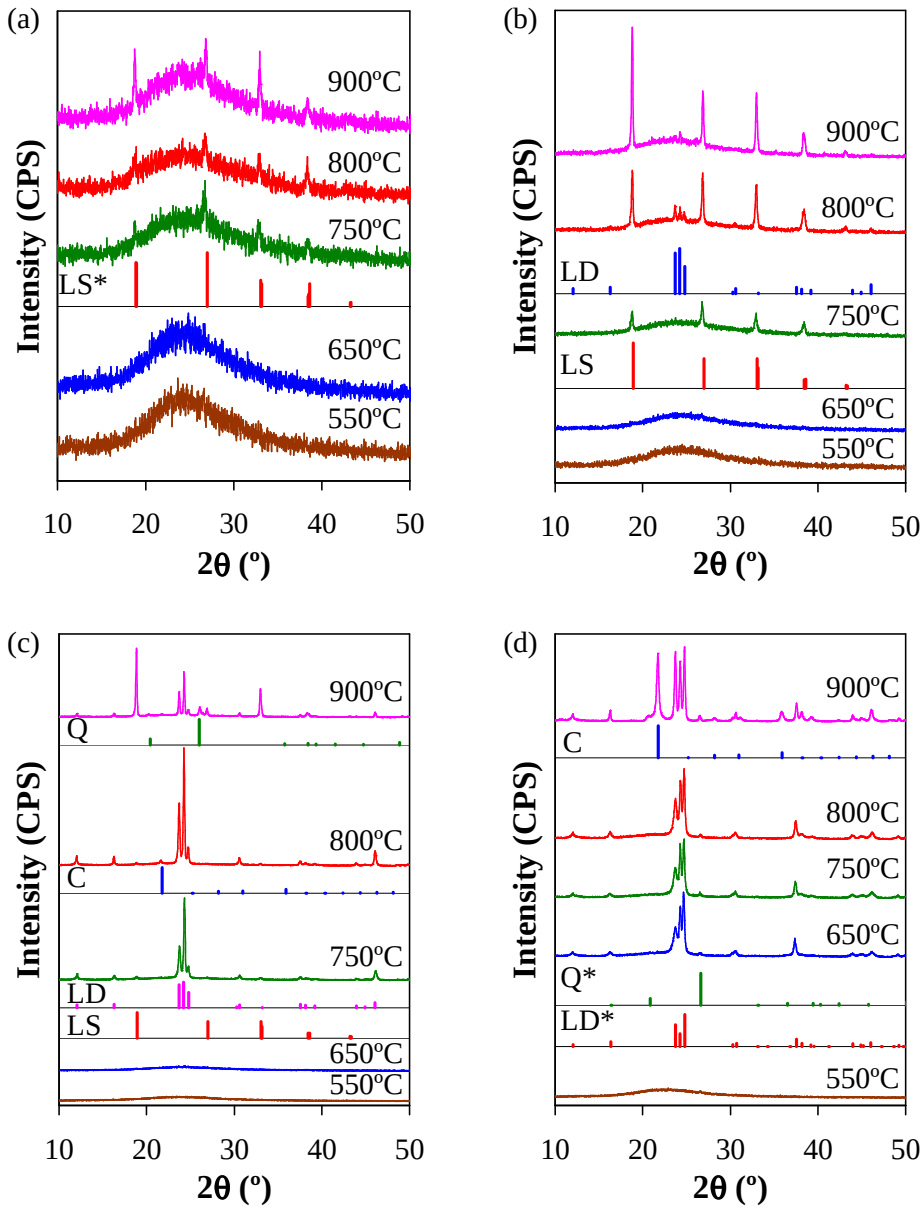

Fig. 4 – X-ray diffractograms of bulk glasses heat treated at 550, 650, 750, 800 and 900 ºC: (a) G1, (b) G2, (c) G3 and (d) $L_{23}S_{77}$. LS*: lithium silicate (Li_2SiO_3, ICCD card 01-070-0330); LS: lithium silicate (Li_2SiO_3, ICCD card 00-029-0828); LD*: lithium disilicate ($Li_2Si_2O_5$, ICCD card 01-072-0102); LD: lithium disilicate ($Li_2Si_3O_5$, ICCD card 01-049-0803); Q: quartz (SiO_2, ICCD card 01-070-2516); Q*: quartz (SiO_2, ICCD card 01-077-1060); C: cristobalite (SiO_2, ICCD card 01-082-0512) [scale bar: (a) 3500, (b) 3500, (c) 70000 and (d) 40000 cps].

Fig. 4 presents the evolution of phases in bulk glasses heated at different temperatures for 1 h. No crystallization events could be detected by XRD analysis in G1, G2 and G3 at both 550

and 650 ºC while strong peaks of LD with quartz (Q) traces were already registered in $L_{23}S_{77}$ at 650 ºC. The same phase assemblage was revealed in $L_{23}S_{77}$ upon further heat treating at 750 and 800 ºC until 900 ºC when cristobalite (C) also appeared. The composition G1 exhibited monomineral Li_2SiO_3 (hereafter referred as LS) as the only crystalline phase at temperatures ≥ 750 ºC. In agreement with GC G1, LS crystallized as the only phase in composition G2 after heat treatment at 750 ºC. However, with further increase in temperature to 800/900 ºC, this crystalline phase was adjoined by LD which precipitated as a secondary phase. The composition G3 with lowest K_2O and Al_2O_3 content exhibited LD as the major phase formed at 750 ºC together with traces of LS.

Surface crystallization and dendritic skeletal crystal growth of LS could be observed by SEM in both G1 and G2 in the temperature interval 750–900 ºC (not shown), being consistent with nucleated droplet phase separation in the inner part of the specimens as previously documented for glass G1.[16] SEM images of G3 support the conclusion that LD crystal growth occurred in the form of rods upon heat treating in the temperature interval of 550–750 ºC (Fig. 5(a) and (b)), nucleated from the nanosize droplet phase revealed in the parent non-annealed glass (Fig. 1). G3 specimens became semi-transparent at 550 ºC (Table 3) before any crystallization could be detectable by XRD.

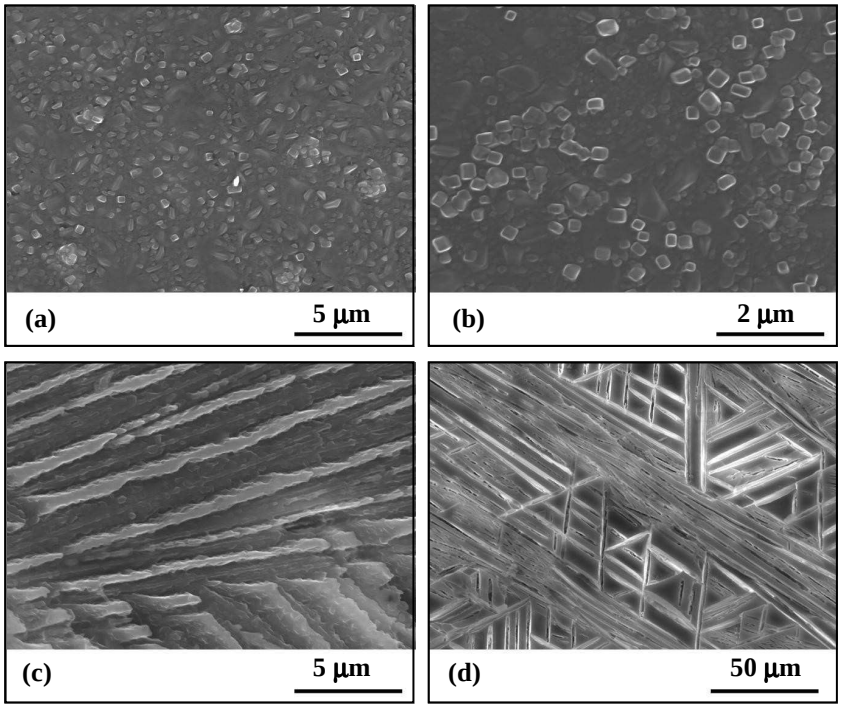

Fig. 5 – SEM images of glass G3 heat treated at several temperatures: (a) 550, (b) and (c) 750, and (d) 900 ºC.

These results suggest that the volume fraction of crystals developed was less than the limit of XRD resolution.[24] Apart from the individual fine rod like crystals observed in the core of G3 specimen at 750 ºC (Fig. 5(b)), there was a structural rearrangement trend towards the formation of oriented fibres (Fig. 5(c)). This is consistent with optical observations made by Morse and Donnay[25] who concluded that the size increase of LD crystals occurs through nucleation and growth of individual rods because every point of the surface of growing fibre can act as a nucleating site for a new rod. Crystal growth of LD in G3 resulted in the formation continuous laminar fibres of LD at 900 ºC (Fig. 5(d)).

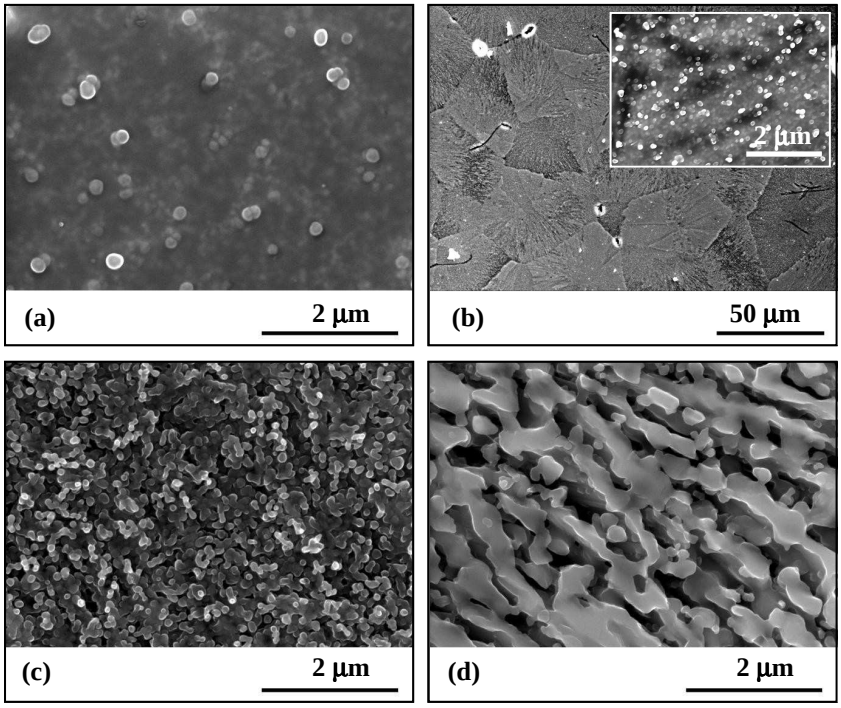

Fig. 6 – SEM images of glass $L_{23}S_{77}$ heat treated at several temperatures: (a) 550, (b) 650, (c) 800, and (d) 900 ºC.

The SEM images of heat treated $L_{23}S_{77}$ specimens show that the nuclei growth up to the critical size at 550 ºC (Fig. 6(a)) has been followed by the formation of LD spherulites at 650 ºC (Fig. 6(b)) as detected by XRD (Fig. 4(d)). At elevated temperatures, 750 and 800 ºC, spherulites were composed by numerous submicron roundly shaped crystals (Fig. 6(c)) followed by a coarsening process at 900 ºC (Fig. 6(d)) with simultaneous formation of cristobalite, as identified by XRD analysis (Fig. 4(d)). Seemingly $L_{23}S_{77}$ was almost fully crystallized at 800 ºC and then residual silica rich glass phase start to devitrify in the form of cristobalite.

Crystallization kinetics studies were performed only for glasses G3 and $L_{23}S_{77}$ because glasses G1 and G2 showed low tendency towards devitrification and exhibited negligible crystallization exothermic curves at the experimental heating rates (β = 2–15 K/min) used in this study. It may be observed that $\left.\frac{d\chi}{dt}\right|_p$ increases with the heating rate (Fig. 7, Eq. (2)). The plots of crystallization fraction *vs* temperature show that crystallization rate of LD decreases with addition of Al_2O_3. This can be attributed to a longer time duration required for the minimum percentage of crystallinity to be detectable by XRD.[24, 26] The values of E_c for glasses $L_{23}S_{77}$ and G3 are 153 and 330 kJ/mol, respectively while the value of n is ~3.04±0.05 and 1.51±0.02, respectively. The corresponding mean values may be taken as the most probable quoted exponents.

3.3 Crystallization of glass powder compacts

The variations in density and bending strength of glass powder compacts with firing temperature in the range 800–900 ºC are plotted in Fig. 8. Well densified GC materials G1 and G2 exhibiting bending strength values of 114±2 and 158±5MPa, respectively, were obtained after sintering at 800 ºC (Fig. 8, Table 4).

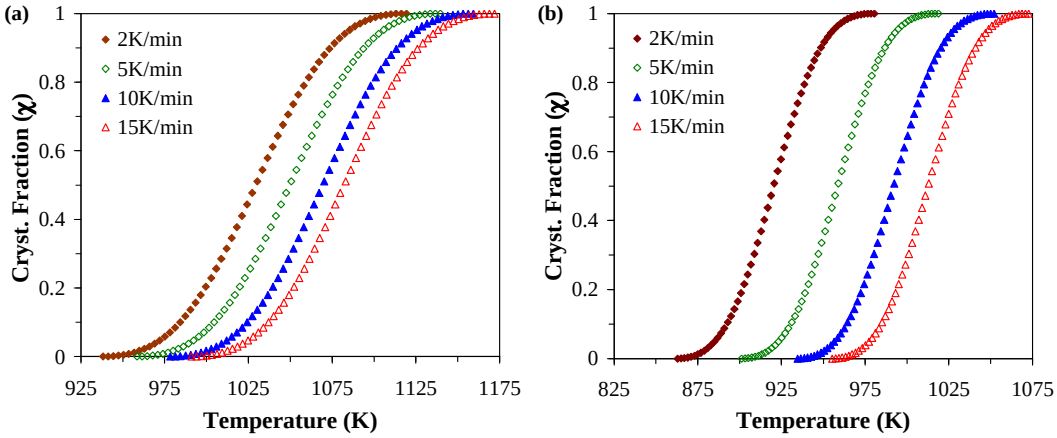

Fig. 7 – Crystallization fraction *vs* heat treatment temperature: (a) G3 and (b) $L_{23}S_{77}$.

Under the same conditions, GC3 featured lower mechanical properties (81±8 MPa) in comparison to GC1 and GC2, while $L_{23}S_{77}$ samples exhibited high fragility and the lowest values of flexural strength (0.7±0.1 MPa) and density (2.03±0.05 g/cm^3) among all investigated compositions. No improvement in densification level was observed for this Al_2O_3

and K_2O free composition after further heat treatment, resulting in mechanically very weak and highly porous samples. On the contrary, GC3 demonstrated the beneficial effect of small addition of Al_2O_3 and K_2O to bicomponent composition $L_{23}S_{77}$. In particular, increases of density (2.25±0.01 g/cm^3), shrinkage (15.9±0.3%) and mechanical strength (216±3 MPa) were observed after firing at 850 ºC followed by further densification and strengthening at 900 ºC (density 2.36±0.01 g/cm^3, bending strength 224±4 MPa). The GCs from glass G1 and G2 showed the maximum density values (2.34 and 2.36 g/cm^3, respectively) at 850 ºC followed by a smooth decrease at 900 ºC. Their maximum flexural strength values of 189±8 MPa for composition GC1 and of 195±9 MPa for composition GC2 were attained at 900 ºC.

X-ray diffractograms revealed LS as the single crystalline phase in GC1 after sintering at 800 ºC (Fig. 9), while GC2 and GC3 comprised LS along with Q and LD as minor phases (Fig. 9(b) and (c)). At 850 and 900 ºC (Fig. 9(c)), GC3 featured almost monomineral composition of LD with peaks of low intensity attributed to Q. From the XRD spectra of the compositions with higher amount of Al_2O_3 and K_2O LD was revealed in G1 and became principle phase in G2 after sintering at 850 ºC. Finally, LD was the main crystalline phase while LS and Q were minor phases in both GC1 and GC2 at 900 ºC.

Table 4 – Properties of the glass powder compacts heat treated at different temperatures.

	$L_{23}S_{77}$	G1	G2	G3
Density (g/cm^3)				
800 ºC	2.03 ± 0.05	2.28 ± 0.05	2.35 ± 0.01	2.19 ± 0.03
850 ºC	2.04 ± 0.07	2.34 ± 0.01	2.36 ± 0.01	2.25 ± 0.01
900 ºC	2.14 ± 0.04	2.33 ± 0.01	2.35 ± 0.01	2.36 ± 0.01
Shrinkage (%)				
800 ºC	0.7 ± 0.1	17.0 ± 0.3	16.9 ± 0.1	12.6 ± 0.1
850 ºC	1.7 ± 0.2	17.9 ± 0.2	17.1 ± 0.1	15.9 ± 0.3
900 ºC	5.2 ± 0.1	18.1 ± 0.1	17.2 ± 0.1	18.0 ± 0.3
Bending strength (MPa)				
800 ºC	0.7 ± 0.1	114 ± 2	158 ± 5	81 ± 8
850 ºC	1.0 ± 0.2	134 ± 4	187 ± 14	216 ± 3
900 ºC	13 ± 2	189 ± 8	195 ± 9	224 ± 4
$CTE_{200\text{-}500\ ºC}$ (10^{-6} /K)[a]	13.45	7.41	7.91	8.69
$CTE_{200\text{-}700\ ºC}$ (10^{-6} /K)[a]	12.51	9.00	9.57	9.94

[a] Samples sintered at 900 ºC.

LD was the main crystalline phase in $L_{23}S_{77}$ glass powder compacts sintered at 800 and 850 ºC (Fig. 9(d)). Most probably, GC $L_{23}S_{77}$ was almost fully crystallized at 800 ºC. Then, the

residual glassy phase depleted from lithium and having high silica content starts to crystallize in the form of quartz and tridymite.[27] Finally, quartz along with LD became the principal crystalline phases at 900 ºC and peaks of tridymite along with cristobalite were also observed in the XRD pattern (Fig. 9(d)) which is, in fact, in good correlation with phase diagram of SiO_2–Li_2O binary system.[28]

The microstructures of the GC1, GC2 and GC3 observed under SEM revealed different morphologies of the crystals developed. The typical microstructure of GC1 sintered at 800 ºC (Fig. 10(a)) features dendrite configuration of LS crystals in SiO_2–Li_2O binary system.[28] Heat treatment of G1 at 850 ºC made LD crystals to grow in the form of submicron sized rods that act as nucleating sites for new rods that increase in size (Fig. 10(b)). Crystal growth of the individual LD rods in G2 and G3 at 900 ºC resulted in the formation of continuous laminar fibres of LD embedded in glassy matrix (Fig. 10(c) and 10(d)) which are responsible for high mechanical strength of these GCs.

Fig. 11 reveals two main steps of sintering for glass powder compacts G1, G2 and G3 during a thermal treatment at a constant heating rate (5 K/min) from ambient temperature to 1000 ºC. Since glass G3 has lower T_g, it starts to sinter earlier than glass G1 and G2 exhibiting the temperature of first initial shrinkage T_{FS1} at 525 ºC.

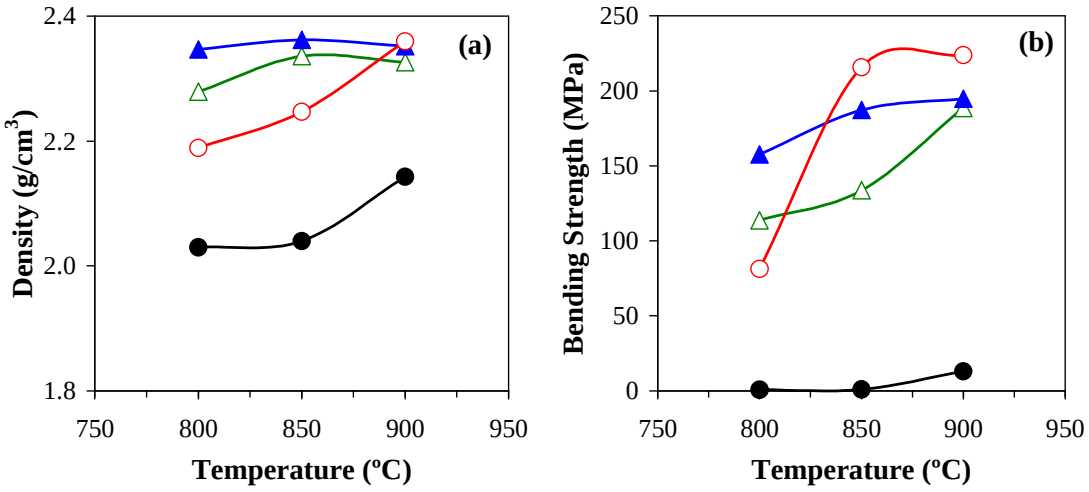

Fig. 8 – Some properties of glass powder compacts heat treated at different temperatures: (a) density and (b) bending strength [●: $L_{23}S_{77}$; △: G1; ▲: G2; ○: G3].

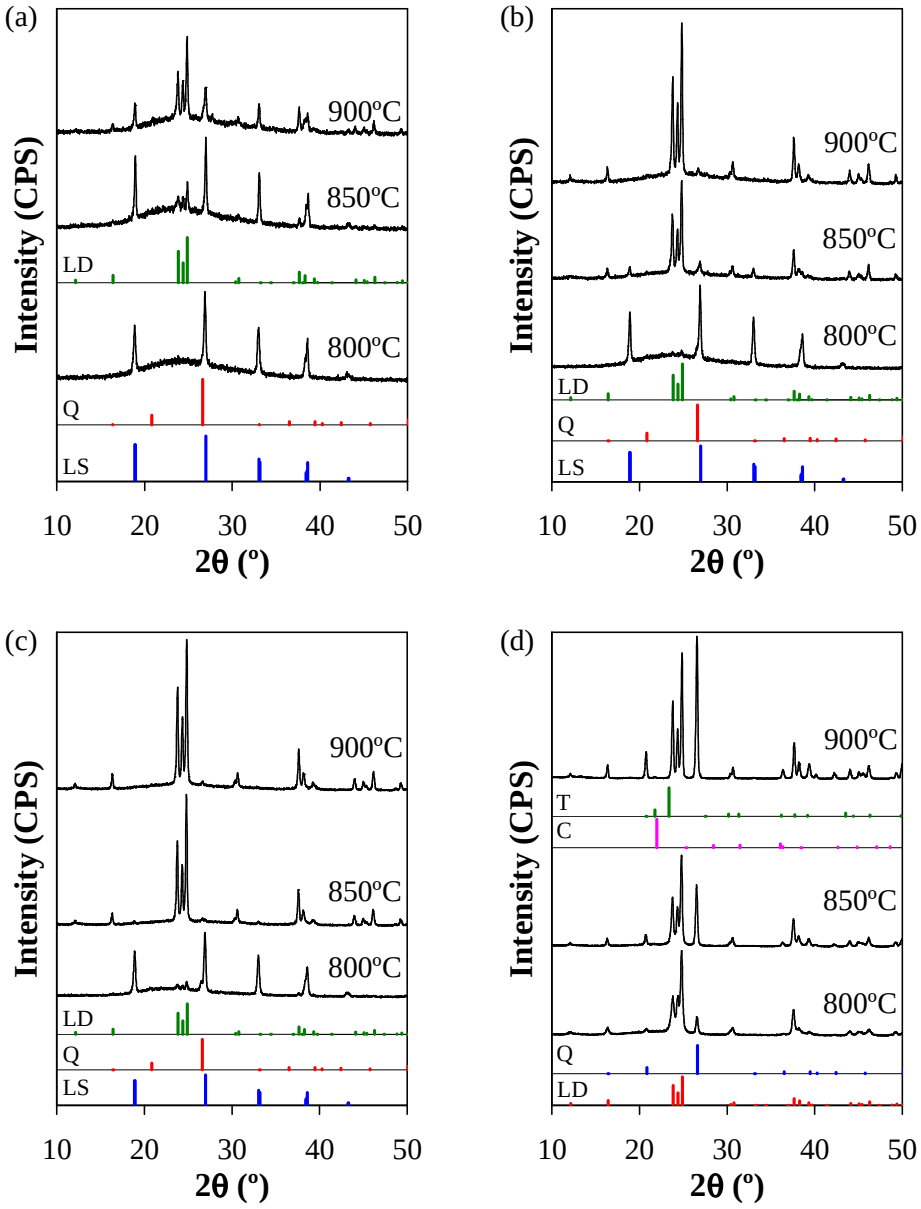

Fig. 9 – X-ray diffractograms of glass powder compacts heat treated at 800, 850 and 900 ºC: (a) G1, (b) G2, (c) G3 and (d) $L_{23}S_{77}$. LS: lithium silicate (Li_2SiO_3, ICCD card 01-070-0330); LD: lithium disilicate ($Li_2Si_2O_5$, ICCD card 01-070-4856); Q: quartz (SiO_2, ICCD card 01-077-1060); T: trydimite (SiO_2, ICCD card 00-042-1401); C: cristobalite (SiO_2, ICCD card 00-039-1425) [scale bar: (a) 12500, (b) 18500, (c) 28000 and (d) 45000 cps].

The first maximum shrinkage (T_{MS1}) for glass G3 was assigned at 570 ºC that was well correlated with first signs of LS crystallization at 550 ºC evidencing from the XRD analysis (not shown). Thus, the interval of first sintering step was wider for G1 (68 ºC) and for G2 (49 ºC) in accordance with their higher T_p values. As soon as the first sintering period finishes, LS start to precipitate from the glass reservoir and crystallization becomes the dominant process.

No shrinkage occurs during this period since crystallization impedes densification. A second shrinkage stage starts almost synchronically at 793–795 ºC for all experimental compositions, the maximum shrinkage (T_{MS2}) being reached at 851, 822 and 924 ºC for G1, G2 and G3, respectively.

4. Discussion

4.1 Bulk glasses

According to Vogel,[8] liquids in pure Li_2O–SiO_2 system containing less than 30 mol.% Li_2O undergo phase separation into droplet like zones of Li-rich phase and SiO_2-rich glass matrix within a metastable immiscibility dome.[29] Consequently, the cloudy appearance of the $L_{23}S_{77}$ glass was expected. Moreover, the droplet size in this glass has remained nearly the same as observed by Vogel.[8]

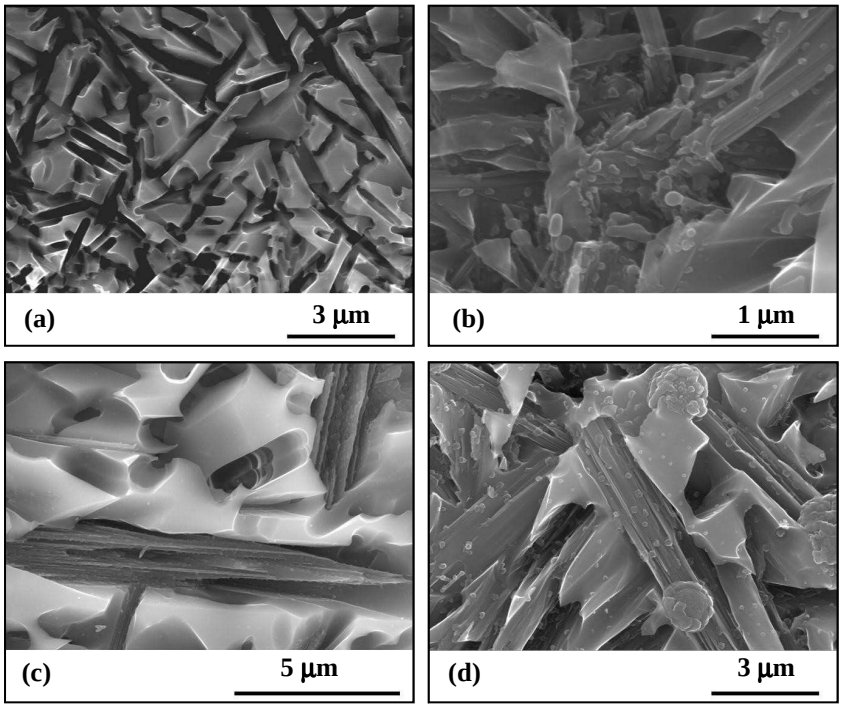

Fig. 10 – SEM images of heat treated glass powder compacts: (a) G1, 800 ºC; (b) G1, 850 ºC; (c) G2, 900 ºC; and (d) G3, 900 ºC.

SEM examination of the segregation effects occurring in bulk glasses (Fig. 1) confirms that incorporation of Al_2O_3 greatly decreases the immiscibility trend. This phenomenon can be

explained by the structural role of Al^{3+} which may exist in four coordinated position due to the presence of alkali cations in the glasses. In order to maintain local charge neutrality, $(AlO_{4/2})^-$ units will be charge compensated by alkali cations (K^+, Li^+) which must be present in the vicinity of each such tetrahedron. Therefore, the $(AlO_{4/2})^-$ tetrahedra will substitute directly into the network for silicon–oxygen tetrahedra and simultaneously tend to suppress the immiscibility while raising the T_g and decreasing the CTE of glasses.[16, 29]

The lack of sharpness featured in FTIR spectra of the experimental glasses G1, G3 and $L_{23}S_{77}$ (Fig. 2) is indicative of the general disorder in the silicate network mainly due to a wide distribution of Q^n units (polymerization in the glass structure, where n denotes the number of bridging oxygens) occurring in these glasses. The broad absorption band in the higher wave number region (850–1300 /cm) is attributed to the stretching vibrations of $[SiO_4]$ tetrahedra. The bands at ~470 and ~800 /cm are linked to bending modes of the silicate network.[30] The FTIR stretching band of SiO_2 tetrahedra slightly broadened in $L_{23}S_{77}$ in comparison with Al_2O_3-containing glasses G1 and G3. Additionally, the appearance of absorption bands at frequencies ~870, ~915 /cm in $L_{23}S_{77}$ proves existence of broader distribution of the non-bridging oxygens among the tetrahedral cation and a less polymerized glass network. On the contrary, a shallow band at frequency ~1170 /cm was observed in the infrared spectra of Al_2O_3-containing glasses, in particular G1 suggesting towards the occurrence of Q^4 units and consequently an increase in cross-linking degree. Nevertheless, further ^{27}Al-MAS-NMR study will be performed to support the hypothesis of Al incorporation in four-fold coordination and its homogeneous mixture within the silicate matrix.

Based on the assumption that Al^{3+} acts as a network former, the numbers of non-bridging oxygen per each tetrahedral cation (NBO/T) were calculated[31] for the glasses G1, G2, G3 and $L_{23}S_{77}$ as 0.36, 0.47, 0.60 and 0.60, respectively (Table 2), suggesting more polymerized glass network structures for G1 and G2. Moreover, from Table 2, G1 exhibits the highest T_g while the lowest T_g values are shown by the G3 and $L_{23}S_{77}$ glasses. The addition of Al_2O_3 in proportion corresponding to G1 and G2 decreased the NBO/T and thus, leading to an increase in T_g. This is consistent with the results reported for the effect of RO_n addition on Li_2O–SiO_2–RO_n glasses (R = P, V, Zr).[14, 32] On the contrary, the lower T_g values measured for $L_{23}S_{77}$ and G3 (Table 2) can be attributed to a less polymerization extent of the silicate network, *i.e.*, higher number of NBO/T, leading to a lower viscosity. At a given temperature, the viscosity of binary silicate melts and super cooled melts generally decreases with increasing concentration of modifiers and NBO/T.[33]

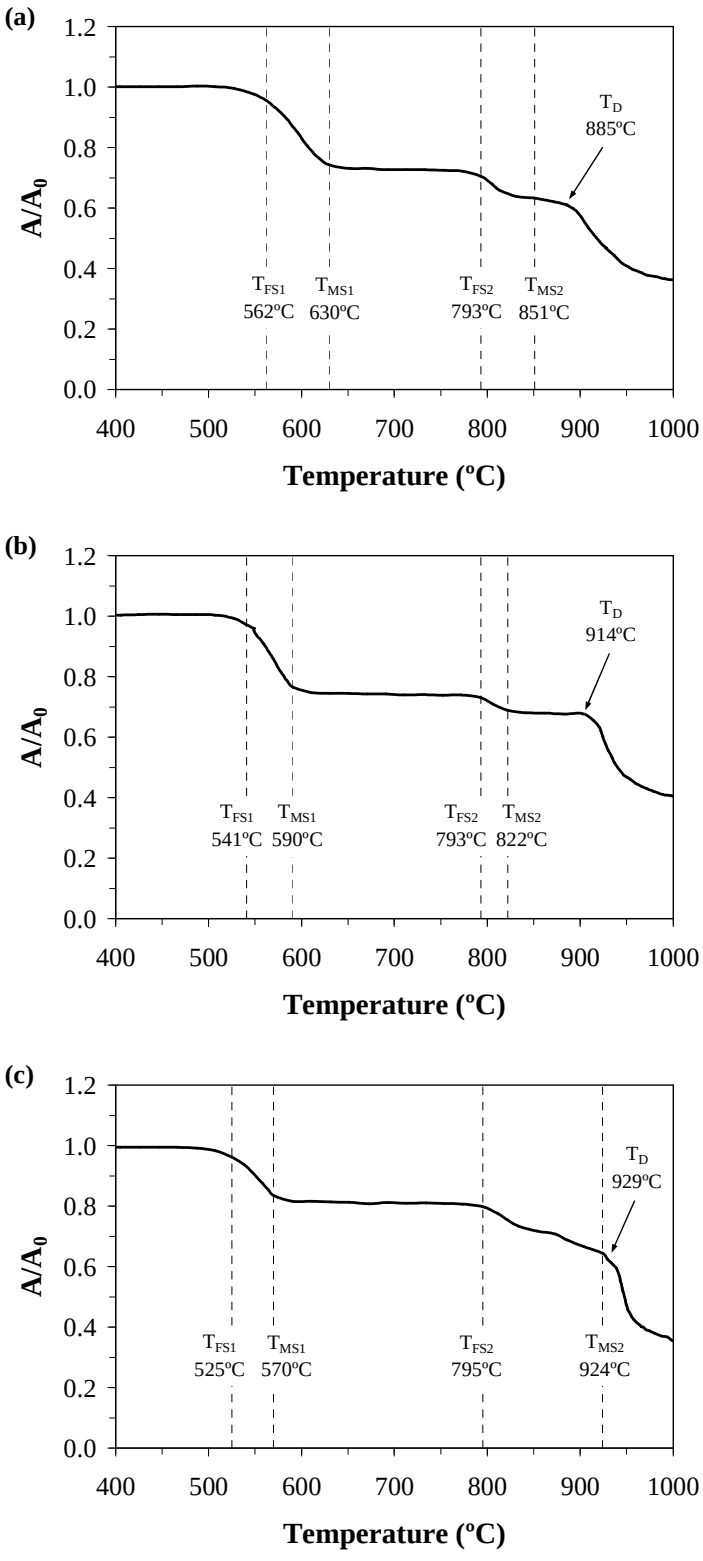

Fig. 11 – Variation in relative area (A/A_0:A_0 is the initial area at room temperature, A is the area at defined temperature) powder samples (a) G1, (b) G2 and (c) G3 during the HSM measurement.

Al^{3+} essentially acts as network former, thus, increasing the molar volume of the glasses G1 and G2. The V_m and V_o values for glass the G3 were higher than for the glass $L_{23}S_{77}$ while an opposite trend was observed for V_e. The lower V_e value for glass G3 in comparison to glass $L_{23}S_{77}$ is likely due to the collapse of the structural skeleton into a closer packing because of the presence of two highly ionic oxides (K_2O and Li_2O) in the former which further leads to higher CTE of glass G3 in comparison to glass $L_{23}S_{77}$.

The peak temperature of crystallization (T_p) tendency to shift towards higher temperatures with addition of Al_2O_3 and K_2O can also be attributed to the structural role of the Al_2O_3 having glass forming units $(AlO_{4/2})^-$ that are larger than $(SiO_4)^{-4}$ tetrahedra due to the different ionic radius of Al^{3+} (0.53 Å) and Si^{4+} (0.40 Å).[34] This leads to an increasing viscosity of the glasses, further reducing the mobility of the different ions and ionic complexes operative in the crystallization process. This result is in good agreement with XRD data and SEM observations of the heat treated specimens.

The Avrami parameter for both the glasses $L_{23}S_{77}$ and G3 suggests bulk crystallization with constant number of nuclei, *i.e.*, the existence of three-dimensional bulk crystallization that is diffusion controlled in the case of G3.[35-36] The higher E_c for glass G3 in comparison to glass $L_{23}S_{77}$ reflects the structural role of Al_2O_3 in the investigated compositions and supports the explanation presented above. The E_c value for glass $L_{23}S_{77}$ (153 kJ/mol) was lower in comparison to that obtained by Freiman and Hench[24] (205 kJ/mol) for a glass with the composition $25Li_2O–75SiO_2$ (mol.%). This difference might be due to different compositions and approaches used to investigate crystallization kinetics.

4.1 Glass powder compacts

Significant changes in crystalline phase assemblage of Al_2O_3 and K_2O containing GCs occurred in the temperature interval of 800–900 ºC. LD precipitated as a secondary phase in GC1 after heat treatment at 850 ºC along with quartz (Q) and LS as major crystalline phases. However, after heat treatment at 900 ºC, LD crystallized to be the primary phase in GC1 along with Q and LS as secondary phases. It is noteworthy LD was not recorded in GC1 prepared through nucleation and crystallization approach in monolithic bulk glasses. This behaviour can be ascribed to the difference in preparation routes of the parent glasses as water quenching of the glass increases the OH content. The hydroxyl groups may act as a modifier and break the silicate network, thus, reducing the viscosity and activation energy of viscous

flow.[16, 37] A large fraction of LD precipitated out to become the major phase in GC2 and GC3 after sintering at 850 and 900 ºC. Crystallization of LD during preparation of glass-powder compacts G1, G2 and G3 predominantly occurs at temperatures above 800 ºC via the precursor LS phase[16, 38] due to the reaction described by the following chemical equation

$$Li_2SiO_3 + SiO_2 \rightarrow Li_2Si_2O_5 \quad (3)$$

No aluminium and potassium associated phases were found by XRD analysis in GC1, GC2 and GC3, resulting in improved mechanical strength compared to data obtained for GCs in the previous study.[16]

For the GC1, GC2 and GC3 the CTE values were higher within the range of 200–700 ºC than within the range of 200–500 ºC (Table 4), but the difference is smaller in case of GC3, compared to GC1 and GC2, most probably due to its lower amount of quartz. The phase inversions of silica polymorphs are completely reversible on cooling and in particular volume changes of tridymite and cristobalite occur at lower temperature than that of quartz when stress relief due to viscous flow in the residual glass phase cannot take place. These changes cause greater stresses during heating and cooling through the inversion temperature ranges leading to weakening of the material. Nevertheless, the main reason for low mechanical performance of $L_{23}S_{77}$ GC was its poor sintering ability due to an early initiation of devitrification process in comparison to Al_2O_3 and K_2O containing glasses. In general, the desired order of events in glass-powder densification process occurs when sintering precedes crystallization. Hence, glasses with large temperature interval between T_g and T_c can possibly be well sintered.[39] When the onset of crystallization occurs before the glass is fully densified, further densification will be impeded by the formation of crystalline phase that increases the matrix viscosity.[40] From the DTA thermographs of glass grains (Fig. 3) the temperature of peak crystallization (T_p), shifted towards higher temperature region with addition of Al_2O_3 and K_2O suggesting an increase in sintering range for experimental compositions in accordance with the trend: $L_{23}S_{77}$ <G3 <G2 < G1. Consequently, the sintering process of $L_{23}S_{77}$ glass powder compacts occurs in narrower T_c–T_g interval compared to Al_2O_3 and K_2O containing compositions and densification was suppressed by the formation of large fraction of LD phase. This phenomenon can explain the behaviour of $L_{23}S_{77}$ that apparently exhibited low flexural strength, density and shrinkage values at 800 ºC (Fig. 8, Table 4).

Further heat treatment at 850 and 900 ºC slightly facilitated densification because the overall volume of the system decreased when residual silica glassy phase (density 2.20 g/cm^3)

crystallized in the form of quartz (density 2.65 g/cm^3) and tridymite (density 2.27 g/cm^3). However, the volume changes occurred in the interval 850 and 900 ºC were not sufficient to cause appreciable increase of density and mechanical strength. Thus, $L_{23}S_{77}$ sample remained porous and highly fragile even at 900 ºC, and densification can only be expected to happen at temperatures close to the *liquidus* line of SiO_2–Li_2O binary system at which abrupt formation of liquid phase occurs.[41]

Unlike to glass $L_{23}S_{77}$, densification process of glass powder compacts G1, G2 and G3 demonstrated excellent sintering ability although, even these compositions also did not follow the desired sequence of events and sintering was partially impeded by crystallization. However, due to a broader T_c–T_g interval, these glass powder compacts attained significant level of densification before crystallization started. The softening point T_D (the temperature at which the first signs of softening are observed by rounded edges of the samples) and half ball point T_{HB} (the temperature at which the section of the sample forms a semicircle on the microscope grid) increase in the order G3 > G2 > G1.

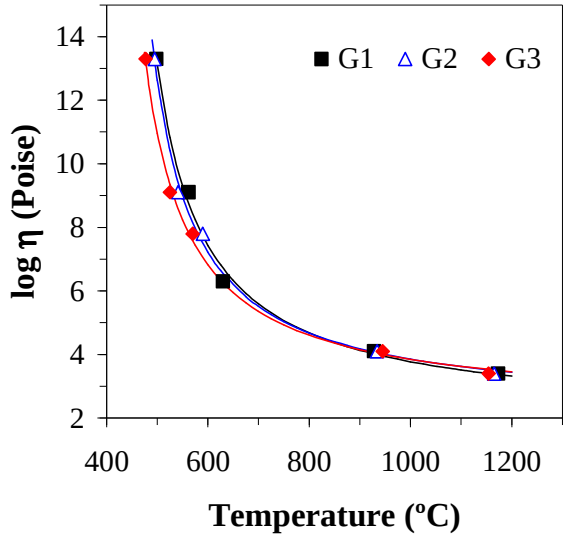

Fig. 12 – Viscosity–temperature curve of the experimental glasses.

The viscosity-temperature curves for G1, G2 and G3 glasses can be built considering their dilatometric T_g ($log\ \eta$ = 13.3) and the experimental temperatures received from the HSM (first and maximum shrinkage, half ball and fluency). The softening point is very much affected by crystallisation and corresponding viscosity cannot be evaluated. The viscosity data might be fitted to the Vogel–Fulcher–Tamman, VFT, Eq. (4), employing a regressive method with all the viscosity experimental points in the studied range.

$$\log \eta = A + \frac{B}{T - T_0} \quad (4)$$

The values of the constants obtained from the fit are the following for each glass (T in ◦C): G1: A = 1.9699, B = 1072.96, T_0 = 403.763; G2: A = 2.23717, B = 955.356, T_0 = 408.105; G3: A = 2.28236, B = 951.887, T_0 = 390.219.

From the approximate viscosity–temperature curve (Fig. 12) the increasing Al_2O_3 content of the glass has a decisive influence on viscosity. Particularly, glass G3 exhibited lowest viscosity at temperatures below 850 ºC and at the constant temperature *log η*(G1) > *log η*(G2) > *log η*(G3). These results are in accordance with Fluegel[42] reporting that Al_2O_3 usually increases the viscosity of glasses, most significantly at low temperatures, caused by the elimination of non-bridging oxygen sites. Within the scope of optimization of material, Fig. 12 supports our assumption that addition of Al_2O_3 reduces the mobility of the different ions and ionic complexes operative in the nucleation and crystallization process. The opposite trends can be observed when temperatures exceeded 850 ºC: compositions G2 and G3 demonstrated higher viscosity than G1. This can be explained by formation of a larger fraction of LD in GC2 and GC3 at 850 ºC and 900 ºC (Figs. 9(a)–(c)) that cause in shifting of their T_D and T_{HB} values to higher temperature region.

Nevertheless, further quantitative XRD analysis will be required to estimate the amount of glassy phase and its role in the second sintering step of the samples.

5. Conclusions

In context of monolithic bulk glasses, liquid–liquid phase separation occurred in all investigated compositions as illustrated by the nanosize droplets precipitated in the glassy matrixes. Al^{3+} acting as network former decreases the volume fraction and mean diameter of droplet phase resulting in transparent glasses G1, G2 and G3, while the opposite effect was observed in the Al_2O_3 and K_2O free glass that became cloudy on cooling. Surface nucleation and crystallization was dominant in glasses G1 and G2 with LS as the primary crystalline phase while volume nucleation and crystallization was observed in glasses G3 and $L_{23}S_{77}$ with LD as the primary crystalline phase. The values of E_c for glasses $L_{23}S_{77}$ and G3 were 153 and 330 kJ/mol, respectively.

Sintered glass powder compacts featured enhanced mechanical properties in comparison to materials earlier prepared in alumina crucibles. In compositions with higher amounts of Al_2O_3 and K_2O, both LS and Q were found as minor crystalline phases at 850 and 900 ºC, while GC-G3 under the same heat treatment conditions featured almost monomineral LD composition.

The narrowing of the T_c–T_g interval in the $L_{23}S_{77}$ glass powder compacts in comparison to Al_2O_3 and K_2O containing compositions hindered the densification process and led to the early formation of large fraction of LD phase resulting in poorly densified samples. Small addition of Al_2O_3 and K_2O to pure Li_2O–SiO_2 system enhanced the densification behaviour and the ultimate mechanical strength. Nevertheless, two main steps of sintering were observed by HSM for glass powder compacts G1, G2 and G3, separated by the temperature range within which LS crystallization occurs and temporarily hinders densification.

Acknowledgments

Hugo R. Fernandes is grateful for the financial support of CICECO and for the PhD grant (SFRH/BD/41307/2007) from the FCT, Portugal. Ashutosh Goel is thankful to CICECO and FCT, Portugal (SFRH/BPD/65901/2009) for the post-doctoral research grant.

References

1. Anspach O, Keding R, Rüssel C. Oriented lithium disilicate glass–ceramics prepared by electrochemically induced nucleation. Journal of Non-Crystalline Solids 2005;351:656-62.
2. Borom MP, Turkalo AM, Doremus RH. Strength and microstructure in lithium disilicate glass-ceramics. Journal of the American Ceramic Society 1975;58(9-10):385-91.
3. Doremus RH, Turkalo AM. Crystallization of Lithium Disilicate in Lithium Silicate-Glasses. Physics and Chemistry of Glasses 1972;13(1):14-&.
4. Headley TG, Loehman RE. Crystallization of Glass–Ceramics by Epitaxial Growth. Journal of the American Ceramic Society 1984;67:620-25.
5. James PF, McMillan PW. Quantitative Measurements of Phase Separation in Glasses Using Transmission Electron Microscopy. Part 1. Experimental Technique and Method of Analysis. Physics and Chemistry of Glasses 1970;11(3):59-&.
6. Ota R, Mishima N, Wakasugi T, Fukunaga J. Nucleation of Li_2O–SiO_2 glass and its interpretation based on a new liquid model. Journal of Non-Crystalline Solids 1997;219:70-74.

7. Ray CS, Day DE, Huang W, Narayan KL, Cull TS, Kelton KF. Non-isothermal calorimetric studies of the crystallization of lithium disilicate glass. Journal of Non-Crystalline Solids 1996;204(1):1-12.
8. Vogel W. Structure and Crystallization of Glasses. Leipzig: Pergamon Press; 1971.
9. Zanotto ED. Metastable phases in lithium disilicate glasses. Journal of Non-Crystalline Solids 1997;219:42-48.
10. Iqbal Y, Lee WE, Holland D, James PF. Crystal nucleation in P_2O_5-doped lithium disilicate glasses. Journal of Materials Science 1999;34(18):4399-411.
11. Von Clausbruch CS, Schweiger M, Höland W, Rheinberger V. The effect of P_2O_5 on the crystallization and microstructure of glass–ceramics in the SiO_2–Li_2O–K_2O–ZnO–P_2O_5 system. Glastechnische Berichte-Glass Science and Technology 2001;74:223-29.
12. Wen G, Zheng X, Song L. Effects of P_2O_5 and sintering temperature on microstructure and mechanical properties of lithium disilicate glass-ceramics. Acta Materialia 2007;55(10):3583-91.
13. Arvind A, Sarkar A, Shrikhande VK, Tyagi AK, Kothiyal GP. The effect of TiO_2 addition on the crystallization and phase formation in lithium aluminum silicate (LAS) glasses nucleated by P_2O_5. Journal of Physics and Chemistry of Solids 2008;69(11):2622-27.
14. Lin CC, Shen PY, Chang HM, Yang YJ. Composition dependent structure and elasticity of lithium silicate glasses: Effect of ZrO_2 additive and the combination of alkali silicate glasses. Journal of the European Ceramic Society 2006;26(16):3613-20.
15. Rukmani SJ, Brow RK, Reis ST, Apel E, Rheinberger V, Höland W. Effect of V and Mn colorants on the crystallization behaviour and optical properties of Ce-doped Li-disilicate glass–ceramics. Journal of the American Ceramic Society 2007;90(9):706-11.
16. Fernandes HR, Tulyaganov DU, Goel IK, Ferreira JMF. Crystallization process and some properties of Li_2O–SiO_2 glass-ceramics doped with Al_2O_3 and K_2O. Journal of the American Ceramic Society 2008;91(11):3698-703.
17. Johnson WA, Mehl KF. Reaction kinetics in processes of nucleation and growth. Transactions of the American Institute of Mining Engineers 1939;135:416-72.
18. Avrami M. Kinetics of phase change. I — general theory. Journal of Chemical Physics 1939;7:1103-12.
19. Avrami M. Kinetics of phase change. II — transformation-time relations for random distribution of nuclei. Journal of Chemical Physics 1940;8:212-24.
20. Avrami M. Avrami M. Kinetics of phase change. III — granulation, phase change, and microstructure. Journal of Chemical Physics 1941;9:177-84.
21. Goel A, Shaaban ER, Ribeiro MJ, Ferreira JMF. Influence of NiO on the crystallization kinetics of near stoichiometric-cordierite glasses nucleated with TiO_2. Journal of Physics: Condensed Matter 2007;19:386231.
22. Pascual MJ, Duran A, Prado MO. A new method for determining fixed viscosity points of glasses. Physics and Chemistry of Glasses 2005;46(5):512-20.
23. Pascual MJ, Pascual L, Duran A. Determination of the viscosity-temperature curve for glasses on the basis of fixed viscosity points determined by hot stage microscopy. Physics and Chemistry of Glasses 2001;42(1):61-66.
24. Freiman SW, Hench LL. Kinetics of Crystallization in Li_2O–SiO_2 Glasses. Journal of the American Ceramic Society 1968;51(7):382-&.
25. Morse HM, Donnay JDH. Optics and structure of three dimensional spherolites. American Mineralogist 1936;21(7):391-426.

26. Vázquez J, Wagner C, Villares P, Jiménez-Garay R. Glass transition and crystallization kinetics in $Sb_{0.18}As_{0.34}Se_{0.48}$ glassy alloy by using non-isothermal techniques. Journal of Non-Crystalline Solids 1998;235-237:548-53.
27. von Clausbruch CS, Schweiger M, Holand W, Rheinberger V. The effect of P_2O_5 on the crystallization and microstructure of glass-ceramics in the SiO_2–Li_2O–K_2O–ZnO–P_2O_5 system. Journal of Non-Crystalline Solids 2000;263(1-4):388-94.
28. Höland W, Beall G. Glass-ceramic Technology. Westerville, Ohio: The American Ceramic Society; 2002.
29. Shelby JE. Introduction to glass science and technology. Cambridge: The Royal Society of Chemistry; 1997.
30. Branda F, P. G, G. L, A. C. Structural role of La_2O_3 in La_2O_3–CaO–Na_2O–SiO_2 glasses. Physics and Chemistry of Glasses 2001;42(6):385-88.
31. White WB, Minser DG. Raman spectra and structure of natural glasses. Journal of Non-Crystalline Solids 1984;67:45-59.
32. Matusita K, Sakka S, Maki T, Tashiro M. Study on crystallization of glass by differential thermal analysis. Effect of added oxide on crystallization of Li_2O–SiO_2 glasses. Journal of Materials Science 1975;10:94-100.
33. Bansal NP, Doremus RH. Handbook of glass properties. San Diego: Academic Press; 1986.
34. Callister Jr WD. Fundamentals of materials science and engineering. New York: John Wiley & Sons; 2001.
35. Donald IW. Crystallization kinetics of a lithium zinc silicate glass studied by DTA and DSC. Journal of Non-Crystalline Solids 2004;345-346:120-26.
36. Goel A, Tulyaganov DU, Kansal I, Shaaban ER, Ferreira JMF. Crystallisation kinetics of diopside-Ca-Tschermak based glasses nucleated with Cr_2O_3 and Fe_2O_3. International Journal of Materials Engineering Innovation 2009;1(1):40-60.
37. Cattell MJ, Chadwick TC, Knowles JC, Clarke RL. The crystallization of an aluminosilicate glass in the K_2O–Al_2O_3–SiO_2 system. Dental Materials 2005;21:811-22.
38. Oliveira APN, Manfredini T, Barbieri L, Leonelli C, Pelacani CC. Sintering and crystallization of a glass powder in the Li_2O–ZrO_2–SiO_2 system. Journal of the American Ceramic Society 1998;81(3):777-80.
39. Siligardi C, D'Arrigo MC, Leonelli C. Sintering behavior of glass-ceramic frits. American Ceramic Society Bulletin 2000;79(9):88-92.
40. Boccaccini AR, Stumpfe W, Taplin DMR, Ponton CB. Densification and crystallization of glass powder compacts during constant heating rate. Materials Science and Engineering 1996;A219:26-31.
41. Tulyaganov DU, Agathopoulos S, Fernandes HR, Ventura JM, Ferreira JMF. Crystallization of glasses in the system tetrasilicic mica-fluorapatite-diopside. Journal of the European Ceramic Society 2004;24(13):3521-28.
42. Flugel A. Glass viscosity calculation based on a global statistical modelling approach. Glass Technology 2007;48(1):13-30.

3.3 Structural characterisation and thermo-physical properties of glasses in the $Li_2O–SiO_2–Al_2O_3–K_2O$ system

Hugo R. Fernandes[a], Dilshat U. Tulyaganov[a,b], Ashutosh Goel[a], José M. F. Ferreira[a]

[a] Department of Ceramics and Glass Engineering, University of Aveiro, CICECO, 3810-193 Aveiro, Portugal

[b] Turin Polytechnic University in Tashkent, 17 Niyazova str., 100174 Tashkent, Uzbekistan

Journal of Thermal Analysis and Calorimetry (2011) 103:827–834

DOI: 10.1007/s10973-010-1049-5

Abstract

This article aims to shed some light on the structure and thermo-physical properties of lithium disilicate glasses in the system $Li_2O–SiO_2–Al_2O_3–K_2O$. A glass with nominal composition $23Li_2O–77SiO_2$ (mol.%) (labelled as $L_{23}S_{77}$) and glasses containing Al_2O_3 and K_2O with SiO_2/Li_2O molar ratios (3.13–4.88) were produced by conventional melt-quenching technique in bulk and frit forms. The glass-ceramics (GCs) were obtained from nucleation and crystallisation of monolithic bulk glasses as well as via sintering and crystallisation of glass powder compacts. The structure of glasses as investigated by magic angle spinning-nuclear magnetic resonance (MAS-NMR) depict the role of Al_2O_3 as glass network former with fourfold coordination, *i.e.*, Al(IV) species while silicon exists predominantly as a mixture of Q^3 and Q^4 (Si) structural units. The qualitative as well as quantitative crystalline phase evolution in glasses was followed by differential thermal analysis (DTA), X-ray diffraction (XRD) adjoined with Rietveld-reference intensity ratio (R.I.R.) method, Fourier transform infrared spectroscopy (FTIR) and scanning electron microscopy (SEM). The possible correlation amongst structural features of glasses, phase composition and thermo-physical properties of GCs has been discussed.

Keywords: Sintering; Thermo-physical properties; Glass; Glass–ceramics; Lithium disilicate

1. Introduction

Glass-ceramic (GC) materials are obtained by the controlled nucleation and crystallisation of glasses. The choice of glass composition is crucial to ensure that a high rate of internal, rather than surface, nucleation occurs. An excessively high crystal growth rate is to be avoided since such materials do not develop fine-grained microstructure, necessary for the achievement of high mechanical strength.[1-2] The binary alkali silicate systems show liquid–liquid phase separation or immiscibility at temperatures below the *liquidus* temperature of crystallisation. This type of phase separation is often called metastable because crystalline phases are more stable than liquid at the temperature of phase separation.[2-3] The presence of metastable immiscibility region is the main cause of S-like course of the *liquidus* curve and binary Li_2O–SiO_2 system is a typical example in this regard which demonstrates S-like course of the *liquidus* curve in silica-rich region. According to Vogel,[3] Li_2O–SiO_2 liquids containing less than 30 mol.% Li_2O lead to opalescent or opaque glasses on cooling owing to phase separation. However, mechanical properties and chemical durability of these glasses after devitrification are low.

Study of nucleation and crystallisation processes in parent glasses is essential, enabling to produce final materials of desired properties. In the previous study,[4] we observed that glasses with composition in the Li_2O–K_2O–Al_2O_3–SiO_2 system comprising equimolar amount of Al_2O_3 and K_2O were prone to volume nucleation and crystallisation, resulting in formation of fine $Li_2Si_2O_5$ (LD) crystals within the temperature interval of 650–900 ºC. Also, it has been demonstrated that Al_2O_3 and K_2O might also improve chemical durability of Li_2O–SiO_2 glasses.[3, 5-6]

The aim of this study is to present an in-depth analysis pertaining to study the structure of Li_2O–Al_2O_3–K_2O–SiO_2 glasses and their devitrification mechanism in relevance with Al_2O_3 and K_2O content. Although the role of Al_2O_3 as glass network former with four-fold coordination of Al(IV) species was hypothesised in our previous study,[4] we felt the need of investigating this issue in detail so as to gain a better understanding regarding the structural role of Al_2O_3 in these glasses. Therefore, in this study, ^{29}Si and ^{27}Al magic angle spinning-nuclear magnetic resonance (MAS-NMR) have been employed to study glass structure and derive relevant information with respect to the local environment of silicon and aluminium in experimental glasses. The sintering behaviour and properties of the corresponding glass powder compacts have also been targeted in the framework of this investigation, in particular

using Fourier transform infrared spectroscopy (FTIR), scanning electron microscopy (SEM), and X-ray diffraction (XRD) to evaluate qualitative and quantitative phase assemblage. The obtained results demonstrated significant differences between binary 23 mol.% Li_2O and 77 mol.% SiO_2 composition and its Al_2O_3 and K_2O containing derivatives in terms of structure, crystallisation kinetics and thermo-physical properties.

2. Experimental procedure

2.1 Glass preparation

Powders of technical grade SiO_2 (purity > 99.5%) and of reactive grade Al_2O_3 (Alcoa, Germany, purity > 99.5%), Li_2CO_3 and K_2CO_3 (Sigma–Aldrich, Germany, purity > 99.5%) were used to prepare the experimental glasses. Glasses were prepared in both bulk and frit form by melt-quenching technique in Pt crucible. Table 1 presents the composition of the glasses investigated in this study. The addition of Al_2O_3 and K_2O to the binary Li_2O–SiO_2 system was performed on equimolar basis, and the amount of additives decreased from glass G1 to G3. A binary composition $L_{23}S_{77}$, containing the same amount of Li_2O as glass G3, but richer in SiO_2 was also synthesised.

Table 1 – Compositions of the experimental glasses.

Oxides (mol.%)	G1	G2	G3	$L_{23}S_{77}$
Li_2O	15.23	19.08	22.96	22.96
K_2O	5.24	3.94	2.63	–
Al_2O_3	5.24	3.94	2.63	–
SiO_2	74.30	73.04	71.78	77.04
$K_2O + Al_2O_3$	10.48	7.88	5.26	0.00

Two sets of bulk glasses for each composition were obtained by pouring the glass melt on preheated bronze mould: (1) the first set of glasses was allowed to cool down in the air; (2) the second set of glasses was subjected to annealing at 450 ºC for 1 h. In order to study the evolution of crystalline phases in monolithic glasses, the annealed glasses were cut into cubes ($1 \times 1 \times 1$ cm^3) and heat treated non-isothermally at 550, 650, 750, 800 and 900 ºC for 1 h, at heating rate of 2 K/min.

Glasses in frit form were dried and then milled in a high speed porcelain mill to obtain fine glass powders with mean particle size of 5–10 μm. Rectangular bars with dimensions of $4 \times 5 \times 50$ mm^3 were prepared by uniaxial pressing (80 MPa). The bars were sintered under non-isothermal conditions for 1 h at 800, 850 and 900 ºC using a low heating rate of 2 K/min aimed to prevent deformation of samples.

2.2 Thermo-physical properties of glasses

The glass transition temperature (T_g), softening point (T_s) and coefficient of thermal expansion (CTE) were obtained from dilatometry measurements which were carried out on prismatic glass samples with a cross section of 4×5 mm^2 (Bahr Thermo Analyze DIL 801 L, Hüllhorst, Germany; heating rate 5 K/min). differential thermal analysis (DTA) of glass grains with sizes in the range of 415–1,000 μm, collected by sieving of grounded non-annealed glass blocks, was carried out in air (Netzsch 402 EP, Germany) from room temperature to 1000 ºC at different heating rates (β = 2, 5, 10 and 15 K/min).

2.3 Structural characterisation

The ^{29}Si MAS-NMR spectra were recorded on a Bruker ASX 400 spectrometer operating at 79.52 MHz (9.4 T) using a 7-mm probe at a spinning rate of 5 kHz. The pulse length was 2 μs, and a 60-s delay time was used. Kaolinite was used as the chemical shift reference. ^{27}Al MAS-NMR spectra were recorded on a Bruker ASX 400 spectrometer operating at 104.28 MHz (9.4 T) using a 4-mm probe at a spinning rate of 15 kHz. The pulse length was 0.6 μs, and a 4s delay time was used. $Al(NO_3)_3$ was used as the chemical shift reference.

2.4 Sintering and crystallisation behaviour of glass powder compacts

Infrared spectra of the GCs were obtained using an Infrared Fourier spectrometer (FTIR, model Mattson Galaxy S-7000, USA). For this purpose, samples were crushed to powder form, mixed with KBr in the proportion of 1/150 (by weight) and pressed into a pellet using a hand press.

The qualitative and quantitative crystalline phase analysis in the GCs (crushed to particle size < 45 μm) was made by XRD analysis using a conventional Bragg–Brentano diffractometer

(Philips PW 3710, Eindhoven, The Netherlands) with Ni-filtered Cu-Ka radiation. The quantitative phase analysis of GCs was made by combined Rietveld-reference intensity ratio (R.I.R.) method. A 10 wt.% of corundum (NIST SRM 676a) was added to all the GC samples as an internal standard. The mixtures, ground in an agate mortar, were side loaded in aluminium flat holder to minimise the problems to due to non-random orientations. Data were recorded in 2θ range = 5–115º (step size 0.02º/50 s). The phase fractions extracted by Rietveld refinements, using GSAS-EXPGUI software[7] were rescaled on the basis of the absolute weight of corundum originally added to their mixtures as an internal standard, and therefore, internally renormalised. The background was successfully fitted with a Chebyshev function with a variable number of coefficients depending on its complexity. The peak profiles were modelled using a pseudo-Voigt function with one Gaussian and one Lorentzian coefficient. Lattice constants, phase fractions, and coefficients corresponding to sample displacement and asymmetry were also refined.

Microstructural observations were done on polished (mirror finishing) surface of samples (etched by immersion in 2 vol.% HF solution for 2 min) by scanning electron microscopy (SEM; SU-70, Hitachi, Japan).

3. Results and discussion

3.1 Bulk glasses

3.1.1 Glass casting ability

Transparent and colourless glasses G1, G2 and G3 were obtained by melting at 1550 ºC for 1 h, while in case of $L_{23}S_{77}$ transparent melt transformed into a cloudy hazy glass on cooling. Figure 1 shows both the appearance of the experimental non-annealed glasses and the corresponding microstructures which reveal the precipitation of a nanosize droplet phase in glassy matrices suggesting the occurrence of liquid–liquid phase separation in all the investigated compositions. However, the phase separation phenomenon was not observed at naked eye for compositions G1, G2 and G3 comprising Al_2O_3 and K_2O. The mean droplet diameter and the population density of droplets (Fig. 1) diminished by increasing amount of Al_2O_3 and K_2O in the Li_2O–SiO_2 system. Consequently, G1 possesses a microstructure comprising rarer smaller droplets compared to the other compositions, evidencing that Al_2O_3 has a strong tendency to reduce phase separation.

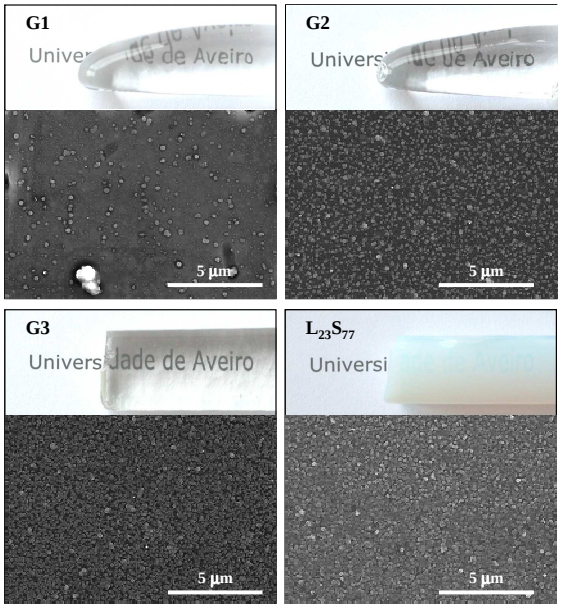

Fig. 1 – Physical appearance of the experimental non-annealed bulk glasses and their respective SEM images for glass compositions G1, G2, G3 and $L_{23}S_{77}$, respectively.

The finer scale morphology and a relatively lower volume fraction of the droplets observed in the glasses G1, G2 and G3 result in the nonexistence of Tyndall effect which can explain the homogeneous and transparent appearance in this compositions when observed with naked eye.[3] On the other hand, the bigger droplets and their higher concentration presented in the microstructure of composition $L_{23}S_{77}$ lead to the cloudy appearance, as expected since the droplet size in this glass has remained nearly the same as observed by Vogel in $Li_2O–SiO_2$ glasses.[3]

3.1.2 Thermo-physical properties and structural features of the glasses

The addition of Al_2O_3 and K_2O in the as-investigated proportions favoured an increase in T_g and T_s of the glasses (Fig. 2a, b). From the linear part of the dilatometric curves, the values of $CTE_{200–400\ ^oC}$ for glasses G1, G2, G3 and $L_{23}S_{77}$, were obtained as 8.47, 8.69, 9.65 and 8.16 $\times 10^{-6}$ /K, respectively. Considering that Al^{3+} Acts as a network former, the number of non-bridging oxygens per each tetrahedral cation (NBO/T) suggested more polymerised glass network structures for G1 (NBO/T = 0.36) and G2 (NBO/T = 0.47) than for G3 (NBO/T = 0.60) and $L_{23}S_{77}$ (NBO/T = 0.60). Diminishing the NBO/T led to an increase in T_g and decrease in CTE values. The higher CTE value of glass G3 compared with $L_{23}S_{77}$ can be explained by the effect of incorporation of potassium cation in the glass network. In general,

alkali ions fill up the glass structure interstices, thus preventing bond bending which consequently increases CTE. This effect, however, can be compensated by addition of intermediate oxides (such as Al_2O_3) that reduce the concentration of NBOs, provided that molar concentration of Al does not exceed that of the charge-balancing cations (*e.g.* alkalis).[2]

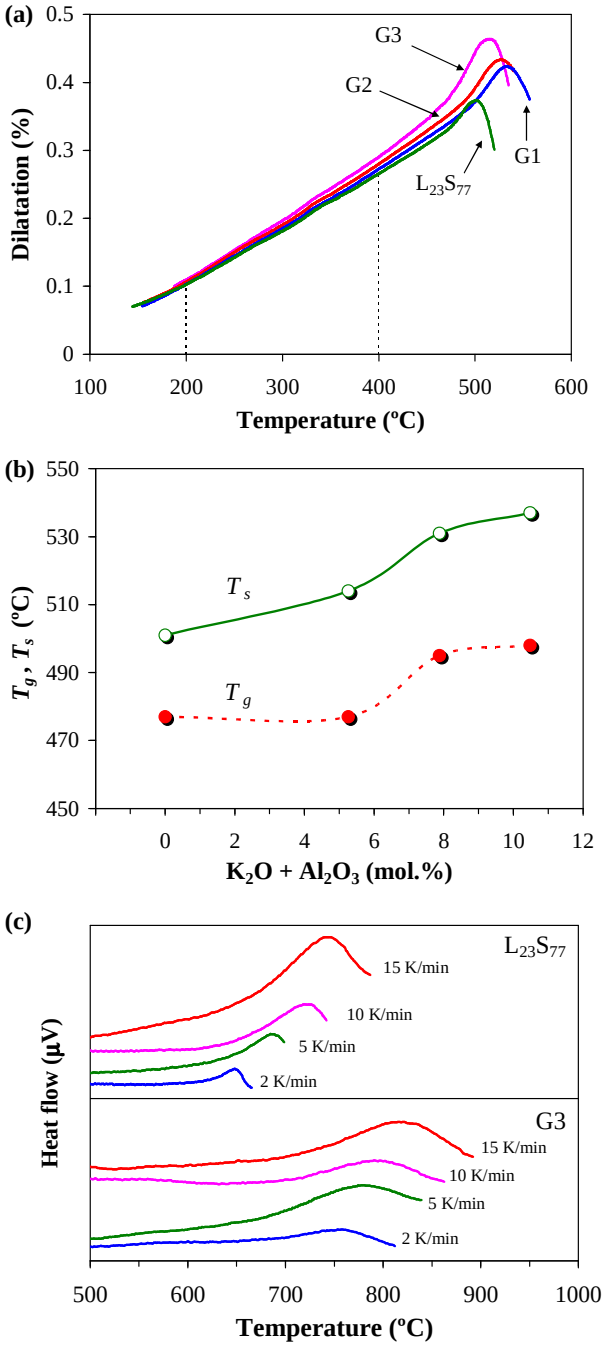

Fig. 2 – Thermo-physical properties of the experimental annealed bulk glasses (K_2O and Al_2O_3 content in mol%): (a) Dilatometry, (b) T_g and T_s versus additives content, and (c) differential thermal analysis (DTA) thermograph of glasses G3 and $L_{23}S_{77}$ at different heating rates (β = 2, 5, 10 and 15 K/min).

Figure 2c presents the DTA thermographs of glasses G3 and $L_{23}S_{77}$ at different heating rates to reveal the influence of Al_2O_3 + K_2O introduction on devitrification behaviour of glass $L_{23}S_{77}$. As is evident from Fig. 2c, the crystallisation curve for glass G3 is shallower and exhibits a considerable shift to high temperature with respect to glass $L_{23}S_{77}$. These data clearly demonstrate stronger ability of glass $L_{23}S_{77}$ for devitrification due to coarser scale morphology and a relatively higher volume fraction of the droplets observed in parent glass (Fig. 1d). Similar to the other glasses in the Li_2O–SiO_2 system containing less than 30 mol.% Li_2O, nucleation in $L_{23}S_{77}$ glasses was initiated by metastable liquid–liquid immiscibility[3] that was more extended than in Al_2O_3 and K_2O containing derivates. The activation energy of ystallisation (E_c) as obtained in our previous study for glasses $L_{23}S_{77}$ and G3 are 153 and 330 kJ/mol,[4] respectively, reflecting the structural role of Al_2O_3 which is probably contributing towards decreasing the immiscibility trend, thus reducing mobility of the glass-forming ions and ionic complexes operative in the crystallisation process.

The ^{29}Si and ^{27}Al MAS-NMR spectra of the samples (Figs. 3a, b, respectively) exhibit broad bands which indicate the amorphous nature of investigated materials.[8-9] Glass $L_{23}S_{77}$ exhibited two characteristic peaks in ^{29}Si MAS-NMR spectra at about −92 and −108 ppm (Fig. 3a), which can be assigned to a mixture of Q^3 and Q^4 species, respectively. The addition of Al_2O3 and K_2O resulted in a broadening of spectra and shifting the peak centred at −92 ppm to lower values. These features imply towards decreasing number of Q^3 species at the expense of more polymerised Q^4 units and are consistent with calculated NBO/T, evolution of CTE, T_g and T_s values.

The ^{27}Al MAS-NMR data are shown in Fig. 3b. A signal at ~52 ppm evidenced about dominant presence of tetrahedral aluminium in all the Al_2O_3 + K_2O containing glasses and especially in G1 and G2. It is noteworthy that Al(IV) species are characteristic networking-forming units of aluminosilicate glasses causing increase in crosslinking of the glass structure.[10] Therefore, as the sum of Al_2O_3 and K_2O increased the ($AlO_{4/2}$) glass forming units are incorporated in the network as Q^4 species. To maintain local charge neutrality, $(AlO_{4/2})^-$ units will be charge compensated by alkali cations (K^+, Li^+) which must be present in the vicinity of each such tetrahedron. The results of ^{27}Al MAS-NMR study strongly support our previous presumption[4] concerning the role of Al_2O_3 as glass network former with four-fold coordination of Al(IV) species in the experimental compositions G1, G2 and G3.[10-11]

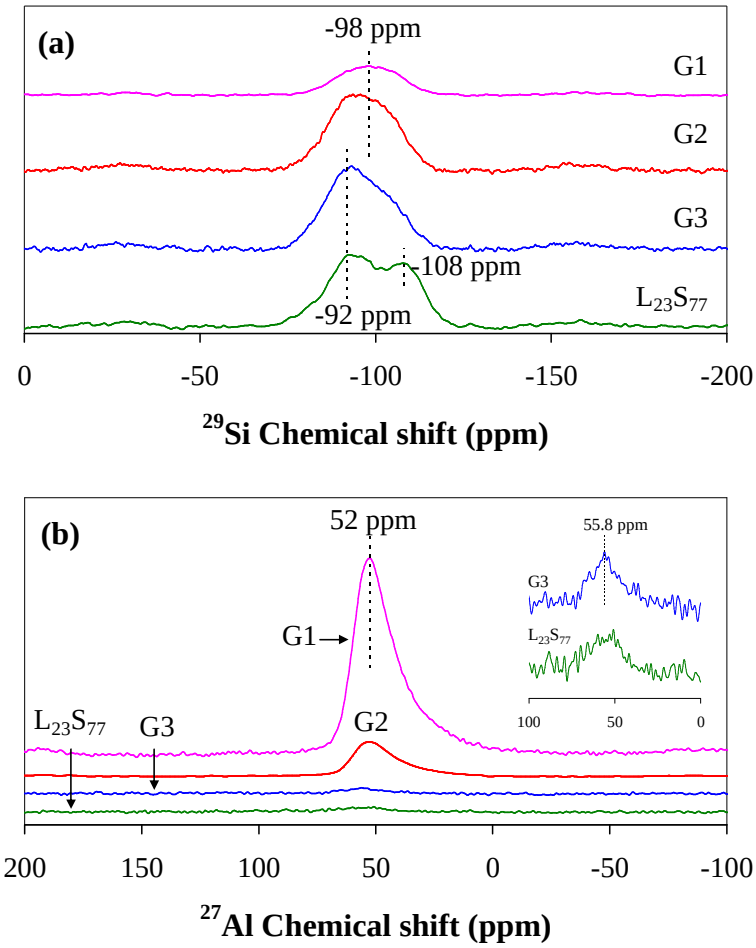

Fig. 3 – ^{29}Si MAS-NMR (a) and ^{27}Al MAS-NMR (b) spectra of glasses. The insertion shows the ^{27}Al MAS-NMR spectrum for glass G3.

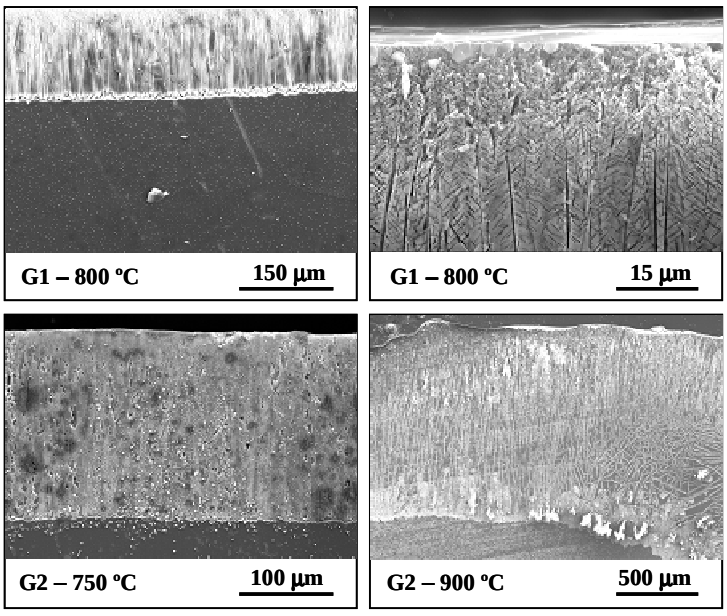

Fig. 4 – SEM of bulk glasses heat treated at different temperatures.

Surface crystallisation and dendritic skeletal crystal growth which can be observed in SEM images of both G1 and G2 glasses (Fig. 4), being a further evidence of the structural role of Al^{3+} that apparently increased viscosity of those glasses and greatly decreased the immiscibility trends. On the contrary, fine grained volume crystallisation has been observed in low alumina G3 glass.[4]

3.2 Glass powder compacts

Well-sintered GCs demonstrating flexural strength values 114 ± 2, 158 ± 5 and 81 ± 8 MPa for G1, G2 and G3, respectively, were obtained after heat treatment of glass powder compacts at 800 ºC for 1 h. Further heat treatment at 850 ºC significantly improved densification of G3 compared to G1 and G2 whereas maximum bending strength values as 189 ± 8 (G1), 195 ± 9 (G2) and 224 ± 4 (G3) MPa were revealed after sintering at 900 ºC for 1 h. Figure 5 presents the SEM images of glass powder compacts G1 and G3 heat treated at 800, 850 and 900 ºC. At the lowest temperature, structural features of Li_2SiO_3 (LS) crystals which possess a chain silicate structure and crystallised dendritically can be observed. It is known that LS crystals are particularly easy to dissolve from GC by dilute hydrofluoric acid while the surrounding aluminosilicate glassy matrix is considerably more resistant to acid attack.[1] At 850 ºC, LD crystals start up to grow in the form of submicron-sized rods and act as nucleating sites for new rods. LD crystals uniformly embedded in glassy matrix were responsible for high mechanical strength of these GCs at 900 ºC. According to XRD data (spectra are not shown), LS was revealed as the single crystalline phase in GC1 after sintering at 800 ºC, while GC2 and GC3 comprised LS along with quartz (Q) and LD as minor phases.

At 850 and 900 ºC, GC3 exhibited almost monomineral composition of LD with peaks of low intensity attributed to quartz. In compositions G1 and G2, both LS and Q were found as minor crystalline phases at 850 and 900 ºC. Unlike Al_2O_3 and K_2O containing GCs, binary $L_{23}S_{77}$ composition featured very poor sinterability thus exhibiting bending strength of 13 ± 2 MPa and density of 2.14 ± 0.04 g/cm^3 at 900 º for 1 h (Fig. 5a). This phenomenon can be explained by lower E_c for $L_{23}S_{77}$ compared to G3 causing formation of large fraction of LD phase that hinders the densification process.[12] Indeed, LD was the main crystalline phase in $L_{23}S_{77}$ glass powder compacts sintered at 800 and 850 ºC. At 900 ºC both LD along with quartz became the principal crystalline phases while tridymite along with cristobalite were also recorded.

The FTIR spectra of glass powder compacts heat treated at 800, 850 and 900 ºC are presented in Fig. 6. In all Al_2O_3 and K_2O containing compositions. transmittance bands of LS phase, *i.e.* 525–527, 604, 635–638, 728–732, 846–851, 932, 973 and 1054–1057 /cm were revealed at lower temperatures.[13] For instance, FTIR spectrum of G1 at 800 ºC exhibited well resolved bands at ~527, 609, 730, 850 and 923 /cm, and a shallow band at ~1060 /cm, which resembles the above mentioned typical values for LS (Fig. 6a).

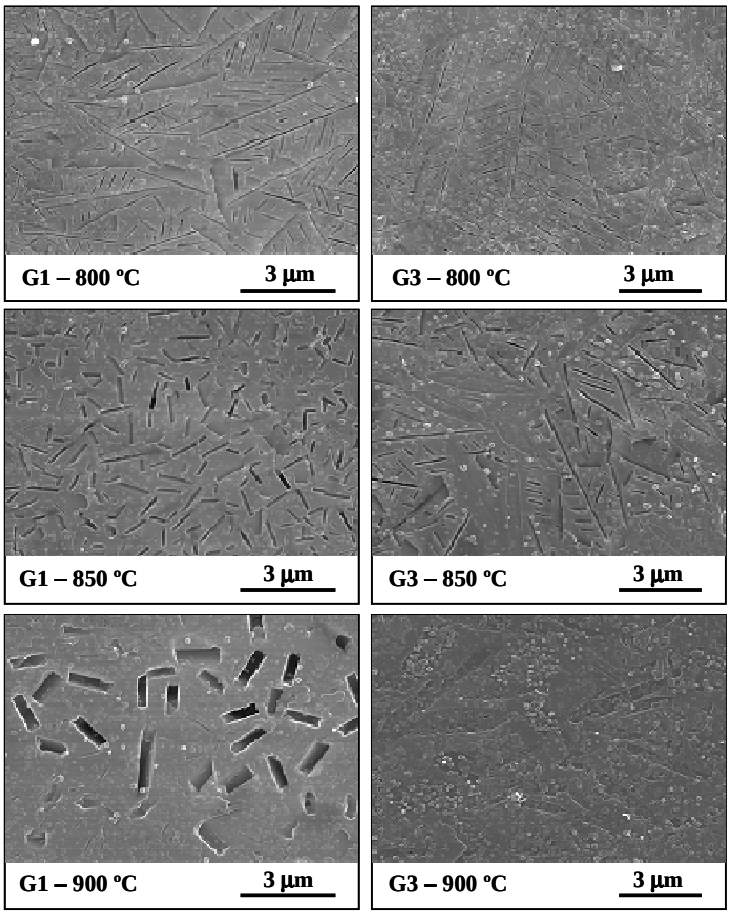

Fig. 5 – SEM of glass powder compacts G1 and G3 heat treated at 800, 850 and 900 ºC.

The absence of other significant bands suggested that LS is the only crystalline phase formed in G1 at this temperature. The sharpness and intensity of these bands tend to be diminished and shifted slightly to higher frequency values with increasing sintering temperature. Thus, at 850 ºC new peaks characteristic for transmittance of LD phase were revealed and become more pronounced at 900 ºC. The FTIR patterns of G2 and G3 glasses sintered at 800 ºC (Fig. 6b) are quite similar to spectrum of G1. However, transmittance bands in the spectra of G1, G2 and G3 at 850 and 900 ºC mostly correspond to LD crystalline phase. Binary Al_2O_3 and K_2O free $L_{23}S_{77}$ composition featured several peaks at ~475, 563, 633, 760, 788, 940 and

1108 /cm (Fig. 6d). These transmittance bands can be assigned to LD control-crystal (470, 548, 635, 756, 782, 936, 1022, 1108 and 1212 /cm).[13] At 850 and 900 ºC FTIR spectra presented similar profile coupled with appearance of small peaks at ~450 and 692 /cm corresponding to standard quartz.[14]

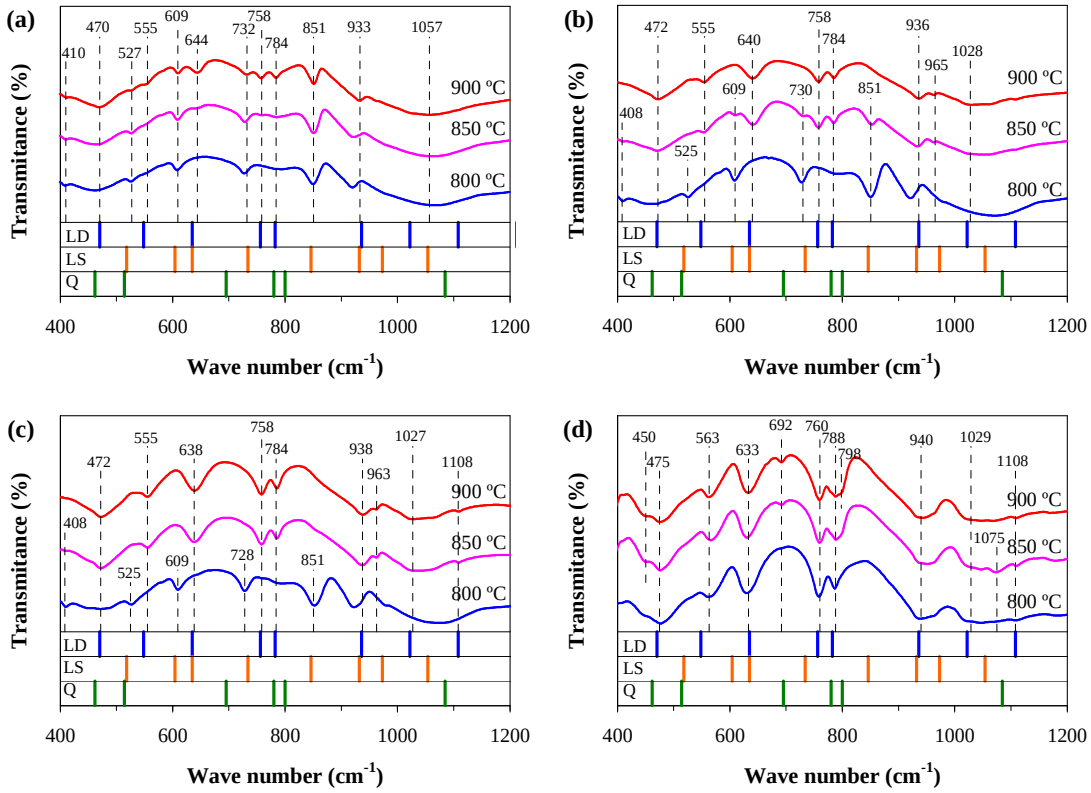

Fig. 6 – FTIR spectra of the investigated glass powder compacts (a) G1, (b) G2, (c) G3 and (d) $L_{23}S_{77}$ after heat treatment at 800, 850 and 900 ºC for 1 h, respectively. Typical spectra for quartz (Q), lithium disilicate (LD) and lithium metasilicate (LS) are indicated in the figure.

From the hot stage microscopy observation performed in the previous study two main steps of sintering were revealed for G1, G2 and G3 compositions.[4] First sintering step was initiated at temperatures slightly higher than T_g and retarded by crystallisation of LS at around 600 ºC whereas a second shrinkage step started almost synchronically at about 800 ºC for all Al_2O_3 and K_2O containing compositions. Moreover, the interval for first sintering step was wider for G1 (68 ºC) and G2 (49 ºC) than for G3 (45 ºC).

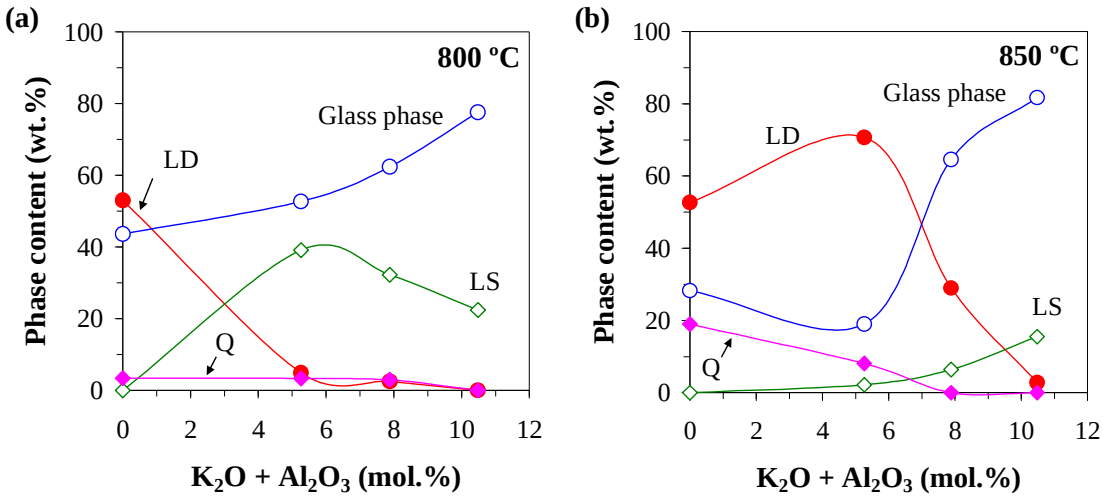

Fig. 7 – Quantitative crystalline phase evolution in GCs as obtained from Rietveld-R.I.R. refinement at (a) 800 ºC and (b) 850 ºC. Phases are indicated in the figure as Q (quartz, SiO_2), LD (lithium disilicate, $Li_2Si_2O_5$) and LS (lithium metasilicate, Li_2SiO_3).

Nevertheless, deeper investigation was required for quantifying content of crystalline and amorphous phase. Therefore, Rietveld-R.I.R. refinement was conducted for the samples sintered at 800 and 850 ºC, i.e. in the interval when a second phase of sintering took place and was accompanied with new phase transformations. From Fig. 7a, it is clear that $L_{23}S_{77}$ composition at 800 ºC contained about 53.0 wt.% LD, 3.4 wt.% quartz and 43.6 wt.% amorphous phase. In comparison to $L_{23}S_{77}$, compositions G1, G2 and G3 featured lower crystalline content (mainly LS and quartz), but higher amount of residual amorphous reservoir (52.7, 62.4 and 77.6 wt.% for G3, G2 and G1, respectively). After heat treatment at 850 ºC, no deviation in LD content was revealed in $L_{23}S_{77}$ although quartz content increased up to 19 wt.% at the expense of silica rich amorphous phase (Fig. 7b). It is due to the precipitation of residual silica glassy phase (density 2.20 g/cm^3) in the form of quartz (density 2.65 g/cm^3) that overall volume of the system decreased. However, the occurred volume changes were not sufficient to cause appreciable increase of density and mechanical strength even after 900 ºC.

Unlike $L_{23}S_{77}$, the volume changes in G3 at 850 ºC were associated with both reaction of residual glass with LS causing formation of large fraction LD (up to 70.7 wt.%) and simultaneous densification of residual amorphous phase owing to its lower crystallinity (Fig. 7a). The densification was less pronounced in G2 and G1 since LD was formed in low amount and mostly due to reaction between LS and quartz whereas the amount of glassy phase remained almost constant. The reason for this was that significant level of densification

of G1 and G2 was attained during the first sintering stage before crystallisation started.[4] Formation of LD was advanced in G2 and mostly in G1 in the interval 850–900 ºC. The results of Rietveld-R.I.R. refinement are well correlated with the viscosity–temperature curves for G1, G2 and G3 glasses[4] evidencing that the glass G3 exhibited lowest viscosity at temperatures below 850 ºC and at the constant temperature $log\ \eta$ (G1) > $log\ \eta$ (G2) > $log\ \eta$ (G3). The opposite trend was observed at temperatures higher than 850 ºC when compositions G2 and G3 demonstrated higher viscosity than G1. This can be explained by formation of a larger fraction of LD in GC3 and GC2 at 850 ºC (Fig. 7b).

4. Conclusions

This study demonstrates that slight changes in lithium silicate glass composition may have significant effects on chronology and morphology of phases. A careful selection of additive's amount is crucial to ensure that internal nucleation and moderate crystal growth rate in parent glass occurs. The following conclusions can be drawn from the above discussed results:

1. Liquid–liquid phase separation occurred in all the investigated monolithic bulk glasses. The mean droplet diameter and the population density of droplets diminished by increasing amount of Al_2O_3 and K_2O demonstrating that aluminium greatly decreased the immiscibility trends in the Li_2O–SiO_2 system.
2. Al_2O_3- and K_2O-free $L_{23}S_{77}$ glass demonstrated higher rate of crystal growth due to extended phase separation.
3. The addition of Al_2O_3 and K_2O in the as-investigated proportions favoured the decrease of CTE and an increase of T_g and T_s. The surface crystallisation and dendritic skeletal crystal growth was observed in compositions G1 and G2 with higher Al_2O_3 and K_2O content whereas bulk crystallisation with fine-grained microstructure has been attained in low alumina G3 glass.
4. ^{29}Si MAS-NMR spectra evidenced a decreasing number of Q^3 species at the expense of Q^4 implying towards polymerised structure of Al_2O_3 and K_2O containing compositions.
5. The peaks of ^{27}Al MAS-NMR spectra of G1 and G2 glasses were centred at ~52 ppm corresponding to tetrahedral four-coordinated Al(IV) species confirming the role of Al_2O_3 as glass network former.

6. The sintering and crystallisation of Al_2O_3- and K_2O containing compositions in the silica reach region of $Li_2O–SiO_2$ system, which resulted in well-densified and mechanically strong fine-grained GCs with LD as the major crystalline phase.
7. Glass G3 exhibited most promising thermo-physical properties due to careful selection of Al_2O_3 and K_2O additives promoting internal nucleation and moderate crystal growth rate.

Further investigations of new materials will be required to study chemical durability, mechanical properties (fracture toughness, Weibull modulus, etc.) as well as to optimise their processing parameters.

Acknowledgements

Hugo R. Fernandes is grateful for the financial support of CICECO and for the PhD grant (SFRH/BD/41307/2007) from the FCT, Portugal. Ashutosh Goel is thankful to CICECO and FCT, Portugal (SFRH/BPD/65901/2009) for the post-doctoral research grant.

References

1. Höland W, Beall G. Glass-ceramic Technology. Westerville, Ohio: The American Ceramic Society; 2002.
2. Shelby JE. Introduction to glass science and technology. Cambridge: The Royal Society of Chemistry; 1997.
3. Vogel W. Structure and Crystallization of Glasses. Leipzig: Pergamon Press; 1971.
4. Fernandes HR, Tulyaganov DU, Goel A, Ribeiro MJ, Pascual MJ, Ferreira JMF. Effect of Al_2O_3 and K_2O content on structure, properties and devitrification of glasses in the $Li_2O–SiO_2$ system. Journal of the European Ceramic Society 2010;30(10):2017-30.
5. Barrett JMG, FL), Clark, David E. (Gainesville, FL), Hench, Larry L. (Gainesville, FL), inventor; The Board of Regents, State of Florida, University of Florida (Tallahassee, FL), assignee. Glass-ceramic dental restorations. 1980.
6. Wu J-mT, TW), Cannon, Warren R. (East Brunswick, NJ), Panzera, Carlino (Belle Mead, NJ), inventor; Johnson & Johnson Dental Products Company (East Windsor, NJ), assignee. Castable glass-ceramic composition useful as dental restorative. 1985.
7. Larson AC, von Dreele RB. GSAS: general structure analysis system LANSCE, MS-H805. Los Alamos: Los Alamos National Laboratory; 1998.
8. Engelhardt G, Nofz M, Forkel K, Wihsmann FG, Magi M, Samoson A, et al. Structural studies of calcium aluminosilicate glasses by high resolution solid state ^{29}Si

and ^{27}Al magic angle spinning nuclear magnetic resonance. s Chem Glasses. Physics and Chemistry of Glasses 1985;26(157-65).
9. Mackenzie KJD, Smith ME. Multinuclear solid-state NMR of inorganic materials. Amsterdam: Pergamon; 2002.
10. Abo-Mosallam HA, Hill RG, Karpukhina N, Law RV. MAS-NMR studies of glasses and glass-ceramics based on a clinopyroxene–fluorapatite system. Journal of Materials Chemistry 2010;20:790-97.
11. Stebbins JF, Kroeker S, Lee SK, Kiczenski TJ. Quantification of five- and six-coordinated aluminium ions in aluminosilicate and fluoride-containing glasses by high-field, high-resolution ^{27}Al NMR. Journal of Non-Crystalline Solids 2000;275:1-6.
12. Siligardi C, D'Arrigo MC, Leonelli C. Sintering behavior of glass-ceramic frits. American Ceramic Society Bulletin 2000;79(9):88-92.
13. Fuss T, Mogus-Milankovic A, Ray CS, Lesher CE, Youngman R, Day DE. Ex situ XRD, TEM, IR, Raman and NMR spectroscopy of crystallization of lithium disilicate glass at high pressure. Journal of Non-Crystalline Solids 2006;352:4101-11.
14. Bhaskar JS, Parthasarathy G, Sarmah NC. Fourier transform infrared spectroscopic estimation of crystallinity in SiO_2 based rocks. Bulletin of Materials Science 2008;31(5):775-9.

3.4 Effect of K_2O on structure–property relationships and phase transformations in Li_2O–SiO_2 glasses

Hugo R. Fernandes[a], Dilshat U. Tulyaganov[a,b], Ashutosh Goel[c], José M. F. Ferreira[a]

[a] Dep. of Ceramics and Glass Engineering, University of Aveiro, CICECO, 3810-193 Aveiro, Portugal

[b] Turin Polytechnic University in Tashkent, 17 Niyazova str., 100174 Tashkent, Uzbekistan

[c] Glass Processing Group, Radiological and Nuclear Science and Technology Division, Pacific Northwest National Laboratory, Richland, WA 99354, United States

Journal of the European Ceramic Society 32 (2012) 291–298

DOI: 10.1016/j.jeurceramsoc.2011.09.017

Abstract

Glass compositions with formula (71.78−*x*) SiO_2 – 2.63 Al_2O_3 – (2.63+*x*) K_2O –23.7 Li_2O (mol.%, *x* = 0–10) and SiO_2/Li_2O molar ratios far beyond that of stoichiometric lithium disilicate ($Li_2Si_2O_5$) were prepared by conventional melt-quenching technique to investigate the influence of K_2O content on structural transformations and devitrification behaviour of glasses in the Li_2O–SiO_2 system. The scanning electron microscopy (SEM) examination of as cast non-annealed glasses revealed the presence of nanosized droplets in glassy matrices suggesting occurrence of liquid–liquid phase separation. An overall trend towards depolymerization of the silicate glass network with increasing K_2O content was demonstrated by employing magic angle spinning-nuclear magnetic resonance (MAS-NMR) spectroscopy. The distribution of structural units in the experimental glasses was estimated using ^{29}Si MAS-NMR spectroscopy suggesting the appearance of Q^2, enhancement of Q^3 and diminishing of Q^4 groups with increasing K_2O contents. X-ray diffraction (XRD) and differential thermal analysis (DTA) were used to assess the influence of K_2O on devitrification process and formation of lithium disilicate ($Li_2Si_2O_5$) and/or lithium metasilicate (Li_2SiO_3) crystalline phases.

Keywords: Glass; Glass ceramics; Lithium disilicate; Thermo-physical properties

1. Introduction

The immiscible region between the $Li_2O–2SiO_2$ and SiO_2 end members is an important feature in the $Li_2O–SiO_2$ system. The synthesis of glass-ceramic (GC) materials in the $Li_2O–SiO_2$ system is based on controlled nucleation and crystallization of lithium metasilicate and/or lithium disilicate phases which govern the properties for the final product. The glasses with SiO_2 contents higher than the stoichiometric $Li_2O·2SiO_2$ (33.33 mol.% Li_2O–66.66 mol.% SiO_2) tend to separate into a matrix phase with a composition almost similar to that of lithium disilicate along with an isolated droplet SiO_2 rich phase,[1] while glasses with Li_2O contents <30 mol.% usually turn out to be opalescent or opaque on cooling owing to phase separation.[1-3] Although, nucleation of base glass with stoichiometric composition of lithium disilicate has been widely investigated for GC manufacture,[4] the GCs derived from this parent binary system exhibit some unfavourable characteristics in terms of their mechanical and chemical properties which hinder their potential applications in several technological areas.

On the other hand, lithium disilicate GCs derived from non-stoichiometric compositions have proven themselves to be potential candidates for different functional applications, for example: dental restorations,[5-8] metal-glass seals,[9-10] etc. Fundamental research on certain non-stoichiometric lithium disilicate based glass compositions was carried out by Stookey (1959).[11] It is noteworthy that according to Höland and Beal,[4] the term ‘non-stoichiometric’ implies that SiO_2/Li_2O molar ratio deviates greatly from 2:1 and the system in rendered considerably more complex with numerous additional components and nucleating agents. However, the present investigation aims towards investigating a relatively simpler non-stoichiometric lithium disilicate based GC system in the glass forming region of $Li_2O–K_2O–Al_2O_3–SiO_2$ with its SiO_2/Li_2O molar ratio varying between 2.69 and 3.13. The simultaneous incorporating of K_2O and Al_2O_3 is known to significantly improve the chemical durability of lithium disilicate GCs,[1, 12-13] therefore justifying the choice of these two oxides in the present study. One of the main objectives of this study was to investigate the influence of replacing increasing amounts of SiO_2 by equimolar amounts of K_2O on the structural transformations occurring in the non-stoichiometric lithium disilicate glasses, and on their crystallization mechanism.

2. Experimental procedure

2.1 Glass Preparation

The investigated glass compositions were designed according to the general formula $(71.78-x)SiO_2–2.63Al_2O_3–(2.63+x)K_2O–22.96Li_2O$ (mol.%), where x changed from 0 to 10, with SiO_2/Li_2O ratios far from lithium disilicate stoichiometry ($SiO_2/Li_2O = 2$). Accordingly, the glasses have been labelled as GK_x depending on the amount of K_2O being substituted for SiO_2 in the glass compositions. For example: GK_0 corresponds to the parent composition, i.e. $x = 0$ and $K_2O/Al_2O_3 = 1$. Table 1 presents the detailed composition of the glasses along with their corresponding SiO_2/Li_2O, SiO_2/K_2O and K_2O/Al_2O_3 ratios.

Table 1 – Compositions of the experimental glasses.

	Oxides (mol.%)						
	Li_2O	K_2O	Al_2O_3	SiO_2	SiO_2/Li_2O	SiO_2/K_2O	K_2O/Al_2O_3
GK_0	22.96	2.63	2.63	71.78	3.13	27.29	1.00
$GK_{0.5}$	22.96	3.13	2.63	71.28	3.10	22.77	1.19
GK_1	22.96	3.63	2.63	70.78	3.08	19.50	1.38
$GK_{1.5}$	22.96	4.13	2.63	70.28	3.06	17.02	1.57
GK_2	22.96	4.63	2.63	69.78	3.04	15.07	1.76
$GK_{2.5}$	22.96	5.13	2.63	69.28	3.02	13.50	1.95
GK_5	22.96	7.63	2.63	66.78	2.91	8.75	2.90
GK_{10}	22.96	12.63	2.63	61.78	2.69	4.89	4.80

A total of eight glasses were prepared in Pt-crucibles using melt quenching technique. The powders of technical grade SiO_2 (purity >99.5%) and of reactive grade Al_2O_3, Li_2CO_3, and K_2CO_3 were used. Homogeneous mixtures of batches (~100 g), obtained by ball milling, were calcined at 800 ºC for 1 h and then melted in Pt crucibles at 1550 ºC for 1 h, in air. The glasses were produced in bulk (monolithic) form by pouring glass melts on bronze mould in two different sets. The glasses of one set were immediately annealed at 450 ºC for 1 h; the other set of glasses was preserved in the non-annealed condition.

2.2 Thermo-physical properties of glasses

The coefficient of thermal expansion (CTE) of the annealed glasses was measured by dilatometry using prismatic samples of bulk glasses with cross section of 3×4 mm^2 (Bahr Thermo Analyse DIL 801 L, Germany; heating rate 5 K min^{-1}). The differential thermal analysis (DTA, Setaram Labsys, Setaram Instrumentation, Caluire, France) of glasses was carried out in air from room temperature to 1000 ºC at heating rate (β) of 20 K min^{-1}. The glass powders with sizes in the range of 500–1000 μm (collected by sieving of crushed non-annealed glass blocks) and weighing 50 mg were contained in an alumina crucible and the reference material was α-alumina powder. The value of the glass transition temperature T_g, crystallization onset temperature, T_c and peak temperature of crystallization, T_p were obtained from the DTA scans.

Archimedes' method (*i.e.* immersion in ethylene glycol) was employed to measure the apparent density of the bulk annealed glasses which was further applied along with compositions of glasses to calculate their excess volume (V_e) according to a procedure described elsewhere.[3]

2.3 Structural characterization of glasses

^{29}Si MAS-NMR spectra were recorded on a Bruker ASX 400 spectrometer operating at 79.52 MHz (9.4 T) using a 7 mm probe at a spinning rate of 5 kHz. The pulse length was 2 μs and 60 s delay time was used. Kaolinite was used as the chemical shift reference. ^{27}Al MAS-NMR spectra were recorded on a Bruker ASX 400 spectrometer operating at 104.28 MHz (9.4 T) using a 4 mm probe at a spinning rate of 15 kHz. The pulse length was 0.6 μs and 4 s delay time was used. $Al(NO_3)_3$ was used as the chemical shift reference. The Q^n distributions were obtained by curve fitting and spectral deconvolution using DMFIT program (version 2011).[14]

2.4 Crystalline phase analysis and microstructural evolution in glass-ceramics

Bulk parallelepiped glass samples were heat treated non-isothermaly at 600, 700, 800 and 900 ºC for 1 h, respectively, at a heating rate of 2 K min^{-1}. The amorphous nature of the parent glasses and the nature of crystalline phases present in the GCs were determined by X-ray diffraction (XRD) analysis (Rigaku Geigerflex D/Mac,CSeries, Japan; Cu Kα radiation, 2θ between 10º and 60º with a 2θ-step of 0.02 º s^{-1}). The crystalline phases were identified by

comparing the obtained diffractograms with patterns of standards complied by the International Centre for Diffraction Data (ICDD).

Microstructure observations were done at polished (mirror finishing) and then etched surfaces of samples (by immersion in 2 vol.% HF solution for 1–2 min) by field emission scanning electron microscopy (SEM, Hitachi SU-70, Japan) under secondary electron mode.

3. Results and discussion

3.1 Casting ability and microstructure of glasses

Heating at 1550 ºC for 1 h was adequate to obtain bubble free, homogenous transparent and colourless glasses from all the investigated compositions. The absence of any crystalline inclusions was confirmed by XRD and SEM analyses. The SEM images of as cast non–annealed samples (Fig. 1) revealed nanosized droplets embedded in the glass matrices of all investigated compositions suggesting the occurrence of liquid–liquid phase separation. The droplet size and density distribution observed in the phase separated zones were small enough to avoid Tyndall effect, thus, resulting in transparent glasses. It is noteworthy that liquid separation is often the precursor to nucleation and crystal growth in certain GC compositions and can profoundly influence the crystallization path.[1, 15]

According to Vogel,[1] metastable immiscibility that occurs in binary Li_2O–SiO_2 system causes segregation of glassy phase into droplet-like zones of Li-rich phase and SiO_2-rich glass matrix. Moreover, the mean droplet size was found to be a function of Li_2O and SiO_2 contents. In particular, a bell-shaped curve showed maxima for SiO_2/Li_2O= 4.95 (~16.8 mol.% of Li_2O) and minima for both pure silica glass and stoichiometric lithium disilicate composition. Assuming similar structural roles for Li_2O and K_2O in the investigated glasses, a steady decrease in size of droplet-like zones should be expected with increasing contents of K_2O. However, our experimental results presented in Fig. 1 show an opposite trend with the mean droplet size growing with increasing K_2O contents. This can be explained by the preferential distribution of K_2O in the Li_2O-rich droplets[15] preventing diffusion of Li_2O towards SiO_2 rich region. Consequently, a composition gradient between separated droplet-like zones and silica rich glassy matrix becomes greater with increasing content K_2O leading to less homogeneous glass structures. The gradual lowering of SiO_2 content in glasses and the consequentially decrease in volume fraction of the silica-rich phase is expected to enhance the droplet like Li_2O and K_2O rich phase.[16]

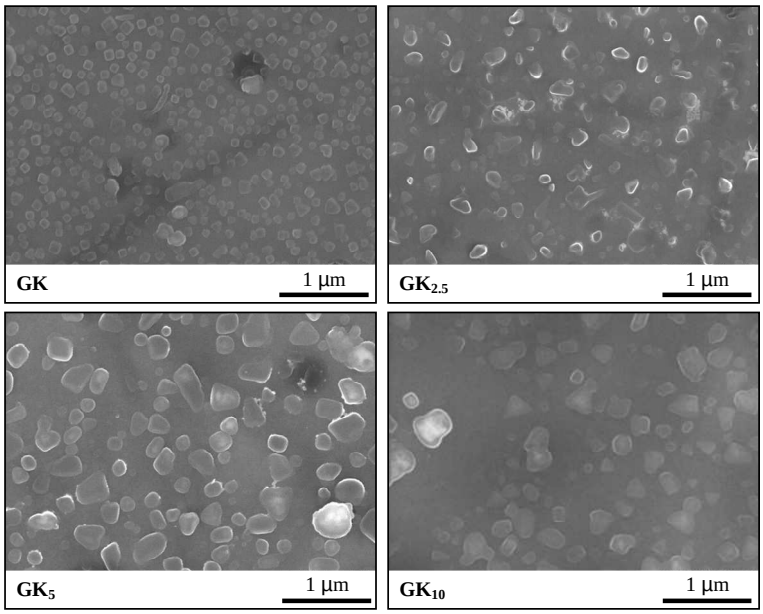

Fig. 1 – SEM images of the experimental non-annealed bulk glasses (etched with 2 vol.% HF solution for 1 min).

3.2 Structure-property relationships in glasses

3.2.1 Density, Ve, CTE and Tg

The density values of annealed glasses varied in the range of 2.36–2.43 g cm^{-3} (Table 2). A slight increase in density was observed from the parent glass composition (GK_0) to the glass $GK_{0.5}$, followed by a broad plateau until glass GK_2, and a new step increment to the glass $GK_{2.5}$. After that, density increased in direct proportion with further added amount of K_2O reaching the highest value for the glass GK_{10}. Since, density of glasses is an additive property, therefore, the constant values of glass density for compositions $GK_{0.5}$, GK_1, $GK_{1.5}$ and GK_2 may be attributed to the small K_2O increments in the glasses. However, sound conclusions regarding the structure of glasses cannot be drawn merely on the basis of density variations.[17] Therefore, in order to obtain a clear trend about the influence of K_2O/SiO_2 ratio on structure of investigated glasses, the values of excess molar volume (V_e) were calculated from density and glasses' molar composition data and featured a decrease of excess volume of glasses with increasing x values (Table 2). The incorporation of the K_2O network modifier alters the glass properties. The formation of less directed ionic bonds makes the structural skeleton to collapse into a closer packing, thus leading to reduced degree of cross-linking, which, in turn, reduces the glass transition temperature (T_g) (Fig. 2). Further, an increased polarizability arising from the negatively charged non-bridging atoms enhances the anharmonicity of thermal vibrations, thus leading to an increase in the CTE of glasses (Table 2; Fig. 2).[18]

Table 2 – Thermo-physical properties of the experimental glasses.

	d (g cm^{-3})	V_e (cm^3 mol^{-1})	NBO/T	CTE ±0.1 (10^{-6} K^{-1})	T_g ±2 (ºC)	T_c ±2 (ºC)	T_p ±2 (ºC)
GK_0	2.36 ± 0.01	1.26 ± 0.01	0.60	9.65	505	702	821
$GK_{0.5}$	2.37 ± 0.01	1.12 ± 0.04	0.61	10.16	504	698	817
GK_1	2.37 ± 0.01	1.08 ± 0.05	0.63	11.52	503	695	806
$GK_{1.5}$	2.37 ± 0.01	1.11 ± 0.04	0.65	11.34	501	663	818
GK_2	2.37 ± 0.01	1.03 ± 0.01	0.67	11.41	502	667	812
$GK_{2.5}$	2.38 ± 0.01	0.97 ± 0.01	0.68	11.51	500	663	800
GK_5	2.40 ± 0.01	0.76 ± 0.01	0.78	12.70	496	658	778
GK_{10}	2.43 ± 0.01	0.34 ± 0.02	0.98	14.68	481	582	723

Furthermore, the kinks observed in the values of CTE and T_g (Fig. 2) as well as in the values of V_e (Table 2), when x ranged from 0.5–1.5, can be attributed to the progressive changes brought by the network modifier, thus making the function of less basic so-called intermediate oxides somewhat ambiguous. In the present system, below a certain Li_2O/K_2O ratio, further adding the basic modifier oxide (*i.e.* K_2O) into the glasses forces Li_2O to enter the glass network. This gives rise to the formation of $(LiO_{4/2})^{3-}$ structural units with a coordination number of 4. Therefore, strengthening the silicate glass network occurs.[18]

3.2.2 MAS-NMR

The ^{29}Si MAS-NMR spectra of glasses GK_0, GK_5 and GK_{10} are plotted in Fig. 3 while chemical shifts (δ), linewidths (Δδ) and area fractions (%) of the signal components are presented in Table 3. In general, the spectra feature broad bands, which indicate the amorphous nature of these materials. For each composition, a resonance line covers the chemical shift range of silicon in several Q^n groups with n = 0, . . ., 4.[19] In particular, the ^{29}Si MAS-NMR spectra for parent glass composition GK_0 is centred at about −94 ppm (Fig. 3), suggesting a mixture of Q^3 and Q^4 (Table 3).

An overall trend towards depolymerization of the silicate glass network with increasing K_2O content can be observed due to the following factors: (a) centering of ^{29}Si MAS-NMR spectra at lower values, (b) formation of Q^2 groups, (c) increasing Q^3 and diminishing Q^4 units. However, the ^{29}Si spectrum for glass GK_1 (not shown) deviates from that trend, exhibiting a

chemical shift centred at about −95 ppm, thus implying towards an increasing polymerization, the reasoning for this was explained in the previous section.

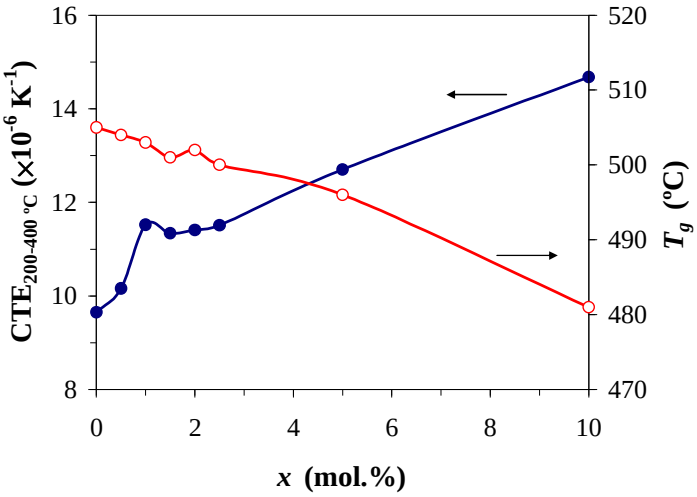

Fig. 2 – Evolution of CTE and T_g with the amount of K_2O added to the parent composition.

Table 3 – Solid state ^{29}Si NMR chemical shifts (δ), linewidths (Δδ) and area fractions (%) of the signal components observed in glasses GK_0, GK_5 and GK_{10}.

	Q^2			Q^3			Q^4		
x (mol.%)	δ (ppm)	Δδ (ppm)	%	δ (ppm)	Δδ (ppm)	%	δ (ppm)	Δδ (ppm)	%
0	–	–	0.0	–92.2	17.2	74.3	–104.7	14.5	25.7
5	–78.4	4.9	1.7	–90.7	14.9	82.7	–102.6	12.8	15.6
10	–79.8	5.6	3.4	–89.1	15.2	90.9	–101.2	13.3	5.8

Schramm *et al.*[20] investigated the extent of Q^n distributions for lithium silicate glasses in the composition region between 15 and 40 mol.% Li_2O by ^{29}Si MAS NMR spectroscopy. Values for the mean chemical shifts used to fit the spectra of those glasses were −107 ppm (Q^4), −92 ppm (Q^3), −82 ppm (Q^2), −69 ppm (Q^1), and −63 ppm (Q^0). The three major species Q^4, Q^3, and Q^2 were revealed. The percentage of Q^4 decreases with increasing Li_2O content, that of Q^3 goes through a maximum at 30 mol.% Li_2O, and the percentage of Q^2 showed tendency to grow at higher Li_2O concentrations. Particular emphasis should be addressed to $22.5Li_2O$–$77.5SiO_2$ and $24Li_2O$–$76SiO_2$ glasses owing to their Li_2O content and SiO_2/Li_2O ratios comparable with the compositions investigated in our work. According to Schramm *et al.*[20]

the $22.5Li_2O–77.5SiO_2$ glass composition featured the distribution of Q^n groups such as 0.1% Q^0 + Q^1, 3.9% Q^2, 63.2% Q^3, 32.8% Q^4 while the $24Li_2O–76SiO_2$ glass composition presented the following distribution: 2.5% Q^0 + Q^1, 11.1% Q^2, 56.6% Q^3, 29.8% Q^4. On the other hand, these glasses of $Li_2O–SiO_2$ system exhibited opalescence characteristic owing to precipitation of a droplet-like zones of Li-rich phase in SiO_2-rich glass matrix.[2, 20] Introduction of additives such as Al_2O_3 and K_2O resulted in glasses of transparent appearance in this metastable liquid immiscibility region due to the diminishing of mean droplet diameter and the packing density of droplet phase.[2-3] Moreover, both activation energy for crystallization and crystallization rate decreased. Analysis of the ^{29}Si MAS-NMR data obtained in our study revealed that the above mentioned phenomenon can be explained by diminishing of Q^2 groups after equimolar addition of Al_2O_3 and K_2O in $Li_2O–SiO_2$ system. Apparently, Q^2 groups are responsible for the enhanced nucleation rate. With regard to immiscibility process, Q^2 units as well as its clustering with Q^3, which is not considered by the Q^n distribution theory, would account for the metastable liquid immiscibility region, whereas Q^4 units represent the silica-rich region.[20]

^{27}Al NMR spectra of our samples (not shown) revealed chemical shifts from 52 ppm (GK_0) to 55 ppm (GK_{10}). The peaks shifting trend in the range of 52–55 ppm usually indicates an increasing predominance of tetrahedral aluminium in the glass structure. Therefore, the results obtained suggest that the K_2O added to the parent glass tends to enhance the role of Al_2O_3 as the glass network former signifying that aluminium in a four-coordinate network-forming species would not participate in the crystallization processes. This is consistent with the need of an associated cation in the vicinity of each tetrahedral unit in order to maintain local charge neutrality of the $(AlO_{4/2})^-$ units with four bridging oxygens.[2-3] In the present case, this neutrality is assured by the presence of K_2O. In such coordination, the Al^{3+} ions strengthen the glass network and diminish crystallization tendency during melt quenching. However, as the ratio K_2O/Al_2O_3 increases, the molar concentration of K_2O exceeds that of Al_2O_3, causing the formation of a larger fraction of NBO (Table 2). These free potassium cations act as glass network modifiers and are distributed in the glass matrix apart from the glass network forming $(AlO_{4/2})^-$ units.

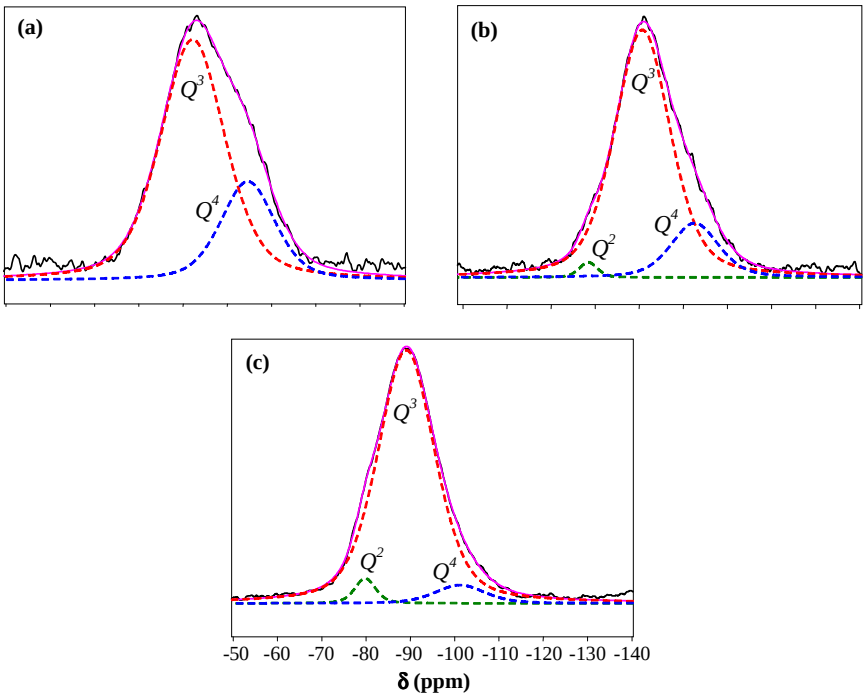

Fig. 3 – ^{29}Si MAS-NMR spectra of glasses: (a) GK_0, (b) GK_5 and (c) GK_{10}. Dashed curves show the spectral deconvolution components used for fitting the data.

3.2.3 Differential thermal analysis

The DTA plots of glasses with a heating rate (β) of 20 K min^{-1}, shown in Fig. 4a, show well-defined features comprising endothermic and exothermic peaks from which transition point (T_g), temperature of onset crystallization (T_c) and peak temperature of crystallization (T_p), were determined (Table 2). In general, T_c and T_p decreased with increasing K_2O content (Fig. 4b) confirming earlier results that crystallization of K_2O containing lithium disilicate glass starts at lower temperatures.[15] Moreover, lowering of T_g values are in accordance with increasing non-bridging oxygens per tetrahedron (NBO/T) for potassium richer compositions suggesting depolymerization of glass network. Additionally it was revealed that the peak temperature of crystallization shifted to higher temperatures with increasing β (figures are not shown).

3.3 Crystallization behaviour of bulk glasses

3.3.1 Phase assemblage

Fig. 5 presents the X-ray diffractograms of glasses heat treated at different temperatures. All the investigated glass compositions were amorphous after heat treatment at 600 ºC for 1 h

except GK_{10} that exhibits traces of lithium metasilicate (Fig. 5a). The trend for the preferential crystallization of lithium metasilicate with increasing potassium content appears clear at 700 ºC (Fig. 5b). As a matter of fact, low intensity peaks of lithium disilicate only appeared in the GK_0 sample heat treated at this temperature. Increasing the heat treatment temperature to 800 ºC (Fig. 5c) favoured the formation of lithium disilicate in detriment of lithium metasilicate within the x range of 0–1, while lithium metasilicate is the only phase present for $x > 1$ (also valid at 900 ºC). However, the parent glass composition GK_0 underwent partial dissolution of lithium disilicate into lithium metasilicate and quartz with increasing the temperature to 900 ºC, while enhanced the intensity of lithium disilicate peaks in the $GK_{0.5}$ and GK_1 compositions (Fig. 5d).

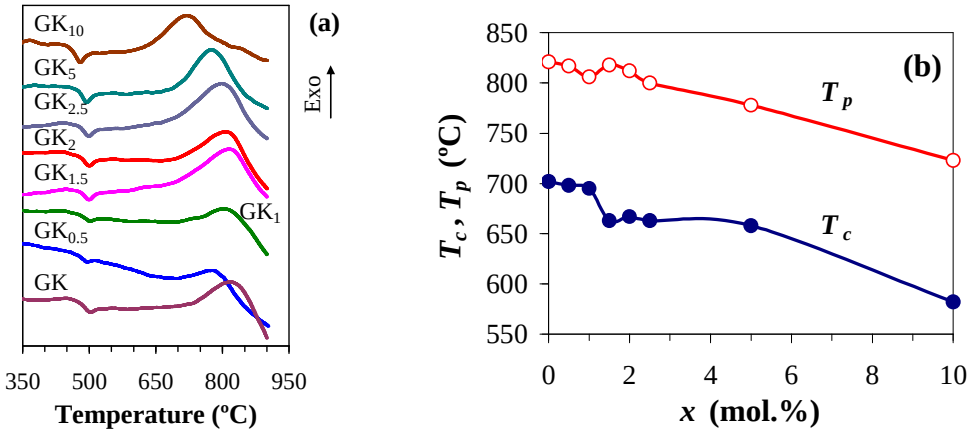

Fig. 4 – Thermal behaviour of glasses: (a) DTA at $\beta = 20$ K min^{-1}; (b) evolution of T_c and T_p with the amount of K_2O added to the parent composition.

The as obtained results suggest that K_2O significantly affects the crystallization process suppressing the crystallization of lithium disilicate and promoting formation of lithium metasilicate for $x > 1$. This conclusion is in agreement with the study on equimolar replacement of 3 mol.% of Li_2O by K_2O in the $73SiO_2$, $2.15Al_2O_3$, $23.7Li_2O$ and $1.15P_2O_5$ (mol.%) base glass.[15] This change in the crystallization behaviour can be explained by the lower value of the activation energy for crystallization of lithium metasilicate in comparison to that of lithium disilicate.[15, 21-22] Moreover, adding alkali oxides to silicate glasses decreases the melt viscosity, increases the fraction of NBO and enhances the tendency of the glass towards devitrification.[23]

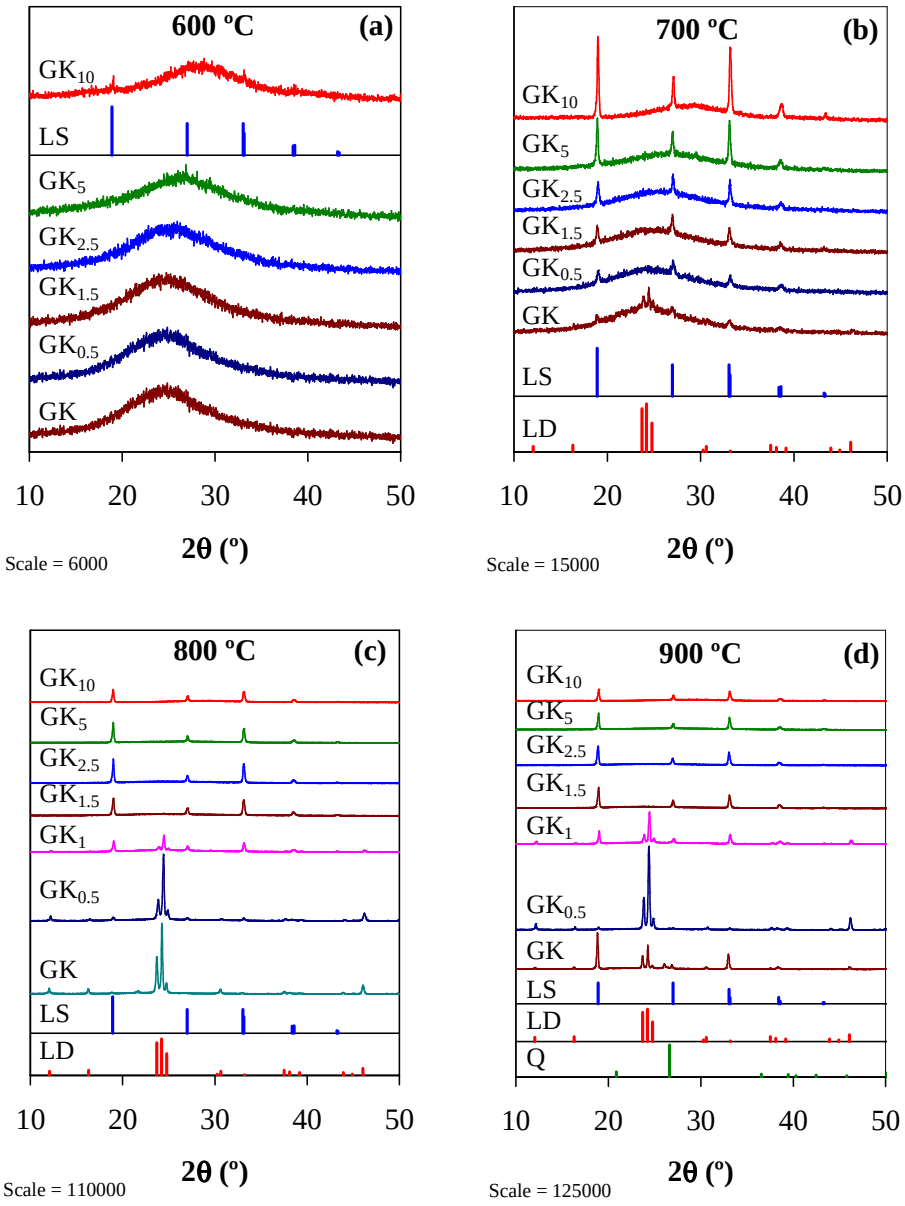

Fig. 5 – X-ray diffractograms of experimental bulk glasses after heat treatment at different temperatures for 1 h. LS: lithium silicate (Li_2SiO_3, ICCD card 01-029-0828); LD: lithium disilicate ($Li_2Si_2O_5$, ICCD card 01-070-4856); Q: quartz (SiO_2, ICCD card 01-077-1060).

Bischoff *et al.*[24] quite recently demonstrated that in series with SiO_2/Li_2O molar ratio 2.39:1, at 650 ºC crystalline Li_2SiO_3 is not only being formed from the Q^2 component present in the glassy precursor material but also via a disproportionation of Q^3 units in the glass according to the reaction (1):

$$2Q^3 \text{ (glass)} \leftrightarrow Q^2 \text{ (cryst.)} + Q^4 \text{ (glass)} \quad (1)$$

Moreover, it was revealed reveals that the Q^3/Q^4 ratio was already significantly decreased in the amorphous sample annealed at 530 ºC, even before crystalline Li_2SiO_3 can be observed in either solid state NMR or X-ray powder patterns. Finally, the formation of crystalline $Li_2Si_2O_5$ in the sample annealed at 850 ºC produced a strong sharp peak near −92 ppm supporting the synproportionation reaction (2):

$$Q^4 \text{ (glass)} + Q^2 \text{ (cryst.)} \leftrightarrow 2Q^3 \text{ (cryst.)} \quad (2)$$

Using this model and ^{29}SiMAS-NMR results (Fig. 3; Table 3) we can explain the effect of suppressing the crystallization of $Li_2Si_2O_5$ and promoting formation of Li_2SiO_3 with increasing of K_2O content. Thus, considering the significant decrease of Q^4 units in K_2O-rich glasses (e.g. GK_5 and GK_{10}) the probability of reaction (2) to occur decreases considerably. This leads to the formation of Li_2SiO_3 as a single phase directly from Q^2 or via reaction (1).

3.3.1 Microstructure

Fig. 6 shows the SEM micrographs for the glasses heat treated at different temperatures. At 600 ºC, composition $GK_{0.5}$ demonstrates coalescence of droplets into bigger agglomerates (Fig. 6a). A superficial layer of crystals with dendritic morphology, characteristic for lithium metasilicate, is clearly observed in the samples heat treated at 800 ºC (Fig. 6b).[3] At 900 ºC, it is possible to observe the droplet-like zones of Li-rich phase, which are responsible for formation of lithium disilicate crystals in bulk region of the specimen (Fig. 6c).

The phase separation in glasses with higher K_2O contents conferred peculiar microstructural features since these glasses separate into two phases, one of which is a continuous phase rich in Li_2O and containing considerable amount of K_2O. Moreover, the addition of K_2O seems to have favoured surface crystallization in glasses, as well as the formation of lithium metasilicate for $x > 1$, in good agreement with the XRD data. Thus, a surface layer of lithium metasilicate crystals grown towards the bulk can be clearly seen in Figs. 6d–f, for the samples heat treated at 700 ºC within the x range of 1.5–10, respectively. The thickness of the crystalline surface layer increased from 125 μm ($GK_{1.5}$, Fig. 6d) to 350 μm (GK_5, Fig. 6e) and 925 μm (GK_{10}, Fig. 6f), an effect that might be due to the preferred distribution of K_2O in liquid–liquid phase separated Li_2O-rich droplets. However, further information on nucleation and crystallization mechanisms needs to be gathered via investigating the crystallization kinetics of experimental glasses.

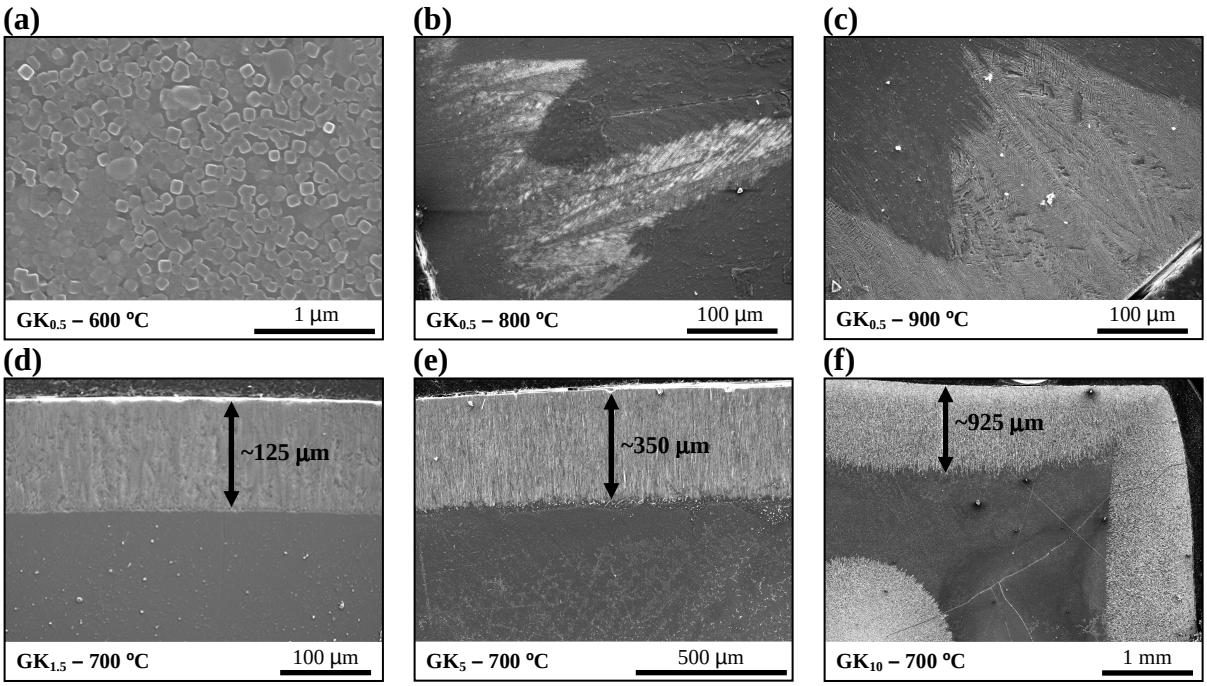

Fig. 6 – SEM images of bulk glasses heat treated at different temperatures for 1 h (etched with 2 vol.% HF solution for 2 min).

4. Conclusions

An insight into the effect of K_2O on structure–property relationships and devitrification behaviour of glasses in the Li_2O–SiO_2 system has been presented. The results can be summarized in the following conclusions:

1. Liquid–liquid phase separation occurred in all investigated glasses and the addition of K_2O to the parent glass led to increasing the mean droplet size and their distribution density due to a decreasing energy barrier towards phase separation caused by the lowering of glass melt viscosity.
2. The ^{29}Si MAS-NMR spectra evidenced a mixture of Q^4 (Si) and Q^3 (Si) as the predominant structural units in all the glasses. Upon increasing K_2O content, new Q^2 groups appeared and the amount of Q^3 units increased, whereas the Q^4 units diminished suggesting depolymerization of the silicate glass network.
3. The ^{27}Al MAS-NMR results suggested that the K_2O added to the parent glass tends to enhance the role of Al_2O_3 as glass network former, signifying

that four-coordinate aluminium network-forming species would not participate in the crystallization processes.

4. According to the ^{29}Si MAS-NMR results, diminishing of Q^4 groups in K_2O-rich glasses (*e.g.* GK_5 and GK_{10}) suppressed the crystallization of $Li_2Si_2O_5$ and promoted the formation of Li_2SiO_3.

Acknowledgments

Hugo R. Fernandes is grateful for the financial support of CICECO and for the PhD grant (SFRH/BD/41307/2007) from the FCT, Portugal.

References

1. Vogel W. Structure and Crystallization of Glasses. Leipzig: Pergamon Press; 1971.
2. Fernandes HR, Tulyaganov DU, Goel A, Ribeiro MJ, Pascual MJ, Ferreira JMF. Effect of Al_2O_3 and K_2O content on structure, properties and devitrification of glasses in the $Li_2O–SiO_2$ system. Journal of the European Ceramic Society 2010;30(10):2017-30.
3. Fernandes HR, Tulyaganov DU, Goel IK, Ferreira JMF. Crystallization process and some properties of $Li_2O–SiO_2$ glass-ceramics doped with Al_2O_3 and K_2O. Journal of the American Ceramic Society 2008;91(11):3698-703.
4. Höland W, Beall G. Glass-ceramic Technology. Westerville, Ohio: The American Ceramic Society; 2002.
5. Borom MP, Turkalo AM, Doremus RH. Strength and microstructure in lithium disilicate glass-ceramics. Journal of the American Ceramic Society 1975;58(9-10):385-91.
6. Guazzato M, Albakry M, Ringer SP, Swain MV. Strength, fracture toughness and microstructure of a selection of all-ceramic materials. Part I. Pressable and alumina glass-infiltrated ceramics. Dental Materials 2004;20(5):441-48.
7. Höland W, Apel E, van Hoen C, Rheinberger V. Studies of crystal phase formations in high-strength lithium disilicate glass-ceramics. Journal of Non-Crystalline Solids 2006;352(38-39):4041-50.
8. Iqbal Y, Lee WE, Holland D, James PF. Metastable phase formation in the early stage crystallisation of lithium disilicate glass. Journal of Non-Crystalline Solids 1998;224(1):1-16.
9. Bengisu M, Brow RK, White JE. Interfacial reactions between lithium silicate glass-ceramics and Ni-based superalloys and the effect of heat treatment at elevated temperatures. Journal of Materials Science 2004;39(2):605-18.
10. Goswami M, Kothiyal GP, Montagne L, Delevoye L. MAS-NMR study of lithium zinc silicate glasses and glass-ceramics with various ZnO content. Journal of Solid State Chemistry 2008;181(2):269-75.

11. Stookey SD. Catalyzed Crystallization of glass in theory and practice. Industrial and Engineering Chemistry 1959;51(7):805-08.
12. Barrett JMG, FL), Clark, David E. (Gainesville, FL), Hench, Larry L. (Gainesville, FL), inventor; The Board of Regents, State of Florida, University of Florida (Tallahassee, FL), assignee. Glass-ceramic dental restorations. 1980.
13. Wu J-mT, TW), Cannon, Warren R. (East Brunswick, NJ), Panzera, Carlino (Belle Mead, NJ), inventor; Johnson & Johnson Dental Products Company (East Windsor, NJ), assignee. Castable glass-ceramic composition useful as dental restorative. 1985.
14. Massiot D, Fayon F, Capron M, King I, Le Calvé S, Alonso B, et al. Modelling one- and two-dimensional solid-state NMR spectra. Magnetic Resonance in Chemistry 2002;40:70-76.
15. Morimoto S. Effect of K_2O on crystallization of $Li_2O–SiO_2$ glass. Journal of the Ceramic Society of Japan 2006;114(1326):195-98.
16. James PF. Liquid-phase separation in glass-forming systems. Journal of Materials Science 1975;10(10):1802-25.
17. Shelby JE. Introduction to glass science and technology. Cambridge: The Royal Society of Chemistry; 1997.
18. Martin JW. Concise Encyclopedia of the Structure of Materials. 1st Edition ed. Amsterdam: Elsevier; 2007.
19. Schneider J, Mastelaro VR, Panepucci H, Zanotto ED. ^{29}Si MAS–NMR studies of Q^n structural units in metasilicate glasses and their nucleating ability. Journal of Non-Crystalline Solids 2000;273:8-18.
20. Schramm CM, de Jong BHWS, Parzialet VE. ^{29}Si Magic Angle Spinning NMR Study on Local Silicon Environments in Amorphous and Crystalline Lithium Silicates. Journal of the American Ceramic Society 1984;106:4396-402.
21. Hammetter WF, Loehman RE. Crystallization kinetics of a complex lithium silicate glass-ceramic. Journal of the American Ceramic Society 1987;70(8):577-82.
22. Oliveira APN, Alarcon OE, Manfredini T, Pellacani GC, Siligardi C. Crystallisation kinetics of a $2.3Li_2O.1.1ZrO_2.6.6SiO_2$ glass. Physics and Chemistry of Glasses 2000;41(2):100-03.
23. Scholze H. Glass: Nature, Structure and Properties. Berlin: Springer; 1991.
24. Bischoff C, Eckert H, Apel E, Rheinberger VM, Holand W. Phase evolution in lithium disilicate glass–ceramics based on non-stoichiometric compositions of a multi-component system: structural studies by ^{29}Si single and double resonance solid state NMR. Physical Chemistry Chemical Physics 2011;13:4540-51.

3.5 The role of K_2O on sintering and crystallization of glass powder compacts in the $Li_2O–K_2O–Al_2O_3–SiO_2$ system

Hugo R. Fernandes[a], Dilshat U. Tulyaganov[a,b], Maria J. Pascual[c], Vladislav V. Kharton[a], Aleksey A. Yaremchenko[a], José M.F. Ferreira[a]

[a] Department of Ceramics and Glass Engineering, University of Aveiro, CICECO, 3810-193 Aveiro, Portugal

[b] Turin Polytechnic University in Tashkent, 17 Niyazova str., 100174 Tashkent, Uzbekistan

[c] Instituto de Cerámica y Vidrio (CSIC), C/Kelsen 5, Campus de Cantoblanco, 28049 Madrid, Spain

Journal of the European Ceramic Society 32 (2012) 2283–2292

DOI: 10.1016/j.jeurceramsoc.2012.02.003

Abstract

The effects of K_2O content on sintering and crystallization of glass powder compacts in the $Li_2O–K_2O–Al_2O_3–SiO_2$ system were investigated. Glasses featuring SiO_2/Li_2O molar ratios of 2.69–3.13, far beyond the lithium disilicate (LD, $Li_2Si_2O_5$) stoichiometry, were produced by conventional melt-quenching technique. The sintering and crystallization behaviour of glass powders was explored using hot stage microscopy (HSM), scanning electron microscopy (SEM), differential thermal (DTA) and X-ray diffraction (XRD) analyses. Increasing K_2O content at the expense of SiO_2 was shown to lower the temperature of maximum shrinkage, eventually resulting in early densification of the glass-powder compacts. Lithium metasilicate was the main crystalline phase formed upon heat treating the glass powders with higher amounts of K_2O. In contrast, lithium disilicate predominantly crystallized from the compositions with lower K_2O contents resulting in strong glass-ceramics with high chemical and electrical resistance. The total content of K_2O should be kept below 4.63 mol.% for obtaining LD-based glass-ceramics.

Keywords: Glass; Glass ceramics; Lithium disilicate; Thermo-physical properties

1. Introduction

Sintering of glass-powder compacts is a common processing route for obtaining glass–ceramic (GC) materials with desired properties.[1-2] The glass powders with high specific surface area intrinsically provide uniformly distributed nucleus sites in the entire volume of the glass.[3-7] The properties of GCs are determined by crystalline phases precipitated from the glass reservoir while an excessively high crystal growth rate is to be avoided to not develop coarse microstructure limiting achievement of high mechanical strength.[1, 8-10] Additionally, sintering should preferably take place prior crystallization thus both events being independent processes.

Lithium disilicate GCs have attracted much interest due to a wide range of practical applications such as ceramic composites, ceramic-metal sealing, dental restoration, etc.[11-13] Production of those materials might be alternatively based on sintering and crystallization of glass powder compacts. In particular, dentistry restoration systems IPS Empress® 2 for restoring three-unit fixed partial dentures up to the second premolar have so far been prepared by hot-pressing technology of sintered ingots.[14] Apparently, besides the practical aspects, lithium disilicate glasses have been a subject of many nucleation and crystallization theories for decades.[15-18] These studies focused on the $Li_2O–SiO_2$ binary glass system and discussed the growth interrelation between the $Li_2Si_2O_5$ and Li_2SiO_3 (lithium metasilicate) crystalline phases.[15-20]

In our previous attempts, the glasses containing Al_2O_3 and K_2O and featuring SiO_2/Li_2O molar ratios (3.13–4.88) were produced by conventional melt-quenching technique along with a bicomponent glass $23Li_2O–77SiO_2$ (mol.%).[19-20] Sintering and crystallization studies of glass powder compacts revealed that $23Li_2O–77SiO_2$ composition exhibited high fragility along with low flexural strength and density. Addition of Al_2O_3 and K_2O in equimolar amount to $Li_2O–SiO_2$ compositions resulted in improved densification and mechanical strength.[19]

Recently we attempted to synthesis glasses in the glass forming region of $Li_2O–K_2O–Al_2O_3–SiO_2$ system with SiO_2/Li_2O molar ratios varying between 2.69–3.13.[21] The role of K_2O and K_2O/SiO_2 ratios on structural transformations, properties of new glasses in bulk form along with their crystallization mechanism was investigated. The ^{29}Si MAS-NMR spectra evidenced a mixture of Q^4 (Si) and Q^3 (Si) as the predominant structural units in all the glasses. Moreover, upon increasing K_2O content new Q^2 groups appeared, the amount of Q^3 units increased, whereas Q^4 diminished, suggesting depolymerisation of the silicate

glass network. The addition of K_2O was found to promote surface crystallization in glasses, as well as the predominant formation of lithium metasilicate phase.

This work, as the logical continuation of the recent study,[21] aims at investigating the effects of K_2O on sintering and crystallization of glass powder compacts in the $Li_2O–K_2O–Al_2O_3–SiO_2$ system. The same glass compositions with SiO_2/Li_2O molar ratios varying between 2.69–3.13 have been prepared but in the frit form, and the sintering and crystallization of glass-powder compacts were analysed by hot stage microscopy (HSM), scanning electron microscopy (SEM), differential thermal (DTA) and X-ray diffraction (XRD) analyses. Another objective was to determine the influence of K_2O contents and K_2O/SiO_2 ratios on thermal, mechanical and electrical properties of resultant glass-ceramic materials.

2. Experimental procedure

2.1. Glass preparation

A total of 8 compositions were prepared according to the general formulae 23.7 (71.78–*x*) $SiO_2 \cdot 2.63\ Al_2O_3 \cdot (2.63+x)\ K_2O \cdot 23.7\ Li_2O$, where *x* changed from 0 to 10.[21] Accordingly, the glasses have been labelled as GK_x depending on the amount of K_2O being substituted for SiO_2 in the glass compositions. For example: GK_0 corresponds to the parent composition, *i.e.*, $x = 0$ and $K_2O/Al_2O_3 = 1$. Table 1 presents the detailed compositions of the glasses along with their corresponding SiO_2/Li_2O, SiO_2/K_2O and K_2O/Al_2O_3 ratios.

Powders of technical grade SiO_2 (purity >99.5%) and of reactive grade Al_2O_3, Li_2CO_3, and K_2CO_3 were used. Homogeneous mixtures of batches (~100 g) obtained by ball milling were calcined at 800 ºC for 1 h, melted in Pt crucibles at 1550 ºC for 1 h in air and then quenched in cold water. The obtained frits were dried and milled in a high-speed agate mill. The mean particle size of the glass powders as determined by light scattering technique (Beckman Coulter LS 230, CA USA; Fraunhofer optical model) was about 5-10 µm.

2.2. Sintering and crystallization of glass powder compacts

A side-view hot-stage microscope (HSM, Leitz Wetzlar, Germany) equipped with a Pixera video-camera and image analysis system was used to investigate the sintering behaviour of glass powder compacts. The cylindrical shaped samples from glass powder compacts with

height and diameter of ~3 mm were prepared by cold-pressing the glass powders. The cylindrical samples were placed on a 10×15×1 mm^3 alumina (>99.5 wt.% Al_2O_3) support and the measurements were conducted in air with a heating rate (β) of 5 K/min. The temperature was measured with a chromel–alumel thermocouple contacted under the alumina support. The temperatures corresponding to the characteristic viscosity points [first shrinkage (T_{FS}), maximum shrinkage (T_{MS}), softening (T_D), half ball (T_{HB}) and flow (T_F)] were obtained from the graphs and photomicrographs taken during the hot-stage microscopy experiment.[22-23]

Apart from HSM investigation, the sintering process was explored using non-isothermal heat treatment of glass-powder compacts. Rectangular bars (4×5×50 mm^3) prepared by uniaxial pressing (80 MPa) were sintered at 800, 850 and 900 ºC for 1 h. A heating rate of 2 K/min was maintained in order to prevent deformation of the samples.

Table 1 – Compositions of the experimental glasses.

	Oxides (mol.%)						
	Li_2O	K_2O	Al_2O_3	SiO_2	SiO_2 /Li_2O	SiO_2 /K_2O	K_2O/ Al_2O_3
GK	22.96	2.63	2.63	71.78	3.13	27.29	1.00
$GK_{0.5}$	22.96	3.13	2.63	71.28	3.10	22.77	1.19
GK_1	22.96	3.63	2.63	70.78	3.08	19.50	1.38
$GK_{1.5}$	22.96	4.13	2.63	70.28	3.06	17.02	1.57
GK_2	22.96	4.63	2.63	69.78	3.04	15.07	1.76
$GK_{2.5}$	22.96	5.13	2.63	69.28	3.02	13.50	1.95
GK_5	22.96	7.63	2.63	66.78	2.91	8.75	2.90
GK_{10}	22.96	12.63	2.63	61.78	2.69	4.89	4.80

The following characterization techniques were employed to analyse sintered materials: (1) Archimedes' method (*i.e.* immersion in diethylphthalate) to measure the apparent density; (2) dilatometry measurements (Bahr Thermo Analyze DIL 801 L, Hüllhorst, Germany; heating rate 5 K/min) to measure coefficient of thermal expansion (CTE) (standard deviation obtained from 3 samples was $\pm 0.1\times10^{-6}$ /K); (3) differential thermal analysis in air (DTA, Labsys setaram TG-DTA; heating rate 5 and 10 K/min); (4) 3-point bending strength tests were performed on rectified parallelepiped bars of sintered GCs (Shimadzu Autograph AG 25 TA, 0.5 mm/min displacement): the results were obtained from 10 different independent samples; (5) chemical resistance was established according to ISO test standards, *i.e.* immersing the

materials in acetic acid at 80 ºC for 16 h and evaluating possible weight loss ($\mu g/cm^2$);[24] (6) crystalline phases were identified by X-ray diffraction analysis (Rigaku Geigerflex D/Mac, C Series, Japan; Cu K_a radiation, 2θ = 10-60º with a 2θ-step of 0.02 deg/s) comparing the experimental X-ray patterns to standards compiled by the International Centre for Diffraction Data (ICDD); (7) microstructure observations were done on polished (mirror finishing) and then etched samples (immersion in 2 vol.% HF solution for 2 min) by field emission scanning electron microscopy (FE-SEM, Hitachi S-4100, Japan, 25 kV acceleration voltage, beam current 10 μA) under secondary electron mode.

For the measurements of total conductivity, dense ceramic samples sintered at 900 ºC were cut into disks with thickness of 1–3 mm (diameter of 14 mm) and then polished with diamond pastes. Porous Ag electrodes were applied onto both sides of the glass-ceramic disks and sintered at 600 ºC for 5–10 minutes. The total conductivity (σ) was determined by alternating current (AC) impedance spectroscopy using a HP4284A precision LCR meter in the frequency range 20 Hz – 1 MHz. The measurements were performed at 630–800 K in flowing dry and wet air or argon, where the water vapour partial pressure was continuously monitored by a Jumo humidity transducer. The lower temperature limit was associated with increasing electrical resistance of the glass-ceramics on cooling, leading to a higher noise level and lower accuracy; the upper limit was selected in order to avoid possible volatilization of the alkaline metal oxide components. The gas flows were dried by passing through silica gel or humidified by bubbling through water at room temperature.

3. Results

3.1. Glass and glass-ceramic samples preparation

Heating at 1550 ºC for 1 h was adequate to obtain amorphous frits from all the investigated compositions as confirmed by the absence of crystalline inclusions using XRD analysis. Apparently, glass preparation temperature decreases with growing K_2O content. Dense samples of rectangular shape were obtained after sintering of glass-powder compacts at 800, 850 and 900 ºC for 1 h. However, GK_5 and GK_{10} exhibited clear signs of softening at temperature ≥ 800 ºC (Fig. 1) due to their higher contents of alkaline oxides (Li_2O+K_2O).[25-29]

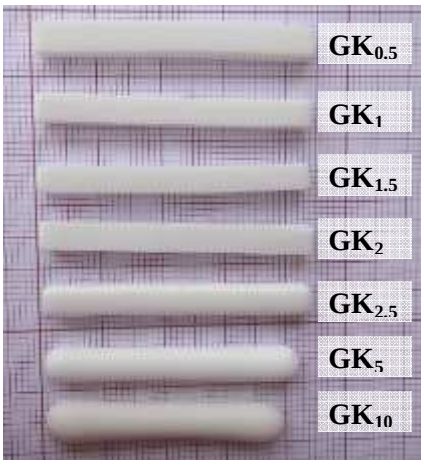

Fig. 1 – Appearance of glass powder compact bars after sintering at 900 ºC for 1 h.

3.2. Sintering process of glass-powder compacts

During sintering of a glass-powder compact, smaller particles get sintered first and sintering kinetics at the first shrinkage is dominated by the neck formation among smallest particles via viscous flow.[30-31] Maximum shrinkage is reached when larger pores have disappeared due to viscous flow that reduces their radii with time.[32] However, some processes, *e.g.* crystallization, occurring at the very end of sintering process might affect the densification kinetics. A comparison between DTA and HSM results under the same heating conditions can be useful to investigate the effect of glass composition on sintering and devitrification phenomena. In general, two different trends related to the sintering and crystallization behaviour of the glasses can be observed:[33] (1) the beginning of crystallization (T_c) occurs after the final sintering stage and, thus, sintering and crystallization are independent processes; (2) T_c appears before the maximum density has been reached, and the crystallization process starts before complete densification, thus, preventing further sintering.

There are several important characteristic viscosity points based on the relation between the temperatures measured by HSM and corresponding viscosities:[22, 34] (1) first shrinkage (T_{FS}): the temperature at which the pressed sample starts to shrink, $\log \eta = 9.1 \pm 0.1$, where η is the viscosity in dPa.s; (2) point of maximum shrinkage (T_{MS}): the temperature at which maximum shrinkage of the glass-powder compact is achieved before it starts to soften, $\log \eta = 7.8 \pm 0.1$; (3) softening point (T_D): the temperature at which the first signs of softening are observed which is generally shown by the disappearance or rounding of the small protrusions at the edges of the sample, $\log \eta = 6.3 \pm 0.1$; (4) half ball point (T_{HB}): the temperature at which the section of the observed sample forms a semicircle on the microscope grid, $\log \eta = 4.1 \pm 0.1$,

and (5) flow point (T_F): the temperature at which the maximum height of the drop of the molten glass corresponds to a unit on the microscopic scale, log η = 3.4 ± 0.1. A/A_0 corresponds to the ratio of final area/initial area of the glass-powder compacts.

The variation in the relative area (A/A_0) and heat flow with respect to temperature is shown in Fig. 2, revealing two steps of sintering. The thermal characteristics and sintering parameters of glasses obtained by means of DTA and HSM are summarized in the Table 2. The initiation of sintering occurred at ~484–491 ºC (T_{FS1}) in all compositions while the extent of densification at the first stage (*i.e.* temperature interval between T_{MS1} and T_{FS1}) significantly decreased with increasing K_2O content and K_2O/SiO_2 ratio. The first sintering stage ended at the point of first maximum shrinkage (T_{MS1}) that was fairly close to the onset of crystallization temperature (T_c).

The second stage of densification occurred in competition with devitrification process (Fig. 2) that subsequently might cause a viscosity increase.[33] However, the viscosity did not raise in such an extent to prevent sintering.[19] In contrast, shrinkage values (Δ_2) of GK_0–GK_2 glasses were comparable with relevant data obtained at the first stage. The subsequent GK_5–GK_{10} compositions exhibited highest values of shrinkage suggesting that the densification processes for these glasses mostly occurred during the second sintering stage. Another feature was that the temperature of second shrinkage (T_{FS2}) and the corresponding point of maximum shrinkage (T_{MS2}) decreased with increasing amounts of K_2O.

The photomicrographs demonstrating a change in the geometrical shape with temperature, as obtained from HSM, are presented in Fig. 3. The value of *TD* for GK_0 is about 929 ºC, which is higher than the maximum sintering temperature used in the experimental procedure (900 ºC). Therefore no deformation sighs in GK_0 samples were revealed (Fig. 1), likewise for GK_1 and GK_2 that exhibited T_D values at about 947 ºC and 928 ºC, respectively (Table 2). Compositions with higher added amounts of K_2O exhibited lower ability to withstand the same temperature range. For instance, compositions GK_5 and GK_{10} reached T_D at 830 and 709 ºC, T_{HB} at 910 and 916 ºC, and T_F at 929 and 939 ºC, respectively (Table 2).

3.3. Phase assemblage and microstructure

Fig. 4 presents the X-ray diffractograms of glass powder compacts after heating at 800, 850 and 900 ºC for 1 h. Lithium metasilicate is the major phase while quartz and lithium disilicate are minor phases in GK_0 at 800 ºC. Low intensive peaks of lithium disilicate also appeared in

the $GK_{0.5}$–GK_2 samples heat treated at this temperature. Increasing the heat treatment temperature to 850–900 ºC favoured formation of lithium disilicate in detriment of lithium metasilicate within the *x* range of 0–2.

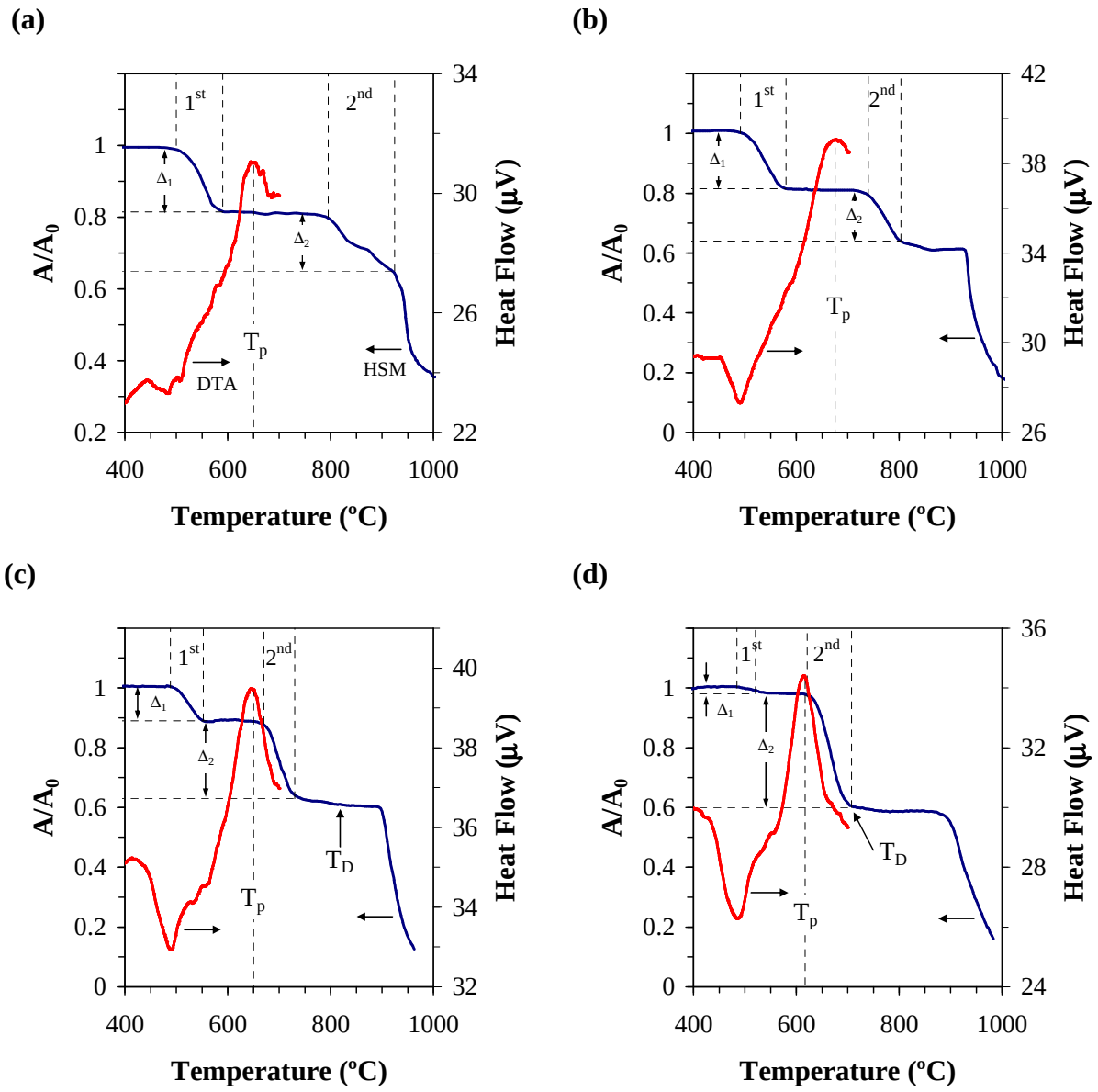

Fig. 2 – DTA and HSM curves for glass-powders (a) GK_0, (b) GK_2, (c) GK_5, (d) GK_{10}.

However, the intensity of lithium disilicate peaks decayed with increasing K_2O contents and the observed results suggest that the total amount of K_2O in a glass should be less than 4.63 mol.% (or *x* should vary in the range of 0–2) to obtain lithium disilicate as the predominate crystalline phase. Thus, lithium metasilicate was the only crystalline phase formed in the

glasses containing higher amounts of K_2O after sintering at 800, 850 and 900 ºC (in GK_5 weak peaks of orthoclase were also identified).

Table 2 –Thermal characteristics of glasses and their sintering parameters.

	DTA			HSM									
x	T_g	T_c	T_p	T_{FS1}	T_{MS1}	Δ_1	T_{FS2}	T_{MS2}	Δ_2	A/A_0	T_D	T_{HB}	T_F
	(ºC)			(ºC)			(ºC)				(ºC)		
0	507	599	672	487	611	0.18	774	924	0.17	0.65	929	945	964
1	499	596	669	491	611	0.18	758	874	0.20	0.62	947	957	967
2	494	588	675	487	593	0.19	717	870	0.20	0.61	928	937	954
5	493	563	651	488	565	0.11	658	821	0.28	0.61	830	910	929
10	490	559	616	484	541	0.02	621	707	0.39	0.59	709	916	939

Fig. 3 – HSM images of glass powder compacts on alumina substrates (* corresponds to T_D of composition GK_0).

Fig. 5 presents the SEM images of glass powder compacts of compositions GK_0 $GK_{2.5}$ and GK_5 after heat treatment at 800, 850 and 900 ºC for 1 h. The microstructure of parent composition GK_0 heat treated at 800 ºC (Fig. 5a) reveals the occurrence of dendritic crystal growth of lithium metasilicate and small crystals of quartz dispersed in the matrix, which are in accordance with the results obtained by XRD (Fig. 4a).

It is known that lithium metasilicate crystals are particularly easy to dissolve from GC by diluted hydrofluoric acid (HF) while the surrounding aluminosilicate glassy matrix is considerably more resistant to acid attack.[1] Thus, its presence is recognized by the replica image resultant from acid etching. At 850 ºC the microstructure changed drastically revealing the presence of laminar fibres of lithium disilicate embedded in the glass matrix which further grew with temperature increasing to 900 ºC. With increasing added amounts of K_2O the content of glassy phase increased and lithium metasilicate appeared as the predominant crystalline phase, being in good agreement with the XRD results presented in Fig. 4. In the

case of $GK_{2.5}$ composition, the presence of laminar lithium disilicate crystals is only apparent in the micrograph of the sample heat treated at 900 ºC (Fig. 5d), although traces of lithium disilicate have been detected at 850 ºC (Fig. 4d). The micrographs of GK_5 composition (Fig. 5h-j) are dominated by the morphological features of lithium metasilicate crystals that underwent extensive dissolution by HF attack. The small orthoclase content detected by XRD is also apparent as small equiaxed and whiter crystals.

3.4. Density, bending strength, CTE and chemical resistance of glass-powder compacts

Table 3 presents density and bending strength values of glass powder compacts heat treated at 800, 850 and 900 ºC for 1 h. The glass ceramics GK_0 - GK_2 exhibited maximum density (2.34–2.38 g/cm^3) and bending strength (~173–224 MPa) after heat treatment at 900 ºC. The samples $GK_{2.5}$, GK_5 and GK_{10} having higher K_2O/SiO_2 ratios possessed maximum density (2.34–2.38 g/cm^3) and bending strength values (~89–148 MPa) at the lower temperatures (800 and 850 ºC) that are in accordance with the results of HSM and DTA.

The superior mechanical properties of GK_0 - GK_2 glass-ceramic samples can be explained by the formation of lithium disilicate crystals (Fig. 5) and their higher contribution to mechanical resistance in comparison to lithium metasilicate.[35-36]

Fig. 6 shows the evolution CTE and chemical durability with respect to K_2O content for glass powder compacts heat treated at 900 ºC for 1 h. The chemical resistance of GCs is high for small *x* values but noticeably decreased with increasing K_2O/SiO_2 ratios. This trend was more than expected considering the relatively high solubility of lithium metasilicate in acidic environment.[1]

The change of CTE with respect to K_2O shows almost a linear trend (Fig. 6). In particular, CTE gradually increases with the increments of K_2O in glass-ceramics. Since a GC might be considered as a composite material, its CTE depends on the type and volume fraction of both crystalline and glassy phases.[38-40] The increase of CTE with the increments of K_2O can be explained by the concomitant increase in the volume fraction of glassy phase (Fig. 4), and by the precipitation of lithium metasilicate and orthoclase phases.[41]

The increasing amounts of residual glassy phase for samples with $x > 2.5$, as deduced from the noisy backgrounds in Fig. 4, will also negatively affect the chemical stability of glass-ceramics.[37]

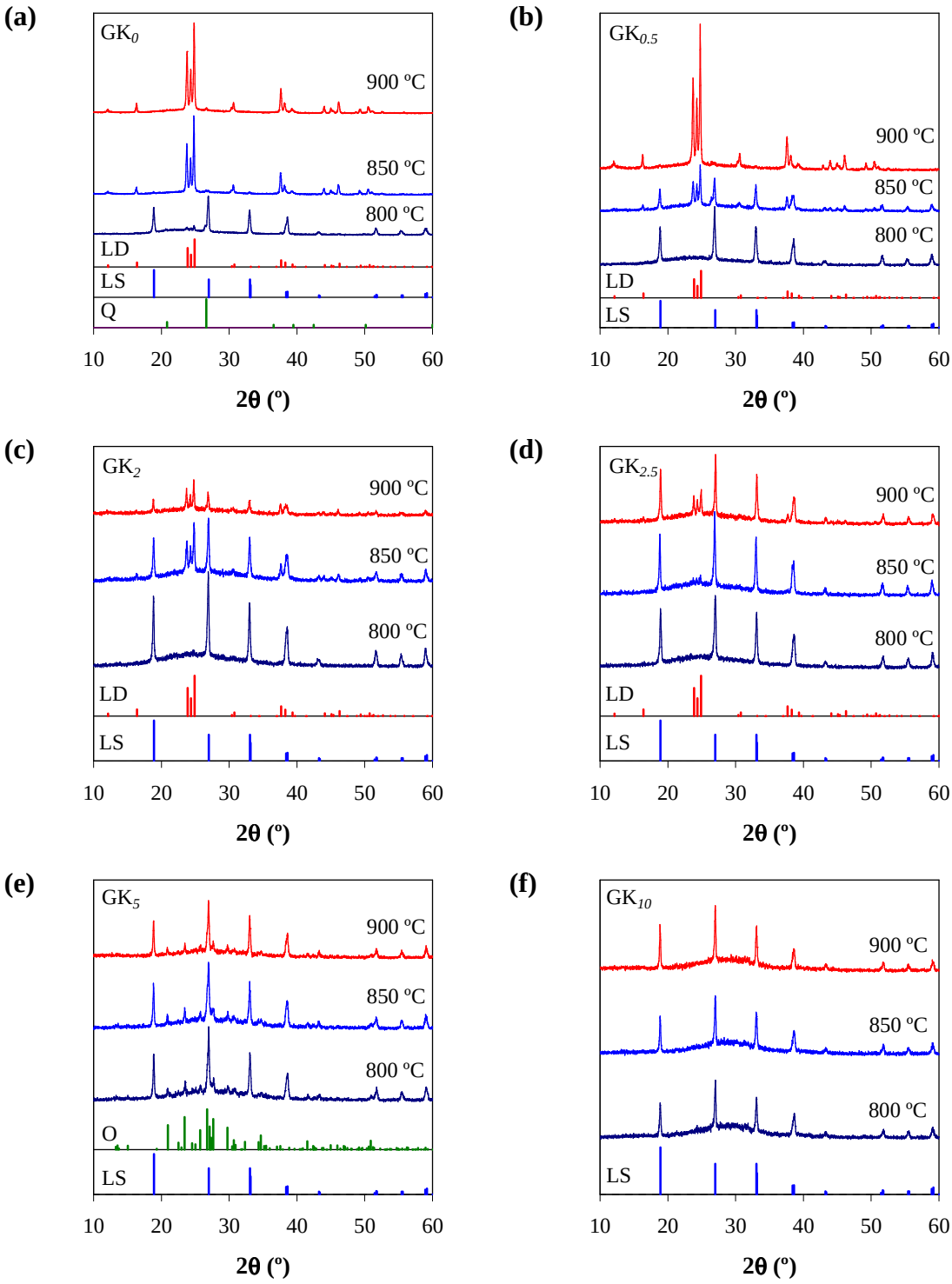

Fig. 4 – X-ray diffractograms of glass powder compacts after heat treatment at different temperatures for 1 h: (a) GK_0, (b) $GK_{0.5}$, (c) GK_2, (d) $GK_{2.5}$, (e) GK_5 and (f) GK_{10}. LS: lithium silicate (Li_2SiO_3, ICCD card 01-029-0828); LD: lithium disilicate ($Li_2Si_2O_5$, ICCD card 01-070-4856); Q: quartz (SiO_2, ICCD card 01-077-1060); O: orthoclase ($K_4Al_4Si_{12}O_{32}$, ICCD card 01-080-2108).

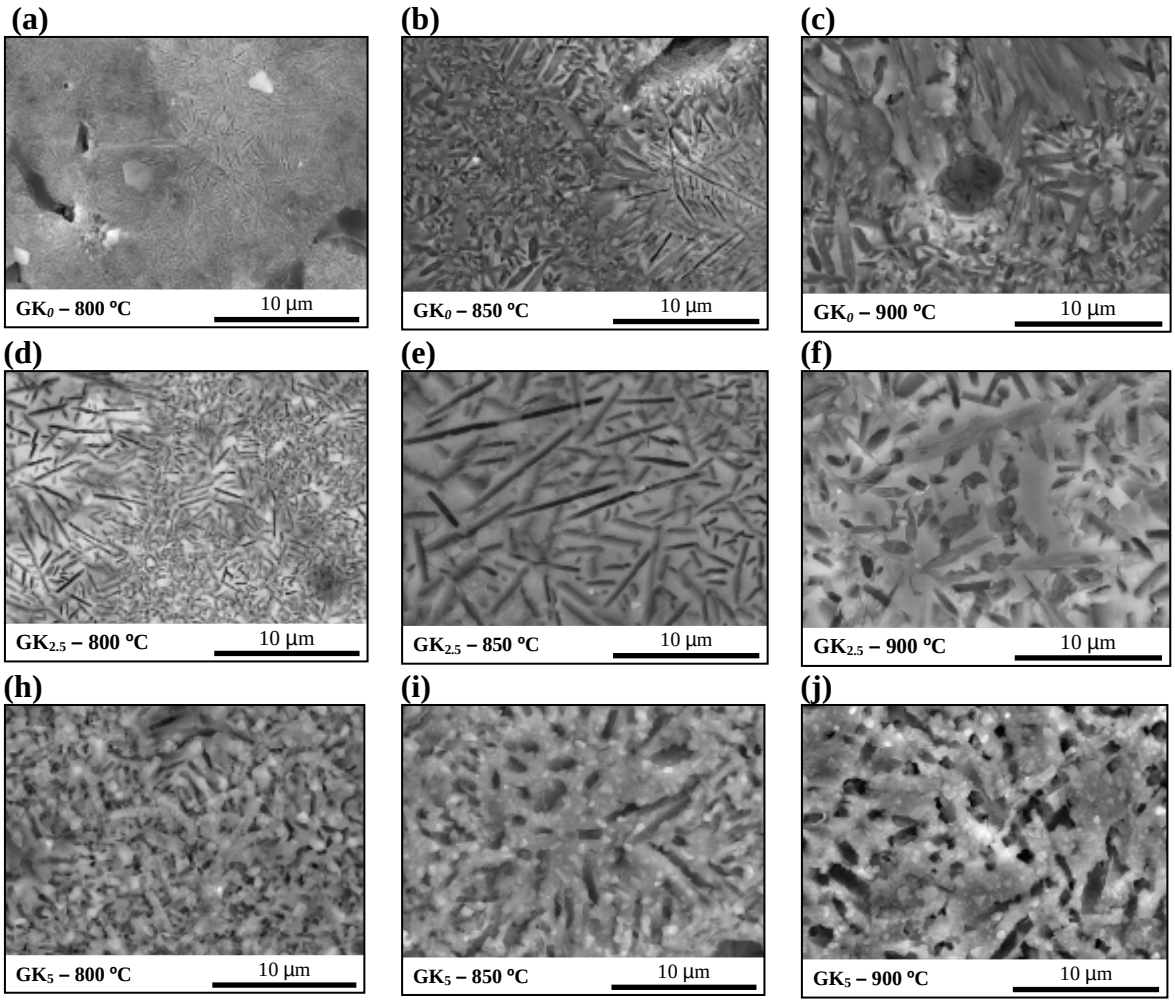

Fig. 5 – SEM images of glass powder compacts heat treated at different temperatures for 1 h.

Table 3 – Properties of the glass powder compacts heat treated at several temperatures in air during 1 hour.

	x (mol.%)					
	0	0.5	1.5	2.5	5	10
Density (g/cm^3)						
800 ºC	2.19 ± 0.03	2.25 ± 0.02	2.35 ± 0.01	2.34 ± 0.03	2.36 ± 0.01	2.38 ± 0.01
850 ºC	2.25 ± 0.03	2.36 ± 0.03	2.35 ± 0.03	2.31 ± 0.03	2.35 ± 0.03	2.30 ± 0.03
900 ºC	2.36 ± 0.03	2.38 ± 0.03	2.35 ± 0.03	2.28 ± 0.03	2.28 ± 0.03	2.22 ± 0.03
Bending strength (MPa)						
800 ºC	81 ± 8	88 ± 19	125 ± 6	148 ± 9	126 ± 4	89 ± 8
850 ºC	216 ± 3	151 ± 11	176 ± 11	138 ± 10	139 ± 12	76 ± 10
900 ºC	224 ± 4	173 ± 8	205 ± 13	107 ± 12	79 ± 6	–

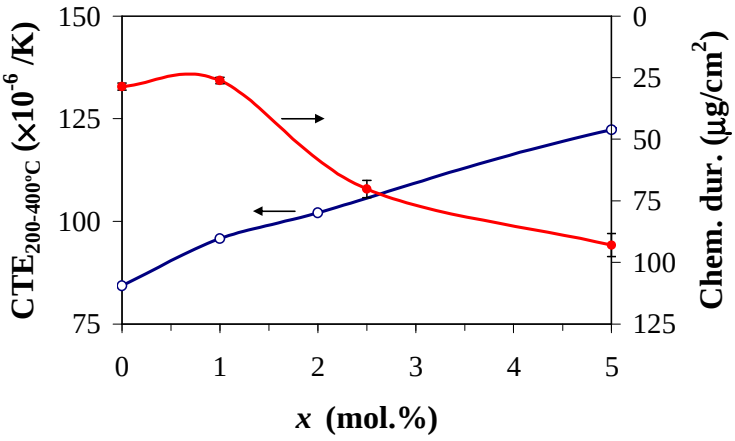

Fig. 6 – Evolution of $CTE_{200\text{-}400\,^{\circ}C}$ and chemical durability with the amount of K_2O for glass powder compacts heat treated at 900 ºC for 1 h.

3.5. Electrical properties

Typical examples of the impedance spectra of glass-ceramic disks with porous Ag electrodes are presented in Fig. 7. In all cases, the spectra consist of one semicircle with a small electrode tail in the low-frequency range. In general, this form is characteristic of dielectric materials, in agreement with high values of the electrical resistance which can be calculated from low-frequency intercept of the semicircles on the real axis.

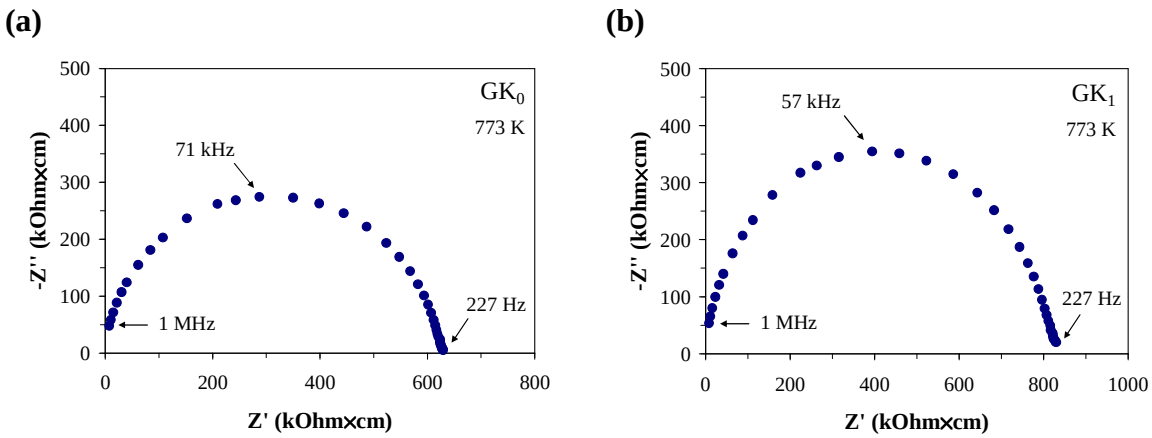

Fig. 7 – Examples of impedance spectra of the glass-ceramics with Ag electrodes, in dry air: (a) GK_0 and (b) GK_1.

The total conductivity (Fig. 8) follows Arrhenius dependence and tends to moderately decrease in the high-temperature range with incremental amounts of K_2O. The latter trend

originates from decreasing activation energy (E_a) when K_2O content increases. Fig. 9 displays the activation energy values calculated by the Arrhenius equation:

$$\sigma = \frac{A_0}{T}\exp\left(\frac{E_a}{RT}\right)$$

were A_0 is the pre-exponential factor. Although the observed variations of both σ and E_a are relatively minor at K_2O concentrations varying in the narrow range of 2.63 to 7.63 mol.%, these are higher than instrumental and statistical errors.

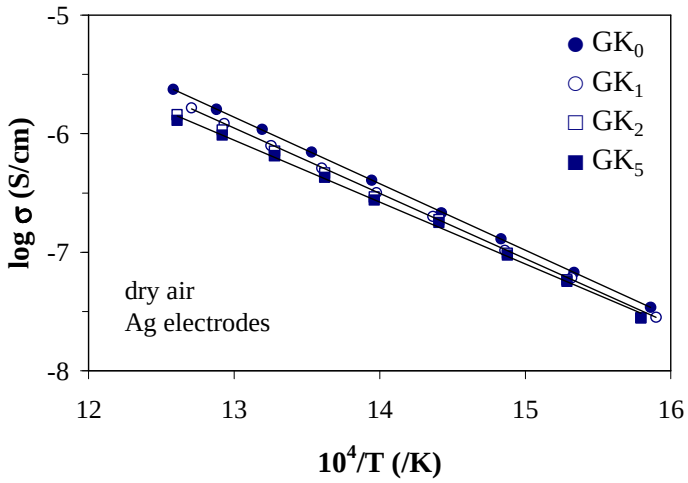

Fig. 8 – Temperature dependence of the total conductivity of glass-ceramic materials in dry air.

Attempts to determine the type of prevailing charge carriers using concentration cells, where the dense glass-ceramic disks are placed under oxygen, water vapour and lithium chemical potential gradient, failed due to the very high resistivity of the studied materials. Nonetheless, the tendency to lowering the conductivity activation energy with K_2O additions may indicate a significant ionic contribution to transport processes. In the latter case, the ionic charge carriers may include either metal cations (Li^+, K^+) or protons formed due to water incorporation, promoted by potassium doping. Indeed, the total conductivity of the glass-ceramics was found essentially independent on the oxygen partial pressure, varied from 0.21 atm (dry air) down to approximately 10^{-5} atm (flowing argon). At the same time, increasing humidity at 633 K resulted in a slow increase of the conductivity (Fig. 10). Again, this effect is small but significant with respect to the experimental error (2–3%). Notice also that keeping of the glass-ceramics in humid atmospheres at 300–400 K during 2 weeks did not

lead to any significant changes in their bulk conductivity, thus suggesting that minor hydration is only observed at elevated temperatures, probably due to kinetic reasons.

Whatever the microscopic mechanisms, the glass-ceramic materials exhibit excellent insulating properties at low temperatures. The estimates of their total conductivity at room temperature, obtained by extrapolation of the Arrhenius dependencies, vary from 2×10^{-18} S/cm (GK_0) to 1×10^{-17} S/cm (GK_5). Regardless of the slight decrease in the electrical resistivity induced by K_2O doping, the overall resistance level is very high.

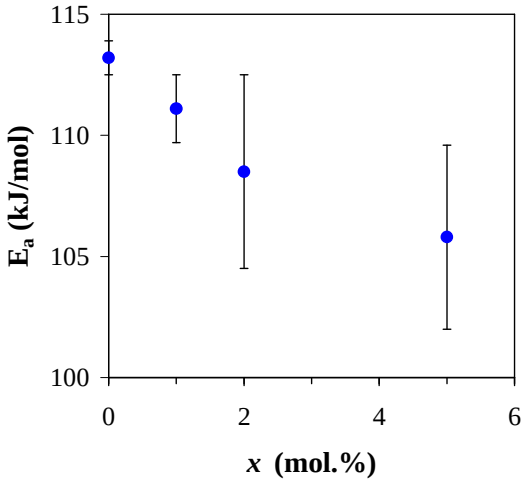

Fig. 9 – Composition dependence of the activation energy for total conductivity of the glass-ceramic materials in dry air.

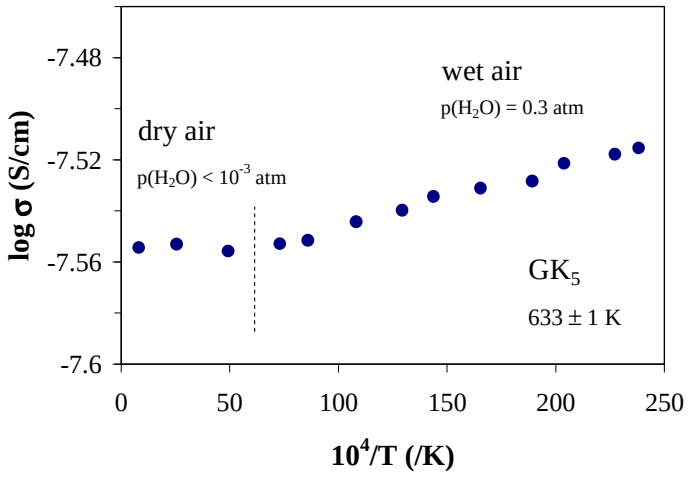

Fig. 10 – Time dependence of the total conductivity of GK_5 glass-ceramics in dry and wet air.

4. Discussion

From the results of our recent study [21] the addition of K_2O at the expense of SiO_2 in the $Li_2O–K_2O–Al_2O_3–SiO_2$ system was found to promote surface crystallization in bulk glasses, as well as the predominant formation of lithium metasilicate phase. However, considering that the production of lithium disilicate GCs for most of the intended applications involves the sintering and crystallization of glass powder compacts, it is of paramount importance to evaluate how these thermal events are affected by the composition. Therefore, the current work is focused on studying the influence of K_2O amount and K_2O/SiO_2 ratio on sintering/crystallization behaviour of glass powder compacts.

Glasses have been produced at 1550 ºC for 1 h to escape any signs of nonhomogeneity in the form of crystalline inclusions. Volatilization of chemical species should be very low. As a matter of fact, analogous glasses from the $SiO_2–Li_2O–Al_2O_3–K_2O–ZrO_2–P_2O_5$ system that were firstly melted at 1370 ºC for 2 h and subsequently heat treated at 1500 ºC for 1.5 h demonstrated to have almost the same chemical compositions after analysis as the planed starting compositions.[42]

Densification of glass powder compacts is obtained through viscous flow at temperatures slightly higher than the glass transition temperature (T_g). The desired order of events in a glass-powder sintering process occurs when the sintering process is completed before crystallization begins. Under these conditions, dense materials are obtained.[33] From HSM and DTA data it can be concluded that increasing K_2O/SiO_2 ratio led to diminishing of T_{FS1}, T_{MS1}, T_{FS2} and T_{MS2} parameters and temperature intervals between T_{MS} and T_{FS} at both the first and the second sintering stages. Consequently, K_2O-richer samples get sintered during shorter temperature interval and at lower temperatures than compositions with lower K_2O contents. Therefore, the GK_5 and GK_{10} compositions reached half ball point (T_{HB}) even earlier than softening point (T_D) was attained in $GK_0–GK_2$ glasses (Table 2 and Fig. 3). This behaviour is in a good correlation with the trend observed in the ^{29}Si NMR spectra of corresponding glasses pointing towards depolymerisation of the silicate glass network when K_2O/SiO_2 ratio increased.[21]

In general, the sintering and crystallization events occurring in the experimental compositions appear as independent processes only during the first sintering stage. Although these compositions did not strictly follow the desired sequence of events and sintering was partially impeded by crystallization, all glass–powder compacts demonstrated excellent sintering

ability and achieved the maximum expected density (A/A_0~0.6).[33] Similar trends were observed in our previous work where sintering and devitrification processes were investigated in $Li_2O–SiO_2$ compositions with equimolar additions of Al_2O_3 and K_2O.[19]

Additionally, the difference between T_c and T_g must be also taken into account. From the Table 2 this difference is about 92–97 °C for GK_0–GK_2 glasses and 69–70 °C for GK_5–GK_{10} glasses confirming that compositions with lower K_2O contents show smaller tendency to crystallization and greater glass stability.

XRD and SEM results demonstrated that K_2O content plays a crucial role in the crystallization process of glass-powder compacts. As a matter of fact, the trend for the preferential crystallization of lithium metasilicate with increasing potassium content resemble data received from crystallization of relevant bulk glasses.[21] Using the model proposed by Bischoff *et al.*[36] and ^{29}Si MAS-NMR results from our previous work [21] we can attempt explaining the effect of suppressing the crystallization of $Li_2Si_2O_5$ and promoting the formation of Li_2SiO_3 with increasing K_2O contents. In particular, considering significant decrease of Q^4 groupings in K_2O-rich glasses (*e.g.* GK_5 and GK_{10}), the feasibility of the reaction Q^4 (glass) + Q^2 (cryst.) ↔ 2 Q^3 (cryst.) diminishes considerably. This leads to the formation of single phase Li_2SiO_3 directly from Q^2 or via reaction 2 Q^3 (glass) ↔ Q^2 (cryst.) + Q^4 (glass).[36]

Another interesting aspect is that the glass powder compacts are more prone to the formation of lithium disilicate for $x \leq 2$, than the corresponding bulk glasses where $x \leq 1$. This behaviour can be ascribed to the difference in preparation routes of the parent glasses as water quenching of the glass increases the OH^- content. The hydroxyl groups may act as a modifier and break the silicate network, thus, reducing the viscosity and activation energy of viscous flow.[19]

Sintered glass powder compacts with K_2O content less than 4.64 mol.% featured enhanced mechanical properties (bending strength ~173–224 MPa) and high chemical resistance (~25–50 μg/cm^2) due to the predominant crystallization of lithium disilicate crystalline phase. The chemical durability of the experimental compositions is similar to that reported for IPS Empress® 2 (50 μg/cm^2), but materials are more resistant than IPS Empress® 1 (122 mg/cm^2) for layering technique.[1]

The 3-point bending strength values are lower than those reported for IPS Empress® 2 (400 ± 40 MPa).[1, 43] It is known, however, that hot pressing technique used to prepare samples of

commercial GC can significantly improves bending strength.[1] To prove this assumption, additional experiments were attempted on the synthesis and processing of a commercial glass-ceramic composition: 69.6 SiO_2, 1.10 Al_2O_3, 3.90 P_2O_5, 3.30 K_2O, 15.4 Li_2O, 0.50 TiO_2, 0.30 CeO_2, 0.30 La_2O_3, 5.20 ZnO, 0.20 MgO, 0.20 Fe_2O_3 (wt.%).[43] A bending strength of 341±98 MPa was reported for this material when processed by hot pressing.[43] According to the specifications given,[43] the glass was melted in a platinum crucible at 1550 °C for 1 h followed by quenching in water, drying and milling the frit to an average particle size of 20 to 30 microns. Then, rectangular bars (4×5×50 mm^3) were prepared by uniaxial pressing (80 MPa) following the same experimental procedure used for compositions GK_0–GK_{10}. The as obtained bars were also similarly fired at 500 °C for 1 h and then at 850 °C for 2 h (the rate of heating was 30 K/min) as recommended in.[43] Thus, hot pressing procedure has been excluded from sample preparation. The average flexural strength (for 10 samples) measured in a testing machine (Shimadzu Autograph AG 25 TA) was 199±14 MPa, which is comparable to other experimental values reported for LD GCs (190–234 MPa [1, 44-46], 204.75 ± 49.81 MPa [47]).

The activation energies for total conductivity of the glass-ceramic materials are significantly higher than those found for lithium disilicate glass [48-49] and close to value obtained for 100% crystallized lithium disilicate.[50] In general, GCs materials featured low total conductivity (~2×10^{-18} S/cm for GK_0) suggesting a number of practical applications in which this property is relevant.

5. Conclusions

The data gathered and discussed in the frame of the present work enable the following conclusions to be drawn:

1. The sintering/densification of the glass powder compacts occurred in two steps. Sintering started at ~484–491 ºC (T_{FS1}) in all compositions while the extent of densification along the first stage significantly decreased with increasing the added amounts of K_2O and the K_2O/SiO_2 ratio. The second stage of densification occurred in competition with crystallization process.
2. Increasing the K_2O/SiO_2 ratio led the thermal parameters T_{FS1}, T_{MS1}, T_{FS2} and T_{MS2} to decrease, a trend that was also observed for the temperature intervals between T_{MS} and T_{FS}. This suggests that K_2O-richer samples

($GK_{2.5}$, GK_5 and GK_{10}) get sintered within a shorter temperature interval and at lower temperatures.

3. The gradual substitution of SiO_2 by K_2O in glass compositions suppressed the crystallization of $Li_2Si_2O_5$ and promoted the formation of Li_2SiO_3 upon sintering the glass powder compacts.
4. The glass powder compacts demonstrate wider range of the lithium disilicate formation with $x \leq 2$ ($\leq$4.63 mol.% K_2O) than the corresponding bulk glasses with $x \leq 1$ ($\leq$3.63 mol.% K_2O).
5. The predominant crystallization of lithium disilicate in low-K_2O compositions resulted in glass-ceramics with high mechanical strength (~173–224 MPa), chemical resistance (~25–50 $\mu g/cm^2$) and low total conductivity (~2×10^{-18} S/cm for GK_0) making the materials suitable for a number of practical applications.

Acknowledgments

Financial support from CICECO, University of Aveiro, and from the FCT, Portugal (grant SFRH/BD/41307/2007 and project PTDC/CTM-CER/114209/2009) are gratefully acknowledged.

References

1. Höland W, Beall G. Glass-ceramic Technology. Westerville, Ohio: The American Ceramic Society; 2002.
2. Lira C, Oliveira APNd, Alarcon OE. Sintering and crystallisation of $CaO–Al_2O_3–SiO_2$ glass powder compacts. Glass Technology 2001;42(3):91-96
3. Boccaccini AR, Schawohl J, Hern H, Schunck B, Rincon JM, Romero M. Sintered glass ceramics from municipal incinerator fly ash. Glass Technology 2000;41(3):99-105.
4. Fan CL, Rahaman MN. Factors controlling the sintering of ceramic particulate composites I: conventional processing. Journal of the American Ceramic Society 1992;75(8):2056-65.
5. Siligardi C, D'Arrigo MC, Leonelli C. Sintering behavior of glass-ceramic frits. American Ceramic Society Bulletin 2000;79(9):88-92.

6. Toya T, Kameshima Y, Yasumori A, Okada K. Preparation and properties of glass-ceramics from wastes (Kira) of silica sand and kaolin clay refining. Journal of the European Ceramic Society 2004;24(8):2367-72.
7. Toya T, Tamura Y, Kameshima Y, Okada K. Preparation and properties of $CaO–MgO–Al_2O_3–SiO_2$ glass-ceramics from kaolin clay refining waste (Kira) and dolomite. Ceramics International 2004;30(6):983-89.
8. Arnault L, Gerland M, Riviere A. Microstructural study of two LAS-type glass-ceramics and their parent glass. Journal of Materials Science 2000;35(9):2331-45.
9. Barbieri L, Leonelli C, Manfredini T, Siligardi C, Corradi AB. Nucleation and crystallization of a lithium aluminosilicate glass. Journal of the American Ceramic Society 1997;80(12):3077-83.
10. Riello P, Canton P, Comelato N, Polizzi S, Verita M, Fagherazzi G, et al. Nucleation and crystallization behavior of glass-ceramic materials in the $Li_2O–Al_2O_3–SiO_2$ system of interest for their transparency properties. Journal of Non-Crystalline Solids 2001;288(1-3):127-39.
11. Kuzielova E, Palou M, Kozankova J. Crystallization mechanism and bioactivity of lithium disilicate glasses in relation to CaO, P_2O_5, CaF_2 addition. Ceramics-Silikaty 2007;51(3):136-41.
12. Lynch ME, Folz DC, Clark DE. Effect of microwaves on the migration of lithium and silicon from lithium disilicate ($Li_2O–2SiO_2$) glass. Food Additives and Contaminants 2008;25(4):519-26.
13. Wen G, Zheng X, Song L. Effects of P_2O_5 and sintering temperature on microstructure and mechanical properties of lithium disilicate glass-ceramics. Acta Materialia 2007;55(10):3583-91.
14. Schweiger M, Höland W, Frank M, Drescher H, Rheinberger V. IPS Empress 2: A new pressable high-strength glass-ceramic for esthetic all-ceramic restoration. Quintessence Dent Technol 1999;24(7):876-82.
15. Burgner LL, Lucas P, Weinberg MC, Soares PC, Zanotto ED. On the persistence of metastable crystal phases in lithium disilicate glass. Journal of Non-Crystalline Solids 2000;274(1-3):188-94.
16. Freiman SW, Hench LL. Kinetics of Crystallization in $Li_2O–SiO_2$ Glasses. Journal of the American Ceramic Society 1968;51(7):382-&.
17. Ray CS, Huang WH, Day DE. Crystallization kinetics of a lithia–silica glass: Effect of sample characteristics and thermal analysis measurement techniques. Journal of the American Ceramic Society 1991;74(1):60-66.
18. Soares PC, Zanotto ED, Fokin VM, Jain H. TEM and XRD study of early crystallization of lithium disilicate glasses. Journal of Non-Crystalline Solids 2003;331(1-3):217-27.
19. Fernandes HR, Tulyaganov DU, Goel A, Ribeiro MJ, Pascual MJ, Ferreira JMF. Effect of Al_2O_3 and K_2O content on structure, properties and devitrification of glasses in the $Li_2O–SiO_2$ system. Journal of the European Ceramic Society 2010;30(10):2017-30.
20. Fernandes HR, Tulyaganov DU, Goel IK, Ferreira JMF. Crystallization process and some properties of $Li_2O–SiO_2$ glass-ceramics doped with Al_2O_3 and K_2O. Journal of the American Ceramic Society 2008;91(11):3698-703.
21. Fernandes HR, Tulyaganov DU, Goel A, Ferreira JMF. Effect of K_2O on structure-property relationships and phase transformations in $Li_2O–SiO_2$ glasses. Journal of the European Ceramic Society 2012;32(2):291-98.
22. Pascual MJ, Duran A, Prado MO. A new method for determining fixed viscosity points of glasses. Physics and Chemistry of Glasses 2005;46(5):512-20.

23. Pascual MJ, Pascual L, Duran A. Determination of the viscosity-temperature curve for glasses on the basis of fixed viscosity points determined by hot stage microscopy. Physics and Chemistry of Glasses 2001;42(1):61-66.
24. ISO 6872. International Standards for Dental Ceramics. Geneva, Switzerland: International Organization for Standardization; 1995.
25. Abdurakhmanov K, Éminov AM, Maslennikova GN. Stages of ceramic structure formation in the presence of additives. Glass and Ceramics 2000;57(9 - 10):354-56.
26. Bernardin AM, de Medeiros DS, Riella HC. Pyroplasticity in porcelain tiles. Materials Science and Engineering A 2006;427:316-19.
27. Liu H, Lu H, Chen D, Wang H, Xu H, Zhang R. Preparation and properties of glass-ceramics derived from blast-furnace slag by a ceramic-sintering process. Ceramics International 2009;35:3181-84.
28. Pranckeviciene J, Balkevicius V, Spokauskas AA. Investigations on Properties of Sintered Ceramics out of Low-Melting Illite Clay and Additive of Fine-Dispersed Nepheline Syenite. Materials Science 2010;16(3):231-35.
29. Torres P, Fernandes HR, Olhero S, Ferreira JMF. Incorporation of wastes from granite rock cutting and polishing industries to produce roof tiles. Journal of the European Ceramic Society 2009;29:23-30.
30. Frenkel J. Viscous flow of crystalline bodies under the action of surface tension. Journal of Physics (USSR) 1945;9:385-91.
31. Prado MO, Zanotto ED, Muller R. Model for sintering polydispersed glass particles. Journal of Non-Crystalline Solids 2001;279(2-3):169-78.
32. Mackenzie JK, Shuttleworth R. A Phenomenological theory of sintering. Proceedings of the Physical Society. Section B 1949;62 (12):833-52.
33. Lara C, Pascual MJ, Duran A. Glass-forming ability, sinterability and thermal properties in the systems RO–BaO–SiO_2 (R = Mg, Zn). Journal of Non-Crystalline Solids 2004;348:149-55.
34. Scholze H. Influence of viscosity and surface tension on Hot Stage Miscroscopy measurements on glasses. Ver. Dtsch. Keram. Ges. 1962;391:63-8.
35. Apel E, van't Hoen C, Rheinberger V, Holand W. Influence of ZrO_2 on the crystallization and properties of lithium disilicate glass-ceramics derived from a multi-component system. Journal of the European Ceramic Society 2007;27:1571-77.
36. Bischoff C, Eckert H, Apel E, Rheinberger VM, Holand W. Phase evolution in lithium disilicate glass–ceramics based on non-stoichiometric compositions of a multi-component system: structural studies by ^{29}Si single and double resonance solid state NMR. Physical Chemistry Chemical Physics 2011;13:4540-51.
37. Strnad Z. Glass-ceramic Materials. Amsterdam: Elsevier; 1986.
38. Pisciella P, Pelino M. Thermal expansion investigation of iron rich glass-ceramic. Journal of the European Ceramic Society 2008;28:3021-26.
39. Volf MB. Mathematical approach to glass. Amsterdam Elsevier; 1988.
40. Xiao Z, Zhou J, Wang Y, Luo M. Microstructure and Properties of $Li_2O–Al_2O_3–SiO_2–P_2O_5$ Glass-Ceramics. The Open Materials Science Journal 2011;5:45-50.
41. Borrelli NF, Goetschius KL, Morse DL, Smith CM, inventors; Corning Incorporated (Corning, NY, US), assignee. Low CTE photomachinable glass. 2010.
42. Höland W, Apel E, van Hoen C, Rheinberger V. Studies of crystal phase formations in high-strength lithium disilicate glass-ceramics. Journal of Non-Crystalline Solids 2006;352(38-39):4041-50.
43. Schweiger M, Frank M, Rheinberger V, Höland W, inventors; Ivoclar AG, assignee. Lithium disilicate glass ceramics dental product 1999.

44. Beall G. Design of glass-ceramics. Solid State Science 1989;3:333–54.
45. Beall G. Glass-ceramics: Recent developments and application. Ceramic Transactions 1993;30:241-66.
46. Echevería LM. New lithium disilicate glass-ceramics. Boletin da la Sociedad Espanola de Cerámica e Vidrio 1992;5:183–88.
47. Drummond JL, King TJ, Bapna MS, Koperski RD. Mechanical property evaluation of pressable restorative ceramics. Dental Materials 2000;16(3):226-33.
48. Hench LL, Frieman SW, Kinser DL. Early stages of crystallization in a $LI_2O–2SiO_2$ Glass. Physics and Chemistry of Glasses 1971;12(2):58-&.
49. Kone A, Ribes M, Souquet JL. The structure of glasses in the $SiO_2–Li_2O–Li_2SiO_4$ system studied by means of electrical measurement. Physics and Chemistry of Glasses 1982;23(1):18-22.
50. Campos-Junior AA, Rodrigues ACM. Ionic blocking effect in partially crystallized lithium disilicate. Journal of Applyed Physics 2006;100:053709.

3.6 Structure, properties and phase formation in Al_2O_3/K_2O-containig non-stoichiometric lithium disilicate based glasses

Hugo R. Fernandes[a], Dilshat U. Tulyaganov[a,b], Maria J. Pascual[c], José M.F. Ferreira[a]

[a] Dep. Ceramics and Glass Engineering, University of Aveiro, CICECO, 3810-193 Aveiro, Portugal

[b] Turin Polytechnic University in Tashkent, 17 Niyazova str., 100174 Tashkent, Uzbekistan

[c] Instituto de Cerámica y Vidrio (CSIC), C/Kelsen 5, Campus de Cantoblanco, 28049 Madrid, Spain

Materials Research Bulletin (2012, submitted)

DOI:

Abstract

The main objective of this work was to evaluate the effect of Al_2O_3 in the $Li_2O–SiO_2$ glass system followed by investigation of structure, properties and phase formation phenomenon in glasses of 3 different systems, *i.e.* $Li_2O–SiO_2$, $Li_2O–Al_2O_3–SiO_2$ and $Li_2O–K_2O–Al_2O_3–SiO_2$. Contribution of both Al_2O_3 and K_2O to the surface tension and subsequently to the segregation process in $Li_2O–SiO_2$ glasses was discussed. The distribution of structural units in the experimental glasses was estimated using ^{29}Si MAS-NMR spectroscopy suggesting enhancement of Q^2, and diminishing of Q^3 and Q^4 groups with addition of Al_2O_3 demonstrating its dual role as network former and modifier in the pure $Li_2O–SiO_2$ system.

Less polymerised network in the $Li_2O–SiO_2$ and $Li_2O–Al_2O_3–SiO_2$ glasses caused significant decrease in $T_c–T_g$ processing window completely hindering the densification of the corresponding glass powder compacts. On the contrary, glass-powder compacts in the $Li_2O–K_2O–Al_2O_3–SiO_2$ system featured excellent densification behaviour and high mechanical strength that was attributed to the formation of a more rigid glass network comprising four coordinated $(AlO_{4/2})^-$ units and K^+ cations in its vicinity.

Keywords: Glass; Lithium disilicate; Metastable phase separation

1. Introduction

The binary alkali silicate glasses may be considered as the original type of all silicate glasses consisting of several components.[1-3] Among the binary alkali silicate glasses the lithia-silica system has gained a great interest for the preparation of glasses and glass-ceramic materials.[4-6] Lithium meta- and disilicate phases might be formed depending on the SiO_2/Li_2O ratio, presence of nucleating agents, thermal history of parent glasses, etc..[7] The S-shaped path of the melting curve in the $Li_2O–SiO_2$ system shows that it has to certain extent a tendency to segregation. According to Vogel [2] the glasses with SiO_2 contents higher than the stoichiometric lithium disilicate $Li_2Si_2O_5$ (here after referred as LD) tend to separate into a matrix phase with a composition almost similar to that of LD along with an isolated droplet SiO_2 rich phase, while glasses with Li_2O contents <30 mol.% usually turn out to be opalescent or opaque on cooling owing to phase separation. Electron microscopic examination successfully demonstrated segregation into droplet-like zones of Li-rich phase and SiO_2-rich glass matrix even in compositions with Li_2O contents <10 mol.%.[2]

It was further assumed that the composition of the droplet phase tended to a limiting value, *i.e.* towards the disilicate compound that was reached within the Li_2O content of 14–16 mol.% in the entire glass, which thereafter remained constant until a composition of 33.3 mol.%. Absolute surface tension measurements of the pure silica and lithium disilicate glasses at 1300 ºC gave the values of 283 and 320.2 dynes cm^{-1} (mN m^{-1}), respectively.[2] This was the main reason for the segregation zones formation in glasses with a range of compositions from 0 to 33.3 mol.% of Li_2O (maximum).

The glass-ceramics derived from this parent binary system exhibit some unfavourable characteristics in terms of their mechanical strength and chemical durability which hinder their use in several technological areas. Although chemical durability, which is of major importance for dental materials, has been improved via adding Al_2O_3 and K_2O to stoichiometric LD compositions,[8-9] special attention was drawn to non-stoichiometric LD glass-ceramics. The latter have proven to be potential candidates for different functional applications due their improved mechanical, chemical and thermal properties.[10-15] It is noteworthy that according to Höland and Beal [7] the term ‘non-stoichiometric’ implies that SiO_2/Li_2O molar ratio deviates greatly from 2:1 and the system is rendered considerably more complex with numerous additional oxides, including nucleating agents. The introduction of SiO_2-excess to stoichiometric lithium disilicate glass along with additives, such as ZrO_2,

Al_2O_3, ZnO, CaO, K_2O, and P_2O_5, has been suggested by Echeverria and Beall.[16-18] Later, P_2O_5 was found to play a crucial role in lithium disilicate transformation and crystallization:[19-20] P_2O_5 (as nucleating agent) at the amount of 1.5–2.5 mol.% resulted in glass-ceramics with fine-grained interlocking microstructures, conferring the final products with high mechanical strength. A powder processing of lithium disilicate glass-ceramics in a multi-component system with a wide compositional range (in wt.%) 57–80 SiO_2, 11–19 Li_2O, 0–13 K_2O, 0–5 Al_2O_3, 0–8 ZnO, 0.1–6, La_2O_3, and 0.1–11 P_2O_5, was thoroughly investigated by Ivoclar-Vivadent company to produce the material IPS Empress®2.[21-24]

In spite of the numerous studies found on non-stoichiometric glasses in the Li_2O–SiO_2 system, compositions with SiO_2/Li_2O molar ratios > 3:1 were scarcely investigated.[3, 25-26] We have recently reported on glass compositions with SiO_2/Li_2O molar ratios far beyond that of lithium disilicate stoichiometry,[27-31] namely within the range of 3.13–4.88 and containing Al_2O_3 and K_2O, which were compared with a bicomponent glass $23Li_2O$–$77SiO_2$ (mol.%).[27, 29-30] The later composition exhibited a cloudy appearance upon cooling while the Al_2O_3 and K_2O containing compositions resulted in transparent glasses due to the presence of Al^{3+}, which acted as network former decreasing the volume fraction and mean diameter of droplet phase. Sintering and crystallization studies of $23Li_2O$–$77SiO_2$ glass powder compacts revealed high fragility, and low flexural strength and density. In contrast, good densification behaviour resulted from adding equimolar amounts of Al_2O_3 and K_2O to the Li_2O–SiO_2 system to obtain the composition $22.96Li_2O$–$2.63Al_2O_3$–$2.63K_2O$–$71.78SiO_2$ (mol.%) (SiO_2/Li_2O molar ratio of 3.13), and a glass-ceramic with improved mechanical strength.[30] A further insight into the effect of K_2O on structure–property relationships and devitrification behaviour of glasses was made starting from the above referred glass ($22.96Li_2O$–$2.63Al_2O_3$–$2.63K_2O$–$71.78SiO_2$) and adding incremental amounts of K_2O.[28, 31] These studies revealed that excess K_2O contents within the range of 2.63–12.63 (mol.%) enhanced the liquid-liquid immiscibility as denoted by an increasing of the mean droplet size and their distribution density. On the other hand, increasing K_2O contents resulted in ^{29}Si MAS-NMR spectral changes: decreasing Q^4 units accompanied by an increase of Q^3 units and the appearance a new Q^2 population, suggesting depolymerisation of the silicate glass network, while ^{27}Al MAS-NMR revealed an enhanced role of Al_2O_3 as glass network former. This role implies the association of a cation in the vicinity of each tetrahedral unit in order to maintain local charge neutrality of the $(AlO_{4/2})^-$ units with four bridging oxygens (BO). However, for K_2O/Al_2O_3 molar ratios > 1, there was the formation of a larger fraction of non-

bridging oxygens (NBO) due to the excess of K_2O. Additionally K_2O was found to promote surface crystallization in glasses with the predominant formation of lithium metasilicate (LMS) phase. Only in low-K_2O compositions LD was formed, resulting in glass-ceramics with high mechanical strength (~173–224 MPa), good chemical resistance (~25–50 μg cm^{-2}) and low total conductivity (~2×10^{-18} S cm^{-1} for GK_0) making the materials suitable for a number of practical applications.[31]

To deepen the study of the structure of LD glasses the role of Al_2O_3 in Li_2O–SiO_2 glasses needs to be further clarified. Accordingly, the main objective of this work is to evaluate the effect of Al_2O_3 on the structure, properties and phase formation in glasses of 3 different systems: (i) Li_2O–SiO_2; (ii) Li_2O–Al_2O_3–SiO_2; (iii) and Li_2O–K_2O–Al_2O_3–SiO_2. The contribution of both Al_2O_3 and K_2O to the surface tension and subsequently to the segregation process in Li_2O–SiO_2 glasses will be discussed. Solid state magic angle spinning nuclear magnetic resonance (MAS-NMR) was employed to provide information on the local environment of silicon and aluminium in experimental glasses. The sintering behaviour and properties of the corresponding glass powder compacts was also a target subject during this study, in particular using a hot stage microscopy technique.

2. Experimental procedure

2.1. Glass preparation

Table 1 presents the detailed compositions of the experimental glasses along with their corresponding SiO_2/Li_2O ratios. A total of 9 glasses divided into 3 groups namely A, B and C belonging to the Li_2O–SiO_2, Li_2O–Al_2O_3–SiO_2 and Li_2O–K_2O–Al_2O_3–SiO_2 system, respectively, were synthesised. Compositions of group B were prepared from A series replacing SiO_2 by Al_2O_3 while glasses in group C (similar to those investigated in the study[28]) derived from B glasses series by replacing Li_2O by K_2O. Powders of technical grade SiO_2 (purity >99.5%) and of reactive grade Al_2O_3, Li_2CO_3, and K_2CO_3 were used. Homogeneous mixtures of batches (~100 g), obtained by ball milling, were calcined at 800 ºC for 1 h and then melted in Pt crucibles at 1550 ºC for 1 h, in air. The glasses were produced in bulk (monolithic) form by pouring glass melts on bronze mould (in two different sets: the glasses of one set were immediately annealed at 450 ºC for 1 hour while the other set of glasses was preserved in the non-annealed condition) and frit form by quenching the glass melt in cold water. The obtained frits were dried and milled in a high-speed agate mill. The mean particle

size of the glass powders as determined by light scattering technique (Beckman Coulter LS 230, CA USA; Fraunhofer optical model) was about 5–10 µm.

Table 1 – Compositions of the experimental glasses (mol.%).

	$Li_2O–SiO_2$			$Li_2O–Al_2O_3–SiO_2$			$Li_2O–K_2O–Al_2O_3–SiO_2$		
#	A1	A2	A3	B1	B2	B3	C1	C2	C3
Li_2O	26.59	28.09	30.59	26.59	28.09	30.59	22.96	22.96	22.96
K_2O	–	–	–	–	–	–	3.63	5.13	7.63
Al_2O_3	–	–	–	2.63	2.63	2.63	2.63	2.63	2.63
SiO_2	73.41	71.91	69.41	70.78	69.28	66.78	70.78	69.28	66.78
SiO_2/Li_2O	2.76	2.56	2.27	2.66	2.47	2.18	3.08	3.02	2.91

2.2. Thermo-physical properties of glasses

Glass samples with particle sizes in the range of 500–1000 µm (collected by sieving of crushed non-annealed glass blocks) and weighing 40 mg were contained in an alumina crucible (the reference material was α-alumina powder) to perform differential thermal analysis (DTA, Setaram Labsys, Setaram Instrumentation, Caluire, France) in order to evaluate the glass transition temperature T_g, the crystallization onset temperature, T_c and peak temperature of crystallization, T_p (β = 20 K min^{-1}).

The coefficient of thermal expansion (CTE) of the annealed glasses was measured by dilatometry using prismatic samples of bulk glasses with cross section of 3×4 mm^2 (Bahr Thermo Analyse DIL 801 L, Germany; heating rate 5 K min^{-1}).

Archimedes' method (*i.e.* immersion in ethylene glycol) was employed to measure the apparent density of the bulk annealed glasses which was further applied along with compositions of glasses to calculate their excess volume (V_e) according to a procedure described elsewhere.[30]

2.3. Structural characterization of glasses

^{29}Si MAS-NMR spectra were recorded on a Bruker ASX 400 spectrometer operating at 79.52 MHz (9.4 T) using a 7 mm probe at a spinning rate of 5 kHz. The pulse length was 2 µs and 60 s delay time was used. Kaolinite was used as the chemical shift reference. ^{27}Al MAS-NMR

spectra were recorded on a Bruker ASX 400 spectrometer operating at 104.28 MHz (9.4 T) using a 4 mm probe at a spinning rate of 15 kHz. The pulse length was 0.6 µs and 4 s delay time was used. $Al(NO_3)_3$ was used as the chemical shift reference. The Q^n distributions were obtained by curve fitting and spectral deconvolution using DMFIT program (version 2011).[32]

2.4 Crystalline phase analysis and microstructural evolution in glass-ceramics

Bulk parallelepiped glass samples were non-isothermally heat treated at 600, 700, 800 and 900 ºC for 1 h, respectively, at a heating rate of 2 K min^{-1}. Glass powder compacts were heat treated at 800, 850 and 900 ºC for 1 h at the heating rate of 2 K min^{-1}. The amorphous nature of the parent glasses and the nature of crystalline phases present in the glass-ceramics were determined by X-ray diffraction (XRD) analysis (Rigaku Geigerflex D/Mac, C Series, Japan; Cu K_a radiation, 2θ between 10º and 60º with a 2θ-step of 0.02 deg s^{-1}). The crystalline phases were identified by comparing the obtained diffractograms with patterns of standards complied by the International Centre for Diffraction Data (ICDD).

Archimedes' method was employed to measure the apparent density of the sintered glass-powder compacts. Microstructure observations were done at polished (mirror finishing) and then etched surfaces of samples (by immersion in 2 vol.% HF solution for 2 min) by field emission scanning electron microscopy (SEM, Hitachi SU-70, Japan) under secondary electron mode.

2.5. Sintering and crystallization of glass powder compacts

A side-view hot-stage microscope (HSM, Leitz Wetzlar, Germany) equipped with a Pixera video-camera and image analysis system was used to investigate the sintering behaviour of glass powder compacts. The cylindrical shaped samples from glass powder compacts with height and diameter of ~3 mm were prepared by cold-pressing the glass powders. The cylindrical samples were placed on a 10×15×1 mm^3 alumina (>99.5 wt.% Al_2O_3) support and the measurements were conducted in air with a heating rate (β) of 5 K min^{-1}. The temperature was measured with a chromel–alumel thermocouple contacted under the alumina support. The temperatures corresponding to the characteristic viscosity points (first shrinkage (T_{FS}), maximum shrinkage (T_{MS}), softening (T_D), half ball (T_{HB}) and flow (T_F)) were obtained from the graphs and photomicrographs taken during the hot-stage microscopy experiment.[33]

Apart from HSM investigation, the sintering process was explored using non-isothermal heat treatment of glass-powder compacts. Rectangular bars ($4\times5\times50$ mm^3) prepared by uniaxial pressing (80 MPa) were sintered at 800, 850 and 900 ºC for 1 h. A heating rate of 2 K min^{-1} was maintained in order to prevent deformation of the samples.

3. Results

3.1 Casting ability and microstructure of glasses

Melting at 1550 ºC for 1 h was adequate to obtain bubble-free homogenous glasses from all the investigated compositions. The absence of any crystalline inclusions was confirmed by XRD and SEM analyses (not shown). Cloudy appearance was characteristic of A1, while the other glasses were completely transparent. The SEM images of as cast non–annealed samples (Fig. 1) revealed nanosize droplet phase embedded in the glass matrix suggesting occurrence of liquid-liquid phase separation in all investigated glasses. The droplet size and density distribution seemingly decreased from glass A1 to A3 (series A) and from glass B1 to B3 (series B) while increased from C1 to C3 in series C.

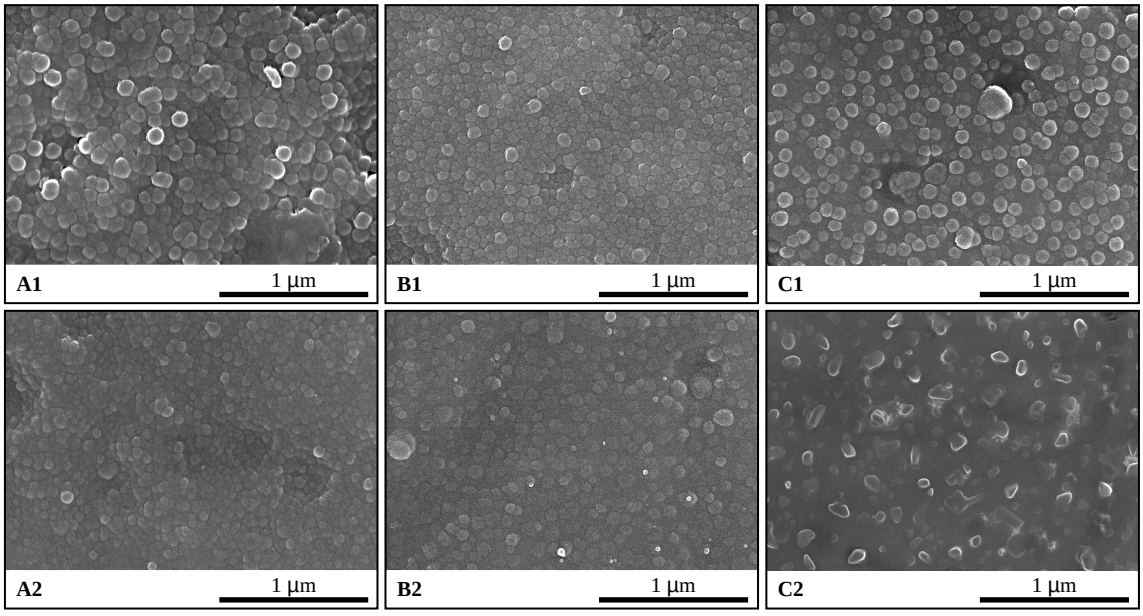

Fig. 1 – SEM images of the experimental non-annealed bulk glasses (etched with 2 vol.% HF solution for 1 min).

3.2 Structure and thermo-physical properties of glasses

3.2.1 Density, excess molar volume and thermal properties

The density values of glasses varied in the range 2.32–2.40 g cm^{-3} (Fig. 2(a), Table 2). The observed general trend indicates that density increases in the sequence C > B > A and, consequently, glasses from the $Li_2O–K_2O–Al_2O_3–SiO_2$ system featured the highest density while the binary glasses ($Li_2O–SiO_2$) exhibited are the less dense ones. Density increments with addition of Al_2O_3 (density ~4.00 g cm^{-3}) were expected assuming additive properties argument. But the same reasoning seems to fail when decreasing SiO_2/Li_2O and SiO_2/K_2O ratios. This might be explained considering the decreasing trend observed in the excess molar volume (V_e) of the glasses (Fig. 2(b), Table 2). Apparently, diminishing of both SiO_2/Li_2O and SiO_2/K_2O ratios enhanced the packing ability of the constituent oxides resulting in a more efficient filling of the glass network interstices and thus in a more compact structure. The coefficient of thermal expansion (CTE) values of the glasses followed the sequence C > B > A (Table 2, Fig. 2(b)), being in good agreement with the variation trends observed for density. Accordingly, within each group, the CTE increased upon decreasing of SiO_2/Li_2O or SiO_2/K_2O ratios (*e.g.* C3 > C2 > C1).

Table 2 – Thermo-physical properties of the experimental glasses.

	d (g cm^{-3})	V_e (cm^3 mol^{-1})	NBO/T	CTE ±0.1 (10^{-6} K^{-1})	T_g ±2 (ºC)	T_c ±2 (ºC)	T_c-T_g (ºC)	T_p ±2 (ºC)
A1	2.32 ±0.03	1.05 ±0.03	0.72	9.9	498	587	89	737
A2	2.33 ±0.01	0.90 ±0.03	0.78	10.8	495	606	111	733
A3	2.35 ±0.04	0.66 ±0.03	0.88	11.1	491	612	121	717
B1	2.36 ±0.01	1.17 ±0.01	0.63	9.6	504	662	158	781
B2	2.36 ±0.04	1.08 ±0.04	0.68	10.6	500	639	139	773
B3	2.37 ±0.02	0.92 ±0.02	0.78	11.7	499	620	117	746
C1	2.37 ±0.01	1.08 ±0.04	0.63	11.5	503	695	192	806
C2	2.38 ±0.01	0.97 ±0.05	0.68	11.5	500	663	163	800
C3	2.40 ±0.01	0.76 ±0.04	0.78	12.7	496	658	162	778

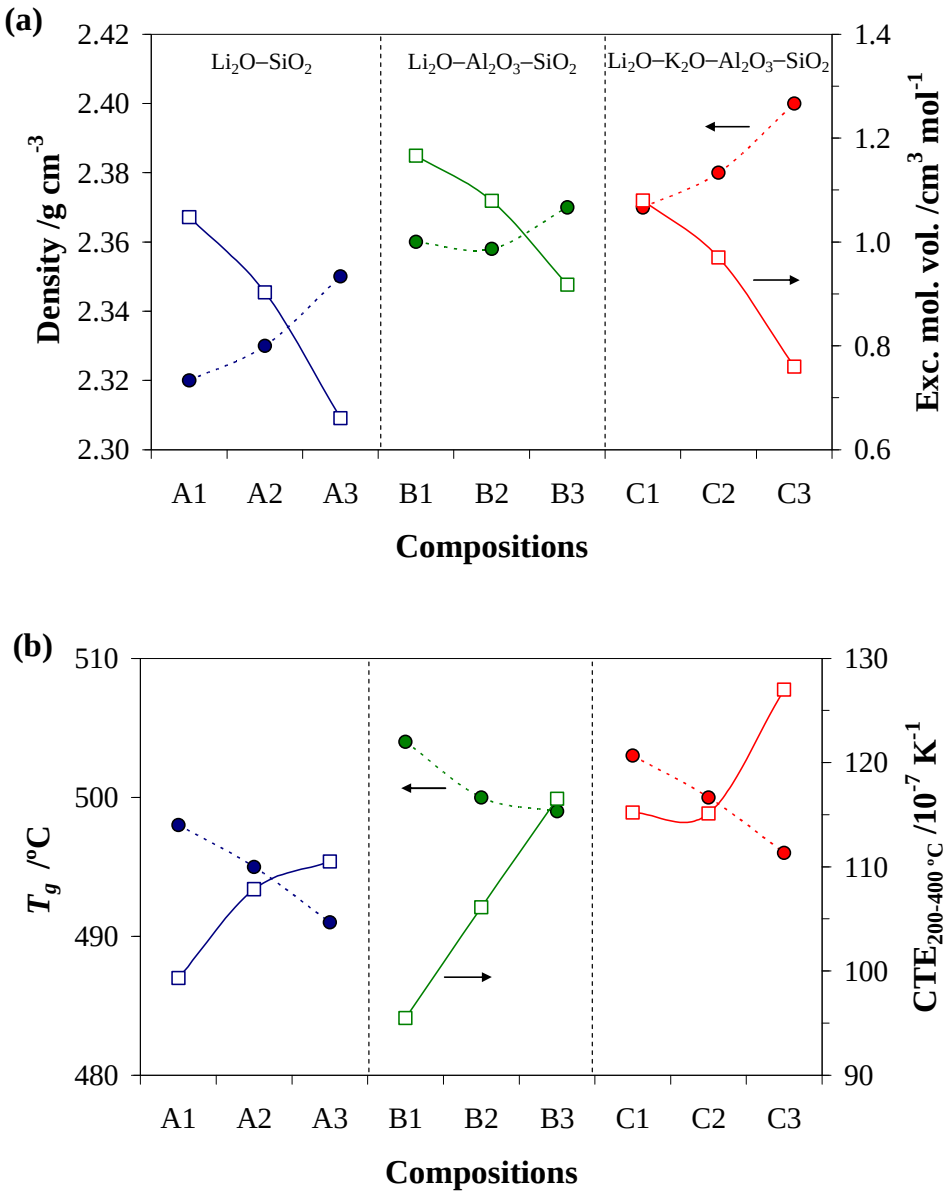

Fig. 2 – Thermo-physical properties of bulk glasses: (a) Evolution of density and excess molar volume, and (b) evolution T_g of and CTE with the composition.

The DTA plots of glasses with a heating rate (β) of 20 K min^{-1} (Fig. 3) revealed well-defined features comprising endothermic and exothermic peaks from which transition point (T_g), temperature of onset crystallization (T_c) and peak temperature of crystallization (T_p), were determined (Table 2). General decreasing trends of T_c and T_p with decreasing the SiO_2/Li_2O ratio can be depicted from data reported in Table 2 and Fig. 2(b), being accompanied by a similar variation trend of T_g in each group. The observed lowering of T_g is in accordance with the calculated increasing number of non-bridging oxygens per tetrahedron (NBO/T) further supporting the hypothesis of depolymerisation of the glass network.

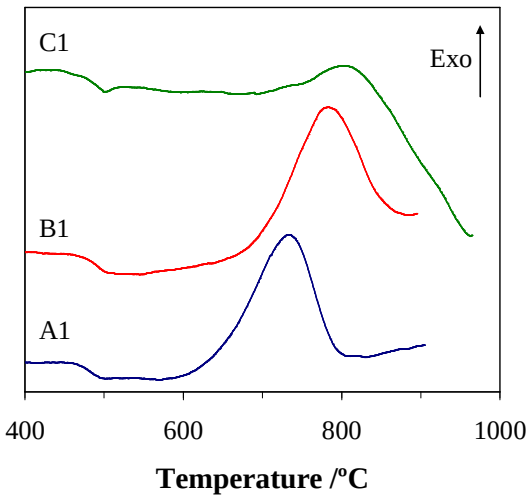

Fig. 3 – DTA of glasses A1, B1 and C1.

3.2.2 Structure analysis by MAS-NMR

^{29}Si MAS-NMR spectra of glasses A1, B1 and C1 are shown in Fig. 4, while the Q^n distributions of glasses obtained from ^{29}Si MAS-NMR spectra and corresponding deconvolution are plotted in Fig. 5. In general, the spectra displayed in Fig. 4 feature broad bands, denoting the amorphous nature of these materials. For each composition, a resonance line covers the chemical shift range of silicon in several Q^n groups with n ranging from *0–4*.[34] Q^3 and Q^4 units predominate in series A and C, revealing higher degrees of polymerization in comparison to B series. For each series, there is a general depolymerisation trend with decreasing SiO_2/Li_2O and SiO_2/K_2O ratios as can be deduced from the diminishing intensity band of Q^4 units. The fading intensity trend of Q^4 signal is accompanied by a significant intensity increase of Q^3 units and smaller increments in Q^2 for both A and C series. A stronger depolymerisation trend was observed with the partial replacement of SiO_2 by Al_2O_3 in B series. The incorporation of Al_2O_3 caused an abrupt increase in Q^2 at the expense of Q^3 and Q^4 units (Figs. 4 and 5), suggesting that this oxide is fulfilling dual role of glass network former and network modifier in the B series of glasses.

The role of Al_2O_3 as modifier oxide in the $Li_2O–Al_2O_3–SiO_2$ system is supported by the analysis of ^{27}Al MAS-NMR spectra (Fig. 6). All compositions of group B show ^{27}Al chemical shift towards lower values compared to glasses in group C, indicating increasing coordination numbers, Al[5] and Al[6], in detriment of Al[4].[35-37]

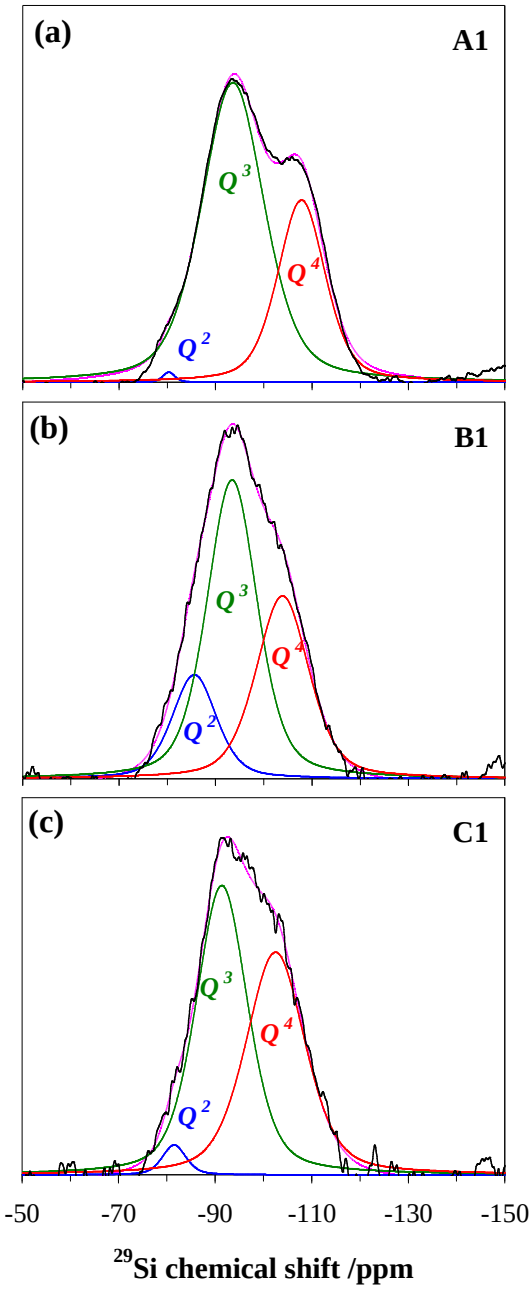

Fig. 4 – ^{29}Si MAS-NMR spectra of glasses: (a) A1, (b) B1 and (c) C1. Dashed curves show the spectral deconvolution components used for fitting the data.

3.3. Crystallization behaviour of bulk glasses

3.3.1 Phase assemblage

All the investigated glass compositions were amorphous after heat treatment at 600 ºC. Figure 7(a-i), presents the X-ray diffractograms of the investigated bulk glasses heat treated within the temperature interval of 700–900 ºC. LD was recorded as the single crystalline phase in the glasses of A series at 700 ºC and 800 ºC (Fig. 7(a,b)). The intensity of the peaks of LD

slightly increased with the rising temperature and traces of cristobalite appeared at 900 ºC (Fig. 7(c)). The addition of Al_2O_3 in the Li_2O–SiO_2 system enhanced the intensity of LD peaks and the formation of lithium aluminium silicate ($LiAlSi_2O_6$, LAS) (Fig. 7(d-f)). On the other hand, earlier studies[28, 31] suggested that adding an excessive amount of K_2O tends to suppress the crystallization of LD and to promote the formation of LMS due to its lower activation energy for crystallization in comparison to LD.[38-39] Moreover, adding alkali oxides to silicate glasses decreases the melt viscosity, increases the fraction of NBO and enhances the tendency of the glass towards devitrification.[40] Indeed, in the C series, LD was formed only in the composition C1 with the lowest K_2O content.[28, 31]

3.3.2 Microstructure

Figures 8, 9 and 10 compare the SEM micrographs of A and B series of glasses heat treated at different temperatures. In the temperature interval 600–700 ºC the small droplets underwent coalescence into bigger agglomerates at a rate that was seemingly higher in B series. LD crystals can be observed at 700 ºC, being more evident in B series, in correlation with XRD data (Fig. 7). Bulk glasses of series A and B demonstrated ability towards bulk nucleation and crystallization of LD, while glasses of series C were prone to surface crystallization with the formation of dendritic crystals characteristic for LMS,[28] clearly observed in the samples heat treated at 800 ºC.

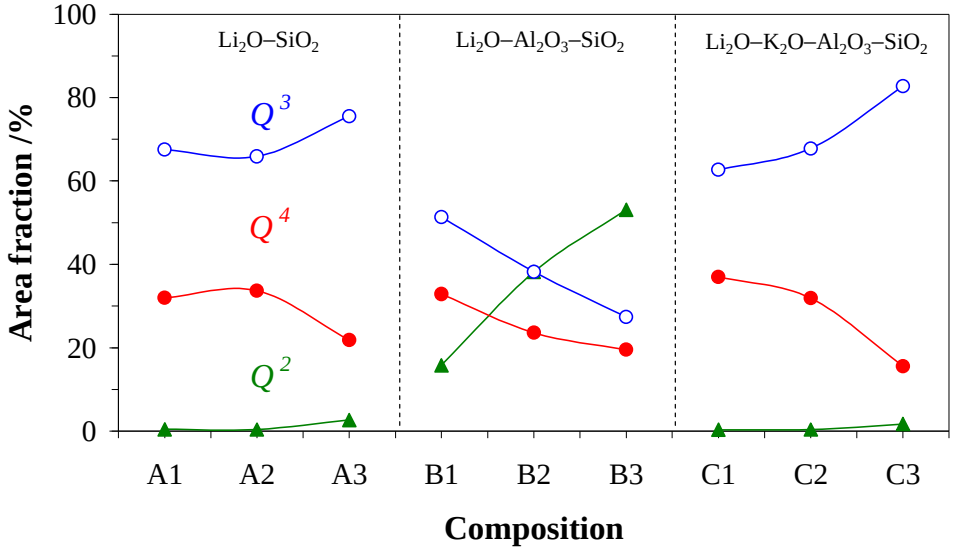

Fig. 5 – Solid state ^{29}Si NMR area fractions (%) of the signal components observed in glasses.

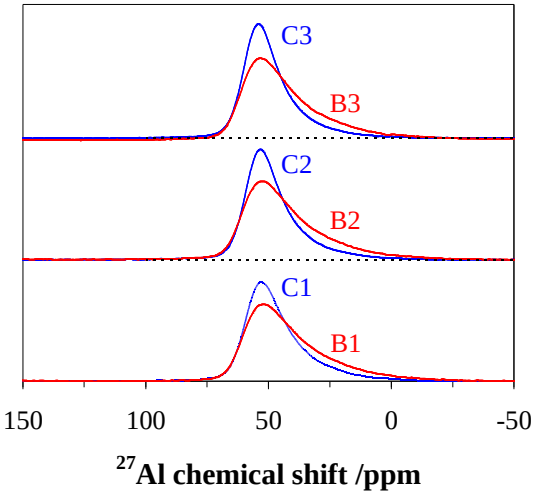

Fig. 6 – ^{27}Al MAS-NMR spectra of glasses of series B and C.

3.4. Sintering and crystallization of glass powder compacts

3.4.1 Sintering process

The experimental compositions from series A and B exhibited poor densification ability and resulted in porous and brittle samples, contrasting with the glass-powder compacts from series C that could be densely sintered.[31] In particular, samples from the binary system (series A) were extremely fragile. The incorporation of Al_2O_3 enhanced the sintering ability but not in desired extent to get proper densification. Samples of the different series heat treated at 900 ºC for 1 h showed the following bending strength values: 2.40 ± 0.3 MPa (A1), 7.40 ± 0.6 MPa (B1) and 201 ± 16.0 MPa (C1). These considerable differences reflect the great importance of selecting the proper doses of both oxides (Al_2O_3 and K_2O) in order tune the densification ability and the final properties of the sintered glass powder compacts in the present systems.

The HSM curves of the glass powder compacts of series B and C plotted in Fig. 11 show that densification generally occurs through viscous flow at temperatures slightly higher than T_g and dense materials are produced when the sintering process is completed before crystallization begins.[34] The glasses of series B exhibit just a single and small sintering step corresponding to a shrinkage volume of about 6–8%, while glasses of series C present two steps of sintering and a total variation of A/A_0 close to 0.60, *i.e.*, a volume shrinkage of about 40%, corresponding to practically full densification.[34]

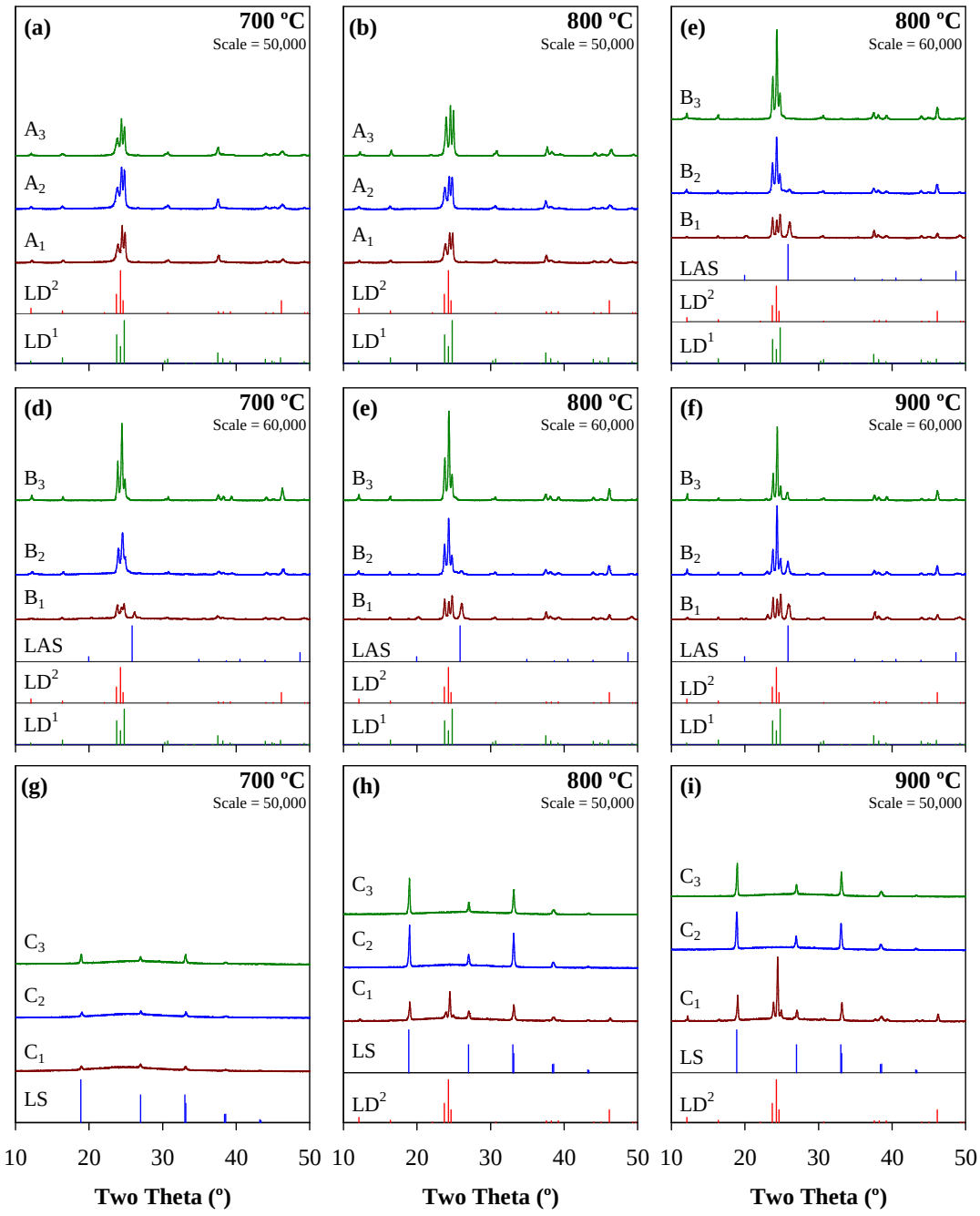

Fig. 7 – X-ray diffractograms of experimental bulk glasses after heat treatment at different temperatures for 1 h. LS: lithium silicate (Li_2SiO_3, ICCD card 01-029-0828); LD^1: lithium disilicate ($Li_2Si_2O_5$, ICCD card 00-072-0102); LD^2: lithium disilicate ($Li_2Si_2O_5$, ICCD card 00-015-0637); LAS: virgilite ($Li_xAl_xSi_{3-x}O_6$, ICCD card 00-031-0707).

The observed changes in the profiles of the samples B3 and C3 during sintering (Fig. 12) reveal that the characteristic temperatures corresponding to softening (T_D), half ball (T_{HB}) and

flow (T_F)) for the $Li_2O–K_2O–Al_2O_3–SiO_2$ (C) system were reached significantly earlier in comparison to those observed in the $Li_2O–Al_2O_3–SiO_2$ (B) system.

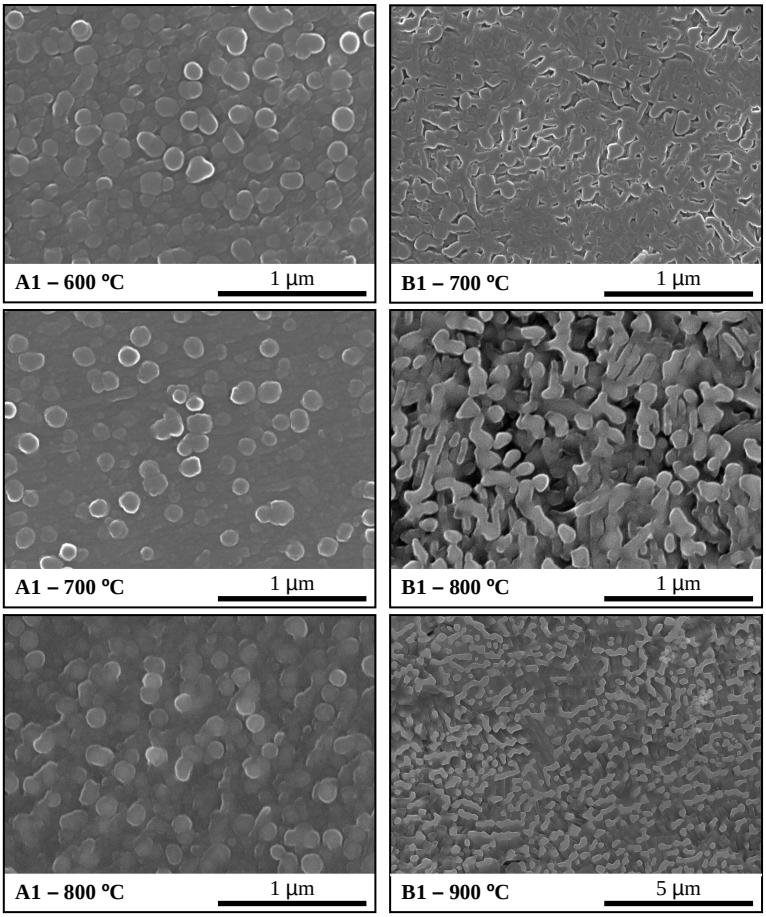

Fig. 8 – SEM images of bulk glasses series A and B heat treated at 700, 800 and 900 ºC for 1 h (etched with 2 vol.% HF solution for 2 min).

4. Discussion

The phenomenon of amorphous phase separation in glasses has become an important topic of glass research since the fundamental investigations of Dietzel at the beginning of the 1940s.[41] It is a common phenomenon in silicate glasses that results in a heterogeneous mixture of two immiscible amorphous phases.[1, 3, 41-42] Dietzel explained this phenomenon on the basic field strength consideration.[3, 41] Thus, in case of cooling binary silicates both cations compete for the oxygen ions so as to surround themselves with the closest possible packing. When the field strengths of both the cations are the same dissociation into the two separate pure oxide phases often occurs. Below the solidus temperature, glass immiscibility is called a metastable

phase separation and above that temperature it is called a stable one.[42] Metastable immiscibility has been observed in many glass systems and the compositional range of the miscible gap varies with glass forming system. Among different types of alkali silicate glasses, lithium silicate glasses have the widest immiscibility range, between pure SiO_2 and close to $Li_2O{\cdot}2SiO_2$.[3, 41-42] Understanding this phenomenon in the 3 different systems studied in the present work, *i.e.* $Li_2O–SiO_2$, $Li_2O–Al_2O_3–SiO_2$ and $Li_2O–K_2O–Al_2O_3–SiO_2$ is essential to correlate the microstructure with phase formation and final properties.

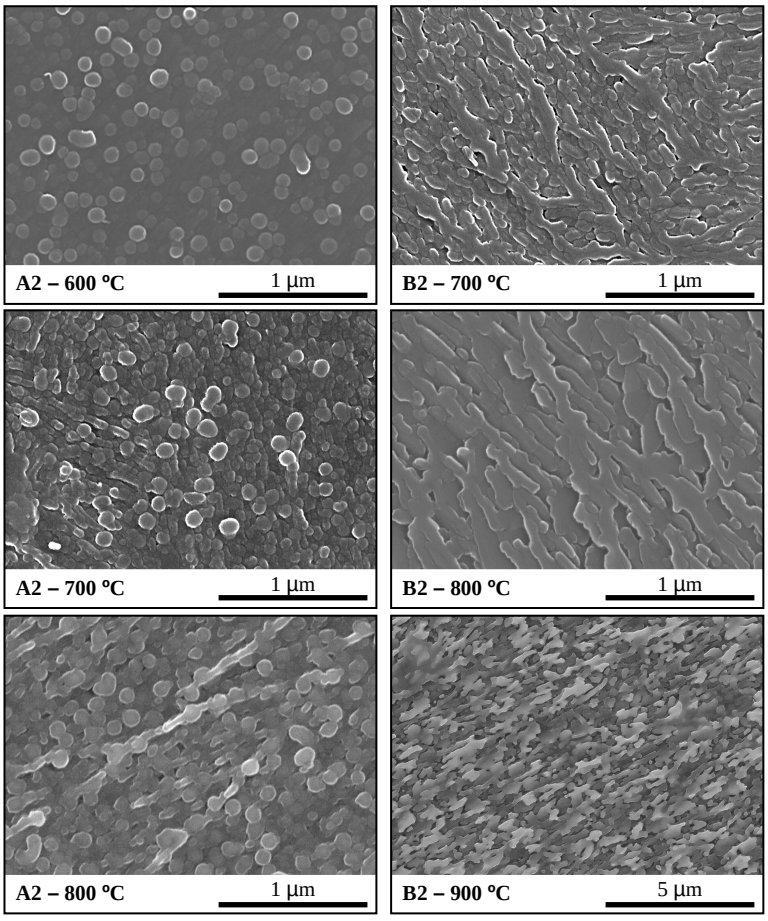

Fig. 9 – SEM images of bulk glasses A2 and B2 heat treated at 700, 800 and 900 ºC for 1 h (etched with 2 vol.% HF solution for 2 min).

According to Dietzel, the contribution of Li_2O to the surface tension is more significant than that of SiO_2.[3, 41] Therefore, further adding Li_2O to the $Li_2O–SiO_2$ glasses that already contain droplet-like zones of Li-rich phase and SiO_2-rich matrix, was aimed at equalizing the surface tension of the different phases and weaken the degree of segregation. The SEM images of non-annealed glasses (Fig. 1) show that the increase of Li_2O content from A1 to A2 made the

droplet size and density distribution to decrease. Further increment in Li_2O in the entire glass reduces the surface tension of the two phases because Li_2O entered into the SiO_2-rich phase surrounding the droplets and the size of the droplets reduced continuously.[2-3] The incorporation of Al_2O_3 in the $Li_2O–SiO_2$ system at the expenses of SiO_2 might slightly increase the difference in surface tension since the former one has smaller contribution to the surface tension than the latter.[2-3, 41] Contrarily, more significant changes in surface tension are likely upon adding K_2O to the $Li_2O–Al_2O_3–SiO_2$ system because of the small efficiency factor of K_2O relative to surface tension.[2, 41]

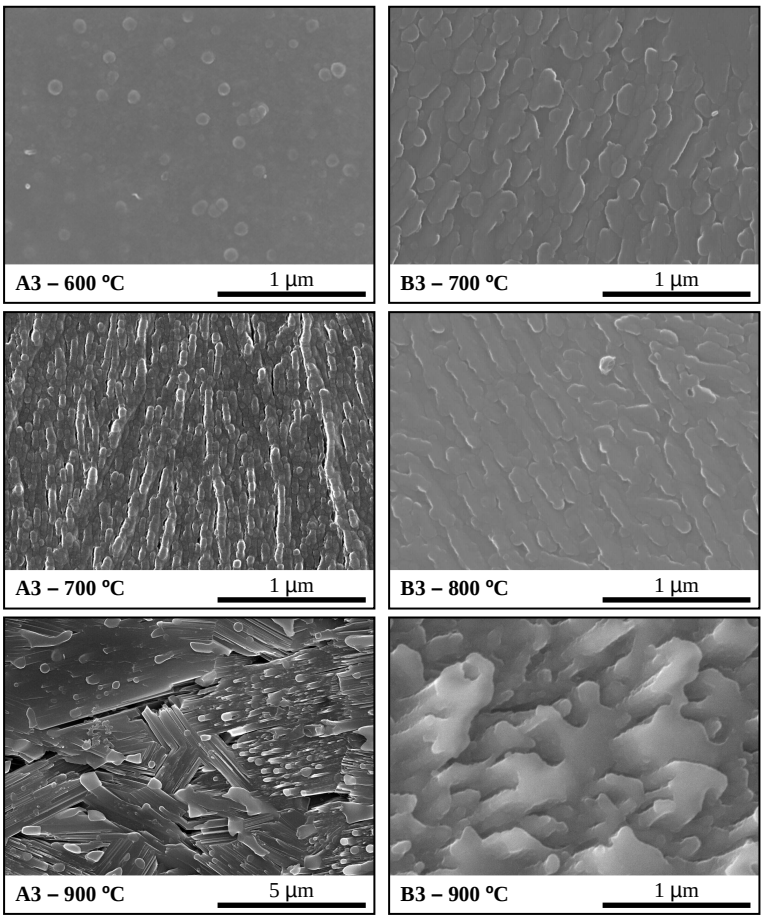

Fig. 10 – SEM images of bulk glasses A3 and B3 heat treated at 700, 800 and 900 ºC for 1 h (etched with 2 vol.% HF solution for 2 min).

Considering Dietzel's hypothesis that a network modifier will migrate preferentially into the phase of the network former which has the highest field strength to contribute to the latter's maximum coordination with the oxygen ions,[2-3, 41] one can expect the potassium ions to be statistically distributed in the SiO_2-rich matrix. Consequently, it will increase the difference in

surface tension between the SiO_2-rich glass and droplet-like zones of Li-rich phase causing higher degree of segregation. Indeed, the addition of K_2O at the expenses of SiO_2 in $Li_2O–Al_2O_3–K_2O–SiO_2$ glasses enhanced the mean Li_2O-rich droplet size and their distribution density.[28]

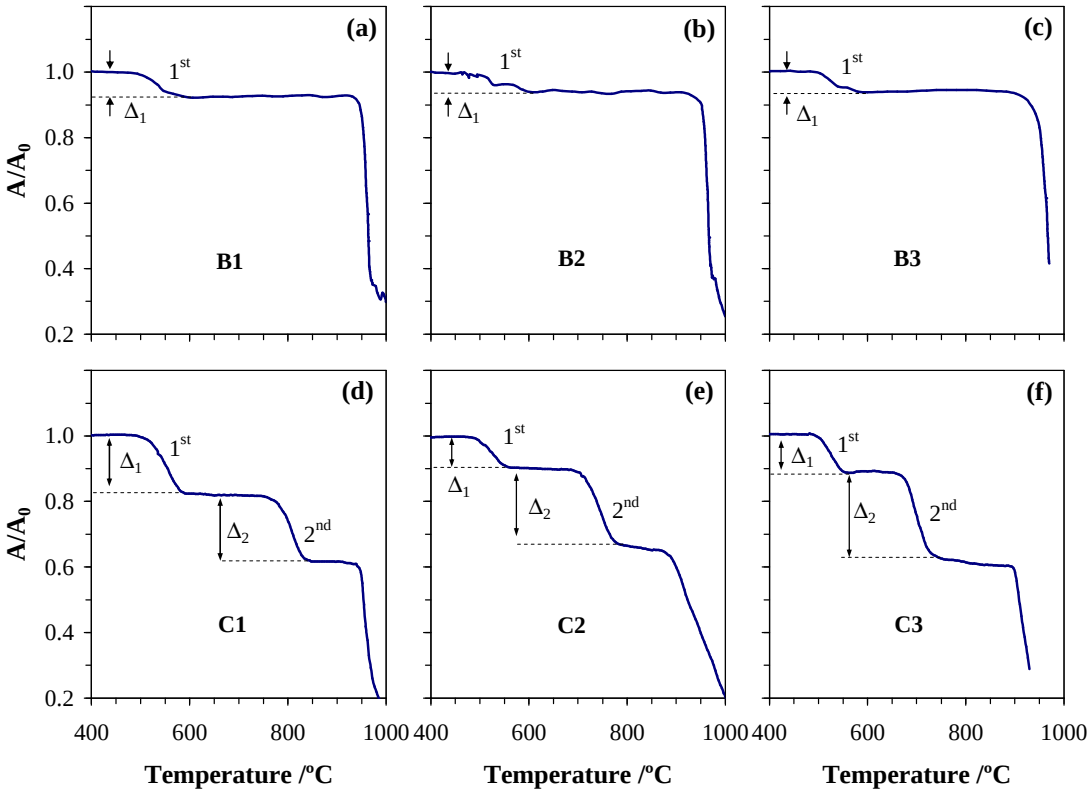

Fig. 11 – HSM curves for glass-powders: (a) B1, (b) B2, (c) B3, (d) C1, (e) C2 and (f) C3.

From the ^{29}Si MAS-NMR spectra (Fig. 4) and the peaks deconvolution derived data presented in the Fig. 5 it is clear that further adding Li_2O to the $Li_2O–SiO_2$ binary system caused depolymerisation of the glass network. These results correlate well with the data reported by Schramm *et al.*[43] who investigated the extent of Q^n distributions for LD glasses in the composition region between 15 and 40 mol% Li_2O: the percentage of Q^4 decreased with increasing amounts of Li_2O, that of Q^3 reached a maximum at 30 mol.% Li_2O, and the percentage of Q^2 showed tendency to grow at higher Li_2O concentrations. On the other hand, adding Al_2O_3 to the $Li_2O–SiO_2$ binary system caused significant decrease in Q^3 and Q^4 units and a rapid grow of Q^2 units (Figs. 4 and 5). These structural changes are consistent with a glass network modifier role of Al_2O_3 as in $Li_2O–SiO_2$ system, which as far as we know, has not been earlier reported although Al_2O_3 has been classified as “randomiser” of the silicate

structure.[2] It is well known that to strengthen the glass network aluminium should be four-coordinated and each tetrahedral unit should be associated with a cation in its vicinity in order to maintain local charge neutrality of the $(AlO_{4/2})^-$ units. In series C glasses this neutrality is assured by the presence of K_2O.[28-29, 31] However, in K_2O-free glasses of series B ($Li_2O–Al_2O_3–SiO_2$), aluminium tends to appear in atomic arrangements of higher coordination number, greatly contributing to depolymerising the glass network. This can be due to a large fraction of lithium cations captured in the Li-rich droplet phase with the remaining lithium amount from the silica rich matrix being insufficient to satisfy the neutrality of the $(AlO_{4/2})^-$ units. The higher coordination number of Al is well supported by the ^{27}Al MAS-NMR spectra of compositions B and C (Fig. 6), namely by the ^{27}Al chemical shifts of B glasses to lower values in comparison to those of group C glasses, indicating growing of Al[5] and Al[6] atomic arrangements in detriment of Al[4].

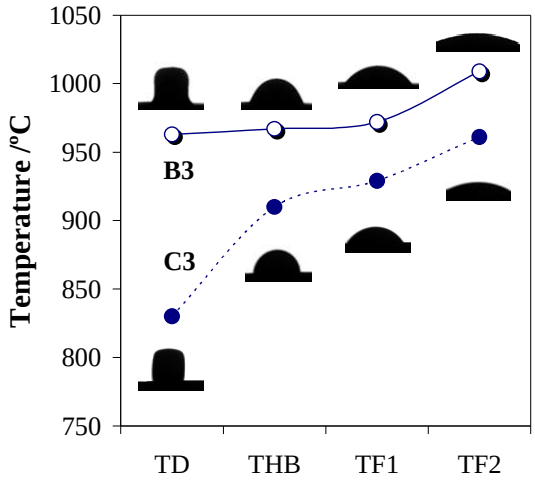

Fig. 12 – Temperature parameters, softening (T_D), half ball (T_{HB}) and flow (T_F)) and images of glass powder compacts as obtained from HSM for glasses B3 and C3.

The structural features of the glasses affect the formation of crystalline phases. Thus, heat treating Al_2O_3-containing bulk glasses of B series resulted in precipitation of LD as the major crystalline phase and LAS as the minor phase (Fig. 7(d-f)). The formation of LAS was favoured by six coordinated aluminium thus supporting NMR results obtained from the $Li_2O–Al_2O_3–SiO_2$ glasses. On the other hand, the preferential formation of LMS in C series of glasses was already explained[27-29] using the model of Bischoff *et al.* and ^{29}SiMAS-NMR results.[44] In particular, suppressing and promoting the formation of $Li_2Si_2O_5$ and Li_2SiO_3, respectively, with increasing K_2O contents was connected to a significant decrease in Q^4 units

according to the reaction $Q^4_{(glass)} + Q^2_{(cryst.)} \leftrightarrow 2Q^3_{(cryst.)}$. Moreover, the second separation process undergone by the LD-rich glass droplets into pure silica-rich glass and LMS-rich glass due to the appreciable contraction on cooling should be taken into account. As a result, LMS is formed as the intermediate crystalline phase in the binary ($Li_2O–SiO_2$) glasses heat treated at temperatures below 500 ºC followed by crystallization of LD.[27-29] The increase in surface tension between LD-rich droplets and SiO_2-rich glass might also contribute for suppressing LD crystallization via the reaction $Q^4_{(glass)} + Q^2_{(cryst.)} \leftrightarrow 2Q^3_{(cryst.)}$.

The comparison of SEM images of bulk glasses A and B heat treated at 700, 800 and 900 ºC for 1 h reveals that a more extended crystallization process has occurred in the B series of glasses. This observation is supported by XRD analysis (Fig. 7) and might implies towards lowering viscosity upon adding Al_2O_3 in $Li_2O–SiO_2$ glasses in a certain temperature range, an issue that could be clarify by performing viscosity measurements, which are out of the scope of this work.

The lower T_c and T_p values of glasses from A and B series in comparison to those of C series (Table 2) mean that the crystallization process is delayed in latter glasses while the resulting larger $T_c–T_g$ differences favour densification of glass-powder compacts, a decisive factor to get strong glass-ceramics. Narrowing the $T_c–T_g$ interval in the less polymerised glass networks of series A and B (Fig. 4 and 5) in comparison to C compositions completely hindered the densification of the glass powder compacts due the early formation of large fraction of LD phase (Fig. 3). From the two steps of densification identified in the HSM curves of C series, only the first one was affected by crystallization. In composition C1 (lowest K_2O content), the first sintering step was separated by the temperature range where LMS was formed followed by a second sintering stage that occurred simultaneously with formation of LD phase.[27-29] This can be attributed to the formation of a more rigid glass network containing four coordinated $(AlO_{4/2})^-$ units and K^+ cations in its vicinity to maintain local charge neutrality. Therefore, a small addition of K_2O to pure $Li_2O–Al_2O_3–SiO_2$ system is crucial to enhance the densification behaviour and the ultimate mechanical strength. In the present study, beneficial effects of adding both K_2O and Al_2O_3 are only observed up to about 3 mol.% of each oxide, being therefore a matter of process optimization.[29]

5. Conclusions

The effect of Al_2O_3 on structure, sintering and devitrification behaviour of glasses in the $Li_2O–SiO_2$ system along with the properties of the resultant glass-ceramics has been investigated. The results can be summarized in the following conclusions:

1. The structure of A and C series of glasses consists predominantly of Q^3 and Q^4 units and the silicate glass network trends to depolymerise with decreasing SiO_2/Li_2O and SiO_2/K_2O ratios, as revealed by an increase of groups Q^3 units, a small increment in Q^2, at the expenses of a decrease in Q^4 units.

2. The partial replacement of SiO_2 by Al_2O_3 in $Li_2O–SiO_2$ glasses (group B) enhanced the trend towards depolymerisation, reflected by an abrupt increase in Q^2 at the expense of Q^3 and Q^4 units, with Al_2O_3 playing dual role of a glass network former and modifier. This latter role of Al_2O_3 in the $Li_2O–Al_2O_3–SiO_2$ system is supported by the analysis of ^{27}Al MAS-NMR spectra. All compositions of group B show ^{27}Al chemical shifts to lower values in comparison to glasses in group C, revealing increasing fractions of Al[5] and Al[6] in detriment of Al[4]. Moreover, crystallization of those glasses resulted in the formation of LD and LAS phases.

3. The experimental compositions from series A and B exhibited poor densification ability resulted in porous samples of brittle nature, contrasting with well sintered glass-powder compacts from series C. This was due to the formation of a more rigid glass network in glasses of series C containing four coordinated $(AlO_{4/2})^-$ units and K^+ cations in its vicinity to maintain local charge neutrality. Therefore, a small addition of K_2O to pure $Li_2O–Al_2O_3–SiO_2$ system is crucial to enhance the densification behaviour and the ultimate mechanical strength.

Acknowledgments

Hugo R. Fernandes is grateful for the financial support of CICECO and for the PhD grant (SFRH/BD/41307/2007) from the FCT, Portugal.

References

1. Mazurin OV, Porai-Koshits EA. Phase Separation in Glasses. Amsterdam: North-Holland; 1984.
2. Vogel W. Structure and Crystallization of Glasses. Leipzig: Pergamon Press; 1971.
3. Vogel W. Glass Chemistry. Berlin: Springer; 1994.
4. Lewis MH. Glasses and Glass-Ceramics. London: Chapman and Hall; 1989.
5. Strnad Z. Glass Science and Technology. New York: Elsevier; 1986.
6. West AR. Solid State Chemistry and its Applications. New York: John Wiley and Sons; 1984.
7. Höland W, Beall G. Glass-ceramic Technology. Westerville, Ohio: The American Ceramic Society; 2002.
8. Barrett JMG, FL), Clark, David E. (Gainesville, FL), Hench, Larry L. (Gainesville, FL), inventor; The Board of Regents, State of Florida, University of Florida (Tallahassee, FL), assignee. Glass-ceramic dental restorations. 1980.
9. Wu J-mT, TW), Cannon, Warren R. (East Brunswick, NJ), Panzera, Carlino (Belle Mead, NJ), inventor; Johnson & Johnson Dental Products Company (East Windsor, NJ), assignee. Castable glass-ceramic composition useful as dental restorative. 1985.
10. Bengisu M, Brow RK, White JE. Interfacial reactions between lithium silicate glass-ceramics and Ni-based superalloys and the effect of heat treatment at elevated temperatures. Journal of Materials Science 2004;39(2):605-18.
11. Borom MP, Turkalo AM, Doremus RH. Strength and microstructure in lithium disilicate glass-ceramics. Journal of the American Ceramic Society 1975;58(9-10):385-91.
12. Goswami M, Kothiyal GP, Montagne L, Delevoye L. MAS-NMR study of lithium zinc silicate glasses and glass-ceramics with various ZnO content. Journal of Solid State Chemistry 2008;181(2):269-75.
13. Guazzato M, Albakry M, Ringer SP, Swain MV. Strength, fracture toughness and microstructure of a selection of all-ceramic materials. Part I. Pressable and alumina glass-infiltrated ceramics. Dental Materials 2004;20(5):441-48.
14. Höland W, Apel E, van Hoen C, Rheinberger V. Studies of crystal phase formations in high-strength lithium disilicate glass-ceramics. Journal of Non-Crystalline Solids 2006;352(38-39):4041-50.
15. Iqbal Y, Lee WE, Holland D, James PF. Metastable phase formation in the early stage crystallisation of lithium disilicate glass. Journal of Non-Crystalline Solids 1998;224(1):1-16.
16. Beall G. Design of glass-ceramics. Solid State Sciences 1989;3:333–54.
17. Beall G. Glass-ceramics: Recent developments and application. Ceramic Transactions 1993;30:241-66.
18. Echevería LM. New lithium disilicate glass-ceramics. Boletin da la Sociedad Espanola de Cerámica e Vidrio 1992;5:183–88.
19. Schweiger M. Microstructure and mechanical properties of a lithium disilicate glass–ceramic in the SiO_2–Li_2O–K_2O–ZnO–P_2O_5 system. Glastechnische Berichte-Glass Science and Technology 2000;73:43–50.
20. von Clausbruch CS, Schweiger M, Holand W, Rheinberger V. The effect of P_2O_5 on the crystallization and microstructure of glass-ceramics in the SiO_2−Li_2O−K_2O−ZnO−P_2O_5 system. Journal of Non-Crystalline Solids 2000;263(1-4):388-94.

21. Frank M, Schweiger M, Rheinberger V, Höland W. High-strength translucent sintered glass-ceramics for dental application. Glastechnische Berichte-Glass Science and Technology 1998;71C:345-48.
22. Höland W. Material science fundamentals of the IPS Empress 2 Glass-Ceramic. Ivoclar-Vivadent Report; 1998. p. 3-10.
23. Höland W, Schweiger M, Frank M, Rheinberger V. A comparison of the microstructure and properties of the IPS Empress®2 and the IPS Empress® glass-ceramics. Journal of Biomedical Materials Research 2000;53(4):297-303.
24. Schweiger M, Frank M, Von Clausbruch CS, Höland W, Rheinberger V. Microstructure and properties of pressed glass–ceramic core to zirconia. Quintessence Dental Technology 1998;21:73-79.
25. Kim KD. Crystallization behavior during cooling and glass-forming ability of Al_2O_3-poor $Li_2O–Al_2O_3–SiO_2$ melts. Journal of Non-Crystalline Solids 2008;354(15-16):1715-20.
26. Morimoto S. Effect of K_2O on crystallization of $Li_2O–SiO_2$ glass. Journal of the Ceramic Society of Japan 2006;114(1326):195-98.
27. Fernandes HR, Tulyaganov DU, Goel A, Ferreira JMF. Structural characterisation and thermo-physical properties of glasses in the $Li_2O–SiO_2–Al_2O_3–K_2O$ system. Journal of Thermal Analysis and Calorimetry 2011;103(3):827-34.
28. Fernandes HR, Tulyaganov DU, Goel A, Ferreira JMF. Effect of K_2O on structure-property relationships and phase transformations in $Li_2O–SiO_2$ glasses. Journal of the European Ceramic Society 2012;32(2):291-98.
29. Fernandes HR, Tulyaganov DU, Goel A, Ribeiro MJ, Pascual MJ, Ferreira JMF. Effect of Al_2O_3 and K_2O content on structure, properties and devitrification of glasses in the $Li_2O–SiO_2$ system. Journal of the European Ceramic Society 2010;30(10):2017-30.
30. Fernandes HR, Tulyaganov DU, Goel IK, Ferreira JMF. Crystallization process and some properties of $Li_2O–SiO_2$ glass-ceramics doped with Al_2O_3 and K_2O. Journal of the American Ceramic Society 2008;91(11):3698-703.
31. Fernandes HR, Tulyaganov DU, Pascual MJ, Kharton VV, Yaremchenko AA, Ferreira JMF. The role of K_2O on sintering and crystallization of glass powder compacts in the $Li_2O–K_2O–Al_2O_3–SiO_2$ system. Journal of the European Ceramic Society 2012:in press.
32. Massiot D, Fayon F, Capron M, King I, Le Calvé S, Alonso B, et al. Modelling one- and two-dimensional solid-state NMR spectra. Magnetic Resonance in Chemistry 2002;40:70-76.
33. Lara C, Pascual MJ, Duran A. Glass-forming ability, sinterability and thermal properties in the systems $RO–BaO–SiO_2$ (R = Mg, Zn). Journal of Non-Crystalline Solids 2004;348:149-55.
34. Schneider J, Mastelaro VR, Panepucci H, Zanotto ED. ^{29}Si MAS–NMR studies of Q^n structural units in metasilicate glasses and their nucleating ability. Journal of Non-Crystalline Solids 2000;273:8-18.
35. Smith ME. Application of ^{27}Al NMR techniques to structure determination in solids. Applied Magnetic Ressonance 1993;4:1-64.
36. Oudadesse H, Derrien AC, Lefloch M, J. D. MAS-NMR studies of geopolymers heat-treated for applications in biomaterials field. Journal of Materials Science 2007:;42:3092-98.
37. Wright PA. Microporous Framework Solids. London: Royal Society of Chemistry; 2007.

38. Hammetter WF, Loehman RE. Crystallization kinetics of a complex lithium silicate glass-ceramic. Journal of the American Ceramic Society 1987;70(8):577-82.
39. Oliveira APN, Alarcon OE, Manfredini T, Pellacani GC, Siligardi C. Crystallisation kinetics of a $2.3Li_2O.1.1ZrO_2.6.6SiO_2$ glass. Physics and Chemistry of Glasses 2000;41(2):100-03.
40. Scholze H. Glass: Nature, Structure and Properties. Berlin: Springer; 1991.
41. Dietzel A. Zusammenhänge zwischen Oberflächenspnnung und Struktur von Glasschmelzen. Kolloid-Z 1942;100(3):368-80.
42. Uhlmann DR, Kolbeck AG. Phase separation and revolution in concepts of glass structure. Physics and Chemistry of Glasses 1976;17(5):146-58.
43. Schramm CM, de Jong BHWS, Parzialet VE. ^{29}Si Magic Angle Spinning NMR study on local silicon environments in amorphous and crystalline lithium silicates. Journal of the American Ceramic Society 1984;106:4396-402.
44. Bischoff C, Eckert H, Apel E, Rheinberger VM, Holand W. Phase evolution in lithium disilicate glass–ceramics based on non-stoichiometric compositions of a multi-component system: structural studies by ^{29}Si single and double resonance solid state NMR. Physical Chemistry Chemical Physics 2011;13:4540-51.

3.7 Al_2O_3/K_2O-containing non-stoichiometric lithium disilicate based glasses: a study of crystallization kinetics

Hugo R. Fernandes[a], Dilshat U. Tulyaganov[a,b], José M.F. Ferreira[a]

[a] Dep. of Ceramics and Glass Engineering, University of Aveiro, CICECO, 3810-193 Aveiro, Portugal

[b] Turin Polytechnic University in Tashkent, 17 Niyazova str., 100174 Tashkent, Uzbekistan

Journal of Thermal Analysis and Calorimetry (published online, 10 October 2012)

DOI: 10.1007/s10973-012-2692-9

Abstract

The crystallization kinetics of experimental glasses in 3 different systems: (A) $Li_2O–SiO_2$, (B) $Li_2O–Al_2O_3–SiO_2$ and (C) $Li_2O–K_2O–Al_2O_3–SiO_2$, was studied under non-isothermal conditions. The DTA results revealed a stronger tendency to crystallization of binary compositions in comparison to the ternary and quaternary compositions comprising Al_2O_3 and K_2O present the lower crystallization, *i.e.* the crystallization propensity follows the trend A > B > C. The devitrification process in the $Li_2O–SiO_2$ and $Li_2O–Al_2O_3–SiO_2$ systems began earlier and the rate was higher in comparison to that of glasses in the quaternary $Li_2O–K_2O–Al_2O_3–SiO_2$ system. Thus, addition of Al_2O_3 and K_2O to glasses of $Li_2O–SiO_2$ system was demonstrated to promote glass stability against crystallization. However, the activation energy for crystallization (E_c) was shown to depend also on the SiO_2/Li_2O ratio with the binary system showing a decreasing trend with increasing SiO_2/Li_2O ratio, while the opposite tendency being observed for compositions with added Al_2O_3 and K_2O.

Key words: Glass; Lithium disilicate; Metastable phase separation.

1. Introduction

Most of the glass-ceramics developed so far for specific tailor-made applications are based on non-stoichiometric materials systems. The search for enhanced processing and properties is usually supported by a deeper understanding of nucleation and crystallization mechanisms in parent glasses.[1] From the experimental approach, differential thermal analysis (DTA) and differential scanning calorimetry (DSC) are among the most common techniques used to study the thermal properties, including the crystallization process and its kinetics. The thermal stability of glassy materials is usually expressed in terms of the glass transition temperature T_g and the glass transition activation energy E_g. The correlation between T_g, E_g and thermal stability arises from the fact that below T_g a glassy material has a large viscosity and the relaxation kinetics is very slow, leaving a few opportunities for local rearrangements of bonds and atomic displacement.[2] Starting from this basic concept, Moynihan *et al.* [3] developed a model to describe the glass transition kinetics, which can be used for determining E_g. According to the theory of crystallization kinetics,[4] for an amorphous glass to transform into a crystalline state, the arranged atoms will have to overcome a certain potential barrier, the height of which is known as the crystallization activation energy E_c. So, as the height of the potential barrier increases, the rate of the nucleation and growth processes becomes smaller and crystallization is retarded. According to the Gao and Wang model,[5] which was developed on the basis of the formal theory of phase transformation,[6-7] the crystallization rate reaches two-thirds of its value at the peak temperature of crystallization T_p. The rate of crystallization at this particular temperature varies with the heating rate, as monitored by thermo-analytical techniques, and could be used to calculate E_c under non-isothermal conditions.

A large variety of theoretical models and functions have been proposed to describe the crystallization kinetics. Two basic calorimetric measurement methods can be used to study the crystallization kinetics: (1) isothermal and (2) non-isothermal.[8-10] In the isothermal method, the sample is brought quickly to a temperature above the glass transition temperature, T_g, and the heat evolved during the crystallization process is recorded as a function of time. In the non-isothermal method, the sample is heated at a fixed rate and the heat evolved is again recorded as a function of temperature or time. The isothermal experiments are generally very time-consuming, while experiments performed at constant heating rate enable a more expeditious gathering of the experimental data. Furthermore, the impossibility of instantaneously reaching the testing temperature under 'isothermal' conditions means that no

measurements are possible while the system is approaching the set temperature. This drawback is absent in the case of non-isothermal (constant heating rate) experiments.[9-10]

In the present study, the kinetic parameters such as E_c and Avrami exponent (n) in Johnson–Mehl–Avrami (JMA) equation [6-7, 11] for binary ($Li_2O–SiO_2$), ternary ($Li_2O–Al_2O_3–SiO_2$), and quaternary ($Li_2O–K_2O–Al_2O_3–SiO_2$) disilicate glasses were determined using non-isothermal methods. The activation energy associated with the glass transition was determined using Kissinger [12] and Moynihan [3] methods. Heating rate dependent glass transition temperature is rationalized using Lascoka equation.[13] Also, the variations of activation energy and Avrami exponent with the fraction of crystallization were examined.

2. Experimental Procedure

Table 1 presents the detailed compositions of the experimental glasses along with their corresponding SiO_2/Li_2O ratios. A total of 9 disilicate glass compositions featuring SiO_2/Li_2O ratios ($2.18 < SiO_2/Li_2O < 3.08$) far from the stoichiometric composition ($SiO_2/Li_2O = 2$) included binary ($Li_2O–SiO_2$), ternary ($Li_2O–Al_2O_3–SiO_2$) and quaternary ($Li_2O–K_2O–Al_2O_3–SiO_2$) systems. The compositions were prepared from powders of technical grade SiO_2 (purity >99.5%) and of reactive grade Al_2O_3, Li_2CO_3, and K_2CO_3. Homogeneous mixtures of batches (~100 g) obtained by ball milling were calcined at 800 ºC for 1 h and then melted in Pt crucibles at 1550 ºC for 1 h, in air, which was adequate to obtain bubble-free homogenous bulk (monolithic) glasses from all the investigated compositions by pouring glass melts on bronze mould.

Table 1 – Compositions of the experimental glasses (mol.%).

	$Li_2O–SiO_2$			$Li_2O–Al_2O_3–SiO_2$			$Li_2O–K_2O–Al_2O_3–SiO_2$		
#	A1	A2	A3	B1	B2	B3	C1	C2	C3
Li_2O	26.59	28.09	30.59	26.59	28.09	30.59	22.96	22.96	22.96
K_2O	–	–	–	–	–	–	3.63	5.13	7.63
Al_2O_3	–	–	–	2.63	2.63	2.63	2.63	2.63	2.63
SiO_2	73.41	71.91	69.41	70.78	69.28	66.78	70.78	69.28	66.78
SiO_2/Li_2O	2.76	2.56	2.27	2.66	2.47	2.18	3.08	3.02	2.91

Differential thermal analysis (DTA, Setaram Labsys, Setaram Instrumentation, Caluire, France) was used to determine the glass transition temperature T_g, the crystallization onset temperature, T_c and peak crystallization temperature, T_p (β = 20 K min^{-1}). For this, glass samples with particle sizes in the range of 500−1000 μm (collected by sieving of crushed non-annealed glass blocks) and weighing 40 mg were contained in an alumina crucible and α-alumina powder was used as reference material. Different heating rates (β = 10, 15, 20, 25 and 30 K min^{-1}) were used to evaluate the crystallization kinetics.

3. Results and discussion

3.1. Glass transition region

According to Lasocka [13], the empirical relation between T_g and β is given by:

$$T_g = A + B \log \beta \qquad (1)$$

where *A* and *B* are constants for a given glass composition at a particular temperature *T*. The value of A indicates the glass transition temperature for the heating rate of 1 K min^{-1}, while the value of B is related to the method of quenching the sample – the lower the cooling rate of the melt is, the lower will be the *B* value.[14] It signifies the response of the configurational changes within the glass transition region to the heating rate. The values of *A* and *B* for all samples are listed in Table 2. T_g values obtained at different heating rates are presented in the Fig. 1. Theoretically, T_g is defined as the temperature at which the relaxation time, τ, becomes equal to the relaxation time of observation, τ_{obs}, with the variations on T_g and τ being inversely proportional.[15] Accordingly, with increasing heating rate, τ_{obs} decreases and hence the glass transition temperature increases. For all systems, T_g increased with increasing heating rate and decreased with diminishing of SiO_2/Li_2O ratio (Fig. 1). This is generally related with the polymerization level of the glass structure and can apparently be explained by the higher content of glass modifying oxides.[16-18] Adding Al_2O_3 and K_2O to binary compositions tend to slightly shifting T_g to higher temperatures. The T_g of a multi-component glass is known to be dependent on several independent parameters such as band gap, co-ordination numbers, bond energy, effective molecular weight, the type and fraction of various structural units formed.[19-20]

Glassy solid state is characterised by very slow relaxation kinetics due to relatively high viscosity which make difficult the local arrangements of bonds and atomic displacements.

This type of thermal relaxation depends upon the thermal treatment and may be quite fast near T_g. Thus, it is reasonable to associate the glass transition temperature with the glass structural rearrangements, a phenomenon that requires an activation energy,[2] and the concept of phase transformation proposed by Kissinger [12, 21] for the amorphous to crystalline phase transition could be formally extended to the elastic-viscoelastic transition.[22] Accordingly, the most commonly used method to estimate the activation energy associated with the glass transition under non-isothermal treatment schedules is the so-called Kissinger plot based on the following equation:[12, 21]

$$\ln\frac{\beta}{T_g^2} = -\frac{E_g}{RT_g} + const. \qquad (2)$$

where E_g is the activation energy associated with the glass transition, R is the universal gas constant and β is the heating rate. Another approach to estimate E_g is the Moynihan equation that relates the heating rate, β, with the right hand side of equation (2):[3]

$$\ln\beta = -\frac{E_g}{RT_g} + const. \qquad (3).$$

The plots of $\ln(\beta/T_g^2)$ and $\ln(\beta)$ *versus* $1000/RT_g$ are straight lines, the slopes of which give the respective E_g values. The E_g values obtained using both methods are presented in Table 2 and the correspondent plots against composition are shown in Fig. 1. It can be clearly seen that E_g values obtained from Kissinger's relation are in good agreement with those obtained using Moynihan's approach. Only small systematic shifts are observed among the predicting ability of both methods, which are consistent with the differences between equations (2) and (3).

The activation energy for glass transition is the amount of energy that is absorbed by a group of atoms in the glassy region so that a jump from one metastable state to another is possible.[23] Thus, the activation energy involves molecular motions and rearrangements of atoms around T_g.[24] When the sample is heated, the atoms undergo infrequent transitions between local potential minima separated by different energy barriers in the configuration space where each local minimum represents a different structure. The most stable local minimum in the glassy region has lowest internal energy. Accordingly, the atoms in a glass having minimum activation energy have higher probability to jump to the metastable (or local minimum) state of lowest internal energy and hence are the most stable ones.[23]

Table 2 – The values *A*, *B* and E_g for the glass transition region.

Composition	Lasocka		Kissinger		Moynihan	
	A /K	*B* /K	E_g /kJ mol^{-1}	R^2	E_g /kJ mol^{-1}	R^2
A1	717.3	41.0	261.5 ± 9.9	0.996	274.3 ± 9.9	0.996
A2	715.0	40.6	262.4 ± 8.9	0.997	275.1 ± 8.8	0.996
A3	712.8	39.8	265.8 ± 5.2	0.999	278.4 ± 5.2	0.999
B1	706.6	54.3	197.8 ± 8.8	0.996	210.7 ± 8.8	0.996
B2	707.0	50.7	210.9 ± 5.3	0.998	223.7 ± 5.3	0.998
B3	707.4	46.6	226.9 ± 7.5	0.996	239.6 ± 7.5	0.996
C1	719.6	43.2	241.5 ± 6.5	0.997	254.4 ± 6.5	0.997
C2	718.4	42.3	259.2 ± 7.4	0.998	273.0 ± 7.3	0.998
C3	716.8	40.1	266.2 ± 9.2	0.999	278.9 ± 9.2	0.999

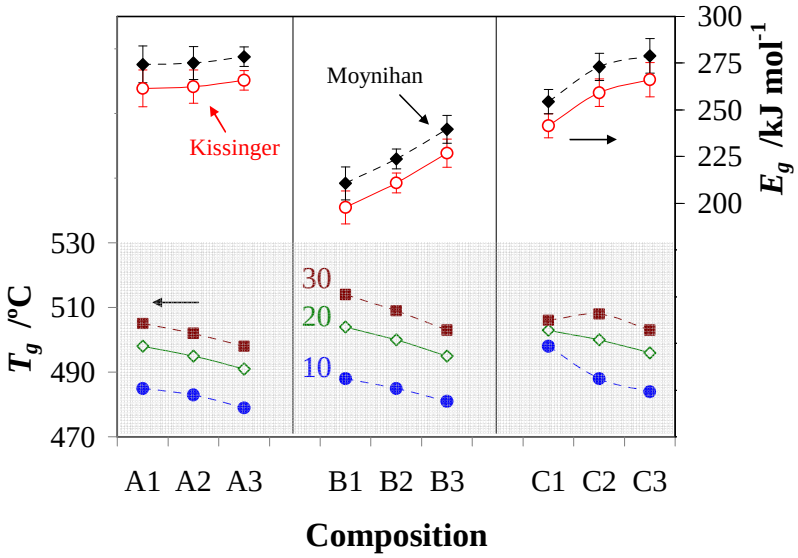

Fig. 1 – Evolution of T_g (at different heating rates) and E_g with composition.

The experimental binary compositions (series A) present the highest values of activation energy for the glass transition (Table 2, Fig. 1). Adding Al_2O_3 to the Li_2O–SiO_2 system (series B) caused a decrease of E_g whereas further adding K_2O (series C) resulted in E_g values similar to those of the binary compositions. Consequently, compositions of series B with the lowest E_g values are seemingly the most stable ones. Moreover, within each system, E_g increases with decreasing the SiO_2/Li_2O ratio. This means that atoms require larger amount of

energy to make transitions between two local minima when the glass compositions are enriched in Li_2O.[25]

3.2. Crystallization region

The DTA plots of the experimental glasses A3, B3 and C3 obtained at different heating rates (10, 15, 20, 25 and 30 K/min) are shown in Figs. 2a-c as an example. Well-defined features comprising endothermic and exothermic peaks with a systematic shift in their position with heating rate, which is tentatively attributed to thermal relaxation phenomena can be observed in all cases. The variation in peak temperature with heating rate is governed by the activation energy (E_c) [12] and the thermal conductivity of the material. At higher heating rates, the activation energy for crystallization follows the same increasing tend as the activation energy for glass transition temperature, because of the decrease of τ_{obs} and the poor thermal conductivity of the material (Fig. 2). Thus by monitoring the shift in the position of the exothermic peak as a function of the heating rate, one could obtain the kinetic parameters as presented in the subsequent sections of this text. Figure 2 shows that the binary composition A3 exhibits the sharper and most intense exothermic peaks. The addition of Al_2O_3 to the binary system (*i.e.* glass B3) caused the broadening of the peaks and slightly shifted T_p to higher temperatures, while more significant variation in the exothermic peak intensity (decreases) and T_p (increases) were observed in the quaternary composition (C3).

The crystallised fraction *versus* temperature plots for compositions A3, B3 and C3, as determined from the Johnson–Mehl–Avrami (JMA) model are shown in Figs. 3a-c. The plots exhibit typical sigmoidal shapes in good agreement to classical literature on glass–ceramics.[6-7, 11, 26] The ratios between the ordinates of the DTA curve and the total area of the peak give the corresponding crystallization rates, which make it possible to build the curves of the exothermal peaks as depicted in Figs. 3d-f. It is observed that the dx/dt increases in direct proportion with the heating rate. Accordingly, a greater volume fraction is crystallized in a shorter time as compared to the low heating rate. This is translated in an increased peak height with increasing heating rate.[27] Apparently, crystallization process moves to higher temperature region hence, the T_p shifts towards higher values.

The plots of DTA suggest that the binary compositions (series A) show stronger tendency to crystallization while compositions comprising Al_2O_3 and K_2O present the lower crystallization propensity, *i.e.*, the crystallization predisposition follows the trend A > B > C

(Figs. 4a-b). In general, crystallization in the systems $Li_2O–SiO_2$ and $Li_2O–Al_2O_3–SiO_2$ begins earlier and occurs at higher rates in comparison to glasses in the $Li_2O–K_2O–Al_2O_3–SiO_2$ system (Figs. 4a-b). Thus, adding of Al_2O_3 and K_2O to the binary system enhanced the glass stability against crystallization.[28-29]

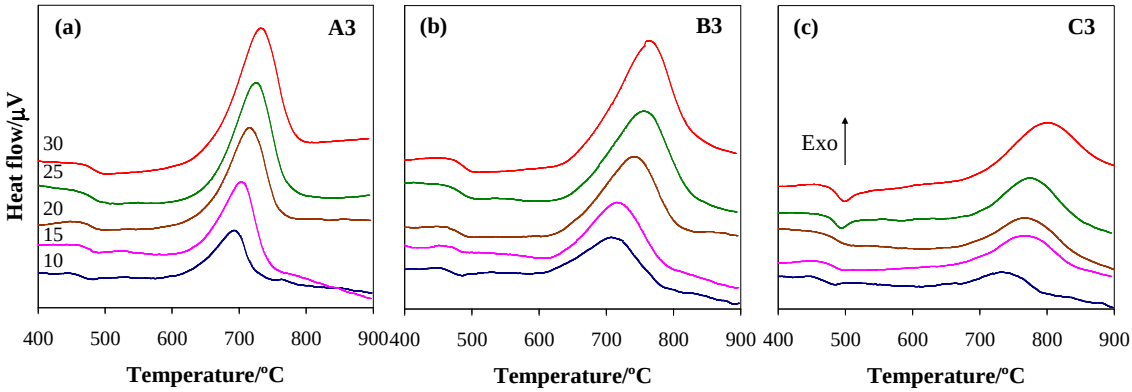

Fig. 2 – DTA plots for glasses A3, B3 and C3 at different heating rates.

The main thermal parameters that influence the crystallization process, *i.e.*, the onset crystallization temperature (T_c), and peak crystallization temperature (T_p), as determined from the DTA plots and are reported in Table 3. The onset temperature of crystallization increases with increasing of SiO_2/Li_2O ratio for the binary compositions, but shows an opposite trend for Al_2O_3 and K_2O containing compositions. Moreover, compositions of series C showed sintering temperature windows ($T_c–T_g$) wider than compositions of series A and B. This can explain their better sintering ability [30]. Regarding the peak temperature of crystallization T_p, the trend is similar to T_g, *i.e.*, T_p decreases with increasing SiO_2/Li_2O ratio. Adding Al_2O_3 to the parent glass led to increasing T_p values. The same trend was observed with the addition of K_2O to the ternary system $Li_2O–Al_2O_3–SiO_2$.

The crystalline phase assemblage of the experimental glasses as determined by X-ray diffraction (XRD) analysis (not shown) revealed that all the investigated glass compositions were amorphous after heat treatment at 600 ºC. Lithium disilicate (LD, $Li_2Si_2O_5$) was recorded as the single crystalline phase in the glasses of series A at 700 ºC and 800 ºC and the intensity of the peaks of LD slightly increased with the rising temperature, while traces of cristobalite appeared at 900 ºC. The addition of Al_2O_3 in the $Li_2O–SiO_2$ system (series B) enhanced the intensity of LD peaks and the formation of lithium aluminium silicate (LAS, $LiAlSi_2O_6$). On the other hand, earlier studies [30-31] suggested that adding an excessive amount

of K_2O tends to suppress the crystallization of LD and to promote the formation of lithium metasilicate (LMS, Li_2SiO_3) due to its lower activation energy for crystallization in comparison to that of LD.[32-33]

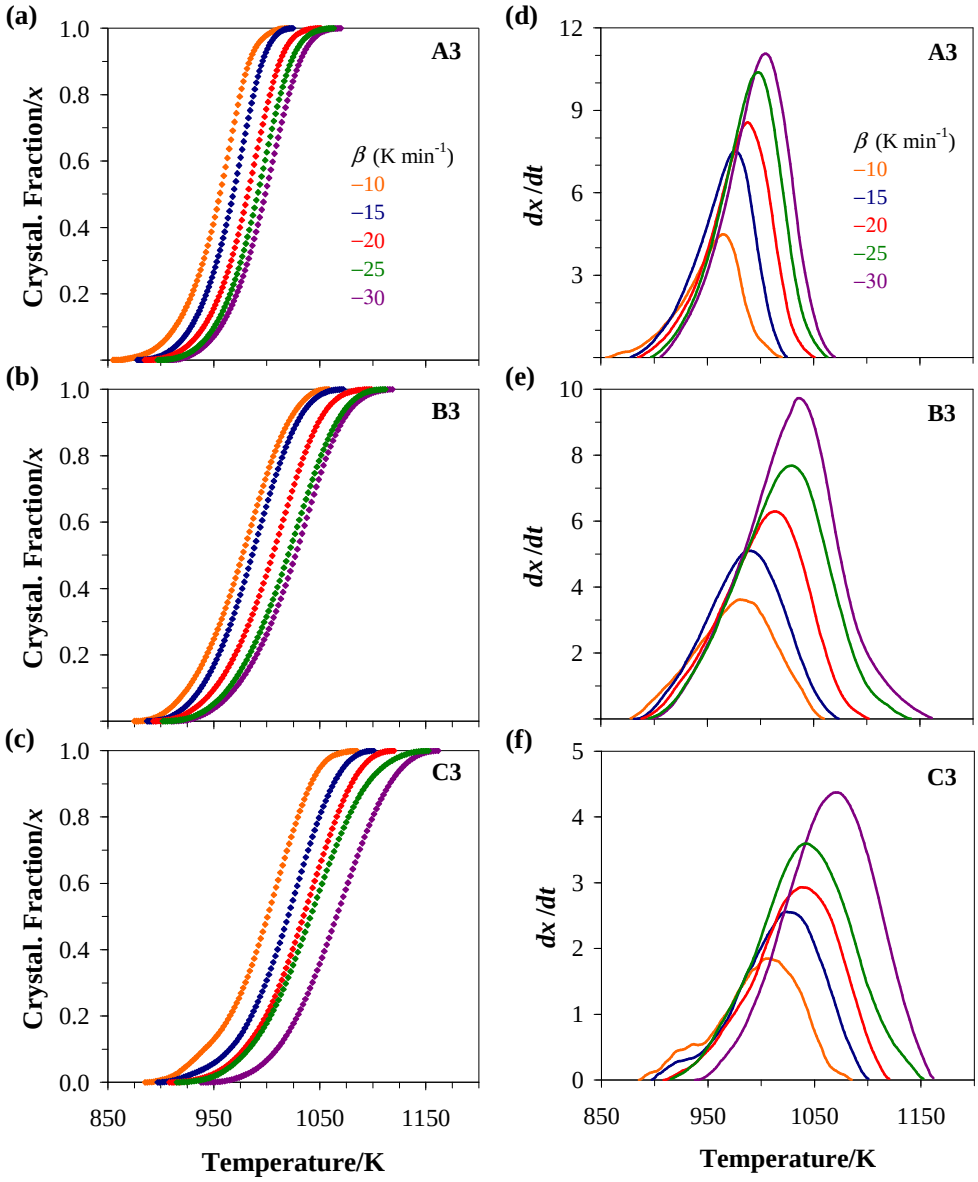

Fig. 3 – Evolution of crystallized fraction *x* and *dx*/*dt* with temperature for A3, B3 and C3 at different heating rates.

Table 3 – Thermal parameters of glasses as determined by DTA at β = 20 K min^{-1}.

	DTA at 20 K min^{-1}		
Composition	T_g /K	T_c /K	T_p /K
A1	498	587	737
A2	495	606	733
A3	491	612	717
B1	504	662	781
B2	500	639	773
B3	495	620	746
C1	503	695	806
C2	500	663	800
C3	496	658	778

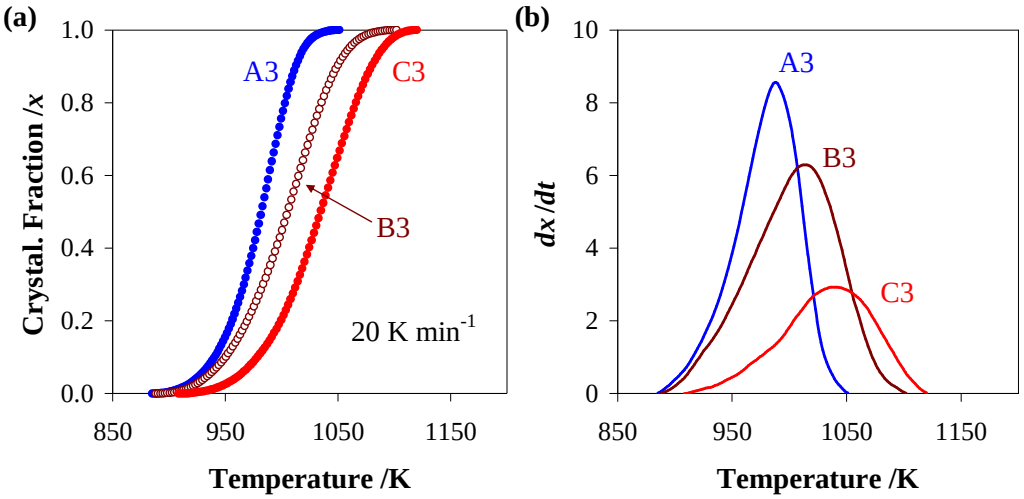

Fig. 4 – Crystallized fraction and *dx*/*dt versus* temperature for A3, B3 and C3 at 20 K min^{-1}.

The activation energy for glass crystallization (E_c) can be estimated using the same Kissinger formalism used in equation (2):[12, 21]

$$\ln\frac{\beta}{T_p^2} = -\frac{E_c}{RT_p} + const. \qquad (4)$$

Plotting the variation of $\ln(\beta/T_p^2)$ as a function of $1000/RT_p$ allows obtaining straight lines, the slopes of which give the activation energy values for crystallization (E_c). The Avrami parameter n was determined according to the method proposed by Augis and Bennett,[34] equation (5):

$$n = \frac{2.5}{\Delta T_{FWHM}} \frac{RT_p^2}{E_c} \quad (5)$$

where ΔT_{FWHM} is the full width of the DTA exothermic peak at the half maximum and E_c was estimated from equation (4).

The kinetic parameters of crystallization have also been estimated using a method suggested specifically for non-isothermal experiments by Matusita *et al.*.[27, 35-36] The crystallized volume fraction (x), precipitated in a glass heated at constant heating rate (β) is related to the effective activation energy of amorphous-crystalline transformation, E_c, through the following expression:

$$\ln[-\ln(1-x)] = -n\ln\beta - 1.052\, m\frac{E_c}{RT} + const. \quad (6)$$

where m is an integer that depends on the dimensionality of growth of the crystal, and n being a numerical factor depending also on the nucleation process. For as-quenched glasses containing no nuclei $m = (n - 1)$ and for glasses containing a sufficiently large number of nuclei, which might occur due to annealing of the as quenched glass, $m = n$.[36] The E_c and n values estimated by both methods are reported in Table 4.

Figure 5 presents the Kissinger plots for compositions A3, B3 and C3 while the variation of ln[–ln(1–x)] with ln(β) and the plot of ln[–ln(1–x)] *versus* 1000/RT_p (derived from Matusita's method) are shown in Figs. 6a-c and Figs. 7a-c, respectively. All plots show straight lines (except at high β), thus indicating the validity of the methods [21] for estimating the values of E_c and n (Table 4). Additionally, similar values could be estimated from Kissinger and Matusita methods as shown in Fig. 8. The binary system shows the lower value of activation energy for crystallization (A1) while quaternary system features the highest one (C1). However, while E_c increases with decreasing the SiO_2/Li_2O ratio for compositions in the system Li_2O–SiO_2, the opposite trend is observed for compositions with added Al_2O_3 and K_2O. Moreover, larger E_c variations as a function of SiO_2/Li_2O ratio were observed for the quaternary compositions (group C), with the lowest E_c value being associated with the highest content of K_2O (C3).

Glasses in groups B and C featured the same alkali oxides content and therefore demonstrated similar values for T_g, which are higher than T_g of glasses in series A. This could be understood considering that the alkaline ions (Li^+, K^+) are likely to be partially associated with Al^{3+} (especially for the lower added amounts) in tetrahedral glass forming units. The

excess of alkaline oxides will tend to act as glass modifiers and to increase the ionic mobility decreasing T_g. With regard to changes in activation energy one can see that initial addition of Al_2O_3 (glass B1) and Al_2O_3 +K_2O (glass C1) resulted in E_c rising. In particular, glass C1 with the lowest K_2O content demonstrated highest E_c among all investigated compositions. On the other hand, further addition of K_2O in series C caused sharp E_c decrease that can be related to mixed alkali effect (Table 3, Fig. 8).

Table 4 – The E_c and n for the crystallization region of experimental glasses obtained from different methods.

Composition	Kissinger			Matusita	
	E_c /kJ mol^{-1}	R^2	n	E_c /kJ mol^{-1}	n
A1	169.2 ± 7.7	0.993	1.42 ± 0.09	170.8 ± 9.0	1.49 ± 0.08
A2	171.1 ± 5.9	0.996	1.64 ± 0.06	190.4 ± 9.9	1.40 ± 0.08
A3	202.2 ± 8.2	0.995	1.67 ± 0.08	198.2 ± 7.3	1.68 ± 0.09
B1	215.1 ± 6.4	0.997	1.22 ± 0.11	178.5 ± 5.1	1.53 ± 0.04
B2	180.4 ± 9.2	0.994	1.35 ± 0.07	175.0 ± 10.4	1.55 ± 0.04
B3	149.2 ± 7.2	0.995	1.55 ± 0.08	155.6 ± 7.2	1.60 ± 0.10
C1	247.4 ± 8.2	0.999	0.85 ± 0.07	258.3 ± 22.5	1.03 ± 0.09
C2	156.9 ± 9.3	0.996	1.27 ± 0.04	161.2 ± 12.5	1.25 ± 0.17
C3	144.1 ± 7.7	0.989	1.64 ± 0.08	145.1 ± 3.2	1.69 ± 0.03

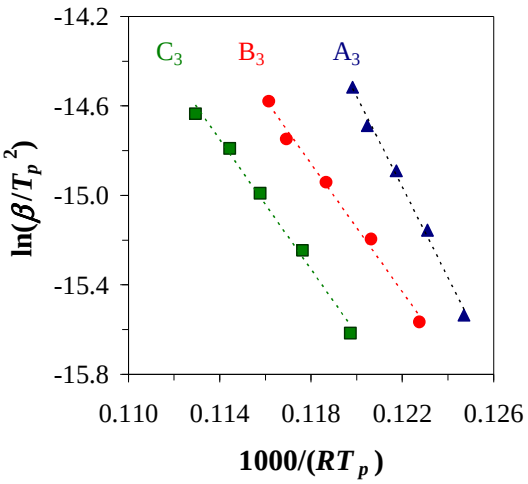

Fig. 5 – Kissinger plots (E_c) for A3, B3 and C3.

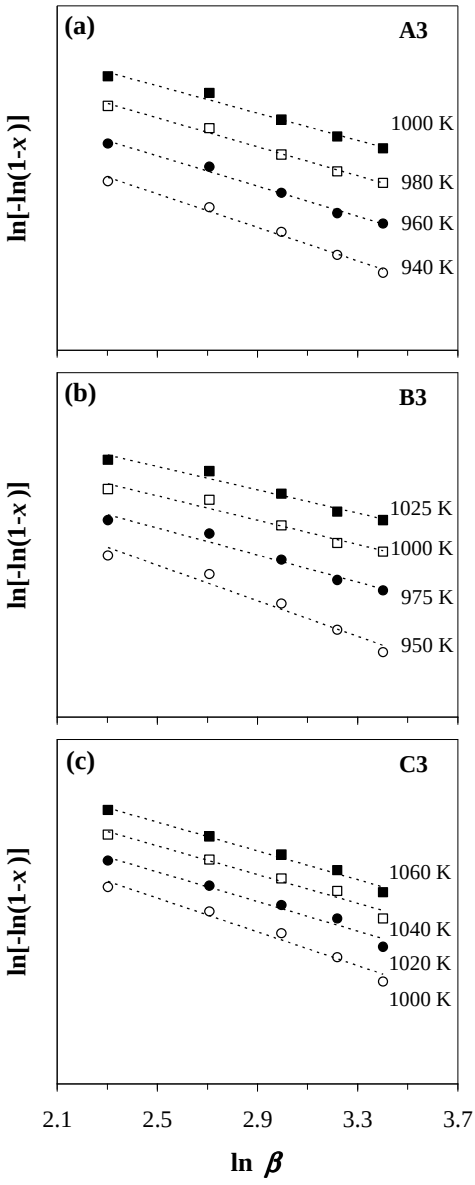

Fig. 6 – Variation of ln[–ln(1–*x*)] with ln(β) for A3, B3 and C3.

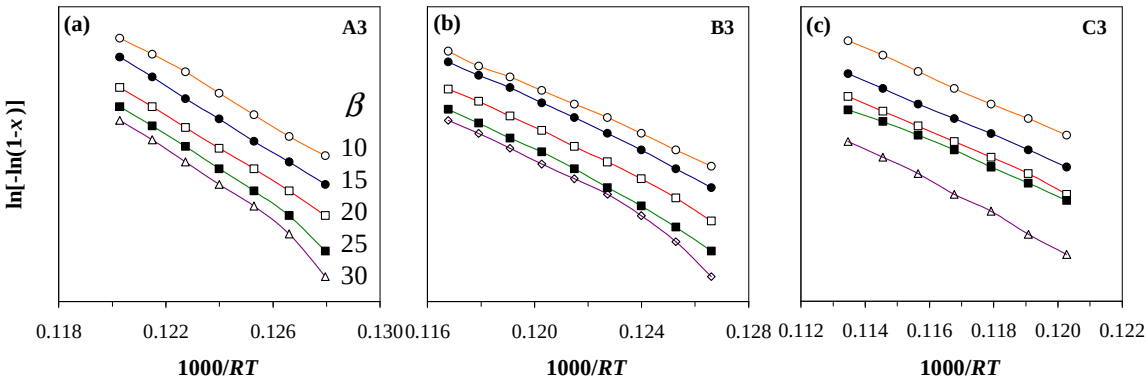

Fig. 7 – Variation of ln[–ln(1–*x*)] with $1000/RT_p$ for A3, B3 and C3.

Significant changes of Avrami parameter *n* are also observed with the variation of glass composition (Fig. 8). The lowest *n* value was obtained for composition C1 (0.85±0.07 and 1.03±0.09, according to Kissinger and Matusita methods, respectively), suggesting that these glasses are prone to surface crystallization, and the general trend for *n* is A > B > C. However, *n* tends to increase with decreasing the SiO_2/Li_2O ratio, suggesting that crystallization occurs via both surface and bulk mechanisms, although surface crystallization appears to be the dominant one (Table 4, Fig. 8). This phenomenon is more pronounced in the glasses of series C that can be clearly observed from the changes in their microstructure after heat treatment (Figs. 9a-b). Thus, composition C1 heat-treated at 800 ºC feature surface crystallization as evidenced by the crystalline layer with about 1 mm thickness (Fig. 9a). Moreover, the inner part of this sample has no evidence of any crystalline phase. On the contrary, glass C3 treated at 700 ºC shows a crystalline layer on the surface along with dispersed crystals in the volume of the sample (Fig. 9b), suggesting the occurrence of both surface and bulk crystallization. These microstructural evolutions are in good agreement with the changes in the Avrami parameter *n* displayed in Fig. 8.

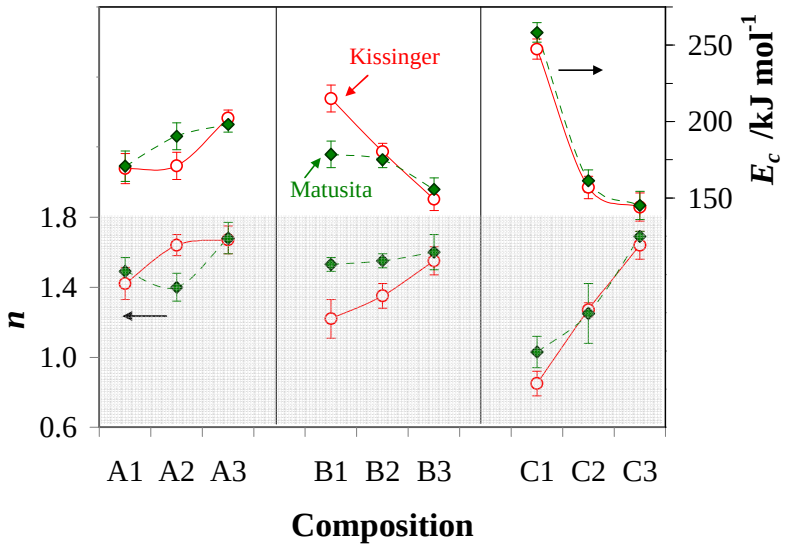

Fig. 8 – Variation of E_c and *n* with composition.

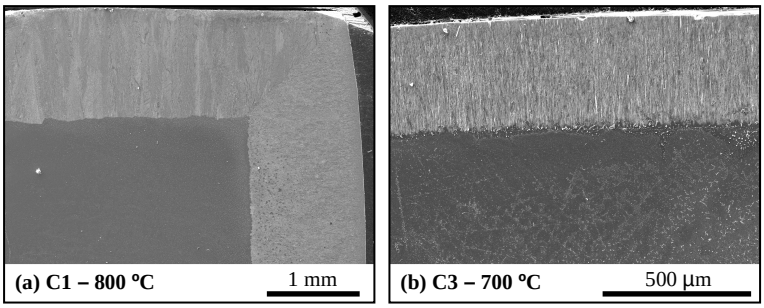

Fig. 9 – Microstructure of C1 heat-treated at 800 ºC (a) and C3 at 700 ºC (b).

4. Conclusions

The results presented and discussed along this work enable the following conclusions to be drawn:

1. The enrichment of the glass composition in Li_2O (decreasing the SiO_2/Li_2O ratio) caused a general increase of the activation energy for glass transition (E_g), enhanced E_c for the binary systems, and decreased E_c for the ternary and quaternary compositions.
2. Binary compositions showed stronger tendency toward crystallization while the addition of Al_2O_3 and K_2O caused slightly shifts in T_g to higher temperatures and enhanced the glass stability against crystallization. The enhanced polymerization of the glassy matrix is consistent with the association of Li^+/Al^{3+} and K^+/Al^{3+} in tetrahedral glass forming units for the lower contents of alkaline elements. The excess of alkaline elements tend to exert an opposite effect.
3. Surface crystallization is the predominant crystallization mechanism especially for the higher SiO_2/Li_2O ratios, being more evident for the ternary and quaternary systems.

Acknowledgment

Hugo R. Fernandes is grateful for the financial support of CICECO and for the PhD grant (SFRH/BD/41307/2007) from the FCT, Portugal.

References

1. Sesták J. Science of Heat and Thermophysical Studies: A Generalized Approach to Thermal Analysis. Amsterdam: Elsevier; 2005.
2. Mehta N, Kumar A. Applicability of Kissinger's relation in the determination of activation energy of glass transition process. Journal of Optoelectronics and Advanced Materials 2005;7(3):1473-78.
3. Moynihan CT, Easteal AJ, Wilder J, Tucker J. Dependence of the glass transition temperature on heating and cooling rate. Journal of Physical Chemistry 1974;78(26):2673-77.
4. Dakui D, Fuding M, Zhengxie Y, Meixin Z. Kinetic study of the crystallization of ZrF_4–BaF_2–LaF_3–AlF_3 glasses. Journal of Non-Crystalline Solids 1989;112(1-3):238-43.
5. Gao YQ, Wang W. On the activation energy of crystallization in metallic glasses. Journal of Non-Crystalline Solids 1986;81(1-2):129-34.
6. Avrami M. Kinetics of phase change. I — general theory. Journal of Chemical Physics 1939;7:1103-12.
7. Avrami M. Kinetics of phase change. II — transformation-time relations for random distribution of nuclei. Journal of Chemical Physics 1940;8:212-24.
8. El-Salam A, Abousehly M. Activation energy of $Se_2Ge_{0.2}Sb_{0.8}$ chalcogenide glass by differential scanning calorimetry. Journal of Thermal Analysis and Calorimetry 1996;46(1):177-86.
9. Starink MJ, Zahra AM. Determination of the transformation exponent s from experiments at constant heating rate. Thermochimica Acta 1997;298 179-89.
10. Vázquez J, López-Alemany PL, Villares P, Jiménez-Garay R. Generalization of the Avrami equation for the analysis of non-isothermal transformation kinetics. Application to the crystallization of the $Cu_{0.20}As_{0.30}Se_{0.50}$ alloy. Journal of Physics and Chemistry of Solids 2000;61:493-500.
11. Avrami M. Avrami M. Kinetics of phase change. III — granulation, phase change, and microstructure. Journal of Chemical Physics 1941;9:177-84.
12. Kissinger HE. Variation of peak temperature with heating rate in differential thermal analysis. Journal of Research of the National Bureau of Standards 1956;57(4):217-21.
13. Lasocka M. Thermal stability of Ge-As-Te-In glasses. Materials Science and Engineering 1976;23:173-77.
14. Lezal D, Zavadil J, Prochazka M. Sulfide, selenide and telluride glassy systems for optoelectronic applications. Journal of Optoelectronics and Advanced Materials 2005;7:2281-91.
15. Joshi SR, Pratap A, Saxena NS, Saksena MP, Kumar A. Heating rate and composition dependence of the glass transition temperature of a ternary chalcogenide glass. Journal of Materials Science Letters 1994;13(2):77-79.
16. Lin C, Li Z, Ying L, Xu Y, Zhang P, Dai S, et al. Network structure in GeS_2–Sb_2S_3 chalcogenide glasses: raman spectroscopy and phase transformation study. Journal of Physical Chemistry C 2012;116(9):5862-67.
17. Shelby JE. Effect of morphology on the properties of alkaline earth silicate glasses. Journal of Applyed Physics 1979;50:8010-15.
18. Vogel W. Structure and Crystallization of Glasses. Leipzig: Pergamon Press; 1971.
19. Giridhar A, Mahadevan S. The T_g versus Z dependence of glasses of the Ge–In–Se system. Journal of Non-Crystalline Solids 1992;151(3):245-52.

20. Rabinal MK, Sangunni KS, Gopal ESR. Chemical ordering in $Ge_{20}Se_{80-x}In_x$ glasses. Journal of Non-Crystalline Solids 1995;188(1-2):98-106.
21. Kissinger HE. Reaction kinetics in differential thermal analysis. Analytical Chemistry 1957;29(11):1702-06.
22. White K, Crane RL, Snide JA. Crystallization kinetics of $As_{2-x}Sb_xS_3$ glass in bulk and thin film form. Journal of Non-Crystalline Solids 1988;103(2-3):210-20.
23. Imran MMA, Bhandari D, Saxena NS. Enthalpy recovery during structural relaxation of $Se_{96}In_4$ chalcogenide glass. Physica B: Condensed Matter 2001;293(3-4):394-401.
24. Agarwal P, Goel S, Rai JSP, Kumar A. Calorimetric studies in glassy Se80−xTe20Inx. Physica Status Solidi (a) 1991;127(2):363-69.
25. Deepika KSR, Saxena NS. Kinetics of phase transformations and thermal stability of $Se_{58}Ge_{42-x}Pb_x$ (x = 15, 18 & 20) Glasses. New Journal of Glass and Ceramics 2012;2:23-33.
26. Johnson WA, Mehl KF. Reaction kinetics in processes of nucleation and growth. Transactions of the American Institute of Mining Engineers 1939;135:416-72.
27. Matusita K, Sakka S. Kinetic study of crystallization of glass by differential thermal analysis - Criterion on application of Kissinger plot. Journal of Non-Crystalline Solids 1980;38-39:741-46.
28. Fernandes HR, Tulyaganov DU, Goel A, Ferreira JMF. Structural characterisation and thermo-physical properties of glasses in the $Li_2O–SiO_2–Al_2O_3–K_2O$ system. Journal of Thermal Analysis and Calorimetry 2011;103(3):827-34.
29. Fernandes HR, Tulyaganov DU, Goel A, Ribeiro MJ, Pascual MJ, Ferreira JMF. Effect of Al_2O_3 and K_2O content on structure, properties and devitrification of glasses in the $Li_2O–SiO_2$ system. Journal of the European Ceramic Society 2010;30(10):2017-30.
30. Fernandes HR, Tulyaganov DU, Pascual MJ, Kharton VV, Yaremchenko AA, Ferreira JMF. The role of K_2O on sintering and crystallization of glass powder compacts in the $Li_2O–K_2O–Al_2O_3–SiO_2$ system. Journal of the European Ceramic Society 2012;32:2283-92.
31. Fernandes HR, Tulyaganov DU, Goel A, Ferreira JMF. Effect of K_2O on structure-property relationships and phase transformations in $Li_2O–SiO_2$ glasses. Journal of the European Ceramic Society 2012;32(2):291-98.
32. Hammetter WF, Loehman RE. Crystallization kinetics of a complex lithium silicate glass-ceramic. Journal of the American Ceramic Society 1987;70(8):577-82.
33. Oliveira APN, Alarcon OE, Manfredini T, Pellacani GC, Siligardi C. Crystallisation kinetics of a $2.3Li_2O.1.1ZrO_2.6.6SiO_2$ glass. Physics and Chemistry of Glasses 2000;41(2):100-03.
34. Augis JA, Bennett JE. Calculation of the Avrami parameters for heterogeneous solid state reactions using a modification of the Kissinger method. Journal of Thermal Analysis 1978;13:283-92.
35. Matusita K, Sakka S. Kinetics study of the crystallization of glass by differential scanning calorimetry. Physics and Chemistry of Glasses 1979;20(4):81-84.
36. Matusita K, Sakka S. Kinetic study on non-isothermal crystallization of glass by thermal analysis. Bulletin of the Institute for Chemical Research 1981;59(3):159-71.

3.8 The role of P_2O_5, TiO_2 and ZrO_2 as nucleating agents on microstructure and crystallization behaviour of lithium disilicate based glass

Hugo R. Fernandes[a], Dilshat U. Tulyaganov[a,b], José M.F. Ferreira[a]

[a] Department of Ceramics and Glass Engineering, University of Aveiro, CICECO, 3810-193 Aveiro, Portugal

[b] Turin Polytechnic University in Tashkent, 17 Niyazova str., 100174 Tashkent, Uzbekistan

Journal of Materials Science (published online, 23 August 2012)

DOI: 10.1007/s10853-012-6793-4

Abstract

The aim of this work was to investigate the effect of different nucleating agents (P_2O_5, TiO_2 and ZrO_2) on the crystallization behaviour and the properties of a parent glass with composition 23.7 Li_2O – 2.63 K_2O – 2.63 Al_2O_3 – 71.78 SiO_2 (mol.%) and SiO_2/Li_2O molar ratio far beyond that of stoichiometric lithium disilicate (LD, $Li_2Si_2O_5$). The scanning electron microscopy (SEM) examination of as cast non-annealed glasses revealed the occurrence of liquid-liquid phase separation for all compositions. P_2O_5 revealed to be effective in promoting bulk crystallization of LD, while TiO_2 and ZrO_2 led to surface crystallization. Moreover, ZrO_2 enhanced the glass polymerization and shifts T_p to higher temperatures hindering crystallization. At 900 ºC, TiO_2-containing glasses feature LD and lithium metasilicate (LMS, Li_2SiO_3), while P_2O_5- and ZrO_2-containing ones present monophasic LD and LMS glass-ceramic, respectively.

Keywords: Glass; Nucleating agents; Crystallization; Thermo-physical properties.

1. Introduction

Glass-ceramics are polycrystalline materials formed through the controlled crystallization of glass during specific heat treatments. Crystallization of glass from the surface or from a small number of sites in the interior usually results in low strength materials with coarse-grained microstructures; in contrast, efficient nucleation of crystals from numerous centres results in fine-grained microstructures and consequently high-strength materials. The role of nucleating agents in initiating glass crystallization from a multitude of centres was the major factor allowing the introduction of glass-ceramics into industrial applications.[1-6]

The lithia–silica glass-ceramics have attracted great interest since the fundamental research of Stookey on the stoichiometric composition of lithium disilicate (LD, $Li_2Si_2O_5$).[7] Later, many comprehensive studies led the development of LD glass-ceramics (GCs) from a variety of compositions.[8-16] It was shown that chronology and morphology of phases formed in this simple binary system could be affected by adding minor amounts of nucleating agents.

The addition of P_2O_5 to LD glass was observed to induce amorphous phase separation and to increase the crystal nucleation rate, simultaneously.[17-19] Recently Bischoff *et al.* [20] provided important insights into the crystallization mechanism of lithium disilicate glass–ceramics starting from non-stoichiometric glass compositions (SiO_2/Li_2O molar ratio was 2.39:1) containing 1.3 mol.% P_2O_5. It was shown that under certain deviations from stoichiometry the formation of LD was preceded by the crystallization of lithium metasilicate (LMS, Li_2SiO_3, SiO_2/Li_2O = 1), contrarily to what is observed in stoichiometric glasses.[11] LMS firstly crystallized at lower temperatures (650–700 ºC) and then reacted with amorphous SiO_2 at higher temperatures to produce LD. Accordingly, the formation of the crystalline silicate phases (LMS, LD) cannot derive from a heterogeneous nucleation processes through epitaxy, but as a heterogeneous nucleation at the interface of an amorphous lithium phosphate phase and the glass matrix.[20]

Titania is an efficient nucleating agent commonly used in the fabrication of glass–ceramics.[2, 21] This oxide is believed to be greatly dissolved in glass melts; however, its high ionic field strength encourages the liquid–liquid phase separation phenomenon to occur during the subsequent heat treatment of solid glass.[2, 21-22] Upon cooling it can precipitate in the form of small titanium oxide or titanium compound species that act as nuclei, facilitating the development of the main crystalline phases.[2, 22] For instance, TiO_2 as nucleating agent in the

$Li_2O–MgO–Zn0–Al_2O_3–SiO_2$ glass-ceramic system led to the formation of Ti-rich droplets leaving the glassy matrix significantly depleted from Ti.[23]

Zirconia (ZrO_2) is another conventional nucleating agent widely used in the several silicate systems,[24-25] which was found to hamper crystal growth and the precipitation of the main crystalline phases (LD and LMS) in the $Li_2O–SiO_2–Al_2O_3–K_2O–P_2O_5$ glasses.[6] Moreover, it was demonstrated that in the $Li_2O–SiO_2$ glass ZrO_2 enhanced the polymerization of the silicate network and amorphous phase separation changing the crystallization route by forming Li_2SiO_3 intermediate prior to $Li_2Si_2O_5$ crystal.[27]

However, the catalytic crystallization of non-stoichiometric lithium silicate glasses with SiO_2/Li_2O molar ratios high than 3:1 was rarely investigated.[28-34] Therefore, the objective of this work was to study the role of P_2O_5, TiO_2 and ZrO_2 on the structural features of the parent glass composition $22.96Li_2O–2.63Al_2O_3–2.63K_2O–71.78SiO_2$ (mol.%) (SiO_2/Li_2O molar ratio of 3.13) and of the glass-ceramics derived thereof.[35]

2. Experimental Procedure

2.1. Glass preparation

A total of 9 new compositions were designed based on the parent composition $22.96Li_2O–2.63Al_2O_3–2.63K_2O–71.78SiO_2$ (mol.%, designated as G). Doping with P_2O_5 was attempted in the amounts of 1, 2 and 3 mol.%, while for TiO_2 and ZrO_2 the added amounts were 1, 3 and 5 mol.%. Nucleating agents were introduced in such a way that either the iO_2/Li_2O molar ratio and the amounts of Al_2O_3 and K_2O remained constant and identical to those of G composition (Table 1).

The powders of technical grade SiO_2 (purity >99.5%) and of reactive grade Al_2O_3, Li_2CO_3, K_2CO_3, TiO_2, ZrO_2, and $NH_4H_2PO_4$, were used. Homogeneous mixtures of batches (~100 g), obtained by ball milling, were calcined at 800 ºC for 1 h and then melted in Pt crucibles at 1550 ºC for 1 h, in air. The glasses were produced in bulk (monolithic) form by pouring glass melts on bronze mould in two different sets: the glasses of one set were immediately annealed at 450 ºC for 1 hour while the other set of glasses was preserved in the non-annealed condition.

2.2. Thermo-physical properties of glasses

The coefficient of thermal expansion (CTE) of the annealed glasses was measured by dilatometry using prismatic samples of bulk glasses with cross section of 3×4 mm^2 (Bahr Thermo Analyse DIL 801 L, Germany; heating rate 5 K min^{-1}). The differential thermal analysis (DTA, Setaram Labsys, Setaram Instrumentation, Caluire, France) of glasses was carried out in air from room temperature to 1000 ºC at heating rate (β) of 20 K min^{-1}. The glass granules with sizes in the range of 500–1000 μm (collected by sieving of crushed non-annealed glass blocks) and weighing 50 mg were contained in an alumina crucible, using α-alumina powder as reference material. The values of glass transition temperature T_g, crystallization onset temperature, T_c and peak temperature of crystallization, T_p were obtained from the DTA scans.

Archimedes' method (i.e. immersion in ethylene glycol) was employed to measure the apparent density of the bulk annealed glasses which was further applied along with compositions of glasses to calculate their excess volume (V_e) according to a procedure described elsewhere.[36]

Table 1 – Compositions of the experimental glasses (mol.%).

#	G	P1	P2	P3	T1	T3	T5	Z1	Z3	Z5
Li_2O	22.96	22.73	22.50	22.27	22.73	22.27	21.81	22.73	22.27	21.81
K_2O	2.63	2.60	2.58	2.55	2.60	2.55	2.50	2.60	2.55	2.50
Al_2O_3	2.63	2.60	2.58	2.55	2.60	2.55	2.50	2.60	2.55	2.50
SiO_2	71.78	71.06	70.34	69.63	71.06	69.63	68.19	71.06	69.63	68.19
P_2O_5	–	1.00	2.00	3.00	–	–	–	–	–	–
TO_2	–	–	–	–	1.00	3.00	5.00	–	–	–
ZrO_2	–	–	–	–	–	–	–	1.00	3.00	5.00

2.3 Crystalline phase analysis and microstructural evolution in glass-ceramics

Bulk parallelepiped annealed glass samples were heat treated non-isothermaly at 600, 700, 800 and 900 ºC for 1 h, respectively, at a heating rate of 2 K min^{-1}. The amorphous nature of the parent glasses and the nature of crystalline phases present in the GCs were determined by X-ray diffraction (XRD) analysis (Rigaku Geigerflex D/Mac, C Series, Japan; Cu K_a

radiation, 2θ between 10º and 60º with a 2θ-step of 0.02 deg s^{-1}). The crystalline phases were identified by comparing the obtained diffractograms with patterns of standards complied by the International Centre for Diffraction Data (ICDD).

Microstructure observations were done at polished (mirror finishing) and then etched surfaces of samples (by immersion in 2 vol.% HF solution for 2 min) by field emission scanning electron microscopy (SEM, Hitachi SU-70, Japan) under secondary electron mode.

3. Results and discussion

3.1. Casting ability and microstructure of glasses

Melting at 1550 ºC for 1 h was adequate to obtain bubble free, homogenous transparent and colourless glasses from the parent composition G, the 1 mol.% P_2O_5–containing P1, and from all the TiO_2 and ZrO_2–containing derivatives. The absence of crystalline inclusions in these compositions was confirmed by XRD and SEM analyses. However, the transparent melts of glasses P2 and P3 (with 2 and 3 mol.% P_2O_5, respectively) tended to acquire a cloudy hazy on cooling. The XRD spectrograms of samples P2 and P3 (not shown) evidenced few and very weak peaks most probably belonging to both silicon oxide and lithium orthophosphate Li_3PO_4 phases. Thus no further examination was performed on those glasses.

The SEM image of the as cast non–annealed parent glass G (Fig. 1(a)) shows liquid–liquid phase separation into droplet like zones of Li-rich phase and SiO_2-rich glass matrix. This type of primary segregation was demonstrated elsewhere.[35] Addition of 1 mol.% P_2O_5 into G did not significantly affect the mean droplet diameter and the population density of droplets, but caused the formation of round shaped zones (Fig. 1(a)). This type of segregation might be related to separation of phosphate phase since no similar observation was revealed in the parent glass G. This type of segregation might be due to the incompatibility of the PO_4 units in the silicate structure.[37] Segregation is promoted by the high field strength of P^{5+} that equals 2.1 [38] and by presence of network modifiers such as the Li^+ ions that will preferably diffuse towards phosphate groups assuming field strength consideration. The separate orthophosphate groups that are charge balanced by lithium,[37, 39] may spontaneously crystallise upon cooling and confer the cloudy appearance to the P2 and P3 glasses.

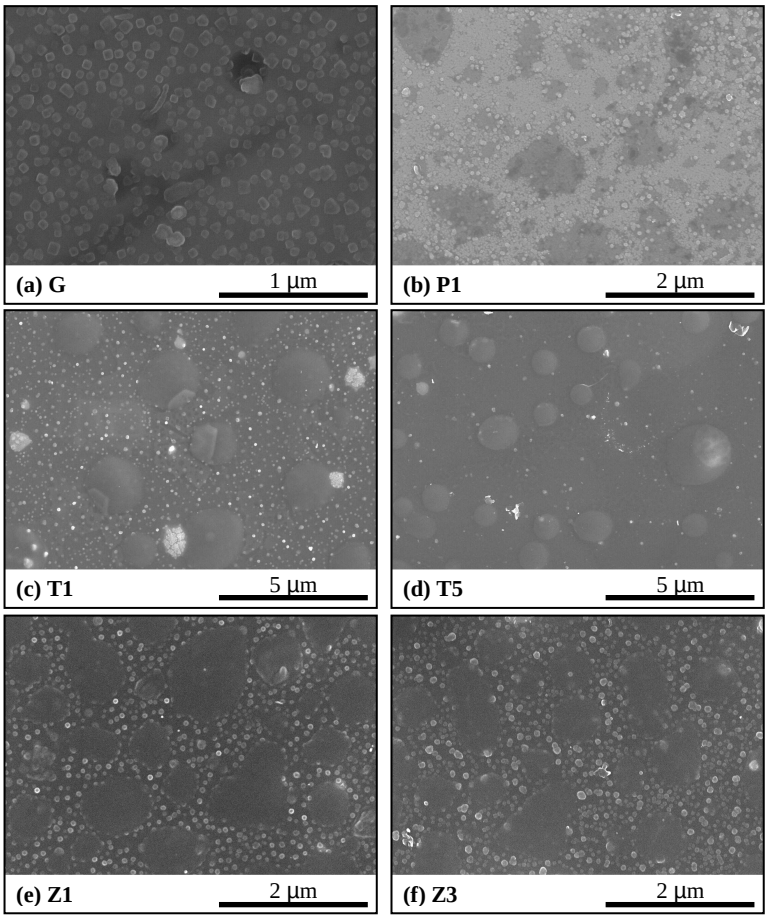

Fig. 1 – SEM images of non-annealed glasses: (a) G, (b) P1, (c) T1, (d) T5. (e) Z1 and (f) Z3.

In the case of TiO_2–containing compositions (Figs. 1(c) and (d)) three glassy phases can be clearly observed: (a) small droplets which resemble a lithium rich phase in the parent glass, (b) bigger spherical droplets, and (c) a silica-rich glass matrix in which both droplet glass phases are embedded. Formation of spherical droplets can be explained by relatively high field strength of Ti^{4+} (1.04 [38]) and ability of titania-rich phase to encourage segregation.[21-22] The SEM images of non-annealed ZrO_2–containing compositions (Figs. 1(e) and (f)) reveal a steady decrease in size of droplet-like zones with increasing ZrO_2 content. According to Dietzel,[40] the contribution of ZrO_2 to the surface tension is more significant than those of SiO_2 and Li_2O. Therefore, adding ZrO_2 to the Li_2O–SiO_2 glasses might lead to equalizing the surface tension of the different phases and weaken the degree of segregation. Moreover, zirconium being in 6-co-ordination number will behave in the glassy lattice as network former ion since Zr occupies a distorted ZrO_6 octahedron which shares corners with SiO_4 tetrahedra with Zr–O–Si angles close to 130°.[40-41]

3.2. Thermo-physical properties of glasses

The properties of the annealed glasses are presented in the Table 2. T_g that is a parameter related to the system viscosity,[40] increased in all the investigated compositions compared to the parent glass. The most significant increment in T_g was revealed for ZrO_2-containing glasses, suggesting increase in the polymerization degree. CTE increased with the first addition of nucleating agents and then decreased for the TiO_2 and ZrO_2 groups. The density values of annealed glasses varied in the range of 2.36–2.52 g cm^{-3}. The observed density variations are composition dependent and can be, in general, explained by atomic weight consideration. Accordingly, the highest values were recorded for the ZrO_2 series, while the lowest ones were measured for the parent glass and P1. Moreover, an increase in density for TiO_2 and ZrO_2 glasses is also a direct consequence of the volume contraction reflected by the significant decreases of structural parameters V_m and V_e.[40]

Table 2 – Thermo-physical properties of the experimental glasses.

	d (g cm^{-3})	V_m (cm^3 mol^{-1})	V_e (cm^3 mol^{-1})	$CTE_{200-400}$ ±0.1 (10^{-7} K^{-1})	T_g ±2 (ºC)	T_{p1} ±2 (ºC)	T_{p2} ±2 (ºC)
G	2.36 ± 0.01	23.38 ± 0.01	1.26 ± 0.01	96.5	505	821	–
P1	2.36 ± 0.01	23.78 ± 0.01	1.20 ± 0.01	112.7	520	661	870
T1	2.38 ± 0.01	23.29 ± 0.04	1.14 ± 0.04	109.1	521	822	–
T3	2.41 ± 0.01	22.96 ± 0.03	0.81 ± 0.03	102.9	526	813	–
T5	2.44 ± 0.02	22.68 ± 0.04	0.53 ± 0.04	102.7	532	808	–
Z1	2.39 ± 0.01	23.41 ± 0.02	1.21 ± 0.02	118.4	522	833	–
Z3	2.45 ± 0.02	23.44 ± 0.01	1.19 ± 0.01	106.0	536	855	–
Z5	2.52 ± 0.03	23.37 ± 0.01	1.06 ± 0.01	97.0	569	856	–

Considering the micro heterogeneous structure of the experimental glasses (Fig. 1) and the prominent role of droplet phases in the nucleation process,[2] further heat treatment for crystal growth was attempted using annealed samples in the interval 600–900 ºC for 1 h. This temperature range was chosen according to the DTA plots of the experimental glasses (β = 20 K min^{-1}) shown in the Fig. 2(a). The glass P1 containing 1 mol.% P_2O_5 exhibits two sharp and well-defined exothermic peaks at 661 and 870 ºC. All the other experimental compositions featured a single exothermic peak but of significantly lower intensity. In particular, DTA

curve of glass containing 1 mol.% ZrO_2 features a single shallow peak that become almost negligible with further ZrO_2 increment (Fig. 2(a)).

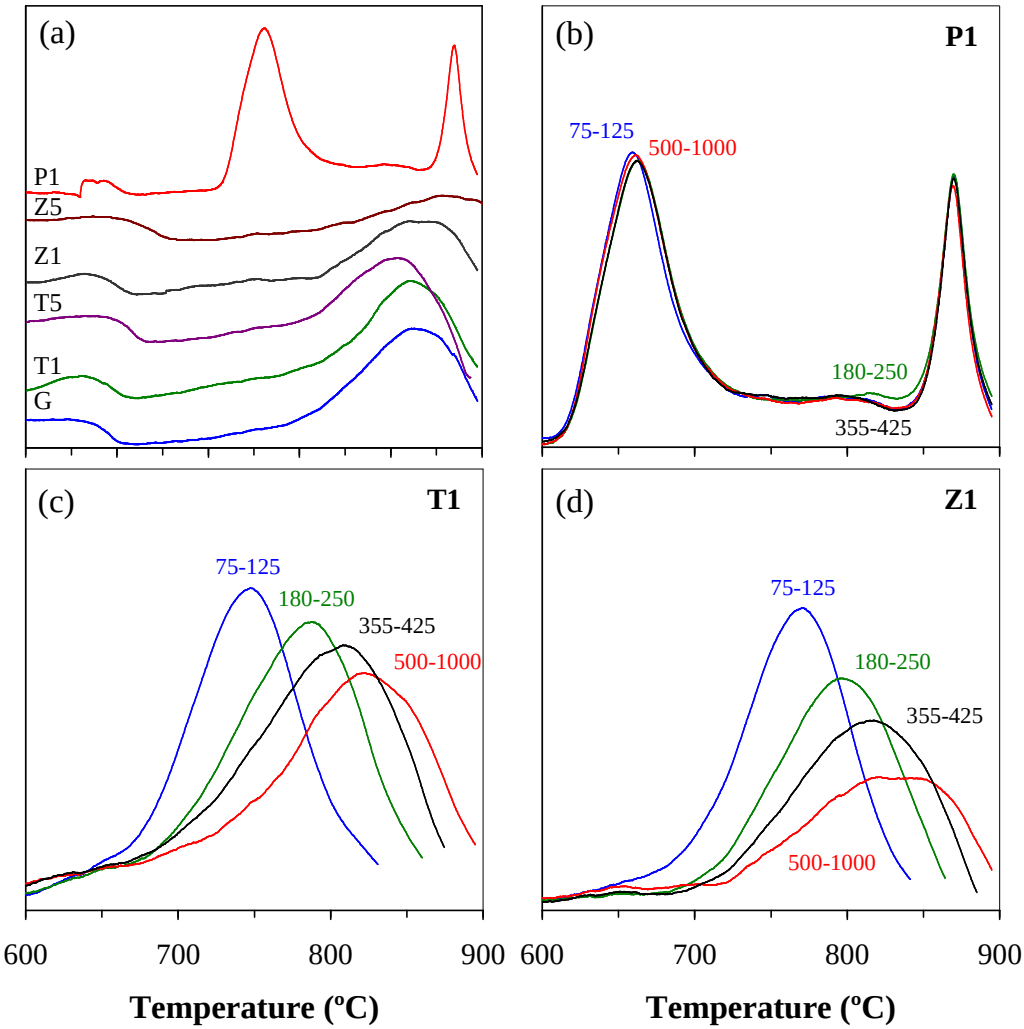

Fig. 2 – The DTA plots (a) glasses with particle size between 500–1000 μm, (b) glass P1 having different particle sizes, (c) glass T1 having different particle sizes, and (d) glass Z1 having different particle sizes (heating rate (β) of K min^{-1}).

In general, as the volume fraction of crystals increases, the heat of crystallization is evolved and the exothermic peak appears on the DTA curves.[29] Consequently, the intensity of the exothermic peak is correlated with the efficiency of nucleating agents to promote nucleation. Additionally, the positioning of the peak temperature of crystallization, T_p, may be a measure of the ease of crystallization; the lower T_p is, more easily the crystallization occurs.[29] The changes in T_p for P1 and ZrO_2 series are in accordance with finding of Matusita *et al.* [29] demonstrating that T_p increases with increasing ionic radius of metal cations in the $25Li_2O{\cdot}75SiO_2{\cdot}3RO_n$ glass (R = Na, K, Cs, Mg, Ca, Sr, Ba, B, A1, In, Ge, Ti, Zr, P or V).

Exception from this tendency was revealed for TiO_2–containing glasses. To explain this phenomenon further crystallization kinetics study of the experimental should be attempted.

DTA curves obtained from the glasses P1, T1 and Z1 having different particle sizes are shown in the Figs. 2 (a-d). For all the glass compositions, except P1, T_p appears at lower temperatures for finer particles, indicating the occurrence of surface crystallization.[42-44] Accordingly, the monoliths from TiO_2 and ZrO_2 series exhibited surface crystallization while P1 glass demonstrated bulk internal crystallization (as will be shown in next subsection 3.3).

3.3. Crystallization of glasses: phase assemblage and microstructure

The general appearance of some experimental glasses after heat treatment at 600, 700, 800 and 900 ºC is presented in Fig. 3. Titania and zirconia containing glasses were still transparent at 600 ºC whilst phosphorous containing composition appeared as semi translucent glass. With increasing the heat treatment temperature to 700 ºC, the TiO_2- and ZrO_2-containing samples turned into opaque glasses, while the translucency degree of P1 glass was almost unaffected. However, the degree of opacity of all the glasses significantly increased with the heat treatment temperature further increasing to 800 and 900 ºC as a consequence of crystals growth.

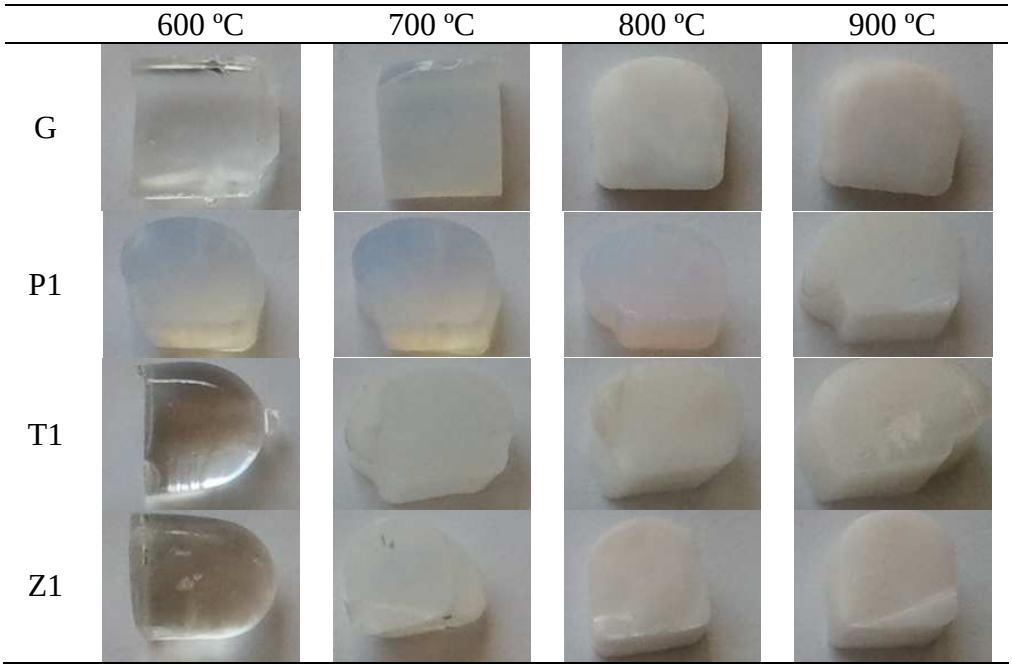

Fig. 3 – The appearance of the bulk heat treated glasses.

Figures 4 (a) to (c) present the XRD spectra of glasses heat treated at different temperatures. All the investigated glasses heat treated for 1 h at 600 ºC were amorphous as evidenced by XRD and SEM (not shown). Crystallization of LMS (Li_2SiO_5) was initiated in P1 at 700 ºC as observed in the XRD spectra (Fig. 4(a)) and SEM image (Fig. 5(a)). LD and small quartz peaks appeared at 800 ºC. LD phase grew up in the temperature range 800–900 ºC turning the P1 heat treated at 900 ºC into a monomineral LD glass-ceramic (Fig. 4(a)). The nucleation process in the parent glass G was initiated from the nanosize Li-rich droplets derived from liquid-liquid phase separation.[35]

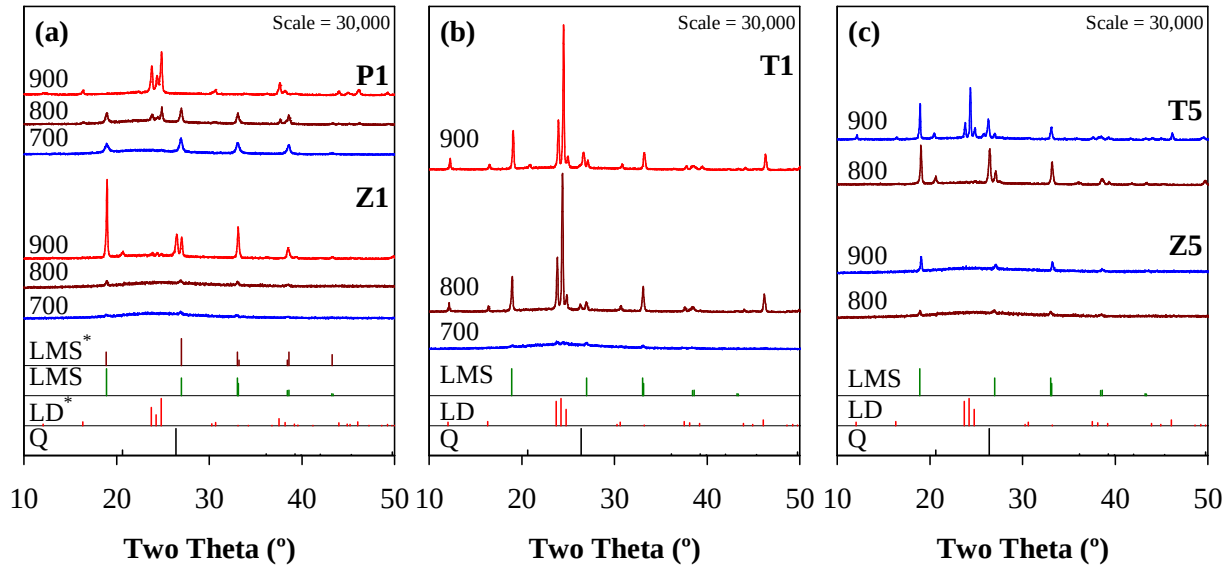

Fig. 4 – XRD of glasses heat treated at different temperatures: (a) P1, (b) T1, (c) Z1, and (d) T5 and Z5.

LD was the major phase with traces of LMS at temperatures <900 ºC, but then opposite trend with growing of former at the expanse of latter was revealed. The mechanism of nucleation and crystal growth in the presence of P_2O_5 seems to be different, leading to the formation of a denser population of tightly interconnected LD crystals (Fig. 5(b) and (c)) but without significant changes in the morphology of LD crystals. A crude epitaxial growth rule has been proposed in some literature reports [37, 45-46] to explain the nucleation and crystallization when at least one of the lattice parameters of the nucleating species and of the growing crystals is within an integer multiple ±15%. The round shaped segregated zones (Fig. 1(a)) formed in the presence of P_2O_5 due to the incompatibility of the PO_4 units in the silicate structure [31] likely consist of Li- and P-rich associations such as Li_3PO_4 a result of the high field strength of P^{5+} (2.1).[38] It is worth noting that for the Li_3PO_4–$Li_2Si_2O_5$ pair, the following proximities can be

registered for the unit cells lattice parameters *a* and *c*: (i) *a* Li_3PO_4 = *a* $Li_2Si_2O_5$ + 8%; (ii) *c* $Li_2Si_2O_5$ = 3*c* Li_3PO_4 − 3%; therefore, being both within the acceptable range.[37] However, the hypothesis of a heterogeneous nucleation at the interface of an amorphous lithium phosphate phase and the glass matrix was considered to be more appropriate to describe the structural changes in this particular system.[20] Similar mechanism of heterogeneous nucleation can be considered when P_2O_5 is incorporated into glasses of the quaternary 22.96Li_2O–2.63Al_2O_3–2.63K_2O–71.78SiO_2 system.

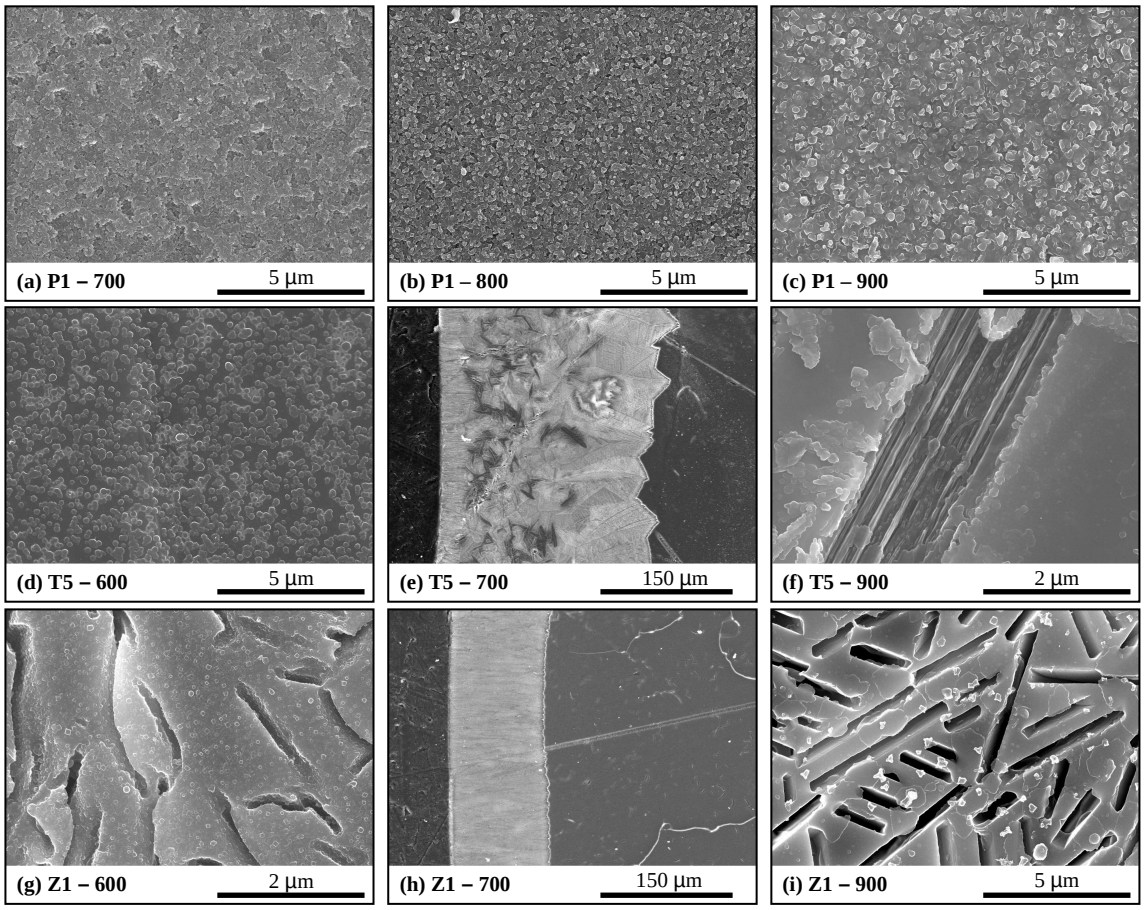

Fig. 5 – SEM of glasses heat treated at different temperatures: (a–c) P1, (d–f) T5, and (g–i) Z1.

The hypothesis of an epitaxial growth mechanism for the LMS in the presence of TiO_2 might be admitted, considering the close proximities of the unit cells lattice parameters *a*, *b* and *c* for the TiO_2–Li_2SiO_3 pair: (i) *a* Li_2SiO_3 = 2*a* TiO_2 + 18%; (ii) *b* Li_2SiO_3 = 2*a* TiO_2 + 2.7 %; (iii) *c* Li_2SiO_3 = 2*c* TiO_2 – 21 %.[38] The fine droplets observed at 600 ºC (about 250 nm) in T5 glass (Fig. 5(d)) are most probably Ti-enriched compounds that act as nuclei and facilitate the development of the main crystalline phases.[2, 22] Unlike to the bulk crystallization observed in

the glass P1, the presence of TiO_2 promoted predominantly surface crystallization as evidenced in (Fig. 5(e)). Typical dendritic crystals of LMS can easily be seen inside this relatively thick crystalline layer.

Both LMS and LD could be identified in the XRD spectra of TiO_2–containing glasses heat treated at 800 and 900 ºC irrespective of the added amount of TiO_2 demonstrating the impossibility of producing monomineral LD GC when this oxide is used alone as nucleating agent. For instance, Fig. 5(f) shows that LMS crystals were almost completely removed during acid etching, while the well-organized interlocking LD crystals are clearly observed in the SEM image due to their high chemical durability.[38]

In the ZrO_2–containing glasses, separated droplets could be seen (Fig. 5(h)) well dispersed in the amorphous matrix heat treated at 600 ºC. Increasing the heat treatment temperature to 700 ºC led to the appearance of a surface crystalline layer, but thinner (Fig. 5(h)) and less expanded that in case of TiO_2 glass, with traces of LMS crystals (Fig. 4(a)). Intensity of LMS did not increase significantly after further heat treatment at 800 ºC while this phase was more pronounced at 900 ºC in Z1. Figure 5 shows the SEM microstructures of Z1 heat treated at 600, 700 ºC and 900 ºC. The amorphous glassy matrix predominates in all of them while some embedded dendrite holes resembling the typical LMS morphology can be seen especially in the sample heat treated at 900ºC. However, LMS formation was significantly suppressed in Z5 (Fig. 4(d) confirming the role of ZrO_2 to hamper crystal growth and the precipitation of the main crystalline phases.[26] No LD was formed in ZrO_2–containing glasses.

4. Conclusions

The effects of single additions of P_2O_5, TiO_2 and ZrO_2 as nucleating agents into non-stoichiometric LD based glass could be summarised as follows:

1. The occurrence of liquid-liquid phase separation was observed in all experimental compositions with some specific and delicate differences, which exert a strong influence in the phase composition and microstructure of GC.
2. Compared to the parent glass, T_g increased with addition of nucleating agents. The most significant increment of T_g was observed for ZrO_2-containing glasses suggesting the highest degree of polymerization. CTE

increased with the first addition and then decreased for the TiO_2 and ZrO_2 groups.

3. Well-defined 2 sharp exothermic peaks were characteristic for the glass P1 the position of which is independent of particle size, denoting bulk crystallization. All the other experimental compositions featured a single exothermic peak with significantly lower intensity and its position was particle size dependent, indicating surface crystallization.
4. Only P_2O_5 led to bulk crystallization, with the formation of LMS at lower temperatures and the crystallization of LD at higher temperatures.
5. Biphasic glass ceramics (LMS + LD) were always obtained in the presence of TiO_2 at 800 and 900 ºC irrespective of the added amount.
6. The addition of zirconia to the parent glass reduces the degree of segregation, increases the polymerization of the glassy matrix, and shifts T_p to higher temperatures hindering crystallization.

Acknowledgment

Hugo R. Fernandes thanks FCT for the PhD grant (SFRH/BD/41307/2007). All authors are grateful for the financial support from CICECO.

References

1. Stookey SD. Catalyzed Crystallization of glass in theory and practice. Industrial and Engineering Chemistry 1959;51(7):805-08.
2. McMillan PW. Glass–Ceramics. London: Academic Press; 1979.
3. Morsi MM, Khater GA, Range KJ. Glass ceramics in the system diopside–anorthite–orthoclase prepared by using some industrial waste materials. Glass Technology - European Journal of Glass Science and Technology Part A 2001;42(6):160-64(5).
4. Beall GH. Advances in Nucleation and Crystallization in Glass. Columbus: American Ceramic Society; 1971.
5. Khater GA, Idris MH. Role of TiO_2 and ZrO_2 on crystallizing phases and microstructure in Li, Ba aluminosilicate glass. Ceramics International 2007;33(2):233-38.
6. Khater GA, Idris MH. Effect of some nucleating agents on thermal expansion behaviour of $Li_2O–BaO–Al_2O_3–SiO_2$ glasses and glass-ceramics. Glass Science and Technology 2005;78(5):189-94.

7. Höland W, Beall G. Glass-ceramic Technology. Westerville, Ohio: The American Ceramic Society; 2002.
8. Barrett JMG (Gainesville, FL), Clark, David E. (Gainesville, FL), Hench, Larry L. (Gainesville, FL), inventor; The Board of Regents, State of Florida, University of Florida (Tallahassee, FL), assignee. Glass-ceramic dental restorations. 1980.
9. Echeverría LM. New lithium disilicate glass-ceramics. Boletin da la Sociedad Espanola de Cerámica y Vidrio 1992;5:183–88.
10. Headley TG, Loehman RE. Crystallization of Glass–Ceramics by Epitaxial Growth. Journal of the American Ceramic Society 1984;67:620-25.
11. James PF. Kinetics of crystal nucleation in silicate glasses. Journal of Non-Crystalline Solids 1985;73:517-40.
12. Ota R, Mishima N, Wakasugi T, Fukunaga J. Nucleation of $Li_2O–SiO_2$ glass and its interpretation based on a new liquid model. Journal of Non-Crystalline Solids 1997;219:70-74.
13. Ray CS, Day DE, Huang W, Narayan KL, Cull TS, Kelton KF. Non-isothermal calorimetric studies of the crystallization of lithium disilicate glass. Journal of Non-Crystalline Solids 1996;204(1):1-12.
14. Schweiger M. Microstructure and mechanical properties of a lithium disilicate glass–ceramic in the $SiO_2–Li_2O–K_2O–ZnO–P_2O_5$ system. Glastechnische Berichte-Glass Science and Technology 2000;73:43–50.
15. von Clausbruch CS, Schweiger M, Holand W, Rheinberger V. The effect of P_2O_5 on the crystallization and microstructure of glass-ceramics in the $SiO_2–Li_2O–K_2O–ZnO–P_2O_5$ system. Journal of Non-Crystalline Solids 2000;263(1-4):388-94.
16. Zanotto ED. Metastable phases in lithium disilicate glasses. Journal of Non-Crystalline Solids 1997;219:42-48.
17. Doremus RH, Turkalo AM. Crystallization of lithium disilicate in lithium silicate-glasses. Physics and Chemistry of Glasses 1972;13(1):14-&.
18. Iqbal Y, Lee WE, Holland D, James PF. Crystal nucleation in P_2O_5-doped lithium disilicate glasses. Journal of Materials Science 1999;34(18):4399-411.
19. James PF, McMillan PW. Quantitative measurements of phase separation in glasses using transmission electron microscopy. Part 1. Experimental technique and method of analysis. Physics and Chemistry of Glasses 1970;11(3):59-&.
20. Bischoff C, Eckert H, Apel E, Rheinberger VM, Holand W. Phase evolution in lithium disilicate glass–ceramics based on non-stoichiometric compositions of a multi-component system: structural studies by ^{29}Si single and double resonance solid state NMR. Physical Chemistry Chemical Physics 2011;13:4540-51.
21. Guignard M, Cormier L, Montouillout V, Menguy N, Massiot D. Structural fluctuations and role of Ti as nucleating agent in an aluminosilicate glass. Journal of Non-Crystalline Solids 2010;356:1368-73.
22. Shelby JE. Introduction to glass science and technology. Cambridge: The Royal Society of Chemistry; 1997.
23. Barbieri L, Leonelli C, Manfredini T, Siligardi C, Corradi AB. Nucleation and crystallization of a lithium aluminosilicate glass. Journal of the American Ceramic Society 1997;80(12):3077-83.
24. Partridge G. Nucleation and crystallization phenomena in low expansion $Li_2O–Al_2O_3–SiO_2$ glass ceramics. Glass Technology 1982;23:133-38.
25. Strnad Z. Glass-ceramic Materials. Amsterdam: Elsevier; 1986.

26. Apel E, van't Hoen C, Rheinberger V, Holand W. Influence of ZrO_2 on the crystallization and properties of lithium disilicate glass-ceramics derived from a multi-component system. Journal of the European Ceramic Society 2007;27:1571-77.
27. Lin CC, Shen PY, Chang HM, Yang YJ. Composition dependent structure and elasticity of lithium silicate glasses: Effect of ZrO_2 additive and the combination of alkali silicate glasses. Journal of the European Ceramic Society 2006;26(16):3613-20.
28. Goharian P, Nemati A, Shabanian M, Afshar A. Properties, crystallization mechanism and microstructure of lithium disilicate glass–ceramic. Journal of Non-Crystalline Solids 2010;356(4-5):208-14.
29. Matusita K, Sakka S, Maki T, Tashiro M. Study on crystallization of glass by differential thermal analysis. Effect of added oxide on crystallization of Li_2O–SiO_2 glasses. Journal of Materials Science 1975;10:94-100.
30. Partridge G. Phases and transformations in lithium-zinc silicate glass ceramics. Glass Technology 1979;20(6):246-51.
31. Ananthanarayanan A, Kothiyal GP, Montagne L, Revel B. MAS-NMR studies of lithium aluminum silicate (LAS) glasses and glass–ceramics having different Li_2O/Al_2O_3 ratio. Journal of Solid State Chemistry 2010;183:120-27.
32. Ananthanarayanan A, Kothiyal GP, Montagne L, Revel B. MAS-NMR investigations of the crystallization behaviour of lithium aluminum silicate (LAS) glasses containing P_2O_5 and TiO_2 nucleants. Journal of Solid State Chemistry 2010;183:1416-22.
33. Zheng X, Wen G, Song L, Huang X. Effects of P_2O_5 and heat treatment on crystallization and microstructure in lithium disilicate glass ceramics. Acta Materialia 2008;56(3):549-58.
34. Höland W, Apel E, van Hoen C, Rheinberger V. Studies of crystal phase formations in high-strength lithium disilicate glass-ceramics. Journal of Non-Crystalline Solids 2006;352(38-39):4041-50.
35. Fernandes HR, Tulyaganov DU, Goel A, Ribeiro MJ, Pascual MJ, Ferreira JMF. Effect of Al_2O_3 and K_2O content on structure, properties and devitrification of glasses in the Li_2O–SiO_2 system. Journal of the European Ceramic Society 2010;30(10):2017-30.
36. Fernandes HR, Tulyaganov DU, Goel IK, Ferreira JMF. Crystallization process and some properties of Li_2O–SiO_2 glass-ceramics doped with Al_2O_3 and K_2O. Journal of the American Ceramic Society 2008;91(11):3698-703.
37. O'Donnella MD, Hill RG, Karpukhina N, Law RV. Real time neutron diffraction and NMR of the Empress II glass-ceramic system. Dental Materials 2011;27:990-96.
38. Vogel W. Structure and Crystallization of Glasses. Leipzig: Pergamon Press; 1971.
39. Brow RK. Review: the structure of simple phosphate glasses. Journal of Non-Crystalline Solids 2000;263-264:1-28.
40. Dietzel A. Zusammenhänge zwischen Oberflächenspnnung und Struktur von Glasschmelzen. Kolloid-Z 1942;100(3):368-80.
41. Dargaud O, Cormier L, Menguy N, Galoisy L, Calas G, Papin S, et al. Structural role of Zr^{4+} as a nucleating agent in a MgO–Al_2O_3–SiO_2 glass-ceramics: A combined XAS and HRTEM approach. Journal of Non-Crystalline Solids 2010;356:2928-34.
42. Brauer DS, Karpukhina N, Law RV, Hill RG. Effect of TiO_2 addition on structure, solubility and crystallisation of phosphate invert glasses for biomedical applications. Journal of Non-Crystalline Solids 2010;356:2626-33.
43. Ray CS, Huang WH, Day DE. Crystallization kinetics of a lithia–silica glass: Effect of sample characteristics and thermal analysis measurement techniques. Journal of the American Ceramic Society 1991;74(1):60-66.

44. Donald IW. The crystallization kinetics of a glass based on the cordierite composition studied by DTA and DSC. Journal of Materials Science 1995;30:904 15.
45. Vogel W. Glass Chemistry. Berlin: Springer; 1994.
46. Smith RI, Howie RA, West AR, Aragon PA, Villafuerte CME. The structure of metastable lithium disilicate, $Li_2Si_2O_5$. Acta Crystallographica 1990;C46:363-65.

3.9 Apatite crystallization from glasses in the $Ca_5(PO_4)_3F$–$CaAl_2Si_2O_8$–$CaMgSi_2O_6$–$NaAlSi_3O_8$ system

Hugo R. Fernandes[a], Dilshat U. Tulyaganov[a,b], Manuel J. Ribeiro[c], José M.F. Ferreira[a]

[a] Dep. of Ceramics and Glass Engineering, University of Aveiro, CICECO, 3810-193 Aveiro, Portugal

[b] Turin Polytechnic University in Tashkent, 17 Niyazova str., 100174 Tashkent, Uzbekistan

[c] UIDM, ESTG, Polytechnic Institute of Viana do Castelo, 4900 Viana do Castelo, Portugal

Journal of Non-Crystalline Solids (2012, accepted)

DOI:

Abstract

The aim of the present study is to investigate the apatite formation process from glasses in the fluorapatite–diopside–anorthite–albite system. The effects of partial and total replacement of anorthite fraction by albite in the ternary composition 26 $Ca_5(PO_4)_3F$ − 44 $CaAl_2Si_2O_8$ − 30 $CaMgSi_2O_6$ (wt.%) on the properties of glasses and glass-ceramics were evaluated. The scanning electron microscopy (SEM) examination of glasses revealed the precipitation of a nanosize droplet phase in the glassy matrices suggesting the occurrence of amorphous phase separation in all annealed glasses. An overall trend towards polymerization of the glass network with increasing albite content was demonstrated by employing MAS-NMR and FTIR spectroscopy. X-ray diffraction (XRD) and differential thermal analysis (DTA) were used to assess the effect of albite content on devitrification process and formation of fluorapatite crystalline phase ($Ca_5(PO_4)_3F$).

Key words: Glass; Apatite; Microstructure; Phase separation; Crystallization.

1. Introduction

Apatite based materials have gained a considerable interest in the last decades due to their application as functional materials in medicine and dentistry [1-5] as well as in optoelectronics.[6-7] Crystallization of glasses is a useful method of obtaining a wide range of apatite containing glass-ceramics, which have unusual microstructures and physical properties.[8-9] The synthesis of the parent glass is an important step of the development of the final glass-ceramic material because the principal components and their proportion in the glass composition govern the precipitation of the crystalline phases. The results of this process endow the resultant glass-ceramic with the desired properties.

Glass-ceramics with fluorapatite (FAp) crystals are durable biomaterials useful for dental restoration. In this regard, a number of glass-ceramic compositions have been proposed by W. Höland *et al*. in recent years exploiting the principles of controlled nucleation and crystallization in various inorganic based glasses.[9-10] A distinction was made by Höland *et al*. [9-10] between two general mechanisms of nucleation and crystallization in glasses that are used for the development of glass-ceramics: surface mechanisms and internal mechanisms. The formation of apatite in glass-ceramics was reported to be controlled by internal nucleation mechanisms where glass-in-glass phase separation played an important role.[11] The glasses exhibited two different types of droplet phases, one enriched in CaO/P_2O_5 oxides, which leads to the nucleation of apatite, and a silica-rich phase that originates the formation aluminosilicate nuclei and the growth of crystalline phases such as leucite ($KAlSi_2O_6$). This amorphous phase separation (APS) thus triggers the double nucleation process and crystallization through surface reactions.[5, 12] This double nucleation and crystallization mechanism from the spherical segregated droplets was confirmed by TEM observations in a glass with a composition: 67.6 SiO_2, 12.8 Al_2O_3, 0.5 Li_2O, 2.8 CaO, 1.2 P_2O_5, 5.7 Na_2O, 8.6 K_2O, 0.8 F (wt.%). An apatitic phase with spherical morphology was firstly formed, which then was fully converted into FAp through a solid state reaction.[11] Fluorapatite was found to easily crystallize from the glass melts with relatively wide compositional ranges: 22.1–45.0 SiO_2, 9.0–21.8 Al_2O_3, 7.3–18.9 CaO, 6.0–19.6 P_2O_5, 16.2–21.0 Na_2O, 0–24.4 K_2O, 7.0–10.1 F (wt.%).[13] Glasses demonstrated phase separation into CaO/P_2O_5-rich droplet phase and silica enriched matrix phase. FAp was the main crystalline phase formed in all glasses studied.

The main aim of the present study is to investigate apatite formation process from glasses in the fluorapatite–diopside–anorthite–albite system. The information gathered will be of high

relevance to select the experimental conditions leading to the preparation of fine grade glass-ceramic coatings on ceramic substrates.[14-15] The base glass (A) was selected from the anorthite primary field of crystallization in the ternary FAp–anorthite–diopside system [26 FAp ($Ca_5(PO_4)_3F$), 44 anorthite ($CaAl_2Si_2O_8$) and 30 diopside ($CaMgSi_2O_6$) (wt.%)] previously studied by Tulyganov.[16]

2. Experimental Procedure

2.1. Glass and glass-ceramic preparation

The chemical composition of the starting glass (hereafter named A) was designed in order to obtain the calculated fractions of the following phases (wt.%): 26 fluorapatite (FAp, $Ca_5(PO_4)_3F$), 44 anorthite (An, $CaAl_2Si_2O_8$), 30 diopside (Di, $CaMgSi_2O_6$). Glasses B, C and D resulted from replacement of 50, 75 and 100 mol.% of An by albite (Al, $NaAlSi_3O_8$) in the parent glass composition, respectively. Table 1 and Table 2 present the detailed mineralogical-based and oxide-based compositions of the experimental glasses. Furthermore, four new B_2O_3-containing compositions were prepared based on the glasses C and D, namely: C–B4 (96 wt.% C and 4 wt.% B_2O_3); C–B8 (92 wt.% C; and 8 wt.% B_2O_3); D–B4 (96 wt.% D and 4 wt.% B_2O_3); and D–B8 (92 wt.% D and 8 wt.% B_2O_3).

Powders of technical grade SiO_2 (purity >99.5%) and of reactive grade Al_2O_3, $CaCO_3$, $MgCO_3$, Na_2CO_3, NH_6PO_4, CaF_2 and H_3BO_3 were used. Homogeneous mixtures of batches (~100 g), obtained by ball milling, were calcined at 800 ºC for 1 h and then melted in Pt crucibles at 1500–1550 ºC for 1 h, in air. The glasses were produced in bulk (monolithic) form by pouring glass melts on bronze mould and were immediately annealed at 450 ºC for 1 hour while another set of glasses was preserved in the frit form by quenching the glass melt in cold water. The obtained frits were dried and milled in a high-speed agate mill. The mean particle size of the glass powders as determined by light scattering technique (Beckman Coulter LS 230, CA USA; Fraunhofer optical model) was about 5–10 µm. Rectangular bars with dimensions of 4×5×50 mm^3 were prepared by uniaxial pressing (80 MPa).

Bulk parallelepiped glass samples were non-isothermally heat treated at 700, 750, 800 and 850 ºC for 5 h, respectively, at a heating rate of 2 K min^{-1}. Glass powder compacts were heat treated at 800, 850 and 900 ºC for 1 h at the heating rate of 2 K min^{-1} aimed to prevent deformation of samples.

Table 1 – Mineralogical compositions of the experimental glasses (wt.%).

wt%	26	44	30
A	$Ca_5(PO_4)_3F$	$CaAl_2Si_2O_8$	$CaMgSi_2O_6$
B	$Ca_5(PO_4)_3F$	$Ca_{0.5}Na_{0.5}Al_{1.5}Si_{1.25}O_8$	$CaMgSi_2O_6$
C	$Ca_5(PO_4)_3F$	$Ca_{0.25}Na_{0.75}Al_{1.25}Si_{2.75}O_8$	$CaMgSi_2O_6$
D	$Ca_5(PO_4)_3F$	$NaAlSi_3O_8$	$CaMgSi_2O_6$

Table 2 – Compositions of the experimental glasses.

		SiO_2	Al_2O_3	CaO	MgO	Na_2O	P_2O_5	CaF_2
A	mol.%	38.99	10.40	34.74	9.10	–	5.08	1.69
	wt.%	35.65	16.13	29.65	5.58	–	10.98	2.01
B	mol.%	44.41	7.93	29.34	8.99	2.64	2.05	1.67
	wt.%	41.11	12.45	25.35	5.58	2.52	10.98	2.01
C	mol.%	47.19	6.66	26.57	8.93	4.00	4.99	1.66
	wt.%	43.96	10.53	23.10	5.58	3.84	10.98	2.01
D	mol.%	50.01	5.38	23.75	8.87	5.38	4.96	1.65
	wt.%	46.89	8.56	20.78	5.58	5.20	10.98	2.01

2.2. Thermo-physical properties of glasses

The coefficient of thermal expansion (CTE) of the annealed samples was determined by dilatometry using prismatic samples of bulk glasses with cross section of 3×4 mm^2 (Bahr Thermo Analyse DIL 801 L, Germany; heating rate 5 K min^{-1}). DTA of glass powders was carried out in air (Netzsch 402 EP, Germany) from room temperature to 1200 ºC at 40 K min^{-1}.

Mechanical resistance (3-point bending strength) tests were performed on rectified parallelepiped bars of sintered GCs (Shimadzu Autograph AG 25 TA, 0.5 mm min^{-1} displacement, the results were obtained from 10 different independent samples).

Archimedes' method (*i.e.* immersion in ethylene glycol) was employed to measure the apparent density of the bulk annealed glasses which was further applied along with compositions of glasses to calculate their excess volume (V_e) according to a procedure described elsewhere.[17]

2.3. Structural characterization of glasses and glass-ceramics

^{29}Si MAS-NMR spectra were recorded on a Bruker ASX 400 spectrometer operating at 79.52 MHz (9.4 T) using a 7 mm probe at a spinning rate of 5 kHz. The pulse length was 2 µs and 60 s delay time was used. Kaolinite was used as the chemical shift reference. ^{27}Al MAS-NMR spectra were recorded on a Bruker ASX 400 spectrometer operating at 104.28 MHz (9.4 T) using a 4 mm probe at a spinning rate of 15 kHz. The pulse length was 0.6 µs and 4 s delay time was used. $Al(NO_3)_3$ was used as the chemical shift reference. The Q^n distributions were obtained by curve fitting and spectral deconvolution using DMFIT program (version 2011).[18] Infrared spectra of the glass powders were obtained using an infrared Fourier spectrometer (FTIR, model Mattson Galaxy S-7000, USA) in the range of 300–1500 cm^{-1}. For this purpose, each sample was mixed with KBr in the proportion of 1/150 (by weight) for 15 min and pressed into a pellet using a hand press.

Microstructural observations were done on polished (mirror finishing) surface of samples (etched by immersion in 2 vol.% HF solution for 1–2 min) by scanning electron microscopy (SEM; SU-70, Hitachi, Japan). The crystalline phases were determined by X-ray diffraction (XRD) analysis (Rigaku Geigerflex D/Mac, C Series, Cu K_a radiation, Japan). Copper K_α radiation (λ=1.5406 Å), produced at 30 kV and 25 mA, scanned the range of diffraction angles (2θ) between 10º and 60º with a 2θ-step of 0.02 deg s^{-1}. The phases were identified by comparing the obtained diffractograms with patterns of standards complied by the International Centre for Diffraction Data (ICDD).

3. Results and discussion

Melting at 1500–1550 ºC for 1 h was adequate to obtain bubble free transparent colourless glasses A and B, although in the case of the latter one the transparency was slightly disturbed by the appearance of cloudy regions. Further addition of albite (Al) component to the glasses C and D considerably modified their optical properties converting the transparent glass A into cloudy white opaline materials. The degree of opacity was enhanced in glasses C and D containing B_2O_3 component.

The SEM images of annealed samples presented in Fig. 1 reveal the precipitation of a nanosize droplet phase in the glassy matrices, suggesting the occurrence of APS in all annealed glasses. However, the mean droplet diameter and the population density of droplets increased by adding albite at the expenses of anorthite into the $Ca_5(PO_4)_3F$–$CaAl_2Si_2O_8$–

$CaMgSi_2O_6$ system. In particular, glass A remained transparent owing to a low volume fraction of the segregated phase and very fine scale morphology of droplets with the sizes laying in the interval 25–125 nm. In glass B the population density of droplets drastically increased while the size of the droplets remained similar to A. Glasses C and D exhibited higher degree of segregation compared to B with droplets sizes between 100–400 nm. Moreover, crystallization of FAp within separated droplet phase has already occurred upon casting (Fig. 1b-d). FAp peaks of very low intensity were also detected on XRD spectra of all experimental glasses (not shown) except for glass A. However, the rapid quenching of glass frits in water prevented the crystallization of Fap as revealed by their crystalline-free XRD patterns (not shown).

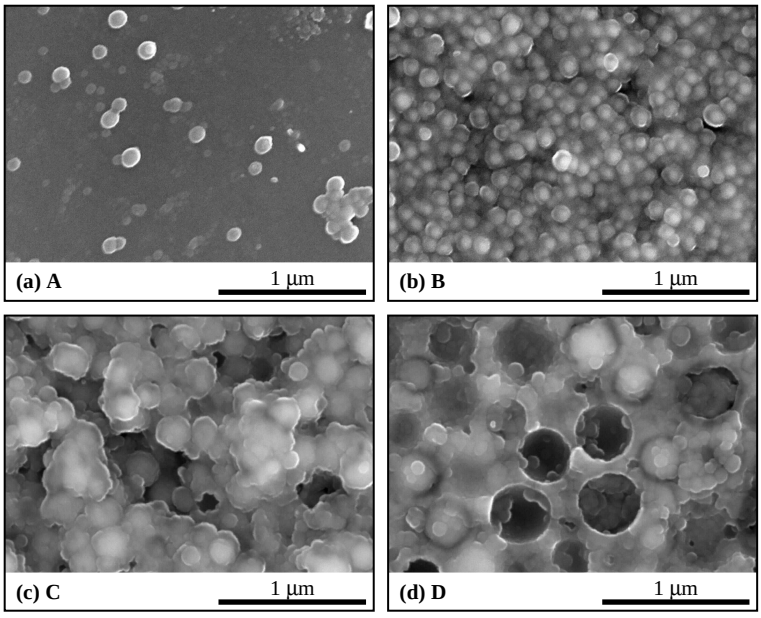

Fig. 1 – SEM images of the experimental glasses etched with 2 vol.% HF solution for 1 min.

The room temperature FTIR transmittance spectra in the region of 300–1300 cm^{-1} of all the experimental glasses are shown in Fig. 2. The most intensive bands lie between 300–600 cm^{-1}, 650–800 cm^{-1} and the 800–1300 cm^{-1}. The broad bands in the 800–1300 cm^{-1} are assigned to the stretching vibrations of the SiO_4 tetrahedron with a different number of bridging oxygen atoms, while the bands in the 300–600 cm^{-1} region are due to bending vibrations of Si–O–Si and Si–O–Al linkages.[19] The transmittance bands in the 650–800 cm^{-1} region are related to the stretching vibrations of the Al–O bonds with Al^{3+} ions in four-fold coordination.[19] The transmittance bands in 800–1300 cm^{-1} region for albite-containing glasses

B, C and D were registered at higher wave numbers than those observed for parent glass A. Thus, the partial or total replacement of An by Al enhances the polymerisation of the glass structure through the formation of more Q^3 units at the expense of Q^2 units.

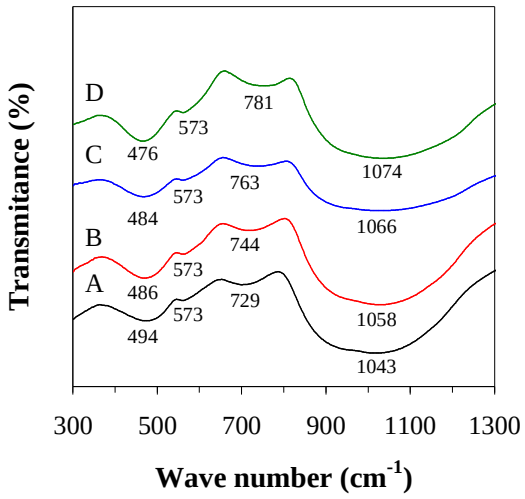

Fig. 2 – FTIR spectra of glass frits.

The ^{29}Si MAS NMR spectra of glasses A and D are shown in Fig. 3a. In general, the spectra feature broad bands, which indicate the amorphous nature of the glass frits. For each composition, a resonance line covers the chemical shift range of silicon in several Q^n groups with n varying from 0 to 4.[20-21] In particular, the ^{29}Si MAS-NMR spectrum for the parent glass A is centred at about −82 ppm (Fig. 3a) and contains ~60% Q^2, ~29% Q^3 and ~11% Q^4 structural units.

The total replacement of An by Al caused a shift of the main ^{29}Si MAS-NMR spectral peak to about −93 ppm (Fig. 3b) and resulted in significant increments in the populations of Q^3 and Q^4 units as can be concluded from the following Q^n distribution: ~39% Q^2, ~42% Q^3 and ~19% Q^4. This enhanced degree of polymerization of the silicate glass network is in good agreement with the FTIR observations. Contrarily, the chemical neighbourhood of Al atoms is less sensitive to glass composition changes. The ^{27}Al MAS NMR spectra of all glasses shown in Fig. 3c are practically identical and centred at 54 ppm, revealing the dominant presence of tetrahedral aluminium, Al(IV).[22]

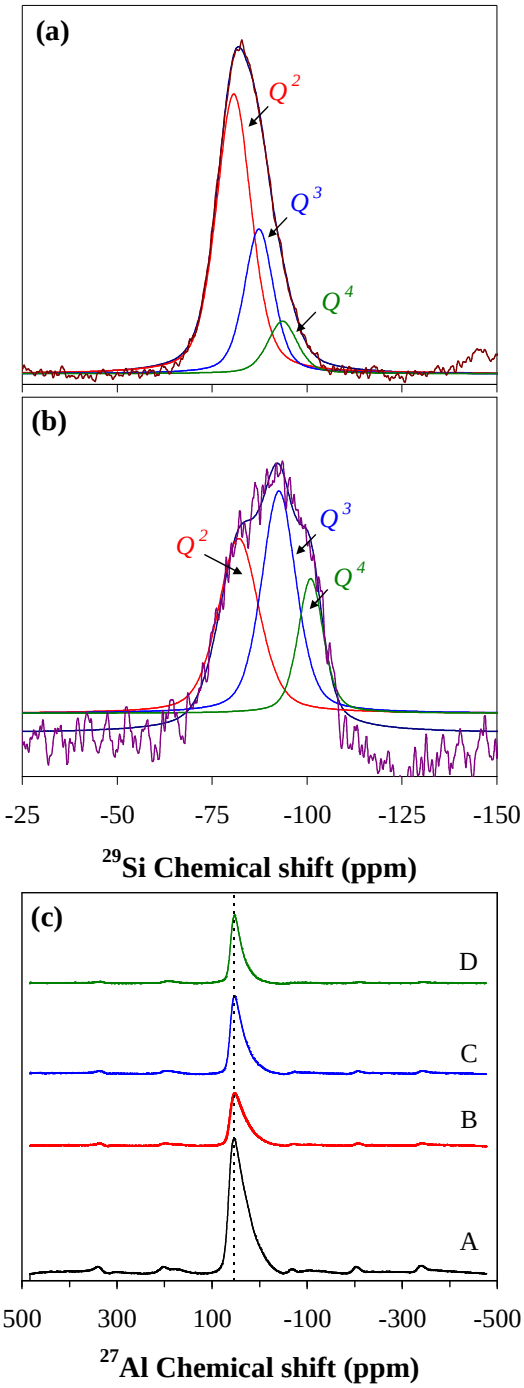

Fig. 3 – MAS-NMR spectra: (a) ^{29}Si MAS-NMR for glass A, (b) ^{29}Si MAS-NMR for glass D and (c) ^{27}Al MAS-NMR spectra of glass frits.

The DTA traces for the glass powder frits with particle sizes in the range of 5–10 µm are shown in Figs. 4a,b. The parent glass (A) has a T_g of 742 ºC and two crystallisation exotherms at 884 ºC (T_{p1}) and 1040 ºC (T_{p2}) (Table 3). The first and the second exothermic peaks are due to the formation of FAp and An, respectively.[22] The shoulder observed in the second exothermic peak suggests the formation of a third crystalline phase, likely diopsite.

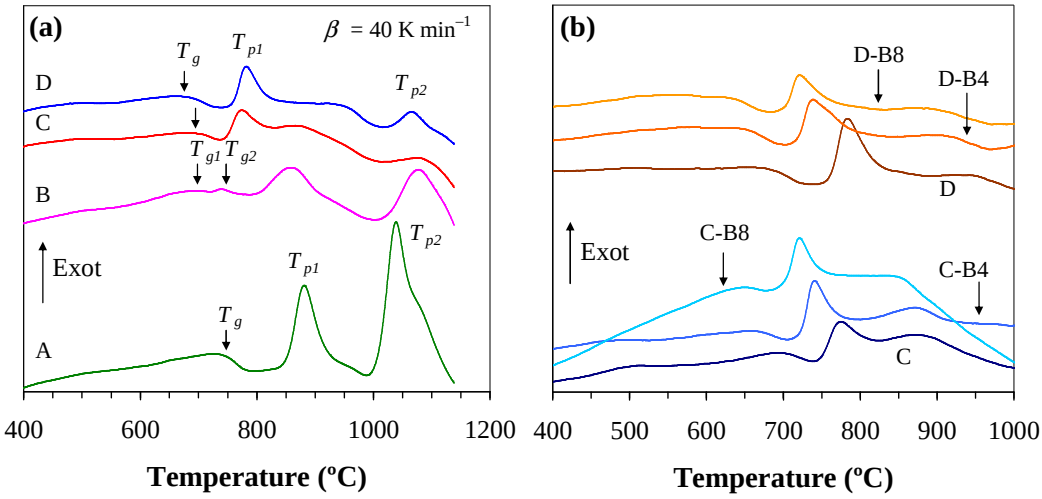

Fig. 4 – DTA of glass frits at $\beta = 40$ K min^{-1}.

Table 3 – Thermo-physical properties of the experimental glasses.

	d (g cm^{-3})	CTE$_{200\text{-}500\ ºC}$ ±0.1 (10^{-6} K^{-1})	T_{g1} ±2 (ºC)	T_{g2}	T_{p1} ±2 (ºC)	T_{p2} ±2 (ºC)
A	2.866 ±0.001	7.86	742	–	884	1040
B	2.800 ±0.001	6.34	700	743	862	1081
C	2.766 ±0.005	9.07	704	unresolved	779	1078
D	2.718 ±0.003	8.98	685	unresolved	785	1068
C-B4	2.734 ±0.004	8.08	671	unresolved	742	unresolved
C-B8	2.700 ±0.002	8.14	657	unresolved	722	unresolved
D-B4	2.691 ±0.002	8.49	654	unresolved	740	unresolved
D-B8	2.667 ±0.003	8.08	639	unresolved	722	unresolved

Adding the lowest amount of Al (glass composition B) shifted the first crystallisation peak to lower temperatures (862 ºC) whilst the second crystallisation peak occurred at higher temperatures (1081ºC). Further, two transition points T_{g1} and T_{g2} were revealed in the DTA spectrum of glass B at 700 ºC and 743 ºC, respectively, whilst only one T_g could be distinguished in the glasses C and D. The position of the first crystallization peak T_{p1} significantly shift to lower temperatures in both C and D glasses in comparison to glass B, but T_{p2} remained almost the same (Table 3). One important feature in DTA traces of glasses C and D is the presence of a distinct hump peak between the T_{p1} and T_{p2} exotherms. Also, the shoulder observed in the second exothermic peak disappeared and the overall intensity of the

peak decreased, suggesting the formation of a solid solution. The addition of 4 and 8 wt.% B_2O_3 to the compositions C and D caused significant shifts of T_g and crystallization exotherms to lower temperatures (Fig. 4,b). These observations suggest that B_2O_3 contributes to decrease the viscosity of the melts and enhances the diffusivity of the atoms.

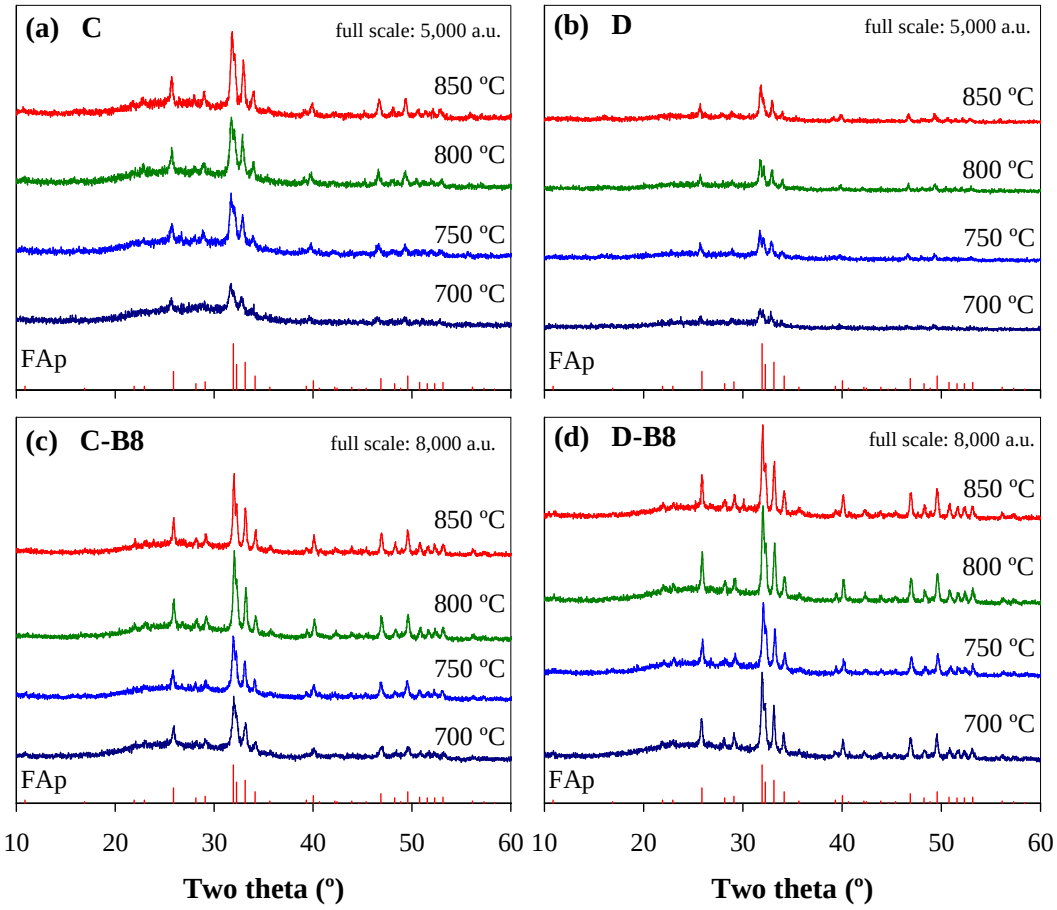

Fig. 5 – X-ray diffractograms of experimental bulk glasses after heat treatment at different temperatures for 5 h: (a) C, (b) D, (c) C-B8, (d) D-B8 (FAp: fluorapatite, $Ca_5(PO_4)_3F$, ICCD card 01-015-0876).

Some properties of the experimental glasses are presented in Table 2. Density decreased with increasing amounts of Al and B_2O_3. The CTE of the glasses show an increasing trend with the addition of Al, while an opposite effect was observed in the case of B_2O_3.

The XRD spectra of bulk glass samples heat treated at 700, 750, 800 and 850 ºC for 5 h presented in the Fig. 5 reveal that FAp was the single crystalline phase formed in all glass-ceramics, irrespective of the sintering temperature within the range studied. The intensities of

FAp peaks decrease with increasing amounts of Al and increased with incremental additions of B_2O_3.

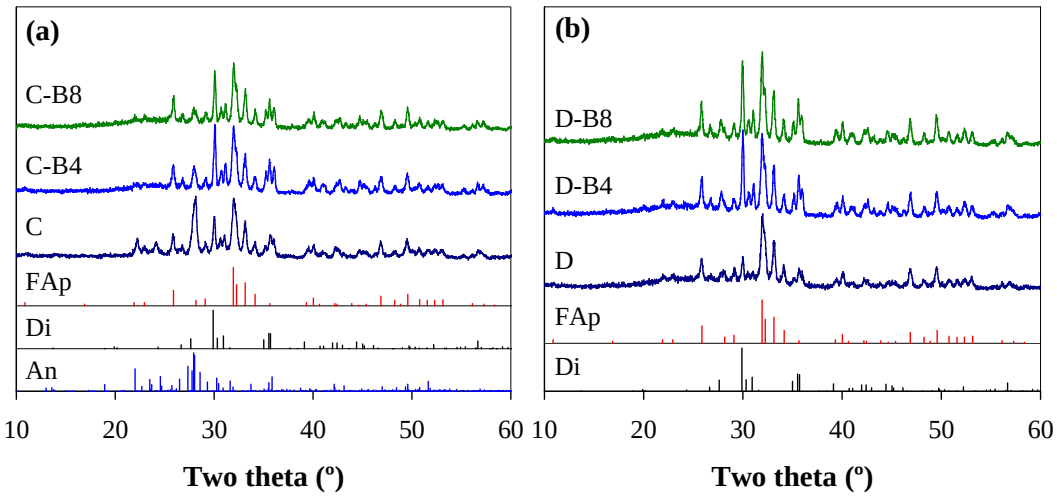

Fig. 6 – X-ray diffractograms of glass powder compacts after heat treatment at 900 ºC for 1 h (FAp: fluorapatite, $Ca_5(PO_4)_3F$, ICCD card 01-015-0876; Di: diopside, $CaMg(SiO_3)_2$, ICCD card 01-073-6374; An: anorthite, $CaAl_2Si_2O_8$, ICCD card 98-000-0012).

Sintering of glass powder compacts at 800, 850 and 900 ºC for 1 h resulted in dense glass-ceramic materials featuring relatively high mechanical strength (Table 4). Figs. 6 and 7 show the XRD spectra and microstructure of glass powder compacts heat treated at 900 ºC for 1 h, respectively. Three crystalline phases, FAp, Di and An were identified in the glass-ceramic C, while only FAp and Di were formed in glass-ceramic D in which An has been completely replaced by Al. The morphological features presented in Fig. 7 show the predominance of spherical crystals, therefore close to those of the liquid-liquid segregated droplets, suggesting again that apatite phase formation is nucleated inside the droplets. However, in the B_2O_3-containing composition D–B8, some areas with rod-like FAp crystals formed from the coalescence of droplets as revealed in Fig. 7b (insert).

4. Discussion

The results presented above showed that nano-scale crystallisation of FAp–An–Di glass-ceramics could be achieved due to two main contributing processes: (a) loss of fluorine and calcium from the glassy phase (CaO/P_2O_5-rich droplets) to form the FAp phase with the concomitant increase of T_g of the residual glass. This ‘freezing’ effect tends to halt the

crystallisation of the system; (b) the boundaries imposed by the nano-scale APS induced phosphate-rich droplets further limit the growth of the apatite crystallites, as proposed by Hill *et al.* [22] who assumed that the APS probably results in one of the phases having a composition close to FAp.

Table 4 – Thermo-physical properties of glass powder compacts.

	C	C-B4	C-B8	D	D-B4	D-B8
Density (g cm^{-3})						
800 ºC	2.560 ±0.033	2.636 ±0.015	2.654 ±0.002	2.532 ±0.013	2.534 ±0.017	2.613 ±0.005
850 ºC	2.637 ±0.003	2.721 ±0.007	2.667 ±0.006	2.541 ±0.009	2.682 ±0.006	2.642 ±0.009
900 ºC	2.776 ±0.002	2.776 ±0.006	2.692 ±0.005	2.712 ±0.008	2.703 ±0.001	2.647 ±0.006
Shrinkage (%)						
800 ºC	3.28 ±0.15	12.98 ±0.18	13.21 ±0.16	2.22 ±0.35	9.68 ±0.62	13.56 ±0.23
850 ºC	12.41 ±0.33	13.94 ±0.13	13.43 ±0.23	11.93 ±0.51	14.18 ±0.17	14.23 ±0.10
900 ºC	14.23 ±0.10	14.72 ±0.18	13.65 ±0.08	13.61 ±0.24	13.94 ±0.06	14.11 ±0.11
Bending strength (MPa)						
800 ºC	18.61 ±2.13	110.93 ±5.40	110.50 ±5.57	17.00 ±2.28	96.79 ±2.48	115.15 ±6.55
850 ºC	89.50 ±7.51	126.22 ±6.83	119.22 ±12.04	83.98 ±8.20	130.47 ±4.67	107.40 ±1.29
900 ºC	110.67 ±3.63	147.95 ±14.18	157.05 ±16.43	105.18 ±4.06	128.50 ±24.22	147.97 ±4.70

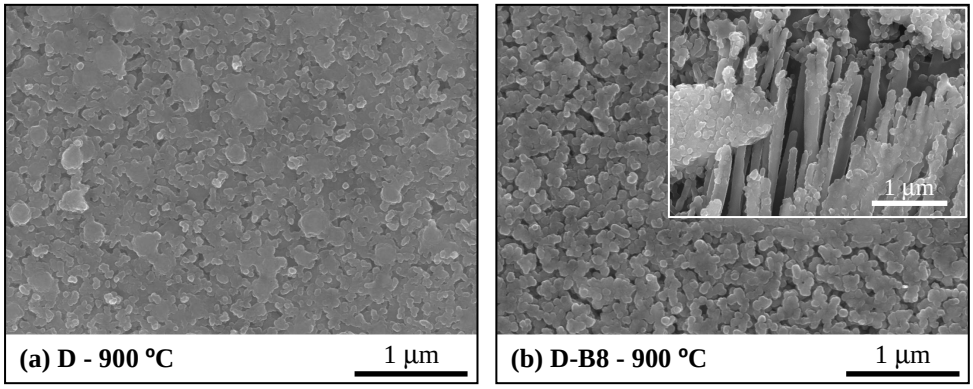

Fig. 7 – Microstructure of glass powder compacts heat-treated at 900 ºC for 1 h: (a) D, (b) D-B8.

In the present work a glass composition previously studied by Hill *et al.* [22] was used as the parent glass (A) for synthesis of three new glasses in the system FAp–An–Di–Al. SEM analyses of annealed glass A performed in our work confirmed the presence of APS in the form of droplets of very fine scale morphology (25–125 nm) dispersed in the glassy matrix

(Fig. 1). T_g, T_{p1} and T_{p2} values of the glass A were similar to those obtained in that earlier study [22] whilst some discrepancies can be explained by the use of different characterization techniques and heat treatment schedules. The two characteristic endotherms presented by glass B at 700 and 743 ºC (Fig. 4, Table 3) are likely due to the enhanced liquid-liquid phase separation that occurred upon replacing 50 mol.% of anorthite by albite (Fig. 1) and the consequent formation of droplets with different compositions, which will exhibit distinguishable transition points.[23] The shifting trend of the thermal events to lower temperatures (Fig. 4) suggests that the second T_g attributed to the transition of the silica rich glassy phase in glasses C and D probably has been masked by its superposition with T_{p1}.[24]

According to the ternary system albite–anorthite–diopside [25], albite and anorthite form a complete solid solution series (the plagioclase series), anorthite and diopside form a eutectic system, as do albite and diopside. The solid solution between albite and anorthite continues into the ternary system and is expressed by the boundary curve connecting the two binary eutectics. However, from the phase diagram of diopside–albite system [26], the narrow crystallization field for albite reflects big differences in the crystallization trends of the two phases. It is known that anorthite features highly ordered structure [22] but albite is even more difficult to crystallize from the silicate glasses.[27]

Karamanov *et al.* [27] investigating diopside–albite glass ceramics mentioned that practically, only diopside formation is expected while the residual glass retains composition similar to albite. The different crystallization behaviour was explained in terms of crystal structures: albite has a complicated framework structure, while diopside consists of a simple chain structure of monoclinic pyroxene. Similar crystallization trends were observed for the experimental B–D compositions since evidences of albite formation could neither be detected by XRD nor by SEM analyses in both heat treated bulk glasses and glass-powder compacts.

The crystallization of apatite phase in the experimental B–D melts through slow cooling rate can be explained by the allowed extension of liquid-liquid phase separation into CaO/P_2O_5-rich droplet phase and silica enriched matrix phase. This phenomenon was earlier observed in similar systems.[13, 28] Fluorapatite-based glass-ceramics featuring relatively high mechanical properties comparable to those reported for similar systems [27, 29], could be produced from the amorphous powder frits obtained by fast quenching the glass melts in cold water and further applying glass-powder processing techniques.

5. Conclusions

The melts of all investigated glass compositions in the system FAp–Di–An–Al were prone to the occurrence of APS reflected in the precipitation of a nanosize droplet phase in the glassy matrices. But this segregation trend increased by adding albite at the expense of anorthite into the $Ca_5(PO_4)_3F$–$CaAl_2Si_2O_8$–$CaMgSi_2O_6$ system.

The structure of glass A consisted predominantly of Q^2 units, but the polymerisation degree of the glass network increased upon replacing anorthite by albite, as revealed by a decrease of relative distribution of Q^2 units and an increase of Q^3 and Q^4 structural groups. All compositions show ^{27}Al chemical shifts centred at about 54 ppm with dominant presence of tetrahedral aluminium, evidencing its role as glass network former.

Apatite monophase glass-ceramics were obtained after heat treatment of bulk glasses in the temperature interval 700–850 ºC for 5 h. Glass powder compacts heat-treated at 900 ºC for 1 h exhibited good densification behaviour after sintering at 900 ºC for 1 h. Formation of rod-like apatite crystals in B_2O_3-containing compositions ensure their higher mechanical strength values in comparison to B_2O_3-free glass-ceramics.

Acknowledgment

Hugo R. Fernandes is grateful for the financial support of CICECO and for the PhD grant (SFRH/BD/41307/2007) from the FCT, Portugal.

References

1. Best SM, Porter JAE, Thian ES, Huang J. Bioceramics: Past, present and for the future. Journal of the European Ceramic Society 2008;28(7):1319-27.
2. Hill RG, Stamboulis A, Law RV, Clifford A, Towler MR, Crowley C. The influence of strontium substitution in fluorapatite glasses and glass-ceramics. Journal of Non-Crystalline Solids 2004;336(3):223-29.
3. Kokubo T. Apatite formation on surfaces of ceramics, metals and polymers in body environment. Acta Materialia 1998;46(7):2519-27.
4. LeGeros RZ, LeGeros JP. Dense Hydroxyapatite. In: Hench LL, Wilson J, editors. An Introduction to Bioceramics. Singapore: World Scientific; 1993. p. 139-80.
5. Höland W. Biocompatible and bioactive glass-ceramics - state of the art and new directions. Journal of Non-Crystalline Solids 1997;219:192-97.

6. DeLoach LD, Payne SA, Smith LK, Kway WL, Krupke WF. Laser and spectroscopic properties of $Sr_5(PO_4)_3F$:Yb. Journal of the Optical Society of America B 1994;11(2):269-76.
7. DeLoach LD, Payne SA, Chase LL, Smith LK, Kway WL, Krupke WF. Evaluation of absorption and emission properties of Yb^{3+} doped crystals for laser applications. IEEE Journal of Quantum Electronics 1993;29(4):1179-91.
8. Abo-Mosallam HA, Hill RG, Karpukhina N, Law RV. MAS-NMR studies of glasses and glass-ceramics based on a clinopyroxene–fluorapatite system. Journal of Materials Chemistry 2010;20:790-97.
9. Höland W, Beall G. Glass-ceramic Technology. Westerville, Ohio: The American Ceramic Society; 2002.
10. Höland W, Rheinberger V, Apel E, van Hoen C, Höland M, Dommann A, et al. Clinical applications of glass-ceramics in dentistry. Journal of Materials Science: Materials in Medicine 2006;17:1037-42.
11. Höland W, Ritzberger C, Apel E, Rheinberger V, Nesper R, Krumeich F, et al. Formation and crystal growth of needle-like fluoroapatite in functional glass-ceramics. Journal of Materials Chemistry 2008(18):1318-32.
12. Höland W, Frank M, Schweiger M, Rheinberger V. Paper presented at: 17th International Congress on Glass, 1995; Beijing.
13. Moisescu C, Jana C, Rüssel C. Crystallization of rod-shaped fluoroapatite from glass melts in the system SiO_2–Al_2O_3–CaO–P_2O_5–Na_2O–K_2O–F^-. Journal of Non-Crystalline Solids 1999;248(2-3):169-75.
14. Bou E, Moreno A, Escardino A, Gozalbo A. Microstructural study of opaque glazes obtained from frits of the system: SiO_2–Al_2O_3–B_2O_3–(P_2O_5)–CaO–K_2O–TiO_2. Journal of the European Ceramic Society 2007;27:1791-96.
15. Reinosa JJ, Rubio-Marcos F, Soleraa E, Bengochea MA, Fernández JF. Sintering behaviour of nanostructured glass-ceramic glazes. Ceramics International 2010;36(6):1845-50.
16. Tulyaganov DU. Phase equilibrium in the Fluorapatite–Anorthite–Diopside system. Journal of the American Ceramic Society 2004;83(12):3141–46.
17. Fernandes HR, Tulyaganov DU, Goel IK, Ferreira JMF. Crystallization process and some properties of Li_2O–SiO_2 glass-ceramics doped with Al_2O_3 and K_2O. Journal of the American Ceramic Society 2008;91(11):3698-703.
18. Massiot D, Fayon F, Capron M, King I, Le Calvé S, Alonso B, et al. Modelling one- and two-dimensional solid-state NMR spectra. Magnetic Resonance in Chemistry 2002;40:70-76.
19. Lin S-L, Hwang C-S. Structures of CeO_2–Al_2O_3–SiO_2 glasses. Journal of Non-Crystalline Solids 1996;202:61-67.
20. Schneider J, Mastelaro VR, Panepucci H, Zanotto ED. ^{29}Si MAS–NMR studies of Q^n structural units in metasilicate glasses and their nucleating ability. Journal of Non-Crystalline Solids 2000;273:8-18.
21. Fernandes HR, Tulyaganov DU, Goel A, Ferreira JMF. Effect of K_2O on structure-property relationships and phase transformations in Li_2O–SiO_2 glasses. Journal of the European Ceramic Society 2012;32(2):291-98.
22. Hill RG, O'Donnell MD, Law RV, Karpukhina N, Cochrane B, Tulyaganov DU. The early stages of nucleation and crystallisation of an apatite glass-ceramic: Evidence for nano-scale. Journal of Non-Crystalline Solids 2010;356:2935-41.
23. Henry DJ, Mackinnon IDR, Chan I, Navrotsky A. Subliquidus glass-glass immiscibility along the albite–diopside join. Geochimica et Cosmochimica Acta 1983;47(2):277-82.

24. Lasocka M. Thermal evidence of overlapping effects of glass transition and crystallization, derived from two different glassy phases in the phase-separated system $Te_{80}Ge_{12.5}Pb_{7.5}$. Journal of Materials Science Letters 1978;13:2055-59.
25. Morse SA. Basalts and Phase Diagrams. Malabar: Krieger Publishing; 1994.
26. Schairer JF, Yoder Jr. HS. Nature of residual liquids from crystallization, with data on the system nepheline–diopside silica. American Journal of Science 1960;258A:273-83.
27. Karamanov A, Arrizza L, Matekovits I, Pelino M. Properties of sintered glass-ceramics in the diopside–albite system. Ceramics International 2004;30:2129-35.
28. Moisescu C, Höche T, Carl G, Kedding R, Rüssel C, Heerdegen WG. Influence of the Ca/P ratio on the morphology of FAp crystals in the SiO_2–Al_2O_3–CaO–P_2O_5–K_2O–F^- glass-ceramics. Journal of Non-Crystalline Solids 2001;289:123-34.
29. Zhang WY, Gao H, Xu Y. Sintering and reactive crystal growth of dipside–albite glass-ceramics from waste glass. Journal of the European Ceramic Society 2011;31:1669-75.

Chapter

4

Conclusions and future direction

"*The value of experience is not in seeing much, but in seeing wisely.*"
William Osler

4.1. Conclusions

The present work aimed at developing lithium disilicate based glass-ceramics in the system $Li_2O–K_2O–Al_2O_3–SiO_2$ featuring SiO_2/Li_2O molar ratios far beyond that of lithium disilicate ($Li_2Si_2O_5$) stoichiometry using simple compositions and traditional glass melt-quenching technique in order to get enhanced mechanical, thermal, chemical and electrical properties which allow the use these materials in functional applications. The effect of Al_2O_3 and K_2O contents on the structure and crystallization of glasses in the system $Li_2O–K_2O–Al_2O_3–SiO_2$ was evaluated. The comparison between 3 systems, *i.e.* $Li_2O–SiO_2$, $Li_2O–Al_2O_3–SiO_2$ and $Li_2O–K_2O–Al_2O_3–SiO_2$, was also performed in order to deeply understand the role Al_2O_3 and K_2O on the structure and properties of the glasses, their crystallization kinetics as well as on phase evolution and thermo-physical properties of corresponding glass-ceramics. Additives, such as P_2O_5, TiO_2 and ZrO_2, were employed to assess their role on glass structure and crystallization process in the parent composition G3. The results obtained throughout these experiments can be summarised as follows:

4.1.1 Bulk glasses

The results revealed that compositions with equimolar addition of Al_2O_3 and K_2O appeared as transparent glasses and exhibited liquid–liquid phase separation with nanosize droplets, while the binary composition ($L_{23}S_{77}$) became cloudy on cooling. The addition of Al_2O_3 and K_2O to the binary system in the as-investigated proportions allowed to control the extent of the phase separation in the system $Li_2O–SiO_2$ due to the formation of tetrahedral four-coordinated Al(IV) species confirming the role of Al_2O_3 as network former. Surface nucleation and crystallization was dominant in high Al_2O_3 and K_2O glasses (G1 and G2) with lithium metasilicate as the primary crystalline phase whilst volume nucleation and crystallization of lithium disilicate was observed in glass containing lowest amount of additives (G3) and in the binary glass composition ($L_{23}S_{77}$).

Adding excess of K_2O to glass G3 (*i.e.* $K_2O/Al_2O_3 > 1$) resulted in an increase of the mean droplet size and droplet distribution density due to a decreasing energy barrier towards phase separation caused by the lowering of glass melt viscosity. Moreover, adding excess of K_2O to glass G3 suppressed the crystallization of $Li_2Si_2O_5$ and promoted the formation of Li_2SiO_3.

Addition of nucleating agents (P_2O_5, TiO_2 and ZrO_2) to the parent composition G3 resulted in higher T_g for all investigated compositions, but only P_2O_5 led to bulk crystallization, with the formation of lithium metasilicate at lower temperatures and the crystallization of lithium disilicate at higher temperatures. Biphasic glass ceramics (lithium metasilicate + lithium disilicate) were always obtained in the presence of TiO_2 at 800 and 900 ºC irrespective of the added amount. The addition of zirconia to the parent glass reduces the degree of segregation, increases the polymerization of the glassy matrix, and shifts T_p to higher temperatures hindering crystallization.

4.1.2 Glass powder compacts

Al_2O_3- and K_2O-free binary glass demonstrated higher rate of crystal growth due to extended phase separation. Sintering of corresponding glass powder compacts resulted in poorly densified samples due to the narrowing of the T_c–T_g interval and early formation of large fraction of lithium disilicate phase. On the other hand, sintering and crystallisation of Al_2O_3- and K_2O-containing compositions in the silica rich region of Li_2O–SiO_2 system resulted in well-densified and mechanically strong fine-grained glass-ceramics with lithium disilicate as the major crystalline phase featuring mechanical strength ~173–224 MPa, chemical resistance ~25–50 μg/cm^2 and low total conductivity (~2×10^{-18} S/cm) making these materials suitable for a number of practical applications.

The sintering/densification of the glass powder compacts of composition derived from G3 with excess of K_2O (*i.e.* $K_2O/Al_2O_3 > 1$) occurred in two steps. The extent of densification along the first stage significantly decreased with increasing the excess amounts of K_2O, while the second stage of densification occurred in competition with crystallization process. The gradual substitution of SiO_2 by K_2O in glass compositions suppressed the crystallization of $Li_2Si_2O_5$ and promoted the formation of Li_2SiO_3 upon sintering the glass powder compacts. The glass powder compacts demonstrate wider range of the lithium disilicate formation than the corresponding bulk glasses.

The fluorapatite–diopside–anorthite–albite (FAp–Di–An–Al) system revealed to be promising for applications as fine grade glass-ceramic coatings on ceramic substrates with compositions similar to that of G3. The FAp–Di–An–Al glass powder compacts heat-treated at 900 ºC for 1 h exhibited good densification behaviour. Moreover, the incorporation of B_2O_3

led to the formation of rod-like apatite crystals which improve their mechanical strength values in comparison to B_2O_3-free glass-ceramics.

4.2. Proposed application fields for the experimental glass-ceramics

The present work is based on the study of glasses in the $Li_2O–K_2O–Al_2O_3–SiO_2$ system, featuring SiO_2/Li_2O molar ratios far beyond that of lithium disilicate ($Li_2Si_2O_5$). The experiments allowed obtaining fine-grained glass-ceramics with lithium disilicate as the major crystalline phase and attractive mechanical, chemical and electrical properties which allow the use of these materials in functional applications such as: (a) dental applications in the form of artificial tooth substitutes; (b) electrical applications as low voltage insulators; (c) chemical industrial applications as acid resistive materials.

4.3. Future directions

During this research work, an attempt has been made to develop lithium disilicate based glass-ceramics in the simple quaternary system $Li_2O–K_2O–Al_2O_3–SiO_2$ for functional applications. We have succeeded in shedding some light on the structure and crystallization of glasses, phase evolution and microstructure of the final materials which render them suitable for further experimentation as potential candidates in various functional applications. However, complementary work still needs to be accomplished before making them geared up for final application. Therefore, in our opinion, the future work in this area may be addressed to the following issues:

1. Further improvement of mechanical properties and chemical durability of developed glass-ceramics via application of hot pressing technique used in the production of commercial dental materials, *e.g.* IPS Empress®2.
2. Investigation of the effect of various additives (CeO_2, V_2O_5, P_2O_5 + ZrO_2, etc.) on translucency and optical properties of glass-ceramics.

3. Development of apatite–based coatings in the system fluoapatite–diopside–anorthite to improve aesthetic properties of glass-ceramics for application as dental materials.
4. *In vitro* and *in vivo* tests of glass-ceramics in physiological media.
5. Further attempts to decrease droplets size in phase separated glasses to achieve nanosize crystallization of lithium disilicate glass-ceramics useful for advanced engineering fields.